Inorganic Hydrazine Derivatives

Inorganic Hydrazine Derivatives

Synthesis, Properties and Applications

Edited by

K. C. Patil
Department of Inorganic and Physical Chemistry, Indian Institute of Science, Bangalore, India

and

Tanu Mimani Rattan
Department of Physics, Sri Sathya Sai Institute of Higher Learning, Prasanthi Nilayam, India

WILEY

This edition first published 2014

Registered office
John Wiley & Sons Ltd, The Atrium, Southern Gate, Chichester, West Sussex, PO19 8SQ, United Kingdom

Library of Congress Cataloging-in-Publication Data

Inorganic hydrazine derivatives : synthesis, properties, and applications /
edited by K.C. Patil and Tanu Mimani Rattan.
pages cm
Includes index.
Includes bibliographical references.
ISBN 978-1-118-71513-0 (hardback)
1. Hydrazines. 2. Hydrazines–Industrial applications. I. Patil, K. C.,
editor of compilation. II. Rattan, Tanu Mimani, editor of compilation.
QD181.N1I57 2014
661–dc23
2013037822

A catalogue record for this book is available from the British Library.

ISBN: 9781118715130

Set in 10.5/13pt, SabonLTStd-Roman by Thomson Digital, Noida, India.

1 2014

Dedicated To
"Eckart W. Schmidt – The Hydrazine man"

Contents

List of Contributors

Singanahally T. Aruna Surface Engineering Division, CSIR-National Aerospace Laboratories, Bangalore, India

Dasaratharam Gajapathy K.M.G. College of Arts & Science, Gudiyathum, India

Subbiah Govindrajan Department of Chemistry, Bharathiar University, Coimbatore, India

K. C. Patil Department of Inorganic and Physical Chemistry, Indian Institute of Science, Bangalore, India

Tanu Mimani Rattan Department of Physics, Sri Sathya Sai Institute of Higher Learning, Prasanthi Nilayam, India

Foreword

Of the two dozen or so known binary compounds of nitrogen and hydrogen, only three are economically significant. Arranged in descending order of importance these are ammonia, hydrazine, and hydrazoic acid. The discovery of phenylhydrazine (1875) and other substituted hydrazines by Fischer preceded that of hydrazine itself by several years. Curtius first prepared hydrazine from ethyl diazoacetate following a circuitous route (1887). Serious research on the structure and reactivity of hydrazine could begin only after its ready availability was assured by Raschig's discovery of its simple and effective synthesis via oxidative coupling of ammonia (1907). A relatively weak N–N bond, two nucleophilic nitrogen sites, multiple replaceable hydrogen atoms, variable reducing power, endothermicity, and high heat of combustion are among the factors that have added unique features to the chemistry of hydrazine. These in turn have prompted extensive uses of hydrazine and its derivatives in the chemical industry, encompassing polymers, agriculture, pharmaceuticals, explosives, water-treatment, and more. Hydrazine and its derivatives also feature in space missions, where the versatility and reliability of hydrazine-powered propellant systems have performed a signal role.

An account of the state of hydrazine chemistry preceding the middle of the last century was chronicled by Audrieth and Ogg in their book *The Chemistry of Hydrazine* (1951). Nearly three decades later, Schmidt's compendium *Hydrazine and its Derivatives, Preparation, Properties, Applications* appeared in 1984. The explosion in hydrazine literature (4400 references) was apparent and in the second edition (2001) of this authoritative book the number of references nearly doubled! Hydrazine and its derivatives very much remains a living arena for continued scrutiny and practical use.

Patil and his students have been intimately associated with several facets of hydrazine chemistry for many years at the Indian Institute of Science, Bangalore. They have enriched the basic chemistry by developing newer methods of preparing hydrazinium salts and by exploring the synthesis and structure of hydrazinium complexes of metal salts. They were also deeply involved with applied aspects such as in the development of energetic oxidizers for solid propellants and of detonators, some of which have commercial success stories to tell. The group also succeeded in preparing technologically important transition metal oxide nanomaterials utilizing combustible carboxylic metal hydrazine salts as starting materials.

The rich contributions of the group to both basic and applied inorganic chemistry of hydrazine have been documented in the literature over the years. Patil and Rattan have now carried out a commendable service by organizing the material into a logical and connected account laid out against the broader background of hydrazine chemistry. The outcome is the present monograph, which has six chapters and is appropriately titled *Inorganic Hydrazine Derivatives: Synthesis, Properties and Applications*. The chapters are divided into sections and subsections for both basic and applied activities and include recent work on these topics by other groups. I expect this book to become a must for all those with direct interest in hydrazine chemistry and technology. It should also arouse considerable general interest in the inorganic chemistry and material science communities. I feel very pleased to write this Foreword for a work that highlights the noteworthy contributions to the pure and applied chemistry of hydrazine derivatives from India in the last few decades. On visits to Bangalore I had the opportunity to watch Patil *et al*. making progress in silent dedication. It is now time for me to congratulate them as I browse through their text.

Animesh Chakravorty
Emeritus Professor and Ramanna Fellow
Indian Association for the Cultivation of Science
Kolkata, India
August 2013

Preface

The chemistry of hydrazine and its derivatives continues to be of interest to chemists, material scientists, and engineers due to their applications in propellants, explosives, polymers, pharmaceuticals, medical, and agricultural fields. Although there are several reviews on this subject there are very few books devoted to the chemistry of hydrazine. The latest voluminous work on hydrazine authored by Eckart W. Schmidt – the hydrazine man – was published over a decade ago in 2001. It contains a wealth of information, citing nearly 8400 references, signifying the importance of hydrazine and its derivatives. The research work of the authors has been cited in this book.

The present monograph, *Inorganic Hydrazine Derivatives: Synthesis, Properties and Applications*, is a compendium of the research work carried out during the last four decades by the authors at the Indian Institute of Science, Bangalore. An attempt has been made to present the work on inorganic hydrazine derivatives over six chapters. Details of the synthesis, spectra, thermal analysis, crystal structure, and applications of inorganic derivatives of hydrazine such as hydrazine salts, metal hydrazines, metal hydrazine carboxylates, and hydrazinium metal complexes are expounded in a systematic manner. Recent contributions by other groups working in similar areas have also been examined. The monograph also highlights current developments and applications of inorganic hydrazine derivatives, including the synthesis of nanostructured materials.

Chapter 1 – Hydrazine and its Inorganic Derivatives briefly describes the chemistry of hydrazine, its physical and chemical properties. A clear distinction is made between hydrazine and hydrazine hydrate in terms of structure and properties. Since there is hardly any difference in the

chemical properties of the two, a case is made for the use of hydrazine hydrate instead of the hazardous and toxic anhydrous hydrazine. A brief literature survey on the synthesis and crystal structure of various hydrazine salts and metal hydrazine complexes is presented. Various thermoanalytical and spectroscopic techniques used in the characterization of hydrazine compounds and metal complexes are discussed.

Chapter 2 – Hydrazine Salts discusses the synthesis and characterization of the inorganic salts of hydrazine. A novel and simple method of preparing hydrazinium salts by the heterogeneous reaction of solid ammonium salts with hydrazine hydrate is presented. The preparation and characterization of numerous N_2H_5A salts, where A = halide, NO_3^-, ClO_4^-, N_3^-, SCN^-, acetate, and so on, are profiled. The formation of $N_2H_5HF_2$ and $N_2H_5HSO_4$ by this method is reported for the first time. These salts are characterized by infrared spectroscopy and differential thermal analysis (DTA), and their properties compared with those of $N_2H_6F_2$ and $N_2H_6SO_4$, respectively. Interestingly, few hydrazine salts form hydrates: for example, $N_2H_5ClO_4{\cdot}0.5H_2O$ and $N_2H_6X{\cdot}2H_2O$, $X = ClO_4^-$. Infrared spectroscopy, thermal analysis, and conductivity measurements show that the water in these compounds is partially present as oxonium ion (H_3O^+) and is involved in hydrogen bonding with N_2H_4.

Chapter 3 – Metal Hydrazines presents the synthesis and properties of metal hydrazine complexes. These compounds are of interest from the point of view of bonding, structure, and reactivity. The hydrazine molecule with its two free electron pairs can coordinate to a metal ion either as a monodentate or bridged bidentate ligand. Several metal hydrazine complexes containing different anions, such as oxalate, perchlorate, nitrate and azide, sulfate, sulfite, hydrazine carboxylate, and so on, are prepared and investigated. In all these complexes hydrazine is usually present as a bridged bidentate and, occasionally, as a monodentate ligand. The thermal reactivity of these metal hydrazines varies from explosion → deflagration → decomposition, depending upon the anion. Transition metal perchlorate, nitrate, and azide hydrazines are primary high energy materials (HEMs). Non-transition metal hydrazines of Li, Mg, and Al perchlorate, nitrate and azide, and so on, and transition metal hydrazine complexes of oxalate, sulfite, and hydrazine carboxylate, deflagrate. The rest simply decompose, with the loss of hydrazine.

Chapter 4 – Metal Hydrazine Carboxylates gives an account of the preparation of various metal hydrazine carboxylate complexes such as $M(N_2H_3COO)_2{\cdot}xH_2O$, M = Ca, Mg, Mn, Cu, and Cr; $Ln(N_2H_3COO)_3{\cdot}3H_2O$, Ln = rare earth ion; $M(N_2H_3COO)_2(N_2H_4)_2$ and $N_2H_5M(N_2H_3COO)_3{\cdot}H_2O$, M = Mn, Fe, Co, Ni, and Zn. These

complexes are investigated by infrared spectroscopy and thermal analysis. The characteristic N–N stretching frequency is used to distinguish between monodentate N_2H_4 (ν_{N-N} 930 cm^{-1}), ionic $N_2H_5^+$ (ν_{N-N} 965 cm^{-1}), and $N_2H_3COO^-$ (ν_{N-N} 990–1005 cm^{-1}) species. Transition metal hydrazine carboxylates decompose in air at low temperatures (75–200 °C) to yield nanosize oxide materials. The decomposition is autocatalytic; once initiated it is accompanied by swelling due to the evolution of large amounts of gases like NH_3, H_2O, H_2, and CO_2.

Chapter 5 – Hydrazinium Metal Complexes highlights the coordinating ability of the hydrazinium cation, $N_2H_5^+$. The synthesis and structure of several hydrazinium metal sulfate and oxalate complexes are presented. Single-crystal structures are showcased of $N_2H_5M(SO_4)_2$ where, M = Mn, Fe, and Cd; $N_2H_5Nd(SO_4)_2{\cdot}H_2O$, $(N_2H_5)_2Cu(C_2O_4)_5{\cdot}2H_2O$, $(N_2H_5)_6(UO_2)_2(C_2O_4)_5{\cdot}2H_2O$, $(N_2H_5)_2(UO_2)_2(C_2O_4)_2{\cdot}H_2O$, and so on. Interestingly, $N_2H_5^+$ ion coordinates to the metal ion in sulfate complexes but is outside the coordination sphere of the metal ion in oxalate complexes.

Several hydrazinium metal chloride complexes $(N_2H_5)_2MCl_4{\cdot}2H_2O$, where M = Fe, Cu, Co, Ni, Pt, and Pd, $N_2H_5CuCl_3$, $(N_2H_5)_2ZnCl_4$, $(N_2H_5)_3MnCl_5$, and $(N_2H_5)_4FeCl_6$ have been synthesized and investigated for their crystal structure. Single-crystal structures presented are of $(N_2H_5)_2MCl_4{\cdot}2H_2O$, M = Fe and Pt, $(N_2H_5)_3MnCl_5$, and so on. In all these complexes $N_2H_5^+$ ions are coordinated to the metal ion. Hydrazinium metal thiocyanates $(N_2H_5)M(NCS)_4{\cdot}2H_2O$, where M = Co and Ni, have been prepared and the single-crystal structure of the cobalt compound is shown.

Chapter 6 – Applications of Inorganic Hydrazine Derivatives summarizes the uses of inorganic hydrazine derivatives. Some interesting properties and reactions of hydrazine salts have emerged from these investigations. These include flame retardancy of hydrazinium phosphates, solid-state rearrangement of hydrazinium thiocyanate to thiosemicarbazide ($N_2H_5SCN \rightarrow N_2H_5CSNH_2$), and the use of N_2H_5SCN as an analytical reagent for the quantitative estimation of copper. Hydrazinium hydrazinecarboxylate formed by the reaction of commercial ammonium carbonate with hydrazine hydrate reacts with acetonitrile at room temperature to give a triazole compound. Triazoles find applications in a wide variety of agrochemicals and medicine. The perchlorate, nitrate, and azide salts of hydrazine, $N_2H_5NO_3$, $N_2H_5N_3$, $N_2H_5ClO_4{\cdot}0.5H_2O$, $N_2H_6(ClO_4)_2{\cdot}2H_2O$, and so on, are potentially energetic oxidizers and are being considered for use in solid propellant compositions. However, they are highly hygroscopic and incompatible with conventional

polymeric fuels and in solid propellants. These problems have been overcome successfully by complexing both hydrazine perchlorates with ammonia as well as by doping with Mg^{2+} ions. Transition metal hydrazines containing anions like nitrate, azide, and perchlorates have been investigated as detonators. Surprisingly, the thermolysis of Mg $(N_3)_2(N_2H_4)_2$ gives a blue colored residue that shows strong IR absorption at 2100 cm^{-1}, which is characteristic of molecular nitrogen.

The deflagrating nature of metal hydrazines is used in the preparation of ferrites and cobaltites. Commonly used recording material like γ-Fe_2O_3 and Co-doped γ-Fe_2O_3, is prepared by the thermal decomposition of iron hydrazine carboxylates in a single step. Similarly, nano-size ferrites (MFe_2O_4, $Ni_xZn_{1-x}Fe_2O_4$, and $Mn_xZn_{1-x}Fe_2O_4$) and cobaltites (MCo_2O_4) are obtained at very low temperatures (300 °C) by the thermal decomposition/combustion in air of solid solution precursors of the type $N_2H_5M_{1/3}Fe_{2/3}(N_2H_3COO)_3{\cdot}H_2O$ and $N_2H_5M_{1/3}Co_{2/3}(N_2H_3COO)_3{\cdot}H_2O$, where M = Mg, Mn, Fe, Co, Ni, and Zn.

Finally, the work carried out and presented in this monograph has been quite exciting, creative, and rewarding to the authors. It is hoped that it will inspire future researchers and entrepreneurs working in academic institutes and defense and space research laboratories.

Acknowledgments

We gratefully acknowledge the collaboration of the following colleagues: Professors C.C. Patel, V.R. Pai Vernekar, S.R. Jain, H. Manohar, and K. Kishore and Drs. Nethaji, Damodar Pujari, and I.I. Mathews (Department of Inorganic and Physical Chemistry, Indian Institute of Science, Bangalore), and Professor Zhu Shanguan (Nanjing University of Science and Technology, China).

We also acknowledge the valuable research contributions of former PhD students: Drs Jayant Budukuley, R. Soundara Rajan, M. Ramanath, J. J. Vittal, C. Nesmani, D. Gajapathy, S. Govindrajan, P. Ravindranathan, N.R.S. Kumar, M.M.A. Sekhar, S. Ekambaram, N. Arul Das, S.T. Aruna, S. Shanmugaraju, Arun Kumar Bar, and Mr. G.V. Mahesh.

We are grateful to Professor A.G. Samuelson, Chairman, Department of Inorganic and Physical Chemistry, Indian Institute of Science, Bangalore for the support and co-operation extended. We thank Professor K. Venkataramaniah and Dr Siva Sankar Sai of Sri Sathya Sai Institute of Higher Learning, Prasanthi Nilayam for their encouragement.

Our sincere thanks are to Sanjay Rattan for editing the manuscript. Finally, we are grateful to Professor Animesh Chakravorty for readily agreeing to write the Foreword to our book.

K. C. Patil

Tanu Mimani Rattan

1

Hydrazine and Its Inorganic Derivatives

Tanu Mimani Rattan[1] and K. C. Patil[2]
[1]*Department of Physics, Sri Sathya Sai Institute of Higher Learning, Prasanthi Nilayam, India*
[2]*Department of Inorganic and Physical Chemistry, Indian Institute of Science, Bangalore, India*

1.1 INTRODUCTION

The chemistry of hydrazine (N_2H_4) acquires significance due to the presence of two free electron pairs and four substitutable hydrogen atoms, in addition to a potent N–N bond (Figure 1.1). Hydrazine is an endothermic molecule ($\Delta H_f = 55.63\,kJ\,mol^{-1}$) with nitrogen in the -2 valence state. Nitrogen's natural tendency is toward the attainment of a zero valence state as in N_2 molecule ($N \equiv N$). As a result, it gives off nearly six times the energy as that stored in the N–N bond. A tremendous amount of energy (ca $-622\,kJ\,mol^{-1}$) is released during the decomposition of N_2H_4 to N_2. This important energetic property of hydrazine was first recognized by the Germans during World War II when they used it as a rocket fuel. Since then hydrazine has been extensively used as a fuel in rocket motors because of its suitable physical properties, endothermicity,

Inorganic Hydrazine Derivatives: Synthesis, Properties and Applications, First Edition.
Edited by K. C. Patil and Tanu Mimani Rattan.

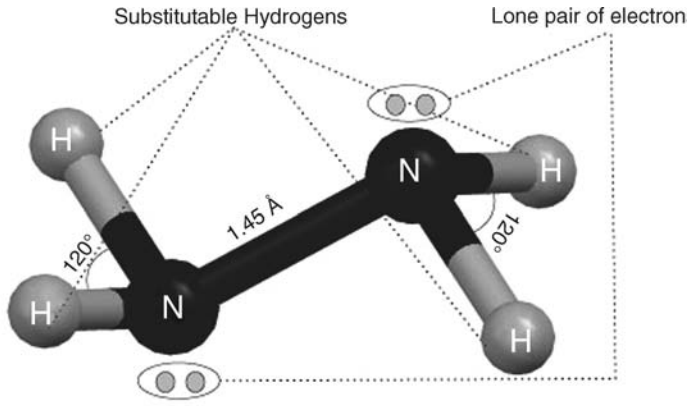

Figure 1.1 Structure of the hydrazine molecule.

and extremely high reactivity with various oxidizers. The ignition of anhydrous hydrazine is achieved simply by passing it through a catalyst bed, producing completely gaseous products, making it an excellent fuel for monopropellant rockets. The other advantage of using hydrazine and its derivatives [e.g., monomethyl hydrazine (MMH) and unsymmetrical dimethyl hydrazine (UDMH)] as propellants stems from the fact that they ignite instantaneously. They are hypergolic on coming in contact with various liquid oxidizers such as HNO_3, N_2O_4, and so on. However, interest in hydrazine and its derivatives has now extended to applications in agriculture (pesticides and fungicides), blowing agents, boiler feed water treatment, pharmaceuticals, and in synthesizing nanostructures. The consumption of hydrazine produced for these latter applications far surpasses that used as rocket propellant.

1.1.1 Properties of Hydrazine

Hydrazine is a strong base, although slightly weaker than ammonia as evident from the respective dissociation constants (k_1 and k_2) in aqueous solution (1.1) and (1.2). It is a much stronger nucleophile than ammonia. The second ionization constant shown in (1.2) being very small, suggests that the $N_2H_6^{2+}$ cation exists at an extremely low pH:

$$N_2H_4 + H_2O \rightarrow N_2H_5^+ + OH^-; k_1 = 8.5 \times 10^{-7} \quad (1.1)$$

$$N_2H_5^+ + H_2O \rightarrow N_2H_6^{2+} + OH^-; k_2 = 8.9 \times 10^{-16} \quad (1.2)$$

In aqueous solutions hydrazine largely exists as the hydrazinium cation ($N_2H_5^+$) while the hydrazonium cation ($N_2H_6^{2+}$) exists only in strong acidic conditions. $N_2H_6^{2+}$ ion reacts completely with solvent water to give back $N_2H_5^+$ in accordance with the equation:

$$N_2H_6^{2+} + H_2O \rightarrow N_2H_5^+ + H_3O^+ \tag{1.3}$$

This suggests that the $N_2H_6^{2+}$ ion does not readily exist in aqueous solutions.

1.1.1.1 Redox Properties

Hydrazine has two lone pairs of electrons on its nitrogen atoms. This makes it a strong reducing agent since it can donate all four electrons. The hydrazinium cation ($N_2H_5^+$) also has a lone pair of electrons on its nitrogen atom and therefore acts as a reducing agent. However, as the hydrazonium cation ($N_2H_6^{2+}$) exists as hydrazinium cation in solution, it also acts as a good reducing agent.

The standard redox potentials of hydrazine and its cation are given below. Reaction 1.4 represents the half-reaction of the molecule as a reductant. It is much less of a reducer in acid medium, where it exists as the hydrazinium cation. As the redox potential (E_0) of hydrazine decreases by nearly 1 V, as shown by (1.5), it is a powerful reducing agent in basic solutions rather than in acidic solutions [1]:

$$N_2H_4 + 4OH^- \rightarrow N_2 + 4H_2O + 4e^- \quad E_0 = +1.16\,V \tag{1.4}$$

$$N_2H_5^+ \rightarrow N_2 + 5H^+ + 4e^- \quad E_0 = +0.23\,V \tag{1.5}$$

Nonetheless, hydrazine, like hydrogen peroxide, can also be an oxidizing agent (1.5) as well as reducing agent (1.4). It can therefore undergo redox reactions that are essentially electron-transfer reactions:

$$N_2H_4 + 2H_2O + 2e^- \rightarrow 2OH^- + 2NH_3 \quad E_0 = +0.1\,V \tag{1.6}$$

Although reactions with hydrazine as an oxidant are possible, these are less frequent. Hydrazine is basically a strong reducing agent and as such reduces many ions to lower oxidation states or even to the bare metal and even beyond, to the hydride. The commonly encountered redox reactions of hydrazine are its autoxidation or atmospheric decay, oxidation in solution, and electro-oxidation. These redox reactions are governed by their reduction potentials and are responsible for its applications in fuel cells, electroless plating, or photographic processes.

Autoxidation of hydrazine occurs due to the presence of atmospheric oxygen. The autoxidation of hydrazine as evidenced by gas analysis and Infrared (IR) absorption measurements for hydrazine detection proceeds as represented in (1.7). The rapid autoxidation of hydrazine in the atmosphere is an advantage, as it means that hydrazine is not categorized as an environmental contaminant:

$$N_2H_4 + O_2 \rightarrow N_2 + 2H_2O \tag{1.7}$$

The above decomposition is catalyzed by metals such as copper and cobalt, and most likely by metallic species leached gradually from pipe systems, particularly nickel. This has led to the deoxygenation of boiler feed water as one of the major applications of hydrazine. The mechanism of autoxidation of hydrazine in aqueous solutions seems to be somewhat different from the mechanism observed in the vapor phase, although the ultimate products are frequently the same.

Autoxidation of hydrazine in solution proceeds only in alkaline and neutral conditions. The oxidation of hydrazine in solution is complex. When the hydrogen is abstracted after oxidation, the two adjacent nitrogen atoms should favor the formation of molecular nitrogen. However, this simple path is hardly followed. Instead, other compounds like ammonia and hydrazoic acid are the products of oxidation as shown by the following reactions:

$$N_2H_5^+ \rightarrow N_2 + 5H^+ + 4e^- \tag{1.8}$$

$$N_2H_5^+ \rightarrow NH_4^+ + 0.5N_2 + H^+ + e^- \tag{1.9}$$

$$N_2H_5^+ \rightarrow 0.5HN_3 + 0.5NH_4^+ + 2.5H^+ + 2e^- \tag{1.10}$$

The reactions shown in (1.8) and (1.9) occur predominantly and simultaneously. The reaction represented by (1.10) occurs when hydrazine is oxidized in hot, concentrated sulfuric acid with hydrogen peroxide. According to the above reaction mechanisms, a four-electron transfer leads to nitrogen formation, a one-electron transfer furnishes a mixture of nitrogen and ammonia, while a two-electron transfer generates hydrazoic acid [2].

The above-mentioned properties of hydrazine make its chemistry interesting as it can react in terms of various species such as molecule, ion, radical, or ligand (N_2H_4, $N_2H_5^+$ and $N_2H_6^{2+}$, $N_2H_3^-$, $N_2H_3COO^-$, $N_2H_3^{\bullet}$). The reactions of these species result in the formation of inorganic salts and coordination complexes with the metal ions as well as organic derivatives. Table 1.1 summarizes the different types of compounds

Table 1.1 Various kinds of species and compounds formed by hydrazine.

Type	Species	Nomenclature	Formula	Product	Example
Molecule	Solvated	Hydrazine	N_2H_4	Metal hydrazine complexes	$M(A)(N_2H_4)_y$ M = metal; A = anion (inorganic/organic); y = 1–4
Ion	Cation	Hydrazinium (monoprotonated)	$N_2H_5^+$	Simple salts	N_2H_5X X = anion (inorganic/organic)
			$(N_2H_5^+)_2$	Dihydrazinium salts	$(N_2H_5)_2X_2$ X = anion (inorganic/organic)
		Hydrazinium	$N_2H_5^+$	Hydrazinium metal complexes	$N_2H_5MA_m.yH_2O$ M = metal, A = anion (inorganic/organic).y = 2–3
		Hydrazonium (diprotonated)	$N_2H_6^{2+}$	Simple salts	$N_2H_5A_2$ A = anion (inorganic/organic)
	Anion	Hydrazide	$N_2H_3^-$	Inorganic hydrazides[a]	MN_2H_3, $M_2N_2H_2$, M = light metal (Na, Al, etc.)
		Hydrazine carboxylate	$N_2H_3COO^-$	Metal hydrazine carboxylates	$M(N_2H_3COO)_2$ M = metal
				Metal hydrazine carboxylates hydrates	$M(N_2H_3COO)_2.yH_2O$ M = metal, y = 2–3
	Neutral radical	Hydrazyl	$N_2H_3^\bullet$	Organic hydrazides	$R(N_2H_3)_2$, R = acyl
Ligand	Monodentate	Hydrazinium	$N_2H_5^+$	Hydrazinium metal complexes	N_2H_5MA M = metal, A = anion (inorganic/organic)
	Monodentate	Hydrazine	N_2H_4	Metal hydrazine complexes	$M(A)(N_2H_4)_2$ A = anion (inorganic/organic)
	Bidentate or bridged	Hydrazine	N_2H_4	Metal hydrazine complexes	$M(A)(N_2H_4)_2$ A = anion (inorganic/organic)

[a] Inorganic hydrazides are stable in solution only.

that can be generated by any one of these species. Hydrazine based compounds have been of great interest and investigated for last one century.

Inorganic hydrazides containing $N_2H_3^-$ species are extremely sensitive. The hydrogen of N_2H_4 in these compounds is replaced by a light metal causing them to explode during attempts at their preparation. As the $N_2H_3^-$ and $N_2H_2^{2-}$ anions have low stability, they are less common and little work on their inorganic salts has been reported. The hydrazyl species, which exists as a radical, forms only organic or organometallic hydrazide derivatives. They are very well known and reported in the literature but do not fall within the scope of this book.

Hydrazine has a high boiling point of 113.5 °C/760 mmHg and a Trouton's constant of 1.83–1.85 D. These values indicate that it is extensively associated through hydrogen bonding in the condensed phase. Consequently, it is miscible with water and forms hydrazine hydrate, $N_2H_4{\cdot}H_2O$. This composition is constant at all proportions of water being added and does not change even on distilling. However, in the gas phase hydrazine is monomeric (N_2H_4) [3].

1.1.2 Hydrazine versus Hydrazine Hydrate

In its anhydrous state, hydrazine is known to be highly explosive, carcinogenic, toxic, and hazardous to handle. However, it has been demonstrated that all chemical reactions of hydrazine can be carried out using hydrazine hydrate ($N_2H_4{\cdot}H_2O$, 64% N_2H_4), which is easy to handle and available commercially. Hydrazine hydrate is much more stable than anhydrous hydrazine [ΔH_f (liq) $-242.9\,kJ\,mol^{-1}$] and can be stored in paraffin-coated sealed vessels for several years without decomposition. Although hydrazine hydrate resembles anhydrous hydrazine in many of its physicochemical properties, some minor differences are observed in physical properties between the two (Table 1.2). This occurs due to the association of hydrazine with water in the hydrated form.

The low melting point of hydrazine hydrate seen in Table 1.2 is consistent with a solid crystal structure that is somewhat different from that of anhydrous hydrazine (Figure 1.2) [4,5]. The low melting point of the hydrate indicates that its crystal is held together by relatively weak chemical forces like hydrogen bonds. Infrared, Raman, microwave, Nuclear Magnetic Resonance (NMR), photoelectron spectra, and X-ray diffraction have been used to elucidate the structure of the crystal and bonding in these molecules. Both hydrazine and hydrazine hydrate

Table 1.2 Comparison of properties of hydrazine and hydrazine hydrate.

Property	Hydrazine (100% N_2H_4)	Hydrazine hydrate (64% N_2H_4)
Melting point (°C)	2.0	−51.5
Boiling point (°C)	113.5	120.1 (azeotrope)
Flash point (°C)	38 °C (open cup)	75 °C (open cup)
Density (g ml^{-1})	1.004	1.032
Surface tension (dyne cm^{-1})	66.7 (25 °C)	74.2 (25 °C)
Vapor pressure (Pa)	1.92×10^3 (1.92 kPa)	1.2×10^3 (1.2 kPa)
Heat of formation (ΔH_f) (kJ mol^{-1})	+55.63	−242.9

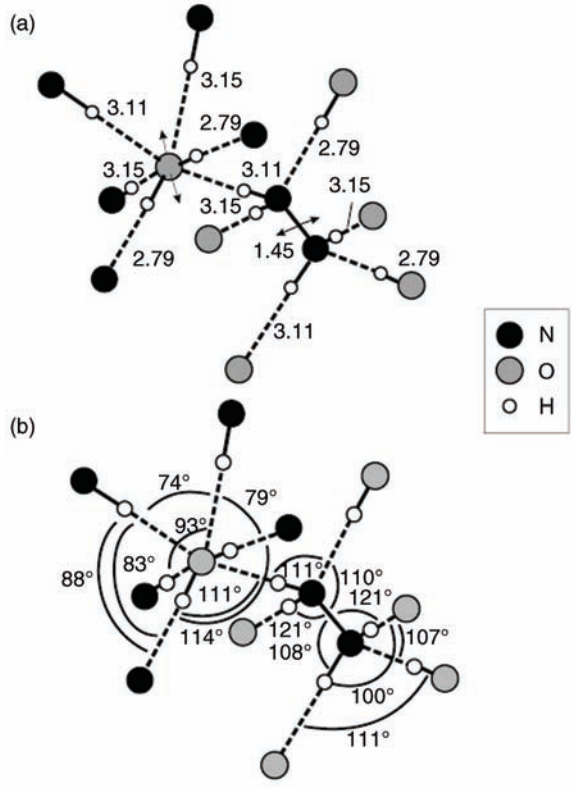

Figure 1.2 Structure of hydrazine hydrate: (a) bond distances (Å) between neighbors of a water molecule and a hydrazine molecule and (b) angles between them. Adapted from [4] with permission from the International Union of Crystallography © 1964.

Table 1.3 Characteristics of hydrazine/hydrazine hydrate.

Property	Effects
Electron donor (readily oxidizable)	Powerful reducing agent
Polar compound (B.P. 113.5 °C, 1.83D)	Surface active and hydrogen-bonding agent
Polyfunctional nature	Organic derivatives
Basic character	Hydrazinium salts, oxygen scavenger, CO_2 converter
As a ligand	Hydrazine and hydrazinium metal complexes
Endothermic compound ($\Delta H_f = 55.34\,kJ\,mol^{-1}$)	Energetic compounds
High toxicity	Therapeutic and protecting agent
High chemical reactivity	Powerful reagent

present conformations in which one NH_2 group is rotated from the transposition. The vacant tetrahedral positions are occupied by lone electron pairs that impart the basic and nucleophilic character to these molecules. The nearly similar physicochemical properties of hydrazine and hydrazine hydrate reflect the equivalence of both forms of hydrazine. Hydrazine hydrate is also considered to be a strong base.

Hydrazine can generate various reactive species (Table 1.1) and it has been known to react with almost every element and their compounds, to produce myriads of hydrazine-derived inorganic and organic substances [6]. Table 1.3 summarizes some important characteristics of hydrazine/hydrazine hydrate that bring about its multifaceted effects, depending on the environment present.

1.1.2.1 Reducing Property of Hydrazine Hydrate

Hydrazine hydrate, being a powerful reductant, is widely used in various chemical operations such as electroless plating and production of metallic nanoparticles [7,8]. It is effectively employed in the reduction of various metal cations (M^{2+}) to their elemental state (M^0) according to the following reaction:

$$2M^{2+} + N_2H_4 + 4OH^- \rightarrow 2M^0 + N_2 + 4H_2O \qquad (1.11)$$

Hydrazine hydrate is used to remove and recover Ni^{2+}, Cu^{2+}, Co^{2+}, and Fe^{2+} from effluents by reduction crystallization. This greatly assists in controlling pollution and eliminating hazardous metals from the

environment [9]. The application of hydrazine hydrate in the recovery of precious metals from wastewater is becoming very popular [10].

Some striking results are obtained on using hydrazine hydrate as a reducing agent, where it lends itself to the production of nanostructures. With hydrazine hydrate these structures form into various geometries, such as nanoparticles, nanowires, nanorods, quantum dots, and so on, under the conditions of hydrothermal/solvothermal, microwave, sonochemical, and micellar methods [11–14]. It is possible to control the morphology of the nanoparticles with a combination of hydrazine hydrate, with or without suitable surfactants.

Of these, the synthesis of one-dimensional nanostructures (Figure 1.3) is very attractive because of their size-dependant electronic and optical properties [15]. It is reported that hydrazine hydrate acts both as a reducing agent and as an *in situ* "soft" template (Figure 1.4) that forms different conformations favoring the formation of one-dimensional nanostructures [16].

Semiconducting chalcogenide nanostructures have received a great deal of attention for application in optoelectronic devices, such as blue laser diodes, light-emitting diodes, solar cells, IR optical windows, optical limiting, and so on [12–17]. To synthesize them as a pure phase is a

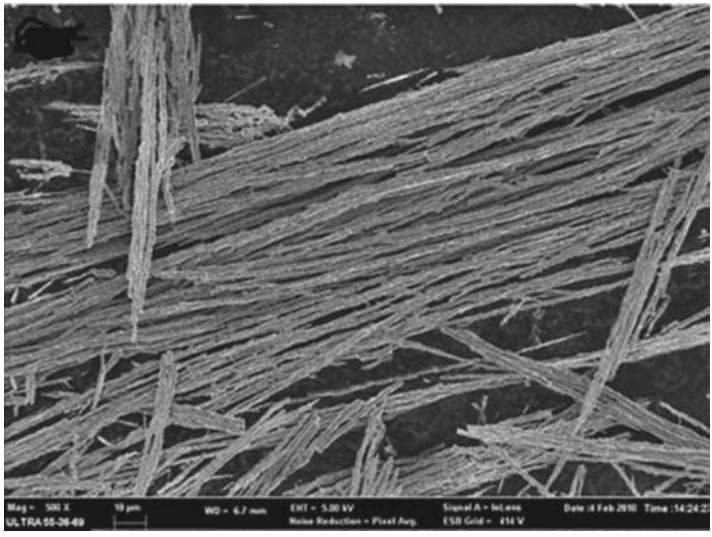

Figure 1.3 SEM image of a 1D cobalt nanostructure. Reproduced from Zhang, Tianmin Lan, Yafei Zhang *et al.*, Template-free Liying Synthesis of One-dimensional Cobalt Nanostructures by Hydrazine Reduction Route, *Nanoscale Res Lett* 2011, **6**:58.

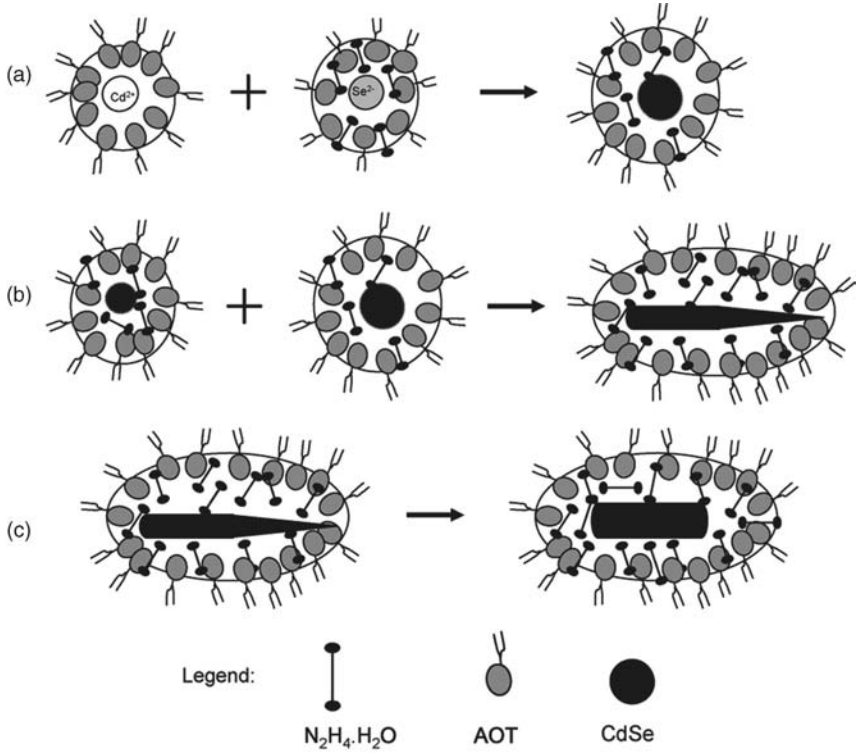

Figure 1.4 Scheme showing how hydrazine hydrate acts as a templating agent favoring the formation of 1D structures. Reproduced from Ref [16] with permission from Elsevier © 2007.

challenge as they form oxides when normal reducing agents are used. The use of hydrazine hydrate, however, overcomes this problem by allowing the formation of pure phases without much difficulty.

1.2 INORGANIC HYDRAZINE DERIVATIVES

1.2.1 Hydrazine Salts

In the presence of acids, hydrazine forms both mono-protonated ions (hydrazinium (1+), $N_2H_5^+$) and diprotonated ions (hydrazonium (2+), $N_2H_6^{2+}$). Both these cations easily form basic salts of the types $N_2H_5^+ \cdot A^-$ and $N_2H_6^{2+} \cdot 2A^-$ [18]. The former type of salts is formed invariably by all acids whereas the latter salts are known to mostly occur

with mineral acids. The $N_2H_5^+$ salts are the more common types of inorganic salts. With monobasic acids of the type HA, compounds as N_2H_5A and $N_2H_6A_2$ are formed. Compounds as $(N_2H_5)_2B$, $N_2H_5{\cdot}HB$, and N_2H_6B are formed with a dibasic acid of type H_2B. The best known salts of these types are N_2H_5A, $(N_2H_5)_2B$, $N_2H_6A_2$, and N_2H_6B.

The synthesis, structure, and physical and chemical properties of various hydrazinium salts have been documented [6]. Several processes have been developed for the synthesis of these salts but, typically, the method of preparation varies with the type of salt made. Furthermore, acids like H_2SO_4 and HF form $N_2H_6^{2+}$ salts exclusively when they react with $N_2H_4{\cdot}H_2O$ because of their low solubility.

1.2.1.1 Synthesis

Early on in the study of hydrazine chemistry, several unusual methods were used to prepare the simple salts of hydrazine. With the availability of aqueous hydrazine, such salts are easily prepared by simple neutralization with the corresponding acid. Some of the other popular methods like double decomposition and the use of barium and ammonium salts are mentioned below:

1. Neutralization of hydrazine hydrate with the corresponding acids yields simple hydrazinium salts. However, the pH of the solution is very important in the preparation of the required salt for this acid–base neutralization:

$$N_2H_4{\cdot}H_2O + HA \rightarrow N_2H_5A + H_2O \ (A = \text{anion}) \tag{1.12}$$

$$N_2H_4{\cdot}H_2O + 2HA \rightarrow N_2H_6A_2 + H_2O \ (A = \text{anion}) \tag{1.13}$$

2. Double decomposition of hydrazine sulfate [$N_2H_6SO_4$ or $(N_2H_5)_2SO_4$] with the corresponding barium salts:

$$(N_2H_5)_2SO_4 + Ba(NO_3)_2 \rightarrow BaSO_4 + 2N_2H_5NO_3 \tag{1.14}$$

3. Reaction of $N_2H_6^{2+}$ salts with anhydrous hydrazine:

$$N_2H_6F_2 + N_2H_4 \rightarrow 2N_2H_5F \tag{1.15}$$

4. Metathetical reaction of ammonium salts with anhydrous hydrazine, where the exchange of anion with hydrazine or its other

salts is observed:

$$NH_4A + N_2H_4 \leftrightarrow N_2H_5A + NH_3 \ (A = \text{anion}) \qquad (1.16)$$

Hydrazinium salts are generally a group of well-crystallized colorless compounds compared to the corresponding ammonium salts. The main difference between ammonium and hydrazinium salts lie in the low reducing property of the ammonium salts and lower thermal stability of hydrazinium salts. Hydrazine salts resemble the corresponding ammonium salts and hence they are quite soluble in water but relatively insoluble in nonpolar organic solvents.

Mono-acid salts (N_2H_5A) are more soluble in water than diacid salts ($N_2H_6A_2$). The diacid salts exist only in solid state and undergo immediate hydrolysis when dissolved in water. Furthermore, $N_2H_5^+$ salts are highly hygroscopic, while $N_2H_6^{2+}$ salts are not so, with the exception of $N_2H_6(ClO_4)_2 \cdot 2H_2O$ (which is highly hygroscopic). Unlike hydrazine, the hydrazinium ion present in acidic conditions is not susceptible to autoxidation. Acidified hydrazinium salt solutions can be stored for many months without change in composition.

1.2.1.2 Structure – Single-Crystal X-Ray Studies

The structures of many simple hydrazinium salts have been determined using single-crystal X-ray crystallography. Neutron diffraction studies have shown that, besides normal hydrogen bonds, bifurcated and probably trifurcated bonds are also common in some of the hydrazinium salts. Table 1.4 lists some of the compounds along with their crystal data and N-N bond distances [6,19].

N–N Bond Lengths in $N_2H_4/N_2H_5^+/N_2H_6^{2+}$

The N–N bond distances in $N_2H_4/N_2H_5^+/N_2H_6^{2+}$ compounds evaluated from single-crystal X-ray data fall in the range 1.40–1.48 Å (Table 1.4). The N–N bond lengths, in general, show a decrease on going from N_2H_4 through $N_2H_5^+$ to $N_2H_6^{2+}$. The decrease in bond length in $N_2H_5^+$ as compared to N_2H_4 is attributed to the diminution of the electron cloud repulsion on nitrogen atoms. Though positive charge repulsion is expected in $N_2H_6^{2+}$ the N–N bond length is shorter than in $N_2H_5^+$ and N_2H_4. This has been explained by the resonance forms occurring in

Table 1.4 Crystal data and N–N bond distance in hydrazine salts.

Compound	Crystal data (a, b, and c are in Å and α, β, and γ are in °)	N–N bond length (Å)
N_2H_5F	$P2_12_12_1$ orthorhombic, $Z = 16$ [$a = 4.592(5)$, $b = 8.217(2)$, $c = 12.341(3)$]	1.463
N_2H_5Cl	Fdd2 orthorhombic, $Z = 16$ ($a = 12.49$, $b = 21.85$, $c = 4.41$)	1.45
N_2H_5Br	C2/c monoclinic, $Z = 8$ ($a = 2.85$, $b = 4.54$, $c = 11.94$; $\beta = 110.15$)	1.45
$N_2H_5N_3$	$P2_1$/b monoclinic, $Z = 4$ [$a = 5.663(2)$, $b = 12.436(3)$, $c = 5.506(2)$; $\beta = 114.0$]	1.45
$N_2H_5BF_4$	C2/c monoclinic, $Z = 8$ [$a = 14.006(8)$, $b = 5.316(4)$, $c = 12.387(3)$; $\beta = 112.87$]	1.425
$N_2H_5ClO_4$	C2/c monoclinic, $Z = 8$ [$a = 14.412(7)$, $b = 5.389(5)$, $c = 12.797(3)$; $\beta = 113.09$]	1.461
$N_2H_5ClO_4 \cdot 0.5H_2O$	C2/c monoclinic, $Z = 8$ [$a = 8.657(3)$, $b = 7.484(3)$, $c = 15.285(5)$; $\beta = 99.36$]	1.474
$N_2H_5COOCH_3$	Cc monoclinic, $Z = 4$ ($a = 7.791$, $b = 8.386$, $c = 7.073$; $\beta = 104.0$)	1.462
$N_2H_5HC_2O_4$	$P2_1$/m monoclinic, $Z = 2$ [$a = 3.583(3)$, $b = 13.318(2)$, $c = 5.103(2)$; $\beta = 102.72$]	1.443
$N_2H_5H_2PO_4$	$P2_12_12_1$ orthorhombic, $Z = 4$ ($a = 5.673$, $b = 7.819$, $c = 10.634$)	1.438
$(N_2H_5)_2SO_4$	$P2_1$/c monoclinic, $Z = 4$ [$a = 5.157(2)$, $b = 11.064(2)$, $c = 10.971(7)$; $\beta = 100.04$]	1.440; 1.427
$N_2H_5N_2H_3CSS$	$P2_1$/c monoclinic, $Z = 4$ [$a = 7.108(6)$, $b = 6.823(3)$, $c = 11.993(7)$; $\beta = 90.65$]	1.436
$N_2H_6F_2$	R3m hexagonal, $Z = 3$ [$a = 4.43(1)$, $c = 14.37(2)$]	1.42
$N_2H_6Cl_2$	Pa3 cubic, $Z = 4$ ($a = 7.89$)	1.42
$N_2H_6SO_4$	$P2_12_12_1$ orthorhombic, $Z = 4$ [$a = 8.232(5)$, $b = 9.145(5)$, $c = 5.535(2)$]	1.416
$N_2H_6(H_2PO_4)_2$	$P2_1$/c monoclinic, $Z = 2$ [$a = 4.483(4)$, $b = 8.039(1)$, $c = 10.701(1)$; $\beta = 99.68$]	1.432

the cation $N_2H_6^{2+}$, which bring positive charges on H and N atoms as well, causing contraction from 1.47 to 1.42 Å.

Conformation of $N_2H_5^+$/$N_2H_6^{2+}$ Ions

The $N_2H_5^+$ group conformations have been reported in neutron diffraction studies of $N_2H_5HC_2O_4$, $N_2H_5H_2PO_4$, and $N_2H_5LiSO_4$. The $N_2H_5^+$ group has a perfectly staggered conformation (projection down N–N bond) in the first case and approximately staggered conformation in the latter two cases (Figure 1.5). An approximate staggered form has also

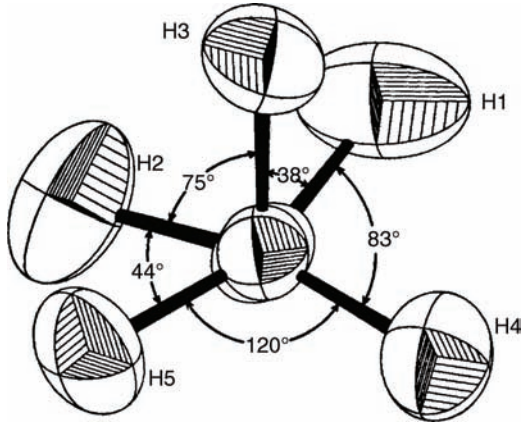

Figure 1.5 Conformation of $N_2H_5^+$ ion. Reproduced with permission from Acta Chem Scand/Royal Society of Chemistry © 1971.

been reported for one of the $N_2H_5^+$ ions in $(N_2H_5)_2SO_4$ while the other independent ion is approximately eclipsed [20]. The staggered form for the $N_2H_5^+$ ion is probably the most stable conformation. However, the $N_2H_5^+$ ion conformation is comparable with methyl amine, for which the staggered configuration is the most stable one, with a barrier to internal rotation of the order of 3 kcal mol^{-1}. Neutron diffraction studies have also shown that the $N_2H_6^{2+}$ ion has a staggered conformation in both $N_2H_6(H_2PO_4)_2$ and $N_2H_6SO_4$.

1.2.2 Metal Hydrazines

The coordination chemistry of hydrazine is of interest because of its ability to serve as an electron-pair donor. The presence of two free-electron pairs, as in other polybasic ligands, offers the possibility of several different types of coordination toward transition metal ions. The two free-electron pairs allow it to function as a monodentate, bidentate, or bridging ligand, which make hydrazine a preferred ligand. Hydrazine may act both as a ligand or a redox reagent in reactions with transition metals to form complexes. In a comprehensive review by Bottomley, the reaction between hydrazine and transition metals has been investigated in detail and summarized [21].

Transition metal complexes containing monodentate and bridging hydrazines are well known. The complexes of transition metal salts of divalent metals like Co^{2+} and Ni^{2+} with anions such as Cl^-, NO_2^-, NO_3^-, SO_4^{2-}, ClO_3^-, and ClO_4^-, with 1, 2, or 3 coordinated molecules

of hydrazine, were reported as early as 1951. The next four decades witnessed a tremendous amount of work on the preparation, characterization, structure and thermal reactivity of hydrazine complexes with varied metals and anions [22,23]. The list includes hydrazine complexes of metal ions such as Ag, Ca, Cd, Ce, Co, Cr, Cu, Dy, Er, Fe, Hg, Ho, Ir, La, Lu, Mn, Mo, Nd, Ni, Pd, Pr, Pt, Re, Sc, and Sm and with anions such as carbonate, halide, nitrate, oxalate, and phosphate.

1.2.2.1 Synthesis

Various methods that have been used for the preparation of metal hydrazine complexes are listed below:

1. The compounds $MA_2(N_2H_4)_n$, where M^{2+} = Mn, Fe, Co, Ni, Zn, and Cd and $A = Cl^-$, Br^-, I^-, NCS^-, CH_3COO^-, N_3^-, ClO_4^-, are prepared by mixing hydrazine hydrate and salts of respective metals in aqueous or alcoholic solution:

$$n N_2H_4 \cdot H_2O + MA_2 \rightarrow MA_2(N_2H_4)_n \qquad (1.17)$$

   where M = divalent metals like Mg, Mn, Fe, Co, and so on.

   The corresponding fluorides $MF_2(N_2H_4)_2$, where M^{2+} = Zn and Fe, are prepared by treating MF_2 with anhydrous hydrazine.
2. The compounds $M(NO_3)_2(N_2H_4)_3$, where M^{2+} = Mn, Fe, Co, Ni, Zn, and Cd, are prepared by mixing hydrazine hydrate and metal nitrate salts in aqueous/alcoholic solution.
3. The compounds $MSO_4(N_2H_4)_2$, where M^{2+} = Fe, Co, Ni, and Cd, are prepared either by mixing hydrazine hydrate with aqueous solutions of metal sulfates or by dissolving the corresponding metal powders in a solution of ammonium sulfate in hydrazine hydrate.
4. The preparation of metal oxalate hydrazines $MC_2O_4 \cdot 2N_2H_4$, where M = Mn, Fe, Co, Ni, Cu, Zn, and Cd, has been reported [6]. The nickel oxalate–hydrazine–water system is shown to form as many as five compounds of the formulae $NiC_2O_4(N_2H_4)_4(1.5–2.5)H_2O$, $NiC_2O_4 \cdot N_2H_4 \cdot 2H_2O$, $NiC_2O_4(N_2H_4)_3 0.75H_2O$, $NiC_2O_4(N_2H_4)_2$-$0.5H_2O$, and $NiC_2O_4 \cdot 3.65N_2H_4 \cdot H_2O$. It appears that these complexes contain saturated hydrazine rather than coordinated hydrazine:

$$MC_2O_4 \cdot 2H_2O + 2N_2H_4 \cdot H_2O \text{ (alcoholic)} \rightarrow MC_2O_4(N_2H_4)_2 + 4H_2O \qquad (1.18)$$

   where M = Mn, Fe, Co, Ni, Zn, and Cd.

5. Metal hydrazine carboxylates $[M(N_2H_3COO)_2{\cdot}(N_2H_4)_2]$ are prepared from aqueous solutions of metals salts with hydrazine carboxylic acid in hydrazine hydrate:

$$M^{2+} + 2N_2H_3COO^- + 2N_2H_4{\cdot}H_2O \rightarrow M(N_2H_3COO)_2(N_2H_4)_2 + 2H_2O \quad (1.19)$$

where M = Fe, Co, Ni, and Zn.

The redox property of hydrazine stabilizes the lowest oxidation state of the metal in all its metal hydrazine complexes. It is not possible to prepare platinum or palladium hydrazines as they are reduced to metals [24].

1.2.2.2 Structure – Single-Crystal X-Ray Studies

Many stable complexes of metal salts with one, two, or more hydrazine molecules are known. However, crystal structural data of only a few have been investigated, probably because of the inherent difficulty in growing single crystals of these complexes. The crystal structure data on complexes of the type $[MA_2(N_2H_4)_2]$, where M = Mn, Co, Ni, Zn, or Cd and $X = Cl^-$, SCN^-, and CH_3COO^-, have been determined. As mentioned earlier, hydrazine coordinates to the metal as a bridged bidentate ligand (Figure 1.6).

These complexes have infinite chain structures with *cis*-bridging hydrazine molecules and respective anions in the *trans* positions. Complexes with corresponding anions are reported to be isomorphous (Table 1.5).

In the compound $[CuCN{\cdot}N_2H_4]_n$ both hydrazine and cyanide are involved in the bridging with copper(I) in a tetrahedral coordination (Figure 1.7).

In all these complexes the N–N bond length is found to range between 1.45 and 1.48 Å, which is the same as in hydrazine or complexes containing monodentate hydrazine. Hydrazine is also present as a monodentate ligand in metal hydrazine carboxylate hydrazine complexes [25].

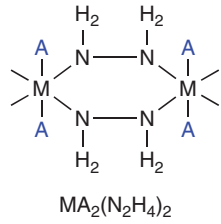

Figure 1.6 Structure of bridged bidentate hydrazine.

Table 1.5 Crystal data and N–N bond distances in metal hydrazine complexes.

Compound	Crystal data (a, b, and c are in Å and α, β, and γ are in °)	N–N bond length (Å)
Bridged bidentate N_2H_4		
$Mn(N_2H_4)_2Cl_2$	$C2_{/m}$ monoclinic, $Z = 2$ [$a = 9.08(1)$, $b = 8.01(1)$, $c = 4.29(1)$; $\beta = 105.5$]	1.459
$Zn(N_2H_4)_2Cl_2$	$C2_{/m}$ monoclinic, $Z = 2$ [$a = 8.99(1)$, $b = 7.92(1)$, $c = 4.13(1)$; $\beta = 105.5$]	1.46
$Zn(N_2H_4)_2(NCS)_2$	$P2_1/a$ monoclinic, $Z = 2$ [$a = 7.141(4)$, $b = 14.756(5)$, $c = 4.214(5)$; $\beta = 105.5$]	1.47
$Zn(N_2H_4)_2(CH_3COO)_2$	$P1^-$ triclinic, $Z = 1$ [$a = 6.58(2)$, $b = 8.52(1)$, $c = 4.14(1)$; $\alpha = 90.0$, $\beta = 90.42$, $\gamma = 96.87$]	1.458
Monodentate N_2H_4		
$[CuCN{\cdot}N_2H_4]_n$	Pbcn orthorhombic, $Z = 4$ ($a = 4.684$, $b = 9.172$, $c = 7.830$)	1.48
$Ba(N_2H_3COO)_2(N_2H_4)_2$	C2 monoclinic, $Z = 2$ [$a = 13.330(3)$, $b = 6.827(1)$, $c = 4.680(2)$; $\beta = 97.63$]	1.43; 1.41

This has been confirmed by the single-crystal structure of the barium compound (Figure 1.8).

1.2.3 Metal Hydrazine Carboxylates

Anhydrous hydrazine reacts to form a syrupy liquid on bubbling carbon dioxide into it. This further solidifies with excess carbon dioxide. The sparingly soluble precipitate so-formed is hydrazine carboxylic acid, also called as carbazic acid [6]:

$$N_2H_4(l) + CO_2(g) \rightarrow N_2H_3COOH\,(s) \tag{1.20}$$

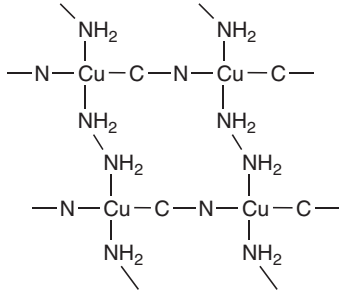

Figure 1.7 Structure of $[CuCN{\cdot}N_2H_4]_n$.

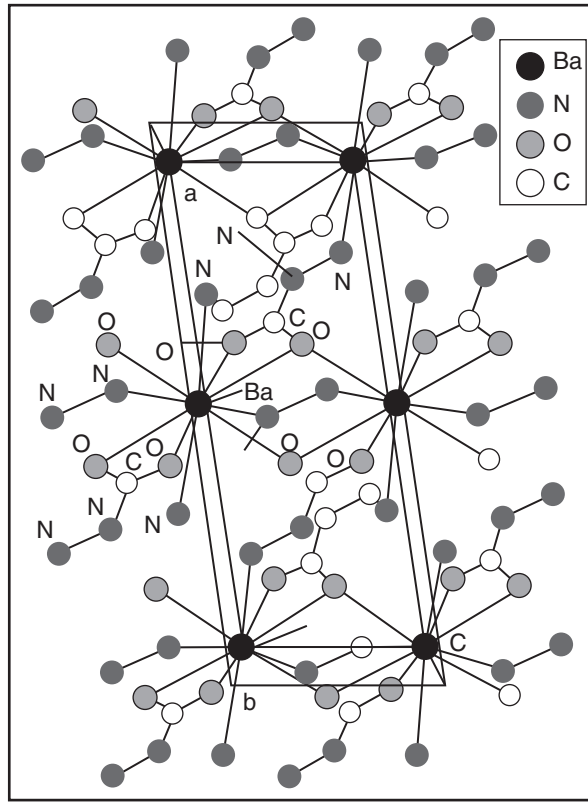

Figure 1.8 Molecular structure of $Ba(N_2H_3COO)_2(N_2H_4)_2$. Reproduced from Ref [25] with permission of The Royal Society of Chemistry © 1993.

This acid is formed by the insertion of carbon dioxide into a hydrazine molecule. It can be visualized as the attack of lone pair of electrons from the nitrogen of hydrazine to the positive carbon center of CO_2 (Figure 1.9).

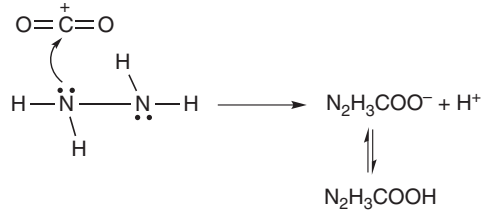

Figure 1.9 Probable mechanism for CO_2 insertion into N_2H_4.

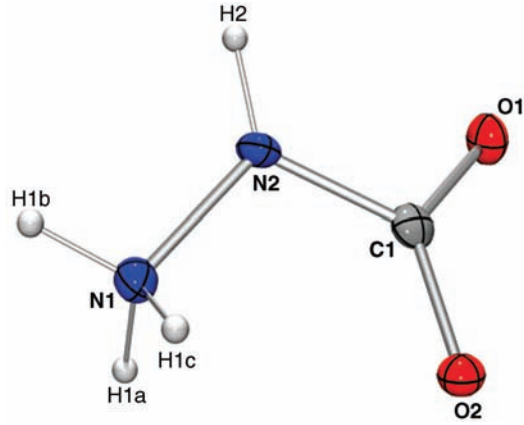

Figure 1.10 Crystal structure of the zwitterion $NH_3^+NHCOO^-$. Reproduced from Ref [26] with permission of The Royal Society of Chemistry © 2011.

Hydrazine carboxylic acid is a weak acid, dissociating into hydrazine carboxylate anion ($N_2H_3COO^-$) and H^+:

$$N_2H_3COOH \rightleftarrows N_2H_3COO^- + H^+ \tag{1.21}$$

Recently, it has been reported that the reaction of hydrazine hydrate with supercritical carbon dioxide forms a stable solid that is a 1 : 1 adduct of hydrazine and CO_2 [26]. Its single-crystal structure (Figure 1.10) shows it to be as a zwitterion ($NH_3^+NHCOO^-$). Its reactivity is similar to that of liquid hydrazine as it produces anhydrous hydrazine locally via the decarboxylation process. Owing to its zwitterionic form, carbazic acid exhibits better selectivity. It also shows excellent reactivity toward carbonyl compounds in the solid state and has been found to be a valuable alternative to liquid hydrazine [27].

When hydrazine carboxylic acid is dissolved in anhydrous hydrazine it probably exists in the form of a hydrazinium carboxylate salt that dissociates into hydrazine carboxylate anion and hydrazinium cation. It is a bidentate ligand and forms coordination compounds with metal ions:

$$N_2H_4(l) + N_2H_3COOH(s) \rightarrow N_2H_5COON_2H_3(l) \tag{1.22}$$

$$N_2H_5COON_2H_3 \rightleftarrows N_2H_3COO^- + N_2H_5^+ \tag{1.23}$$

This hydrazine carboxylate anion is of interest to an inorganic chemist due to its chelating properties. The hydrazine carboxylate anion

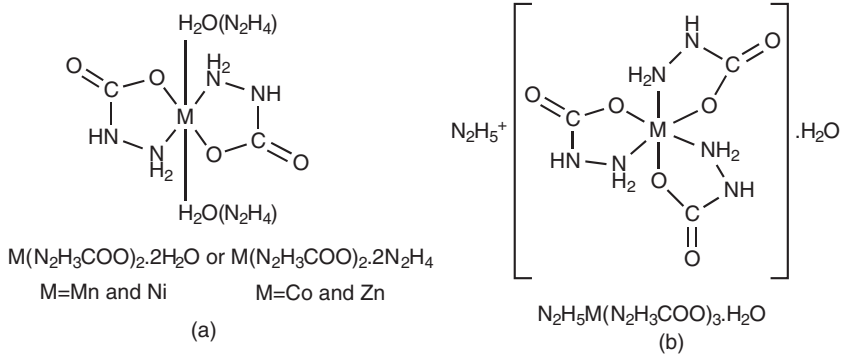

Figure 1.11 Coordination of $N_2H_3COO^-$ bidentate ligand.

$N_2H_3COO^-$ acts a bidentate ligand bonding through N and O atoms. It forms a five-membered ring with bivalent metal ions (Figure 1.11a and b) to afford complexes like $M(N_2H_3COO)_2$, $M(N_2H_3COO)_2{\cdot}nH_2O$, $M(N_2H_3COO)_2(N_2H_4)_2$, or $N_2H_5M(N_2H_3COO)_3{\cdot}H_2O$, where M = Ca, Mg, Mn, Fe, Co, Ni, Cu, Zn, and Cd, as well as rare earth metal complexes of the type $Ln(N_2H_3COO)_3{\cdot}3H_2O$.

1.2.3.1 Synthesis

Metal hydrazine carboxylate complexes can be prepared by the reaction of the respective metal ions with hydrazine hydrate, kept open to atmosphere or saturated with CO_2 gas. Carbon dioxide is absorbed by hydrazine, forming the hydrazine carboxylate anion, which coordinates with the metal ions to give crystalline compounds. Chemical equations for the formation of various complexes are:

$$M^{2+}(aq) + 2N_2H_3COO^-(aq) \rightarrow M(N_2H_3COO)_2(s) \tag{1.24}$$

where M = Mn, Co, Ni, Cu, and Zn.

$$M^{2+}(aq) + 2N_2H_3COO^-(aq) + xH_2O(l) \rightarrow M(N_2H_3COO)_2{\cdot}xH_2O \tag{1.25}$$

where M = Mg, Ca, Cr, Mn, Cu, TiO, and ZrO.

$$LnA_3(aq) + 3N_2H_5COON_2H_3 + 3H_2O \rightarrow Ln(N_2H_3COO)_3{\cdot}3H_2O + 3N_2H_5A \tag{1.26}$$

where Ln = rare earth ion, A = anion.

$$M^{2+} + 2N_2H_3COO^- + 2N_2H_4{\cdot}H_2O \rightarrow M(N_2H_3COO)_2(N_2H_4)_2 + 2H_2O \quad (1.27)$$

where M = Fe, Co, Ni, and Zn.

$$MA_2 + 3N_2H_5COON_2H_3 + H_2O \rightarrow N_2H_5M(N_2H_3COO)_3{\cdot}H_2O + 2N_2H_5A \quad (1.28)$$

where M = Mg, Fe, Co, Ni, and Zn, and A = anion.

It appears that transition metal ions seem to catalyze these reactions, and might be useful in CO_2 conversion.

1.2.3.2 Structure – Single-Crystal X-Ray Studies

Complexes of the type $M(N_2H_3COO)_2(N_2H_4)_2$, where M = Mn, Co, Ni, or Zn, are reported to contain monodentate hydrazine while the hydrazidocarboxylate anions act as bidentate ligands. As both these ligands are coordinated in the *trans* position the coordination around the metal is octahedral. The hydrazinium metal hydrazidocarboxylate hydrate complexes ($N_2H_5M(N_2H_3COO)_3{\cdot}H_2O$) consist of $N_2H_5^+$ cation, complex anions, and water molecules. In these complexes the metal anion is octahedrally coordinated by three bidentate ligands for Ni(II) or four bidentate ligands for Sc(III). The coordination polyhedron is a distorted quadratic antiprism. The $N_2H_5^+$ cation and the water molecules are linked by weak hydrogen bonds to each other and also to some oxygen and nitrogen atoms of the ligands. In all these compounds, since the coordination sphere of the metal is completed by the $N_2H_3COO^-$ groups, the $N_2H_5^+$ ions are not coordinated, and hence exist only as free cations [28]. Table 1.6 gives the crystal structure data of some of the metal hydrazine carboxylates.

1.2.4 Hydrazinium Metal Complexes

Free hydrazine (N_2H_4), hydrazine hydrate, and monoprotonated hydrazine ($N_2H_5^+$) are all good ligands for coordination with transition metals. The monoprotonated hydrazine ($N_2H_5^+$) has a lone pair of electrons and can coordinate to metal ions despite its low basicity. This is due to the presence of a positive charge adjacent to the donor atom that makes it a

Table 1.6 Crystal structure data of metal hydrazine carboxylates.

Compound	Crystal data (a, b, and c are in Å and α, β, and γ are in °)	N–N bond length (Å)
Anhydrous		
$Cd(N_2H_3COO)_2$	$P2_12_12_1$-D_2^3 orthorhombic, $Z = 4$ ($a = 5.372$, $b = 9.116$, $c = 6.444$)	1.39
$Ca(N_2H_3COO)_2$	$P2_{1/c}$ monoclinic, $Z = 4$ [$a = 9.590(15)$, $b = 9.426(10)$, $c = 9.20(1)$; $\beta = 127.8$]	1.416
$Zn(N_2H_3COO)_2$	p_c monoclinic, $Z = 4$ [$a = 6.87(1)$, $b = 5.08(1)$, $c = 9.10(1)$; $\beta = 111.2(1)$]	1.39
Hydrates		
$Ca(N_2H_3COO)_2{\cdot}H_2O$	P1 triclinic, $Z = 2$ [$a = 7.67(1)$, $b = 7.86(1)$, $c = 6.37(1)$; $\alpha = 84.02$, $\beta = 72.88$, $\gamma = 78.65$]	1.43
$Cd(N_2H_3COO)_2{\cdot}H_2O$	Pbcn orthorhombic dipyramidal, $Z = 4$ [$a = 7.402(7)$, $b = 12.360(7)$, $c = 7.828(12)$]	1.41
$Ni(N_2H_3COO)_2{\cdot}2H_2O$	$C_{2/c}$ monoclinic, $Z = 4$ [$a = 11.78(1)$, $b = 12.360(7)$, $c = 7.828(12)$; $\beta = 111.55(10)$]	1.437
$Mn(N_2H_3COO)_2{\cdot}2H_2O$	Pba2 orthorhombic, $Z = 4$ ($a = 11.052$, $b = 9.862$, $c = 7.847$)	1.435
Hydrazines		
$Zn(N_2H_3COO)_2(N_2H_4)_2$	$P2_{1/c}$ monoclinic, $Z = 2$ [$a = 8.412(4)$, $b = 7.384(5)$, $c = 9.852(10)$; $\beta = 125.75$]	1.46; 1.39
$Co(N_2H_3COO)_2(N_2H_4)_2$	$P2_{1/c}$ monoclinic, $Z = 2$ [$a = 9.551(1)$, $b = 7.352(2)$, $c = 8.110(1)$; $\beta = 122.8$]	1.454; 1.425
Hydrazinium complexes		
$N_2H_5Ni(N_2H_3COO)_3{\cdot}H_2O$	Cc monoclinic, $Z = 4$ [$a = 12.129(20)$, $b = 10.858(5)$, $c = 10.225(6)$; $\beta = 121.06$]	1.435
$N_2H_5Sc(N_2H_3COO)_3{\cdot}H_2O$	$P2_{1/c}$ monoclinic, $Z = 4$ [$a = 15.360(3)$, $b = 7.584(1)$, $c = 23.686(3)$; $\beta = 142.14$]	1.439

potential monodentate ligand. The synthesis and structure of several hydrazinium metal complexes have been reported [29–31].

1.2.4.1 Synthesis

Generally, hydrazinium metal complexes are prepared by the variation of any one of the following methods:

1. From aqueous solutions of the corresponding metal salts and hydrazine salts ($N_2H_5^+$ or $N_2H_6^{2+}$). For example:

$$(N_2H_5)_2SO_4 + MSO_4 \rightarrow (N_2H_5)_2M(SO_4)_2 \qquad (1.29)$$

where M = divalent metals like Mg, Mn, Fe, Co, and so on.

2. From the corresponding metal nitrates and hydrazinium oxalate salts:

$$2(N_2H_5)_2C_2O_4 + M(NO_3)_2 \cdot nH_2O \rightarrow (N_2H_5)_2M(C_2O_4)_2 \cdot nH_2O + 2N_2H_5NO_3 \qquad (1.30)$$

where M = Co, Ni, and Cu.

3. From metal salts and hydrazine hydrate or $N_2H_3COON_2H_5$ (hydrazine hydrate saturated with carbon dioxide):

$$MA_2 + 4N_2H_4 \cdot H_2O \rightarrow 2N_2H_5MO \cdot H_2O + 2N_2H_5A \qquad (1.31)$$

where M = Cd and A = anion.

Using these methods numerous hydrazine complexes have been prepared and characterized [6]. Table 1.7 gives actual preparative methods employed for individual complexes.

In these reactions it is interesting to see that $N_2H_6^{2+}$ salts form $N_2H_5^+$ ions in solution to yield hydrazinium metal complexes.

1.2.4.2 Structure – Single-Crystal X-Ray Studies

The most adequately characterized hydrazinium complexes consisting of coordinated metal ions are $(N_2H_5)_2M(SO_4)_2$ (M = Mg, Mn, Fe, Co, Ni, Cu, Zn, Cd, and the halides) [31]. In addition, single crystals have been analyzed of Co and Ni double sulfates synthesized under hydrothermal conditions using metal sulfates, hydrazine hydrate, and HF [32]. Table 1.8 lists various hydrazinium compounds along with their crystal data and N–N bond distances.

The structures of hydrazinium metal sulfate complexes determined by single-crystal X-ray analysis show them to be a chain of metal ions linked by bridging bidentate sulfate groups with *trans* ligands, completing a distorted octahedron (Figure 1.12). The N–N bond length of 1.55 Å in the Zn complex is significantly longer than that found for uncoordinated

Table 1.7 Methods of preparation of hydrazinium metal complexes.

Compound	Preparation
$(N_2H_5)_2M(SO_4)_2$ (M = Mn, Fe, Co, Ni, Cu, Zn, and Cd)	Metal sulfate hydrates + hot aqueous solution of $N_2H_6SO_4$
$N_2H_5Ln(SO_4)_2{\cdot}H_2O$ (Ln = La, Ce, Pr, Nd, Sm)	Hot aqueous solution of $Ln_2(SO_4)_3{\cdot}nH_2O$ in 2N H_2SO_4 + $(N_2H_5)_2SO_4$ or $N_2H_6SO_4$
$N_2H_5Al(SO_4)_2{\cdot}12H_2O$	Aqueous solution of $(N_2H_5)_2SO_4 + Al_2(SO_4)_3{\cdot}16H_2O$
$N_2H_5LiSO_4$	Li_2CO_3 + aqueous solution of $N_2H_6SO_4$
$(N_2H_5)_2M(C_2O_4)_2{\cdot}nH_2O$ [M = Cu, Ni, Co (n = 1–3)]	$M(NO_3)_2{\cdot}xH_2O$ + aqueous solution of $(N_2H_5)_2C_2O_4$ (1 : 4 ratio)
$(N_2H_5)_3V(C_2O_4)_3{\cdot}N_2H_4$	$VCl_3{\cdot}6H_2O$ + excess hot aqueous solution of $(N_2H_5)_2C_2O_4$
$N_2H_5H(UO_2)_2(C_2O_4)_3{\cdot}4H_2O$	Aqueous solution of $N_2H_5Cl + UO_2C_2O_4 + (NH_4)_2C_2O_4$
$(N_2H_5)_2UO_2(C_2O_4)_2{\cdot}2H_2O$	Aqueous solution of $UO_2(NO_3)_2{\cdot}6H_2O + (N_2H_5)_2C_2O_4 + H_2C_2O_4{\cdot}2H_2O$ (1 : 1 : 1 ratio)
$(N_2H_5)_2UO_2(C_2O_4)_2{\cdot}H_2O$	Aqueous solution of $UO_2(NO_3)_2{\cdot}6H_2O + (N_2H_5)_2C_2O_4$ (1 : 2 ratio)
$(N_2H_5)_4UO_2(C_2O_4)_3{\cdot}H_2O$	Aqueous solution of $UO_2(NO_3)_2{\cdot}6H_2O + (N_2H_5)_2C_2O_4 + H_2C_2O_4{\cdot}2H_2O$ (1 : 1 : 2 ratio)
$(N_2H_5)_6(UO_2)_2(C_2O_4)_5{\cdot}2H_2O$	Aqueous solution of $UO_2(NO_3)_2{\cdot}6H_2O + (N_2H_5)_2C_2O_4$ (1 : 4 ratio)
$N_2H_5M(N_2H_3COO)_3{\cdot}H_2O$ (M = Fe, Co, Ni, and Zn)	Corresponding metal salts in excess $N_2H_4{\cdot}H_2O + CO_2$ or $N_2H_3COON_2H_5$
$N_2H_5Sc(N_2H_3COO)_4{\cdot}3H_2O$	Scandium salts in excess $N_2H_4{\cdot}H_2O + CO_2$
$N_2H_5LiBeF_4$	Li_2CO_3 + aqueous $N_2H_6BeF_4$
$N_2H_5CuF_3$	$Cu(N_2H_3COO)_2$ + 85% HF
$N_2H_5MF_3$ (M = Zn and Cd)	$M(NO_3)_2{\cdot}xH_2O + HF + N_2H_4{\cdot}H_2O$
$N_2H_5CoF_3$	CoF_2 + molten $N_2H_6F_2$
$(N_2H_5)_2CoOF_2{\cdot}H_2O$	Cobalt hydroxide + aqueous N_2H_5F
$(N_2H_5)_2CdOF_2$	CdF_2 + excess 80% $N_2H_4{\cdot}H_2O$

$(N_2H_5)_2MnF_4$	$Mn(N_2H_3COO)_2$ + aqueous HF
$(N_2H_5)_3MF_6$ (M = Cr and V)	Solutions of Cr/V salts in saturated aqueous $N_2H_5F + N_2H_4{\cdot}H_2O$ saturated with CO_2
$(N_2H_5)_2M(BeF_4)_2$ (M = Cu, Ni, and Zn)	MF_2 + aqueous $N_2H_6BeF_4$
$(N_2H_5)_2SnF_4$	Aqueous solution of $Sn(OH)_2 + N_2H_4{\cdot}H_2O$ + HF
$N_2H_5SbF_6{\cdot}H_2O$	Sb_2O_5 in aqueous solution of $HF + N_2H_4{\cdot}H_2O$
$(N_2H_5)_2UF_6$	$UF_6 + N_2H_5F$ in anhydrous N_2H_4
$N_2H_5UF_5$	Photolysis of aqueous solution of $UO_2F_2(N_2H_4{\cdot}2HF)$
$N_2H_5InF_4{\cdot}H_2O$	Aqueous solution of $InF_3 + N_2H_5F$
$(N_2H_5)_3CdCl_5$	Aqueous $Cd(NO_3)_2{\cdot}xH_2O + N_2H_5Cl$
$N_2H_5CuCl_3$	$CuCl_2{\cdot}2H_2O$ in 3N HCl + $N_2H_6Cl_2$
$(N_2H_5)_2CuCl_4{\cdot}2H_2O$	$CuCl_2{\cdot}2H_2O$ in 3N HCl + $N_2H_6Cl_2$ heating the resulting solution to 45 °C
$(N_2H_5)_2Cu_3Cl_6$	$CuCl_2{\cdot}2H_2O$ in 3N HCl + $N_2H_6Cl_2$ heating the resulting solution to 75 °C
$(N_2H_5)_2SnCl_6$	$SnCl_4$ in hot dilute HCl+ N_2H_5Cl
$N_2H_5SnBr_3$	$SnBr_2$ in aqueous warm solution of N_2H_5Br
$M[(N_2H_5)_2A_2]Y_2{\cdot}nH_2O$ [M = Pt, Pd; A = Cl, Br, NO_2; Y = Cl, Br, NO_3, $0.5SO_4$; (n = 0, 1)]	Aqueous solution of M(IV) salt + $N_2H_6^{2+}$ salt in cold condition

Table 1.8 Crystal data and N–N bond distances in hydrazinium metal complexes.

Compound	Crystal data (a, b, and c are in Å and α, β, and γ are in °)	N–N bond length (Å)
$N_2H_5LiSO_4$	$Pna2_1$ orthorhombic, $Z = 4$ [$a = 9.929(5)$, $b = 8.973(3)$, $c = 5.181(2)$]	1.427
$(N_2H_5)_2Zn(SO_4)_2$	P1 triclinic, $Z = 1$ [$a = 7.36(3)$, $b = 5.33(3)$, $c = 5.82(3)$; $\alpha = 99.70$, $\beta = 87.45$, $\gamma = 105.70$]	1.55
$N_2H_5Al(SO_4)_2{\cdot}12H_2O$	Pa3 cubic, $Z = 4$ [$a = 12.408(7)$]	—
$(N_2H_5)_2Cr(SO_4)_2$	P-1 triclinic, $Z = 1$ [$a = 7.266(3)$, $b = 5.457(5)$, $c = 5.709(6)$; $\alpha = 97.596(2)$, $\beta = 91.830(2)$, $\gamma = 103.493(2)$]	1.453
$(N_2H_5)_2Co(SO_4)_2$	P-1 triclinic, $Z = 1$ [$a = 5.266(11)$, $b = 5.828(12)$, $c = 7.3005(15)$; $\alpha = 90.57(3)$, $\beta = 105.73(3)$, $\gamma = 98.93(3)$]	1.432
$(N_2H_5)_2Ni(SO_4)_2$	P-1 triclinic, $Z = 1$ [$a = 5.2667(11)$, $b = 5.8284(12)$, $c = 7.3005(15)$; $\alpha = 90.57(3)$, $\beta = 105.73(3)$, $\gamma = 98.93(3)$]	1.441
$N_2H_5Cu(C_2O_4)_2{\cdot}H_2O$	$P2_1/n$ monoclinic, $Z = 2$ [$a = 3.592(1)$, $b = 7.855(2)$, $c = 19.143(3)$; $\beta = 94.3(3)$]	1.429
$N_2H_5LiBeF_4$	$Pna2_1$ orthorhombic, $Z = 4$ [$a = 9.811(4)$, $b = 8.880(8)$, $c = 5.139(4)$]	1.431
$(N_2H_5)_3CrF_6$	$P2_12_12_1$ orthorhombic, $Z = 4$ [$a = 9.223(7)$, $b = 9.223(7)$, $c = 10.536(5)$]	1.390; 1.466; 1.433
$N_2H_5InF_4{\cdot}H_2O$	$P2_12_12_1$ orthorhombic, $Z = 4$ [$a = 6.768(2)$, $b = 8.632(2)$, $c = 9.249(7)$]	1.436
$N_2H_5CuCl_3$	Pnma orthorhombic, $Z = 4$ [$a = 14.439(1)$, $b = 5.705(1)$, $c = 6.859(1)$]	1.457
$N_2H_5CdCl_5$	Cmca orthorhombic, $Z = 16$ [$a = 22.588(18)$, $b = 28.328(12)$, $c = 7.433(8)$]	—
$(N_2H_5)_2SnCl_6$	Pnca orthorhombic, $Z = 4$ [$a = 11.8(4)$, $b = 11.8(4)$, $c = 8.2(3)$]	1.4
$N_2H_6TiF_6$	Ia3 cubic, $Z = 8$ [$a = 10.404(2)$]	1.474
$N_2H_6ZrF_6$	C2/m monoclinic, $Z = 4$ [$a = 8.13$, $b = 12.16$, $c = 5.42(4)$; $\beta = 101.5(4)$]	1.41
$N_2H_6SiF_6$	Pbca orthorhombic, $Z = 4$ [$a = 7.603(2)$, $b = 7.594(3)$, $c = 8.543(4)$]	1.428
$N_2H_6GeF_6{\cdot}H_2O$	Pnma orthorhombic, $Z = 4$ [$a = 8.869(1)$, $b = 9.292(1)$, $c = 7.400(1)$]	1.428
$N_2H_6[TiF_6]F_2$	Pccn orthorhombic, $Z = 4$ [$a = 5.481(1)$, $b = 13.588(3)$, $c = 10.9347(2)$]	1.441
$N_2H_6NbOF_5{\cdot}H_2O$	Pnma orthorhombic, $Z = 4$ [$a = 9.47$, $b = 7.69$, $c = 9.06$]	—
$(N_2H_6)_2[NbOF_5]F_2$	$P2_1$ monoclinic, $Z = 4$ ($a = 14.62$, $b = 10.82$, $c = 5.56$; $\beta = 111.7$)	—

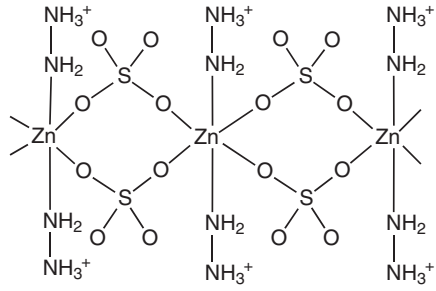

Figure 1.12 Chain structure of $(N_2H_5)_2Zn(SO_4)_2$.

$N_2H_5^+$; this may be due to the twinning of the crystals, which results in a less accurate structure.

In the halide group of hydrazinium metal complexes, the antiferromagnetic compound $N_2H_5CuCl_3$ has, interestingly, coordinated $N_2H_5^+$ (Figure 1.13). This complex is polymeric and the coordination polyhedron around each copper(II) is the tetragonally elongated $(4 + 2)$ octahedron. Its equatorial plane is formed by three chloride ions and the monodentate $N_2H_5^+$ ion. The apical positions are occupied by chloride ions from adjacent units.

The reactivity and bonding of these hydrazinium metal complexes is significantly important from the point of view of their applications.

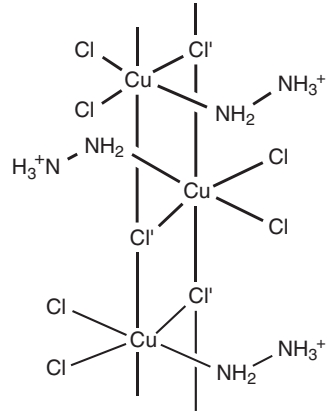

Figure 1.13 Polymeric structure of $N_2H_5CuCl_3$.

1.3 CHARACTERIZATION OF INORGANIC HYDRAZINE DERIVATIVES

Various thermoanalytical and spectroscopic techniques have been employed to characterize the inorganic derivatives of hydrazine. Some of the frequently used techniques for the identification of the composition and molecular structure of inorganic hydrazine solids are considered here.

1.3.1 Analytical Techniques

The redox property of hydrazine is used to estimate hydrazine in its corresponding salts and complexes by volumetric or potentiometric titrations [33]. The redox reactions using potassium iodate in presence of HCl can be represented by the following equations.

Hydrazinium salts:

$$5N_2H_5^+ + 4IO_3^- \rightarrow 5N_2 + 2I_2 + 11H_2O + H_3O^+ \quad (1.32)$$

Hydrazine complexes:

$$N_2H_4 + IO_3^- + 2H^+ + Cl^- \rightarrow ICl + N_2 + 3H_2O \quad (1.33)$$

$$N_2H_4 + 4ICl \rightarrow 2I_2 + N_2 + 4HCl \quad (1.34)$$

The metal content in the complexes is estimated by standard volumetric and gravimetric methods. Of late, the elemental composition of hydrazine species is evaluated with a CHNS/O micro-analyzer for nitrogen, hydrogen, carbon, oxygen, and sulfur content. Metal content is evaluated by inductively coupled plasma optical emission spectroscopy (ICP-OES).

1.3.2 Spectroscopic Methods

1.3.2.1 Infrared Spectroscopy

Infrared spectra of several hydrazine derivatives with N_2H_4, $N_2H_5^+$, and $N_2H_6^{2+}$ moieties have been carried out by simple IR as well as FTIR-Raman spectroscopy. The N–N stretching frequency is of relevance as this frequency is used as a fingerprint to distinguish the various types of hydrazine derivatives and their mode of bonding to metal ions (Table 1.9).

Table 1.9 Assignment of IR absorption frequencies of N_2H_4, $N_2H_5^+$, and $N_2H_6^{2+}$.

Assignments	N_2H_4 (ν cm^{-1})	$N_2H_5^+$ (ν cm^{-1})	$N_2H_6^{2+}$ (ν cm^{-1})
Weakly H bonded	3310	—	—
N–H stretching	3200	3250	—
(N–H···O) group	—	3144	—
Strongly H bonded	—	3050	3070
N–H stretching	—	2965, 2909	2965
(N–H···O) group	—	2716	2780, 2575
NH_3^- deformation	—	—	2115, 2075
NH_2 bending	1655, 1603	1638, 1610	—
NH_3^- bending	—	1562, 1500	1600
$N_2H_5^+$ deformation	—	1420	—
NH_2 wagging	1350, 1304	—	—
NH_3^- rocking	—	1255, 1140	1145
NH_2 rocking	1126, 1066	1107, 1012	1055
N–N stretching	884	975	1025

The N–N stretching frequency is known to vary with the N–N bond distance [34]. Diminution of electron cloud repulsion on nitrogen atoms causes shortening of the bond distance and hence ν_{N-N} frequencies shifts towards higher regions (Table 1.10).

Braibanti *et al.* [35] have given a rule of thumb for the N–N stretching frequency on the basis of earlier studies. In the complexes examined by this group and others, the N–N stretching frequency is found to be in the ranges shown in Table 1.10.

Table 1.10 Variation of stretching frequency with N–N bond distance in hydrazine salts and complexes.

Compound	$\upsilon_{(N-N)}$ cm^{-1}	d_{N-N} Å
N_2H_4 in the gas phase	850	1.47
N_2H_4 in the solid state	884	1.46
$N_2H_5^+$ uncoordinated	965	1.45
$N_2H_6^{2+}$	1023	1.42
N_2H_4, unidentate	930–940	1.43–1.40
N_2H_4, bridging	948–980	1.45–1.47
$N_2H_3COO^-$	986–1012	1.43–1.46
$N_2H_5^+$, coordinated	995–1015	1.43–1.45

1.3.2.2 X-Ray Methods

Hydrazine hydrate dissolves many inorganic salts readily; most of these salts recrystallize from the solution to form stable solvates or adducts that do not dissolve further. Additionally, the reaction of hydrazine with mineral acids/organic acids also leads to the formation of crystalline solids. These colored compounds are mostly single crystals although polycrystalline products can also be obtained. In metal complexes, hydrazine appears as either singly or doubly protonated cation and plays an important role in forming various hydrogen bond networks in their derivatives. For this reason, it is of interest to determine their crystal structures.

X-Ray crystallographic analysis has been extensively used to determine the configuration of such crystalline compounds [36]. Most hydrazine derivatives are characterized by their single-crystal structures, as already mentioned in the respective Sections 1.2.1–1.2.4 on hydrazine salts and metal complexes. Chapter 5 will deal further with the single-crystal characterization of many inorganic hydrazine derivatives.

1.3.3 Thermal Methods

Thermal methods are powerful tools that give valuable information on the nature of decomposition, ignition temperature, heats of formation, heats of combustion, and intermediate and end products formed on heating. Thermal tests conducted on the samples determine the weight loss, endotherms, and exotherms on heating or cooling. These features of the thermograms are indicative of the nature of the compound. As most hydrazine compounds and their metal complexes are high energetic solids, modern thermoanalytical instruments are useful in determining their nature and stability. Table 1.11 summarizes different types of widely used thermal techniques [37].

Combined TG (Thermogravimetry)-DTA (Differential thermal analysis) experiments are useful in determining the decomposition kinetics, activation energies, and thermal stabilities of hydrazine derivatives. The advantage of Differential scanning calorimetry (DSC) technique is the use of a small sample size and quantitative and accurate results. Each thermal analytical method mentioned above has its own unique means of measurement. No single method, however, gives complete information regarding the nature of the compound. Therefore, combined analytical methods like TG-Effluent gas analysis (EGA), DSC-hot-stage microscopy,

Table 1.11 Thermoanalytical techniques.

Technique	Property measured	Applications
Thermogravimetry (TG) or DTG (Differential Thermogravimetry)	Weight change as a function of time or temperature	Composition of intermediates and end products, decomposition kinetics, activation energies
Differential methods:		
1. Differential thermal analysis (DTA), 2. differential scanning calorimetry (DSC)	1. Temperature difference between the sample and reference substance; 2. change in enthalpy	1. Thermal stability, phase transitions, ignition temperature; 2. heats of combustion/ decomposition
Effluent gas analysis (EGA)	Detection of evolved gases	Mechanism of decomposition
Hot-stage microscopy	Microscopic examination during heating or cooling	Micro-structural phase changes and transformations

and pyrolysis-spectroscopic analysis have been developed to better understand these materials.

As hydrazine is an endothermic compound that decomposes exothermically, its derivatives and metal complexes are also highly unstable and some of them fall into the category of high energy materials (HEMs). For such HEMs it becomes essential to test their properties by friction and impact sensitivity tests along with standard techniques like TG/DTA or DSC. This allows for differentiation between HEMs that are classified as primary that is, very sensitive materials which easily explode by the application of fire, spark, impact, friction, and so on, and HEMs that are classified as secondary, that is, materials that are relatively insensitive to both mechanical shock and flame but explode with greater violence when set off [38].

As most of the hydrazine metal derivatives are colored complexes, its coordination geometry is confirmed by electronic spectroscopy (Ultraviolet (UV)/Visual (Vis) range). The electronic transitions of the N–N bond of hydrazine, as well as the $d \rightarrow d^*$ transitions of the transition metal atom, reveal the geometry and coordination around the metal atom as either octahedral or tetrahedral [39].

NMR spectroscopy also contributes a great deal in understanding the molecular structure of hydrazine derivatives. Generally, ^{1}H and ^{15}N or ^{14}N resonances are recorded to observe the chemical shifts that relate to the environment and bonding of the hydrazine moiety. Techniques like Mössbauer spectroscopy, magnetic susceptibility measurement, ESR, and so on have also been used to characterize specific properties.

1.4 APPLICATIONS OF INORGANIC HYDRAZINE DERIVATIVES

The applications of hydrazine and its derivatives are vast and are discussed extensively in References [1,6]. While some key applications of both organic and inorganic derivatives are summarized in Table 1.12, Chapter 6 will further deal with applications of inorganic hydrazine derivatives in detail.

Table 1.12 Important applications of hydrazine and its derivatives.

Compound	Applications
Anhydrous hydrazine	Explosives, rocket monopropellant, fuel for guided missiles, fuel cells
Hydrazine hydrate	Boiler water treatment, metal films, nano structured materials
Inorganic derivatives of hydrazine:	
Hydrazine salts and metal hydrazine complexes of perchlorate, nitrate, azide, hydrazinium nitroformate, or azide	Explosives
Hydrazinium azide	Source for pure nitrogen, automobile safety airbags, foaming agent
Hydrazine sulfate	Drug for cancer treatment
Hydrazine dihydrochloride	Soldering fluxes for aluminum, nanoferrites preparation
Metal hydrazine carboxylates	Precursors to nano metal oxides
Organic derivatives of hydrazine:	
Monomethyl hydrazine (MMH) and unsymmetrical dimethyl hydrazine (UDMH)	Fuel for bipropellant rockets
Isonicotinic acid hydrazide (INH)	Tuberculosis
Hydrazine derivatives	Pharmaceuticals, photographic chemicals
Fatty acid hydrazides, fatty acid aryl hydrazine sulfonic acids	Textile treating agents
Polyhydrazino and amino hydrazine derivatives	Plastics
Phenyl hydrazine, rotenone derivatives, semicarbozones, thiosemicarbozones, sulfonic acid hydrazides	Insecticides, pesticides, fungicides, herbicides
3-Amino-phthalyl hydrazide	Chemiluminescent materials
Phenyl hydrazine and unsymmetrical diphenyl hydrazine (UDPH)	Antioxidant

Apart from the above applications, hydrazine hydrate is also used in preparing organic derivatives, like hydrazones and hydrazides such as carbohydrazide (CH), oxalyl dihydrazide (ODH), malonic acid dihydrazide (MDH), tetra formal tris azine (TFTA) and so on, from the corresponding ketones and aldehydes. Hydrazones have been investigated as solid fuels in hybrid rockets [40]. The hydrazides have been exploited as combustible fuels with metal nitrate oxidizers in the preparation of nanocrystalline oxide materials [41].

REFERENCES

1. Rothgery, E.F. (2004) Hydrazine and its derivatives, in *Kirk-Othmer Encyclopedia of Chemical Technology*, vol. 13, John Wiley & Sons, Inc., pp. 562–607.
2. Stanbury, M.D. (1998) Oxidation of hydrazine in aqueous solution, in *Progress in Inorganic Chemistry*, vol. 47 (ed. K.D. Karlin), John Wiley & Sons, Inc., pp. 511–561.
3. Wiberg, E., Wiberg, N., and Holleman, A.F. (2001) *Inorganic Chemistry*, Academic Press, Part 1 ch. 14.
4. Liminga, R. and Olovsson, R. (1964) The crystal structure of hydrazine monohydrate. *Acta Crystallographica*, **17**, 1523–1528.
5. Collin, R.L. and Lipscomb, W.N. (1951) The crystal structure of hydrazine. *Acta Crystallographica*, **4**, 10–14.
6. Schmidt, E.W. (2001) *Hydrazine and its Derivatives: Preparation, Properties, Applications*, 2nd edn, John Wiley & Sons, Inc..
7. Simpson, D.K. (1985) Hydrazine: a powerful metal reductant. *Metal Finishing*, **83**, 57–60.
8. Lima Jr., E., Drago, V., Bolsoni, R., and Fichtner, P.F.P. (2003) Nanostructured $Fe_{50}Ni_{50}$ alloy formed by chemical reduction. *Solid State Communications*, **125**, 265–270.
9. Chen, J.P. (2012) *Reduction and Oxidation Process, Decontamination of Heavy Metals: Processes, Mechanisms, and Applications*, Advances in Industrial and Hazardous Wastes Treatment Series, CRC Press, Taylor and Francis Group, ch. 5, pp. 125–208.
10. Chen, J.P. and Lim, L.L. (2002) Key factors in chemical reduction by hydrazine for recovery of precious metals. *Chemosphere*, **49**, 363–370.
11. Patil, G.E., Kajale, D.D., Gaikwad, V.B., and Jain, G.H. (2012) Preparation and characterization of SnO_2 nanoparticles by hydrothermal route. *International Nano Letters*, **2**, 17–21.
12. Changwen Hu, L.S. (2008) Low dimensional inorganic materials in Nanotechnology Research, in *New Nanostructures, Nanotubes and Nanofibers* (ed. X. Huang), Nova Science Publishers Inc., ch. 1, pp. 29–30.
13. Salavati, N.M., Esmaeili, Z.M., and Sobhani, A. (2012) Cubic HgSe nanoparticles: sonochemical synthesis and characterisation. *Micro & Nano Letters, IET*, **7**, 1300–1304.
14. Mulpur, P., Mimani, T.R., and Kamisetti, V. (2013) Isolation of colloidal quantum dots of iron selenide exhibiting narrow range fluorescence in the green region. *Journal of Nanoscience*, Article ID 804290.

15. Zhang, L., Wang, T.L.J., Wei, L. *et al.* (2011) Template-free synthesis of one-dimensional cobalt nanostructures by hydrazine reduction route. *Nanoscale Research Letters*, **6**, 58.
16. Xi, L.F. and Lam, Y.M. (2007) Synthesis and characterization of CdSe nanorods using a novel microemulsion method at moderate temperature. *Journal of Colloid and Interface Science*, **316**, 771–778.
17. Molli, M., Parola, S., Chunduri, L.A.A. *et al.* (2012) Solvothermal synthesis and study of nonlinear optical properties of nanocrystalline doped bismuth telluride. *Journal of Solid State Chemistry*, **189**, 85–89.
18. Lee, J.D. (1996) *Concise Inorganic Chemistry*, 5th edn, Chapman & Hall, London, ch. 14, pp. 483.
19. Govindarajan, S. (1983) Structural and thermal studies on hydrazinium (1+) metal sulfate and oxalate complexes. Ph.D Thesis, Indian Institute of Science, Bangalore.
20. Jonsson, P.G. and Liminga, R. (1971) Hydrogen bond studies, Neutron diffraction study of hydrazinium dihydrogen phosphate $N_2H_5H_2PO_4$. *Acta Chemica Scandinavica (Copenhagen, Denmark: 1989)*, **25**, 1729–1741.
21. Bottomley, F. (1970) The reactions of hydrazine with transition-metal complexes. *Quarterly Reviews, Chemical Society*, **24**, 617–638.
22. Ragnarsson, U. (2001) Synthetic methodology for alkyl substituted hydrazines. *Chemical Society Reviews*, **30**, 205–213.
23. Dilworth, J.R. (1976) The coordination chemistry of substituted hydrazines. *Coordination Chemistry Reviews*, **21**, 29–62.
24. Gajapathy, D. (1983) Studies on metal–hydrazine system. Ph.D Thesis, Indian Institute of Science, Bangalore.
25. Edwards, D.A., Keily, J.F., Mahon, M.F. *et al.* (1993) New group 2 metal hydrazinecarboxylates: A novel coordination mode for hydrazinecarboxylate in a polymeric, ten-co-ordinate barium complex. *Journal of the Chemical Society, Dalton Transactions*, 3471–3474.
26. Lee, B., Kang, S.H., Kang, D. *et al.* (2011) Isolation and structural characterization of the elusive 1:1 adduct of hydrazine and carbon dioxide. *Chemical Communications*, **47**, 11219–11221.
27. Lee, B., Lee, K.H., Cho, J. *et al.* (2011) Synthesis of azines in solid state: reactivity of solid hydrazine with aldehydes and ketones. *Organic Letters*, **13**, 6386–6389.
28. Patil, K.C. and Seker, M.M.A. (1994) Synthesis, structure and reactivity of metal hydrazine carboxylates: combustible precursors to fine particle oxide materials. *International Journal of Self-Propagating High-Temperature Synthesis*, **3**, 181–196.
29. Kumar, N.R.S. (1990) Synthesis, spectra and structure of hydrazinium metal chloride and thiocyanate complexes. Ph.D Thesis, Indian Institute of Science, Bangalore.
30. Parkins, A.W., Prince, P.D., Smith, R.A.L., and Steed, J.W. (2001) Chromous hydrazine sulfate. *Acta Crystallographica*, **C57**, 670–671.
31. Patil, K.C., Nesamani, C., and Pai Verneker, V.R. (1983) The nature of water in hydrazine salt hydrates. *Journal of the Chemical Society, Dalton Transactions*, 2047–2049.
32. Jia, L.H., Li, R.Y., Duan, Z.M. *et al.* (2011) Hydrothermal synthesis, structures and magnetic studies of transition metal sulfates containing hydrazine. *Inorganic Chemistry*, **50**, 144–154.
33. Mendham, J., Denny, R.C., Barnes, J.D., and Thomas, M.J.K. (2006) *Vogels' Textbook of Quantitative Chemical Analysis*, 6th Indian edn, Pearson Education Ltd., pp. 441.

34. Nakamato, K. (2009) *Infrared and Raman Spectra of Inorganic and Coordination Compounds*, John Wiley & Sons, Inc., Hoboken.
35. Braibanti, A., Dallavalle, F., Pellinghelli, M.A., and Leporati, E. (1968) The nitrogen-nitrogen stretching band in hydrazine derivatives and complexes. *Inorganic Chemistry*, **7**, 1430–1433.
36. Desiraju, R.G., Vittal, J.J., and Ramanan, A. (2011) *Crystal Engineering. A Textbook*, World Scientific Publishing Co. Pte. Ltd., Singapore.
37. Brown, M.E. (2001) *Introduction to Thermal Analysis: Techniques and Applications*, 2nd edn, Kluwer Academic Publishers.
38. Agarwal, J.P. (2010) *High Energy Materials: Propellants, Explosives and Pyrotechnics*, Wiley-VCH Verlag GmbH, Weinheim.
39. Lever, A.B.P. (1984) *Inorganic Electronic Spectroscopy*, 2nd edn, Elsevier, New York.
40. Jain, S.R., Krishna, P.M.M., and Pai Verneker, V.R. (1979) Hypergolic ignition to various hydrazones with nitric acid. *Journal of Spacecraft and Rockets*, **16**, 69–73.
41. Patil, K.C., Hegde, M.S., Rattan, T., and Aruna, S.T. (2008) *Chemistry of Nanocrystalline Oxide Materials: Combustion Synthesis, Properties, and Applications*, World Scientific Publishing Co. Pte. Ltd., Singapore.

2

Hydrazine Salts

Singanahally T. Aruna[1] and K. C. Patil[2]
[1]*Surface Engineering Division, CSIR-National Aerospace Laboratories, Bangalore, India*
[2]*Department of Inorganic and Physical Chemistry, Indian Institute of Science, Bangalore, India*

2.1 INTRODUCTION

Hydrazine salts are the neutralized products of two important acidic species, hydrazinium ($N_2H_5^+$) and hydrazonium ($N_2H_6^{2+}$) cations that are generated in aqueous solutions of hydrazine (Figure 2.1). During their initial period of development in the first quarter of the twentieth century, hydrazine salts were largely synthesized through (i) neutralization of the corresponding acids; (ii) double decomposition of hydrazine sulfate with the corresponding barium salts; or (iii) the metathetical reaction (exchange of an anion with another salt) of ammonium salts with anhydrous hydrazine, as summarized in Chapter 1 [1]. Such methods of synthesis not only limited the variety of salts formed but made them difficult to produce. A much more versatile method of synthesizing hydrazine salts arises from the metathetical reaction of solid ammonium salts with hydrazine hydrate. This simple, direct, and safe method of making hydrazine salts developed in the last quarter of the twentieth

Inorganic Hydrazine Derivatives: Synthesis, Properties and Applications, First Edition.
Edited by K. C. Patil and Tanu Mimani Rattan.

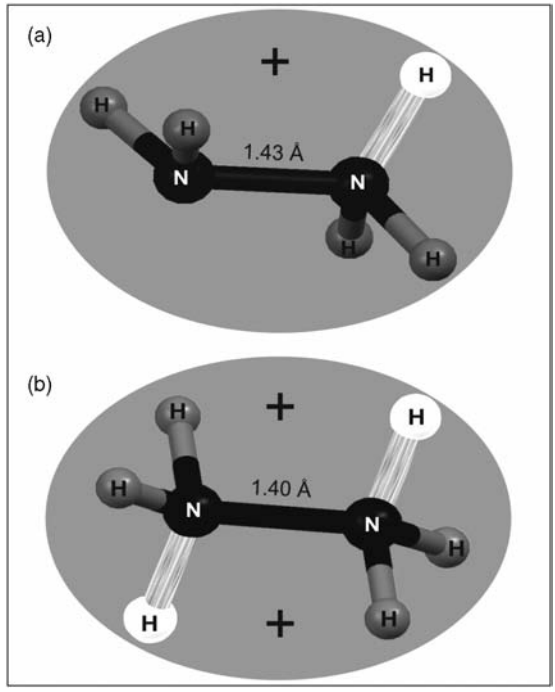

Figure 2.1 Structure of (a) hydrazinium and (b) hydrazonium ions.

century is the main focus of the present chapter [2–4]. Some new hydrazine salts that have been prepared by this method and other methods are reviewed here.

The hydrazinium cation, being the more prominent ionic species of hydrazine hydrate, readily forms hydrazine salts of the type N_2H_5A. In addition, being highly reactive, it can form a dihydrazinum cation $(N_2H_5)_2^{2+}$ in the presence of dibasic acids (H_2B) to form the corresponding salts $[(N_2H_5)_2B]$. However, very few dihydrazinium salts with inorganic anions are known.

Additionally, hydrazine, being a diacidic base, captures H atoms from either HA or H_2B acid molecules to form dicationic hydrazonium ($N_2H_6^{2+}$) salts of the type $N_2H_6A_2$ and N_2H_6B, respectively. As the stability of the $N_2H_6^{2+}$ cation is low, its tendency to form inorganic salts under normal conditions is rare. Raman studies have recently shown that the strong N–N stretching band at 1042 cm^{-1}, which is characteristic of the type of cation, is split into two bands when cooled to −196 °C. It merges again when warmed to room temperature. This indicates that the $N_2H_5^+$ and $N_2H_6^{2+}$ ions are spectroscopically indistinguishable at room

temperature, presumably because of a high rate of phonon-assisted proton tunneling through the barrier [5]. Consequently, as the isolation of these salts is difficult, only a few representative ones are described here. The properties of these hydrazonium ($N_2H_6^{2+}$) salts are compared with their respective hydrazinium ($N_2H_5^+$) and dihydrazinium [$(N_2H_5)_2^{2+}$] salts. Noticeably, both dihydrazinium and hydrazonium cations preferably form salts with organic anions rather than inorganic anions. Some of the recent ones reported in the literature are discussed later in this chapter.

2.2 SALTS OF THE MONOVALENT CATION ($N_2H_5^+$) – N_2H_5A

Of the two ions of hydrazine, the monoprotonated acidic hydrazinium ion is the most easily formed in solution. It is highly reactive and readily combines with various inorganic and organic anions to form salts. However, not all anions can form stable salts: only those hydrazinium salts that are readily attained using hydrazine hydrate are dealt with in this section.

2.2.1 Simple Hydrazinium Salts ($A^- = F$, Cl, Br, I, NO_3, N_3, VO_3, HF_2, HSO_4, SCN, SO_3NH_2, $COOCH_3$)

2.2.1.1 Synthesis

All simple hydrazinium salts are prepared by the reaction of respective ammonium salts with hydrazine hydrate. The general equation for the formation of these hydrazinium salts is:

$$NH_4A + N_2H_4{\cdot}H_2O \rightarrow N_2H_5A + NH_3 + H_2O \qquad (2.1)$$

where $A^- = F$, Cl, Br, I, NO_3, N_3, VO_3, HF_2, HSO_4, SCN, SO_3NH_2, and $COOCH_3$.

In all these reactions (2.1), ammonia gas is given off as a byproduct. To prevent the dissolution of ammonia into the reaction mixture it is essential to remove it by applying suction. Hydrazinium salts are all hygroscopic and need to be handled in a dry atmosphere [6]. A large amount of P_2O_5 in the desiccators ensures complete removal of water from the reaction mixture.

However, when a solution of NH_4I and hydrazine hydrate is evaporated on a water bath, large non-hygroscopic crystals are produced. Chemical analysis of this product reveals the formula $(N_2H_5I)_2{\cdot}N_2H_4$. The probable reaction through initial formation of hydrazinium iodide and its subsequent rearrangement can be written as:

$$3N_2H_5I \rightarrow (N_2H_5I)_2{\cdot}N_2H_4 + HI \qquad (2.2)$$

Interestingly, similar rearranged salts, like hydrazinium azide hydrazinate $[N_2H_5^+]{\cdot}[N_3^-]{\cdot}N_2H_4$, have been reported by heating equimolar amounts of hydrazinium azide and hydrazine. This mixture is heated to 50 °C in an evacuated vessel for 2 days and the product obtained is recrystallized from methanol [7].

In a slightly different method, hydrazinium metavanadate (a brown amorphous solid) is prepared by the addition of solid ammonium metavanadate (NH_4VO_3) to hydrazine hydrate at 0 °C using an ice–salt mixture as this reaction is highly exothermic [8]. The compound formed decomposes at room temperature and so a lower temperature is always maintained during its preparation. In addition, the vanadate ion (VO_3^-) is known to oxidize hydrazine, but this is considerably suppressed if the reaction is conducted at a low temperature. Furthermore, it is extremely difficult to recrystallize hydrazinium metavanadate as it is insoluble in water.

2.2.1.2 Infrared Spectra

The IR (Infrared) spectra of hydrazinium salts show an absorption peak in the region 960–980 cm^{-1}, which is characteristic of ν_{N-N} of $N_2H_5^+$. The IR spectrum of hydrazinium thiocyanate is shown in Figure 2.2 as a representative of the hydrazinium salts. The ν_{N-N} characteristic of $N_2H_5^+$ is observed at 973 cm^{-1} in addition to thiocyanate bands at around 2100 and 1400 cm^{-1} (Figure 2.2a).

In the IR spectrum of hydrazinium metavanadate, apart from the ν_{N-N} frequency of $N_2H_5^+$, absorption frequencies of VO_3^- are seen at 870 and 760 cm^{-1}, confirming the formation of $N_2H_5VO_3$.

2.2.1.3 Thermal Properties

The thermal properties of hydrazinium salts are evaluated in terms of their TG-DTA graphs (TG, thermogravimetry; DTA, differential thermal

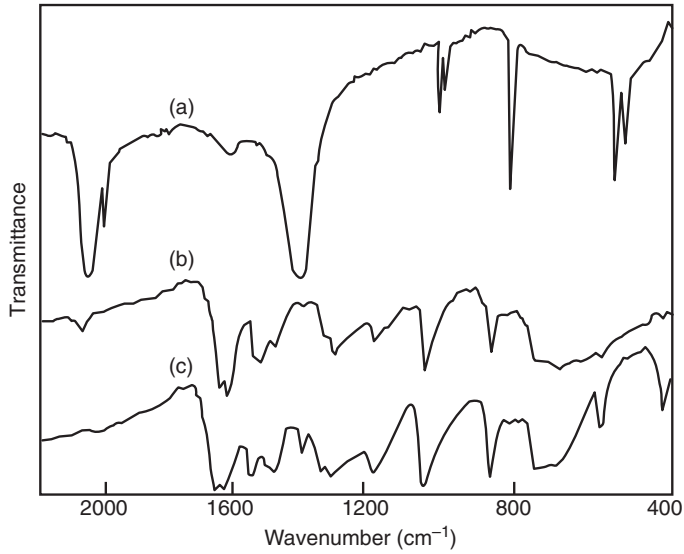

Figure 2.2 Infrared spectra of (a) N_2H_5SCN as synthesized, (b) N_2H_5SCN heated at 100 °C for 9 h, and (c) thiosemicarbazide standard sample. Adapted from Ref [8] with permission from the Indian Academy of Sciences © 1980.

analysis). Table 2.1 summarizes the DTA data of hydrazinium halides. All these salts melt and then decompose exothermically to give the corresponding ammonium halides. The final endotherms are due to the sublimation of *in situ* generated ammonium halides. To confirm this, hydrazinium halides can be heated in a test tube. Initially, the salts melt, and on further heating undergo violent reactions. White sublimates are deposited on the cooler parts of the test tube, and vapors of the corresponding halides (Br_2/I_2) and hydrogen halides (HCl/HBr/HI) are observed. Qualitative analysis of the sublimates identifies them as ammonium halides [9]. The formation of ammonium ion from hydrazinium ion

Table 2.1 DTA data of hydrazinium halides.

Compound	Peak temperature (°C)[a]
N_2H_5F	95(m), 180(−), 230(−)
N_2H_5Cl	89(m), 241(+), 308(−)
N_2H_5Br	180(m), 225(+), 350(−)
N_2H_5I	125(m), 170(+), 330(−)
$(N_2H_5I)_2{\cdot}N_2H_4$	90(m), 165(+), 340(−)

[a] m = Melting; (−) = endotherm; (+) = exotherm.

is so exothermic that partial decomposition of HBr and HI takes place. The reaction sequence is as follows:

$$2N_2H_5A \rightarrow 2NH_4A + N_2 + H_2 \tag{2.3}$$

$$2NH_4A \rightarrow 2NH_3 + 2HA \tag{2.4}$$

$$2HA \rightarrow H_2 + A_2 \tag{2.5}$$

where $A = F^-$, Cl^-, Br^-, and I^-.

The thermal behavior of other hydrazinium salts such as of N_2H_5SCN $N_2H_5SO_3NH_2$, $N_2H_5VO_3$, and $N_2H_5COOCH_3$ have been described [8]. Figure 2.3 shows their simultaneous TG-DTA curves.

Figure 2.3a shows the TG-DTA curves of N_2H_5SCN. The TG of hydrazinium thiocyanate shows no weight loss up to 125 °C. After this temperature it decomposes with a break at 350 °C (weight loss of about 70%). The

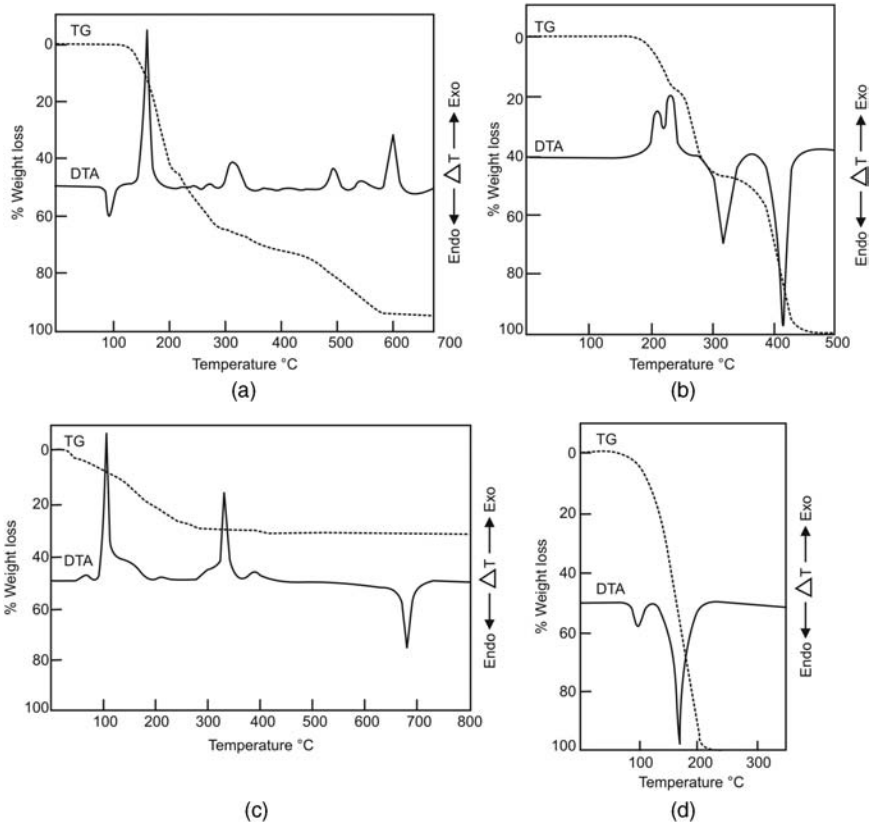

Figure 2.3 Simultaneous TG-DTA curves of (a) N_2H_5SCN, (b) $N_2H_5SO_3NH_2$, (c) $N_2H_5VO_3$, and (d) $N_2H_5COOCH_3$. Reproduced from Ref [8] with permission from the Indian Academy of Sciences © 1980.

DTA shows the first endotherm at 98 °C due to melting; there is some partial rearrangement of hydrazinium thiocyanate to thiosemicarbazide (confirmed by IR spectra – Figure 2.2b). As the process is dynamic there is not enough time for complete conversion. Above this temperature there is equilibrium between these two compounds. The exothermic peak at 156 °C is followed by several exotherms at 242, 266, 310, 490, 540, 590 °C, and so on, as seen from the DTA curve. The exact nature of these peaks is difficult to assign as TG shows no definite steps corresponding to these temperatures. It is more probable that thiosemicarbazide and hydrazinium thiocyanate react to form a cyclic compound or linear polymeric compound.

On heating solid N_2H_5SCN at 100 °C for 9 h at atmospheric pressure, the peaks due to N–N stretching disappear and peaks between 1000 and 800 cm^{-1} due to the CS group of thiosemicarbazide are observed (2.6). It is known that hydrazinium thiocyanate rearranges to thiosemicarbazide similar to the classical rearrangement of ammonium cyanate to urea [8]:

$$N_2H_5SCN \xrightarrow{80-100°C} H_2N-CS-NH-NH_2 \qquad (2.6)$$

The conversion yield of hydrazinium thiocyanate into thiosemicarbazide is about 40% when the isomerization is carried out in solution. It is well known that the conversion yield of N_2H_5SCN into thiosemicarbazide is 74.8% in the solid state. However, when it is heated isothermally the conversion into thiosemicarbazide is almost 100%. The IR spectrum of the converted sample is superimposable with that of a commercial thiosemicarbazide sample (Figure 2.2b and c).

The TG of hydrazinium sulfamate shows that the compound starts decomposing from 190 °C with a little break around 215 °C (Figure 2.3b). The DTA curve shows two exotherms, at 212 and 237 °C, and two endotherms, at 317 and 410 °C. The TG exhibits a two-step decomposition corresponding to the two exotherms, and a single-step weight loss corresponding to the two endotherms. This could be attributed to the initial slow loss of ammonia in the $N_2H_5SO_3NH_2$ liquid, equivalent to a weight loss of 18.6%. The white solid formed thereafter with about 47% weight loss is found to be acidic (pH ~2), giving effervescence with $NaHCO_3$ solution and showing a positive test for ammonium ion. Hydrazinium sulfamate initially decomposes to give sulfamic acid, which appears to decompose instantaneously due to the exothermicity of the first reaction. The acidic residue may be $HN(SO_3NH_4)_2$ or $NH_4N(SO_3H)_2$, similar to the intermediate formed during the decomposition of ammonium sulfamate or sulfamic acid. The acid so formed decomposes to ammonium hydrogen sulfate, which then completely decomposes (100%

weight loss) in the temperature region 350–450 °C, as seen from the TG and DTA with two endotherms. The reaction may be represented as follows:

$$6N_2H_5SO_3NH_2 \rightarrow 3HN(SO_3NH_4)_2 + 5NH_3 + 2N_2 \qquad (2.7)$$

Later, it decomposes exothermically and vigorously, forming a white solid with the evolution of NH_3, H_2O, SO_2, and S and so on, which have been detected by qualitative analysis.

Figure 2.3c shows the TG and DTA curves of hydrazinium metavanadate. As seen in the TG curve, this salt is highly unstable and begins to decompose at room temperature. DTA curve shows two exotherms: one at 104 °C and the other at 330 °C followed by an endotherm at 680 °C. The first exotherm at 104 °C is probably due to the oxidation of hydrazine, leaving a black residue that decomposes to vanadium pentoxide. However, the residue after the exotherm at 330 °C has been identified as V_2O_5 by weight loss in TG as well by the endotherm at 680 °C in DTA, which is due to the melting of V_2O_5.

Figure 2.3d shows TG-DTA curves of hydrazinium acetate ($N_2H_5COOCH_3$). Its DTA shows two endotherms: the first at 105 °C is due to melting of the compound. The second endotherm, occurring at 168 °C, is assigned to the decomposition of the melt into gaseous products containing acetic acid and ammonia, as found by a qualitative test of the gaseous products. The TG shows a single-step decomposition starting around 75 °C and ending near 200 °C, leaving no residue. The thermal decomposition of hydrazinium acetate may be represented as follows:

$$3N_2H_5COOCH_3 \rightarrow 3CH_3COOH + 4NH_3 + N_2 \qquad (2.8)$$

Hydrazinium acetate is one of the few hydrazinium salts to decompose endothermically. The results of TG and DTA are complementary.

2.2.2 Hydrazinium Salts with Oxidizing Anions – N_2H_5A ($A^- = N_3$, NO_2, NO_3, ClO_4, etc.)

2.2.2.1 Synthesis

Hydrazinium salts that form with oxidizing anions are those of the azide, nitrate, perchlorate, and picrate groups. They can be prepared from the metathetical reaction of their corresponding ammonium salts with

hydrazine hydrate [6,10]:

$$NH_4A + N_2H_4{\cdot}H_2O \rightarrow N_2H_5A + NH_3 + H_2O \qquad (2.9)$$

where A = N_3, NO_3, ClO_4, and $C_6H_2(NO_2)_3O$.

Anhydrous hydrazinium perchlorate $N_2H_5ClO_4$ has been prepared by the neutralization of $N_2H_4{\cdot}H_2O$ (99.5%) with 60% perchloric acid at 0 °C [4]. Hydrazinium perchlorate monohydrate ($N_2H_5ClO_4{\cdot}H_2O$) and hydrazinium perchlorate hemihydrate ($N_2H_5ClO_4{\cdot}0.5H_2O$) are prepared by the reaction of ammonium perchlorate with hydrazine hydrate [6]:

$$NH_4ClO_4 + N_2H_4{\cdot}H_2O \rightarrow N_2H_5ClO_4{\cdot}0.5H_2O + NH_3 + 0.5H_2O \qquad (2.10)$$

Hydrazinium perchlorate monohydrate is a white crystalline solid that melts at around 137 °C to a colorless liquid. Anhydrous hydrazinium perchlorate $N_2H_5ClO_4$ is also prepared by the dehydration of $N_2H_5ClO_4{\cdot}0.5H_2O$ kept in an air oven at 100 °C for 5 h.

The IR spectra of hydrazinium azide, hydrazinium nitrate, hydrazinium perchlorate, and hydrazinium picrate solids show ν_{N-N} frequencies in the region 960–980 cm^{-1}, confirming the presence of an $N_2H_5^+$ ion in these salts.

2.2.2.2 Thermal Properties

The DTA data of hydrazinium azide shows an endotherm due to melting at 75 °C and again an endothermic peak at 173 °C corresponding to its volatilization (Figure 2.4a). $N_2H_5N_3$ is reported to decompose explosively into hydrazine, ammonia, and nitrogen gas on rapid heating:

$$12N_2H_5N_3 \rightarrow 3N_2H_4 + 16NH_3 + 19N_2 \qquad (2.11)$$

However, no explosion occurs during DTA experiments because the salt is heated gradually and so simply melts and volatilizes without decomposition. This property of $N_2H_5N_3$ is comparable with ammonium azide (NH_4N_3) which also volatilizes without explosion. It has to be noted that both $N_2H_5N_3$ and NH_4N_3 explode only when heated rapidly.

Hydrazinium azide, utilized as a gun propellant, is unfortunately hygroscopic and volatile and, therefore, not very useful. Instead, the hydrazine adduct of hydrazinium azide, $(N_2H_5^+){\cdot}(N_3^-){\cdot}N_2H_4$, has been more

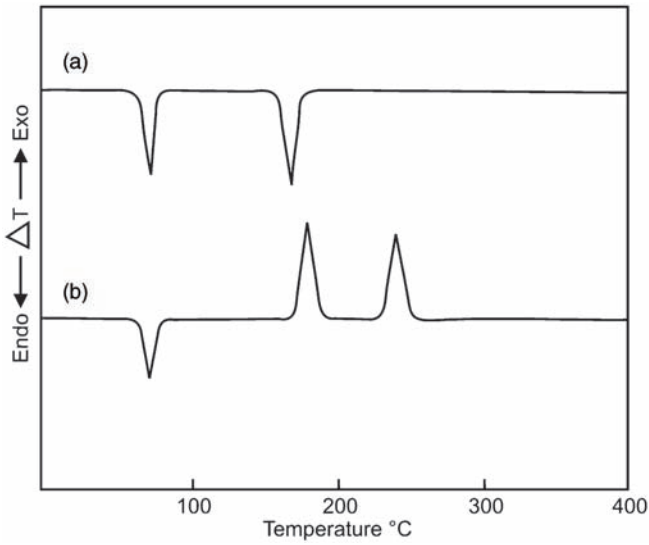

Figure 2.4 DTA curves of (a) $N_2H_5N_3$ and (b) $N_2H_5NO_3$. Adapted from Ref [9] with permission from Elsevier © 1979.

promising as it is neither shock sensitive nor friction or electrostatic discharge sensitive. This hydrazinium azide hydrazinate explodes when heated rapidly or when simply exposed to a hot metal surface [7].

The DTA trace of hydrazinium nitrate [9] shows that it melts at ~60 °C and decomposes in two steps. The intermediate after the first exotherm (~180 °C) is identified as ammonium nitrate by qualitative analysis of the residue left after this exotherm (Figure 2.4b). The peak temperature of the second exotherm (240 °C) also agrees with the decomposition of ammonium nitrate.

The thermal properties of hydrazinium perchlorate salts are discussed in Section 2.4.5.3 along with other perchlorate hydrazine salts.

Figure 2.5 shows the TG and DTA curves of hydrazinium picrate hemihydrate ($N_2H_5C_6H_2(NO_2)_3O{\cdot}0.5H_2O$) [10]. The endotherm at 148 °C in the DTA curve may be attributed to dehydration, since the corresponding TG curve shows a 2.9% weight loss against 3.3% for the loss of half a molecule of water. The exotherm at 167 °C is due to decomposition of the salt, probably to carbonaceous matter, which is further oxidized in air. The small exotherm at 223 °C may well be attributed to this oxidation. During the decomposition at 167 °C, part of the hydrazinium picrate sublimes, as is seen from a yellow deposit of the salt on the sides of the lid in the furnace, and the hydrazine content present

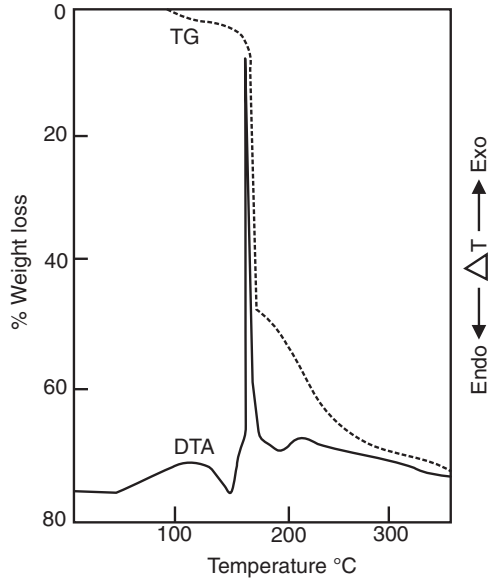

Figure 2.5 Simultaneous TG-DTA curves of $N_2H_5C_6H_2(NO_2)_3O{\cdot}0.5H_2O$. Reproduced from Ref [10] with permission from Akademiai Kiado © 1983.

in the deposit. The exothermic peak at 167 °C seems to be sensitive to the atmosphere, since the exothermic peak is shifted to 198 °C in a nitrogen atmosphere.

More recently, the isolation of the new nitrogen-rich hydrazinium salt $(CN_7^-)(N_2H_5^+)$, with a very high nitrogen content of nearly 84%, has been reported [11, 12]. The molecule, 5-aminotetrazole (AT), behaves as a weak acid and can be used to obtain nitrogen-rich energetic salts, with the hydrazinium cation forming hydrazinium 5-aminotetrazolate. It is a very powerful, environmentally friendly, insensitive propellant material. A DSC (differential scanning calorimetry) trace of hydrazinium 5-aminotetrazolate, (5 °C min^{-1}) shows melting at around 118–122 °C and decomposition at 186 °C. An extensive hydrogen bond network forms between all nitrogen atoms of the anions and the hydrazinium cations. This could be the reason for the stability and low sensitivities of this nitrogen-rich molecule (Figure 2.6).

Hydrazinium salts of the tetrazole family like hydrazinium 5-nitriminotetrazole, dihydrazinium nitriminotetrazolate monohydrate have also been successfully isolated using similar methods [13].

In the class of nitrogen-rich hydrazinium salts there is another category that contains nitro groups (NO_2^-). In this grouping, the most suitable

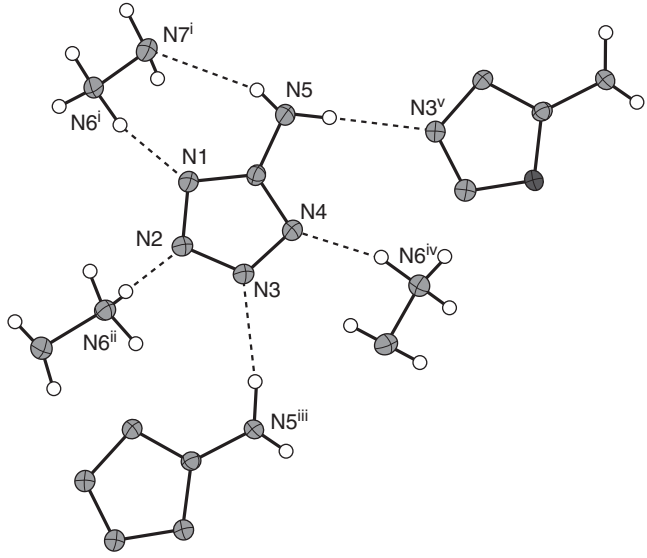

Figure 2.6 Hydrogen bonds of one 5-aminotetrazolate anion: (i) $x, y, 1+z$; (ii) $1-x, -y, z$; (iii) $-0.5+x, 0.5-y, 1-z$; (iv) $1.5-x, 0.5+y, -z$; (v) $0.5+x, 0.5-y, 1-z$. Reproduced from Ref [11] with permission from Institute of Industrial Organic Chemistry © 2008.

synthesized salt is hydrazinium nitroformate (HNF) ($[N_2H_5^+][C(NO_2)_3^-]$) [14, 15]. These salts are solids with ionic structures that are water-soluble and serve as primary propellant oxidizers. HNF is made by a precipitation reaction between hydrazine hydrate (N_2H_4) and nitroform [$HC(NO_2)_3$] according to:

$$N_2H_4{\cdot}H_2O_{(l)} + HC(NO_2)_{3(l)} \rightarrow N_2H_5^+{\cdot}C(NO_2)_3^-(s) + H_2O \qquad (2.12)$$

HNF has certain advantages as its method of synthesis is simple. It is non-hygroscopic in nature and has a higher density and melting point. HNF is an unusual salt of nitroform that has increased thermal stability compared to many nitroform derivatives. This increased stability has been attributed to an extension of the area of charge delocalization within the HNF molecule and extensive hydrogen bonding (Figure 2.7). Other derivatives of the nitroform family are now being explored as green energetic materials.

The IR spectra of hydrazinium 5-aminotetrazolate and hydrazinium nitroformate show peaks at around $960\,cm^{-1}$ corresponding to ν_{N-N} stretching frequency, characteristic of the presence of an $N_2H_5^+$ ion.

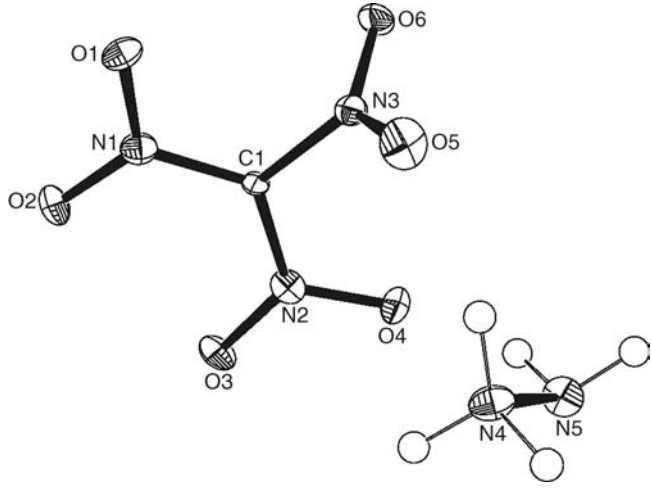

Figure 2.7 Structure of hydrazinium nitroformate in the crystalline state. Reproduced from Ref [19] Copyright © 2007 WILEY-VCH Verlag GmbH & Co. KGaA, Weinheim.

The simple hydrazinium picrate hemihydrate ($N_2H_5C_6H_2(NO_2)_3O \cdot 0.5H_2O$) has also been classified as an explosive even though the oxidizer to fuel ratio is as low as 0.45. Further in this group, energetic salts like hydrazinium dipicrylamine (HDPA) ($[C_{12}H_5(NO_2)_6N^-]$ $[N_2H_5^+]$), consisting of anion of dipicrylamine and the cation of hydrazine and its amino derivatives, have been isolated [16]. They tend to be oxidizers with the potential to form clean burning propellants.

Recently, there has been an increase in research activities to develop propellant formulations based on eco-friendly energetic oxidizers. Energetic salts containing hydrazinium cations and anions built from basic units of N and NO combinations are considered to be high energy materials (HEMs) and have been widely studied as new "green oxidizers," that is, chlorine-free. In addition, nitrogen-rich compounds are suitable ingredients in low smoke propellant charges [17–21]. Simulation studies conducted on structural comparisons between these ionic materials in the liquid and crystalline states have helped to predict their performance [22].

2.3 SALTS OF THE DIVALENT CATION [$(N_2H_5)_2^{2+}$ AND $N_2H_6^{2+}$]

The monoprotonated hydrazinium cation forms a divalent cation called the dihydrazinium ($(N_2H_5)_2^{2+}$) cation. The other divalent cation is the

diprotonated hydrazinium cation of hydrazine called the hydrazonium ($N_2H_6^{2+}$) cation. The salts of both cations are less common since many of them are unstable and decompose easily or rearrange further to form complex structures.

2.3.1 Dihydrazinium Salts ($(N_2H_5)_2^{2+}$) – [$(N_2H_5)_2B$, $B^{2-} = SO_3$, SO_4, C_2O_4, CO_3, HPO_4]

2.3.1.1 Synthesis, Infrared Spectra, and Thermal Properties

The dihydrazinium cation ($(N_2H_5)_2^{2+}$) being a dicationic species forms salts with dibasic acids of the type H_2B. Salts that are generated from the dihydrazinium cation are prepared by the reaction of ammonium salts with hydrazine hydrate [8, 10].

The reaction is as follows:

$$(NH_4)_2B + 2N_2H_4{\cdot}H_2O \rightarrow (N_2H_5)_2B + 2NH_3 + 2H_2O \qquad (2.13)$$

where $B = SO_3$, SO_4, C_2O_4, HPO_4, and CO_3.

A typical synthesis of dihydrazinium sulfite $(N_2H_5)_2SO_3$ is described here. Apart from the above method, one can also start its synthesis with hydrazinium sulfite hydrate. This salt is obtained by the reaction of SO_2 with $N_2H_4{\cdot}H_2O$.

$$2N_2H_4{\cdot}H_2O + SO_2 \rightarrow (N_2H_5)_2SO_3{\cdot}H_2O \qquad (2.14)$$

Anhydrous dihydrazinium sulfite is obtained by dehydration of the hydrated salt [$(N_2H_5)_2SO_3{\cdot}H_2O$] in a vacuum desiccator over phosphorus pentoxide at room temperature. The formed sulfite is characterized by IR spectra where a peak around 960 cm^{-1} corresponding to ν_{N-N} stretching confirms the formation of the dihydrazinium salt.

The DTA of $(N_2H_5)_2SO_3$ shows an endothermic peak at 52 °C due to melting (Figure 2.8). The second endotherm near 100 °C is attributed to dehydration. The anhydrous salt $(N_2H_5)_2SO_3$ decomposes exothermically at 276 °C. The TG shows a three-step decomposition. The first step results from its dehydration; the second is due to decomposition of the anhydrous salt with a weight loss of about 65%. At this stage, qualitative analysis of the residue obtained by heating $(N_2H_5)_2SO_3{\cdot}H_2O$ isothermally at 275 °C gives positive tests for NH_4^+, SO_4^{2-}, $S_2O_3^{2-}$, and polysulfide. It

is possible that $(N_2H_5)_2SO_3$ decomposes exothermically to give sulfur, which probably reacts with undecomposed SO_3^{2-} in the melt to give $S_2O_3^{2-}$. The final step (100% weight loss) is assigned to the decomposition and volatilization of the products. There is a good agreement between the TG and DTA results.

To prepare a carbonate salt of the dihydrazinium cation by the route (2.13), where ammonium carbonate is dissolved in hydrazine hydrate. Notably, when this reaction is attempted, instead of a carbonate salt of hydrazine being formed a viscous, syrupy liquid is obtained. The liquid has been shown to be hydrazinium hydrazine carboxylate ($N_2H_5COON_2H_3$) [23]. This occurs because commercial ammonium carbonate is a mixture of ammonium bicarbonate and ammonium carbamate ($NH_4HCO_3{\cdot}NH_2COONH_4$). The probable reaction is shown below:

$$\begin{aligned} NH_4HCO_3{\cdot}NH_2COONH_4 + 2N_2H_4{\cdot}H_2O &\rightarrow N_2H_5HCO_3{\cdot}NH_2COON_2H_5 + 2NH_4OH \\ &\rightarrow N_2H_5COON_2H_3 + NH_3 + CO_2 + H_2O \end{aligned} \tag{2.15}$$

It is worth mentioning that high nitrogen content salts have been recently formulated using dihydrazinium sulfate salt. The reaction of dihydrazinium sulfate with barium 5,5′-azotetrazolate has generated a

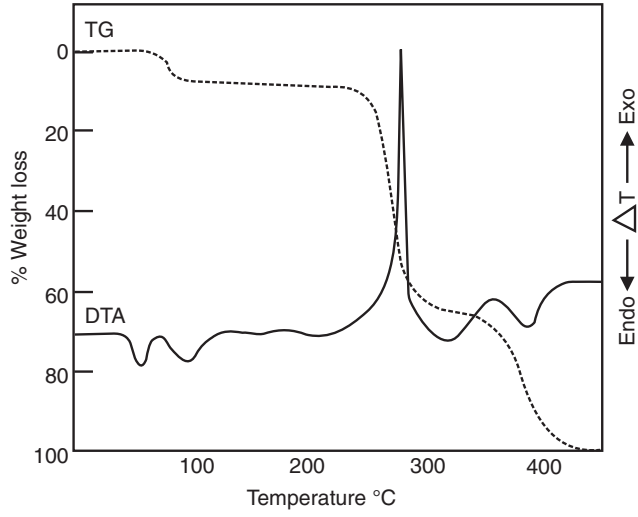

Figure 2.8 Simultaneous TG-DTA curves of $(N_2H_5)_2SO_3{\cdot}H_2O$. Adapted from Ref [8] with permission from the Indian Academy of Sciences © 1980.

series of dihydrazinium 5,5′-azotetrazolate salts of the formula $[N_2H_5]^{2+}[N_4C\text{-}N{=}N\text{-}CN_4]^{2-}$ based on 5,5′-azotetrazolate dianion [24, 25]. This new class of high energy density materials is found to be stable at room temperature, almost insensitive to friction and impact, and displays good detonation characteristics when subjected to rapid heating or use of an initiator. The synthesis, spectra, and thermal properties of other dihydrazinium salts of sulfate, oxalate and phosphate are discussed in Section 2.4.

2.3.2 Hydrazonium Salts ($N_2H_6^{2+}$) –$N_2H_6(A)_2$ or N_2H_6B

Several hydrazonium salts that are known to exist with inorganic anions of the formula $N_2H_6(A)_2$ or N_2H_6B, where A is a monovalent anion, like halide, NO_3, and ClO_4, while B is divalent anion such as C_2O_4, SO_4, and so on [1,4].

2.3.2.1 Synthesis, Infrared Spectra, and Thermal Properties

All hydrazonium salts are synthesized by neutralizing hydrazine hydrate with an excess amount of the corresponding acids:

$$N_2H_4{\cdot}H_2O + 2HA \rightarrow N_2H_6(A)_2 + H_2O \tag{2.16}$$

where $A^- =$ halide, NO_3, and ClO_4.

$$N_2H_4{\cdot}H_2O + H_2B \rightarrow N_2H_6B + H_2O \tag{2.17}$$

where $B^{2-} = C_2O_4$ and SO_4.

The hydrazonium cation is one of the few inorganic cations that allows for hydrogen bonding. Owing to this, most of these salts are present in the form of hydrates.

Hydrazonium salts are characterized by their IR absorption peak at around 1020 cm^{-1}. The $N_2H_6^{2+}$ cation in these salts is also characterized by Raman spectroscopy, where an intensive band at 1042 cm^{-1} confirms the presence of its double charge.

Hydrazonium salts on heating generally decompose to yield the monoacid salts as intermediates, which first melt and then decompose to

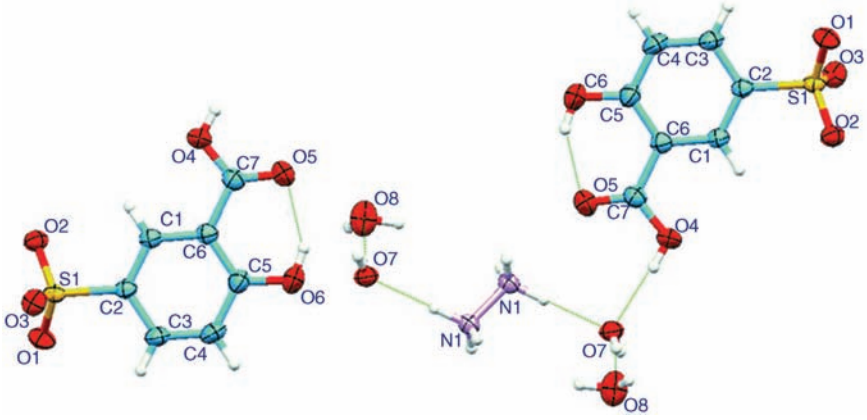

Figure 2.9 Structure of the hydrazonium salt of 5-sulfosalicylic acid. Reproduced from Ref [26] with permission from the International Union of Crystallography © 2011.

ammonium salts:

$$N_2H_6A_2 \rightarrow N_2H_5A + HA \tag{2.18}$$

An unusual hydrazonium salt of a sulfur-containing organic anion has been reported recently. The reaction of 5-sulfosalicylic acid with hydrazine hydrate at pH 1 affords hydrazonium 5-sulfosalicylate salt with the diprotonated cation as $0.5N_2H_6^{2+}\cdot C_7H_5O_6S^-\cdot 2H_2O$ (Figure 2.9). Hydrazine as a diacidic base captures the H atoms of sulfonic groups from two acid molecules to form a dicationic hydrazonium salt. The single-crystal structure of this salt shows intra- and intermolecular O–H···O hydrogen bonds [26].

2.4 SALTS OF MONOVALENT ($N_2H_5^+$) AND DIVALENT [$(N_2H_5)_2^{2+}$, $N_2H_6^{2+}$] CATIONS

Anions like fluoride, sulfate, oxalate, phosphate, and perchlorate form salts with both the monovalent and divalent hydrazine cations. As these salts show some interesting features, their synthesis, spectroscopic characterization, and thermal properties are highlighted here.

2.4.1 Hydrazine Fluorides – Hydrazinium Fluoride (N_2H_5F), Hydrazinium Bifluoride ($N_2H_5HF_2$), and Hydrazonium Fluoride ($N_2H_6F_2$)

Hydrazine is known to form three fluoride derivatives, namely, (i) hydrazinium (1+) fluoride, N_2H_5F, (ii) hydrazinium (1+) bifluoride, $N_2H_5HF_2$, and (iii) hydrazonium (2+) fluoride $N_2H_6F_2$. Since hydrazinium salts are analogous to ammonium salts, one would expect to synthesize a fluoride derivative by the addition of hydrofluoric acid (HF) to the monofluoride, similar to the preparation of acid fluorides like NH_4HF_2 and KHF_2. However, the addition of HF to N_2H_5F does not appear to yield hydrazinium bifluoride ($N_2H_5HF_2$); instead, it produces a new salt of hydrazonium fluoride ($N_2H_6F_2$).

2.4.1.1 Synthesis

Simple hydrazinium fluoride is prepared by the reaction of ammonium fluoride with hydrazine hydrate:

$$NH_4F + N_2H_4{\cdot}H_2O \rightarrow N_2H_5F + NH_3 + H_2O \qquad (2.19)$$

Hydrazinium bifluoride is prepared by the reaction of stoichiometric amounts of ammonium bifluoride with hydrazine hydrate in polythene cups. Ammonia evolves instantaneously. The product is crystallized from solution and dried over P_2O_5 in a vacuum desiccator [27]:

$$NH_4HF_2(l) + N_2H_4{\cdot}H_2O(l) \rightarrow N_2H_5HF_2(s) + H_2O(g) + NH_3(g) \quad (2.20)$$

It can also be prepared by isothermal heating of hydrazinium fluoride at 160 °C:

$$2N_2H_5F(s) \xrightarrow{160°C} N_2H_5HF_2(s) + N_2H_4(g) \qquad (2.21)$$

Hydrazonium fluoride ($N_2H_6F_2$) is obtained by the addition of aqueous HF to alcoholic hydrazine hydrate. Furthermore, it is synthesized by the addition of aqueous HF to an alcoholic solution of N_2H_5F prepared by the reaction (2.19). Hydrazonium fluoride precipitates as a non-hygroscopic crystalline solid.

Table 2.2 Infrared absorption frequencies (cm^{-1})[a] of hydrazine fluorides.

Assignment	N_2H_5F	$N_2H_5HF_2$	$N_2H_6F_2$
Combination of HF_2^-	—	2100 m, 1840 w	—
NH_2 bending	—	1680 sh	—
HF_2^- asymmetric stretching (ν_3)	—	1620 sh	—
NH_3^+ deformation	1550 vb	1550 vb	1550 vb
NH_2 rocking	1260 vb	1260 s, sp	1264 s
HF_2^- deformation (ν_2)	—	1250 sp	—
NH_3^+ bending	1120, 1100 s	1120, 1100 s	1190 s
ν_{N-N} stretching	960 s	960 s	980 s

[a] vb = Very broad; s = strong; sp = sharp; sh = shoulder; m = medium; w = weak.

2.4.1.2 Infrared Spectra

Infrared absorption frequencies of N_2H_5F and $N_2H_5HF_2$ are listed along with those of $N_2H_6F_2$ in Table 2.2. Both N_2H_5F and $N_2H_5HF_2$ show an absorption at 960 cm^{-1}, which has been assigned to ν_{N-N} of $N_2H_5^+$, while $N_2H_6F_2$ shows ν_{N-N} stretching at 980 cm^{-1} due to $N_2H_6^{2+}$. Figure 2.10 shows the infrared spectra of N_2H_5F and $N_2H_5HF_2$ along with that of NH_4HF_2. The bifluoride ion, HF_2^- has characteristic absorptions at 1600 (ν_3) and 1200 cm^{-1} (ν_2). Additional bands due to the combination of fundamentals of HF_2^- or water are observed at 2100 and 1840 cm^{-1}.

The IR spectra of $N_2H_6F_2$ shows a very broad peak at 1550 cm^{-1} and three strong peaks at 1264, 1190, and 980 cm^{-1} corresponding to NH_2 rocking, NH_3^+ bending and ν_{N-N} stretching, respectively. The IR ν_{N-N} frequency observed for $N_2H_6F_2$ at 980 cm^{-1} is noticeably low compared to the expected value of 1024 cm^{-1} for $N_2H_6^{2+}$. The lowering of this frequency could be expected and justified because the N–N bond distance in $N_2H_6F_2$ is reported to be 1.42 Å and the calculated ν_{N-N} frequency agrees with the observed frequency. Thus, the lowering of the ν_{N-N} frequency in $N_2H_6F_2$ can be attributed to the presence of strong hydrogen bonding that is responsible for the increase in N–N bond distance. In addition, the strong hydrogen bonding in $N_2H_6F_2$ probably does not allow the formation of ammonium fluoride during its decomposition.

The following features of the IR spectra make it possible to differentiate between $N_2H_5HF_2$ and $N_2H_6F_2$:

1. the presence of absorptions at 2100 and 1840 cm^{-1} in $N_2H_5HF_2$ as in NH_4HF_2, which are absent in $N_2H_6F_2$;

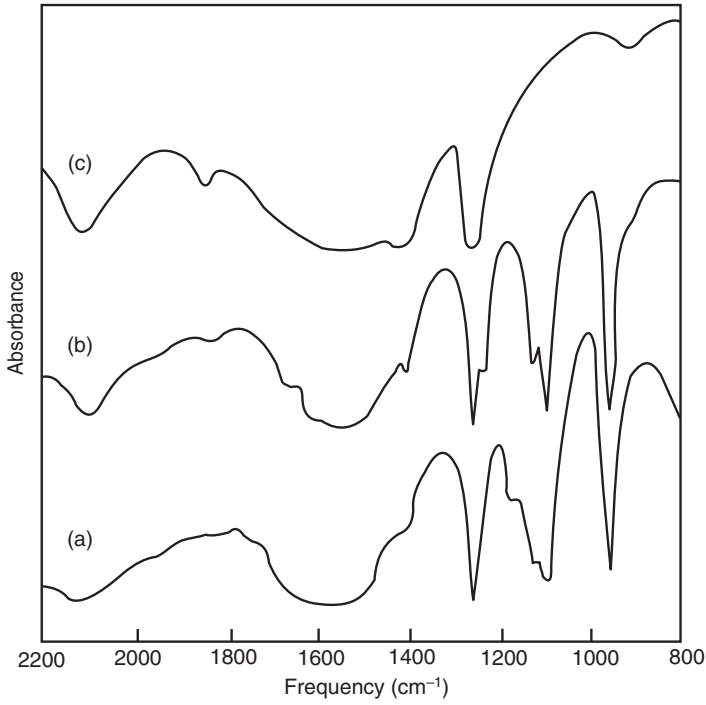

Figure 2.10 Infrared spectra of (a) N_2H_5F, (b) $N_2H_5HF_2$ (heated at 160 °C for 12 h), and (c) NH_4HF_2. Adapted with permission from Ref [27]. © 1979, American Chemical Society.

2. the presence of doublet around 1260 cm^{-1} in $N_2H_5HF_2$ compared to the singlet in $N_2H_6F_2$;
3. the ν_{N-N} frequency of $N_2H_5HF_2$ observed at 960 cm^{-1} compared to the ν_{N-N} of $N_2H_6F_2$ observed at 980 cm^{-1}.

2.4.1.3 Thermal Properties

The DTA data of hydrazine fluorides are tabulated in Table 2.3 and shown in Figure 2.11.

In the DTA of N_2H_5F (Figure 2.11a), the first endotherm is sharp and reversible, which is attributed to melting. The second endotherm is initially broad but becomes narrow during further heating. The resulting third peak is found to be reversible and is assigned to the dissociation of N_2H_5F to $N_2H_5HF_2$.

The DTA of hydrazinium bifluoride, $N_2H_5HF_2$, exhibits three endotherms (Figure 2.11d). The first two endotherms are reversible and are

Table 2.3 DTA data of hydrazine fluorides.

Compound	DTA peak temperature (° C)[a]
N_2H_5F	95(m), 180(−), 230(−)
$N_2H_5HF_2$	142(−), 184(m), 250(−)
$N_2H_6F_2$	184(m), 242(−)
$N_2H_5HF_2$[b]	182(−), 250(−)

[a] m = Melting, (−) = endotherm, (+) = exotherm.
[b] Prepared by heating N_2H_5F at 160 °C for 12 h.

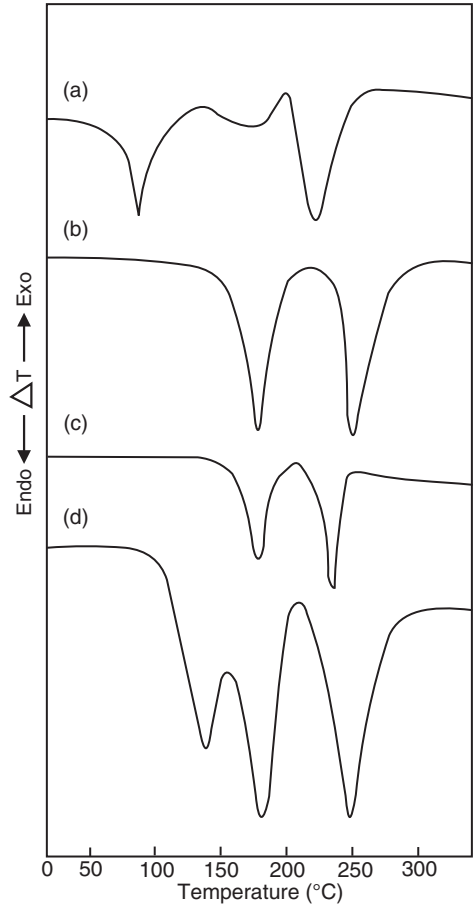

Figure 2.11 DTA curves of (a) N_2H_5F, (b) $N_2H_5HF_2$ obtained by a thermal method, (c) $N_2H_6F_2$, and (d) $N_2H_5HF_2$ obtained by a chemical method. Adapted with permission from Ref [27]. © 1979, American Chemical Society.

assigned to a phase change and melting, respectively. The final endotherm is due to the volatilization of $N_2H_5HF_2$. The phase transition peak at around 140 °C disappears on repeated thermal cycling, probably stabilizing the high-temperature form of $N_2H_5HF_2$.

Formation of $N_2H_5HF_2$ is confirmed by the observed weight loss in the isothermal thermogravimetry of N_2H_5F at 160 °C. The weight loss corresponds to the loss of a hydrazine molecule, which is qualitatively tested by its basic action on pH paper. Further, on analysis of the residue from the isothermal TG for hydrazine content, it is found to contain 44.4% N_2H_4 as in $N_2H_5HF_2$. The DTA of the residue does not show any endothermic peak below 180 °C, indicating the absence of melting of N_2H_5F and the phase-transition peak of $N_2H_5HF_2$. This appears to suggest that a high-temperature form of fluoride salt of formula $N_2H_5HF_2$ is produced by heating N_2H_5F at 160 °C. The possibility of formation of $N_2H_6F_2$ instead of $N_2H_5HF_2$ is ruled out by the IR spectrum, which shows a characteristic infrared absorption of $N_2H_5^+$ at 960 cm^{-1} and not of $N_2H_6^{2+}$, which is observed around 980 cm^{-1}. This property of N_2H_5F in dissociating to $N_2H_5HF_2$ is similar to that of NH_4F. Ammonium fluoride is known to dissociate to ammonium bifluoride and ammonia on heating. The final endotherm in the DTA of N_2H_5F is attributed to the volatilization of $N_2H_5HF_2$ formed.

Hydrazonium fluoride exhibits only two endotherms in DTA (Figure 2.11c). The DTA shows a sharp and reversible peak at 184 °C corresponding to melting of the salt; the second endotherm at 242 °C can be assigned to the volatilization of $N_2H_6F_2$. The presence of strong hydrogen bonding, in both N_2H_5F and $N_2H_6F_2$, probably does not allow the formation of ammonium fluoride during the decomposition of these fluorides.

2.4.2 Hydrazine Sulfates – Hydrazinium Bisulfate ($N_2H_5HSO_4$), Dihydrazinium Sulfate [$(N_2H_5)_2SO_4$], and Hydrazonium Sulfate ($N_2H_6SO_4$)

Hydrazine is known to form three sulfate derivatives, namely, (i) hydrazinium (1+) bisulfate, $N_2H_5HSO_4$, (ii) dihydrazinium (1+) sulfate, $(N_2H_5)_2SO_4$, and (iii) hydrazonium (2+) sulfate $N_2H_6SO_4$. Hydrazonium (2+) sulfate mainly exists as $N_2H_5HSO_4$ in aqueous solution. However, no attempts have been made to isolate the $N_2H_5HSO_4$ salt in the solid state. In this section the synthesis of $N_2H_5HSO_4$ carried out by the

metathetical reaction of ammonium bisulfate with hydrazine hydrate is discussed, and its properties are compared with hydrazonium sulfate ($N_2H_6SO_4$) and dihydrazinium sulfate $(N_2H_5)_2SO_4$. The more common sulfate salt of hydrazine is $N_2H_5HSO_4$ (called hydrazinium bisulfate).

2.4.2.1 Synthesis

Hydrazinium bisulfate ($N_2H_5HSO_4$) is prepared by the reaction of calculated amounts of the corresponding ammonium salts with hydrazine monohydrate [28]. The reaction is represented as follows:

$$NH_4HSO_4 + N_2H_4{\cdot}H_2O \rightarrow N_2H_5HSO_4 + NH_3 + H_2O \qquad (2.22)$$

Dihydrazinium sulfate is prepared by the reaction of stoichiometric quantities of ammonium sulfate with calculated quantities of hydrazine hydrate (99–100%) [10]. Ammonia is evolved instantaneously and the resulting product is dihydrazinium sulfate. The products are crystallized from solution and dried over phosphorus pentoxide in a vacuum desiccator:

$$(NH_4)_2SO_4 + 2N_2H_4{\cdot}H_2O \rightarrow (N_2H_5)_2SO_4 + 2NH_3 + 2H_2O \qquad (2.23)$$

Commercially available $N_2H_6SO_4$ is recrystallized and used for comparative studies.

2.4.2.2 Infrared Spectra

Table 2.4 lists infrared absorption frequencies of $N_2H_5HSO_4$, $(N_2H_5)_2SO_4$ and $N_2H_6SO_4$ along with their assignments. It can be seen that $N_2H_5HSO_4$ and $(N_2H_5)_2SO_4$ show characteristic absorptions of the $N_2H_5^+$ ion at ~1600, ~1400, 1240, 980, and ~963 cm^{-1}. The ν_3 band of the SO_4^{2-} ion in $N_2H_5HSO_4$ is split into two bands at 1105 and 1080 cm^{-1}, indicating the C_{3v} symmetry of HSO_4^-. However, the absorption at 617 cm^{-1} (ν_4) does not show any splitting.

The main feature distinguishing $N_2H_5HSO_4$ from $N_2H_6SO_4$ is the presence of $\nu_{(N-N)}$ of $N_2H_5^+$ at 963 cm^{-1} in the former, compared to $\nu_{(N-N)}$ of $N_2H_6^{2+}$ at 1023 cm^{-1} in the latter. The IR spectra of $N_2H_6SO_4$ shows a weak peak at 3080 cm^{-1}, which can be assigned to N–H stretching of the NH_3^+ group (N–H···O). The weak peak observed at 2100 cm^{-1} may be assigned to NH_3^+ deformation.

Table 2.4 Infrared absorption frequencies (cm^{-1})[a] of hydrazine sulfates.

$N_2H_5HSO_4$	$(N_2H_5)_2SO_4$	$N_2H_6SO_4$	Assignment
3245m	3245m	—	N–H stretching of NH_2 group (N–H···O)
3040w	3040w	3080w	N–H stretching of NH_3^+ group (N–H···O)
2575m	2575m	2590w	NH_3^+ deformation
1576m	1578m	1555m(sh)	N–H bendings
—	1400m	—	$N_2H_5^+$ deformation
—	1180w(sh)	—	NH_3^+ rocking
1105s, br	1110s, br	1057m	$\nu_3(SO_4)$
—	980w	=	NH_2 rocking
970(sh)	970(sh)	969m	$\nu_3(SO_4)$
963s	964m	1023m	N–N stretching
617s	619s	616s	$\nu_4(SO_4)$
498sbr	498s, br	513s	Torsional mode
455(sh)	450(sh)	466s	$\nu_2(SO_4)$

[a] m = Medium, s = strong, sh =shoulder, w = weak.

2.4.2.3 Thermal Properties

The TG-DTA results of $N_2H_5HSO_4$, $(N_2H_5)_2SO_4$, and $N_2H_6SO_4$ are tabulated in Table 2.5 (Figure 2.12). The hydrazinium bisulfate shows an endothermic peak at 105 °C due to melting. It decomposes exothermically with a peak temperature at 250 °C to give a mixture of ammonium sulfate and ammonium bisulfate. Ammonium sulfate decomposes further endothermically at 324 °C to ammonium bisulfate, which decomposes and volatilizes at 404 °C. The DTA of $N_2H_6SO_4$ shows an endotherm at 222 °C which is attributed to phase transformation (Figure 2.12c). This is followed by another endothermic peak at 265 °C due to its melting with decomposition. Hydrazonium sulfate decomposes exothermically to ammonium bisulfate at 271 °C, which decomposes and volatilizes at 400 °C.

The TG of hydrazinium bisulfate indicates that it is thermally stable up to 190 °C and decomposes in the temperature region 190–290 °C (Figure 2.12a), while hydrazonium sulfate is quite stable up to 270 °C (Figure 2.12c). The hydrazonium salt further decomposes in the temperature region 270–290 °C, with a higher rate of weight loss, to ammonium bisulfate. Dihydrazinium sulfate also behaves in a similar way to $N_2H_5HSO_4$ and is stable up to 180 °C but decomposes to ammonium bisulfate in the higher temperature region 180–280 °C (Figure 2.12b).

DTA carried in vacuum clearly differentiates $N_2H_5HSO_4$ from $N_2H_6SO_4$ (Figure 2.13). While $N_2H_5HSO_4$ and $(N_2H_5)_2SO_4$ show almost

Table 2.5 TG-DTA data of hydrazine sulfates.

Hydrazine salts	DTA peak position (°C)[a]	Thermogravimetry			Products
		TG Temperature range (°C)	% Weight loss		
			Obsd.	Calcd.	
$N_2H_5HSO_4$	105(−)	190–290	54	53.15	
	250(+)	—	—	—	$(NH_4)_2SO_4 + NH_4HSO_4$
	324(−)	300–400	100	100	
	404(−)	—	—	—	
$(N_2H_5)_2SO_4$	95(−)	—	—	—	Melting
	250(+)	180–200	57	57.41	$NH_4HSO_4 + H_2O + H_2S + SO_2 + N_2 + NH_3$
	400(−)	300–450	100	100	Decomposition and volatilization of NH_4HSO_4
$N_2H_6SO_4$	222(−)	—	—	—	—
	265(−)	—	—	—	—
	271(+)	270–290	56	55.81	—
	400(−)	300–450	100	100	—

[a] (−) = Endotherm; (+) = exotherm.

identical decomposition patterns, $N_2H_6SO_4$ does not show any significant change up to 190 °C. However after the initial melting, all three sulfates give $(NH_4)_2SO_4$, which further decomposes to NH_4HSO_4.

Hydrazonium sulfate ($N_2H_6SO_4$) is known to exist in orthorhombic and monoclinic modifications at room temperature. The high-temperature phase transformation of Analar grade hydrazonium sulfate has been studied by DSC [29]. The crystal of this salt is ground and sieved to different ranges of particle sizes using STM standard sieves. The cooling curves of DSC are obtained with a linear cooling rate of 6 to 8 °C min^{-1} from 250 to 100 °C. Figure 2.14 shows the heating and cooling curves of the DSC of orthorhombic $N_2H_6SO_4$ of particle sizes between 250 and 300 μm. The DSC data are summarized in Table 2.6, showing the effect of particle size on the phase-transition temperature and the enthalpy of phase transition. The transformation temperature, which is the intersection of the low temperature side of the peak with the base line, is taken as the initial temperature (T_i). It can be seen that the phase-transformation temperature (T_p) decreases as the particle size increases. The particle

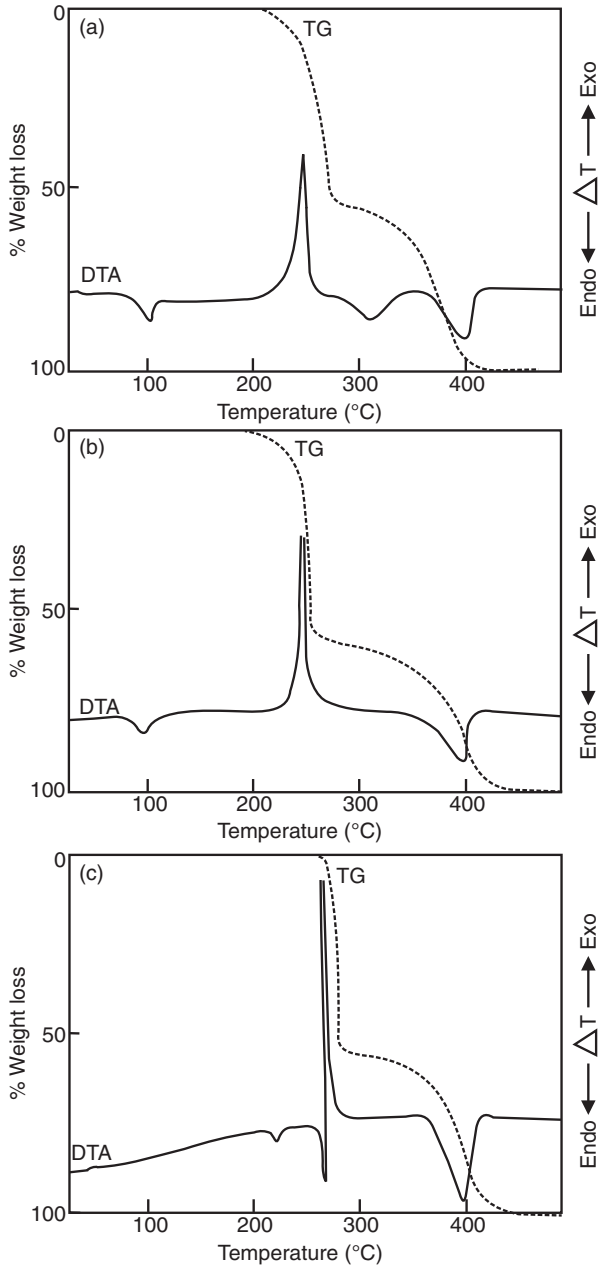

Figure 2.12 Simultaneous TG-DTA curves of (a) $N_2H_5HSO_4$, (b) $(N_2H_5)_2SO_4$, and (c) $N_2H_6SO_4$.

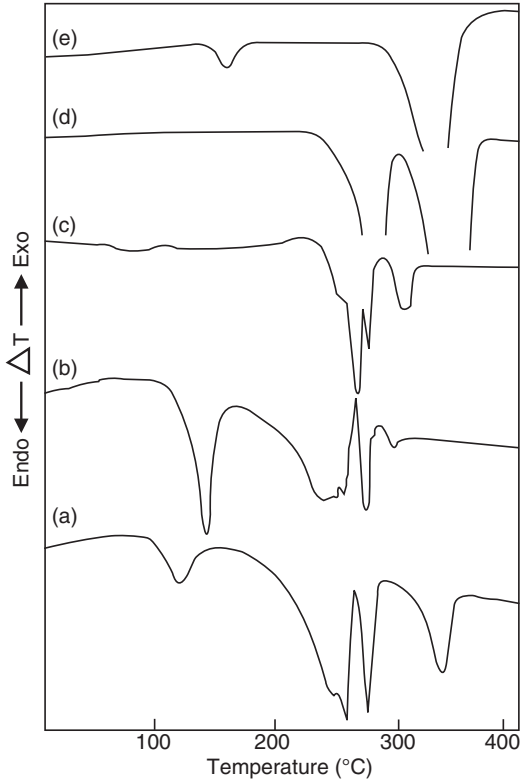

Figure 2.13 DTA curves of (a) $N_2H_5HSO_4$, (b) $(N_2H_5)_2SO_4$, (c) $N_2H_6SO_4$, (d) $(NH_4)_2SO_4$, and (e) NH_4HSO_4 in vacuum (0.5 mmHg pressure) with a heating rate of 13 °C min^{-1}. Adapted from Ref [28] with permission of The Royal Society of Chemistry © 1982.

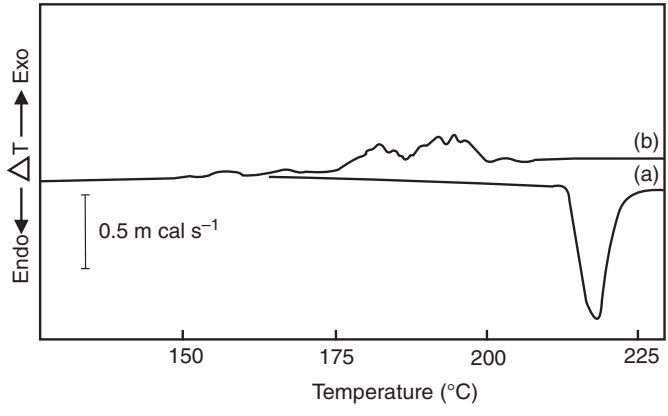

Figure 2.14 DSC curves of orthorhombic $N_2H_6SO_4$: (a) heating curve and (b) cooling curve. Reproduced from Ref [29] with permission from Elsevier © 1982.

Table 2.6 Dependence of phase-transition temperature and heat of phase transition (ΔH) on particle size.

Particle size range (μm)	Amount of sample (mg)	Phase transition temperature (°C)		Enthalpy of phase transition (kJ mol^{-1})
		Initial (T_i)	Peak (T_p)	
40–53	7.560	219.6	228.0	3.60
53–75	8.015	218.0	228.4	3.63
125–150	8.055	216.2	228.0	3.56
250–300	8.750	214.6	221.1	3.61
300–400	12.260	213.5	219.0	3.74

size seems to have no effect on the heat of phase transition. The heat or enthalpy of phase transition is found to be $\approx 3.63 \pm 0.1$ kJ mol^{-1}.

On cooling, the exothermic peak consists of a large number of very small exotherms extending over a wide temperature range. On repeating the heating and cooling cycles, similar effects are observed. Observation of thermal hysteresis (ΔT) over a wide temperature range is due to the absence of thermodynamic equilibrium at all stages of transformation.

When the particle size is smaller, the high-temperature phase becomes stabilized, that is, the phase transition appears to be thermally irreversible for the smaller particle size. When high temperature form of $N_2H_6SO_4$ is aged at room temperature, it slowly converts into the orthorhombic form. The observed behavior is a result of the smaller particle size effect, which has a higher surface area, which in turn allows additional degrees of freedom.

2.4.3 Hydrazine Oxalates – Hydrazinium Hydrogen Oxalate ($N_2H_5HC_2O_4$) and Dihydrazinium Oxalate [$(N_2H_5)_2C_2O_4$]

Hydrazine forms two compounds with oxalic acid, hydrazinium (1+) hydrogen oxalate, $N_2H_5HC_2O_4$, and dihydrazinium (1+) oxalate, $(N_2H_5)_2C_2O_4$. Dihydrazinium oxalate has not been studied extensively as compared to hydrazinium hydrogen oxalate.

2.4.3.1 Synthesis

Hydrazinium hydrogen oxalate, $N_2H_5HC_2O_4$, has been studied extensively. It is obtained by mixing hot aqueous solutions of suitable amounts

of hydrazine hydrate and oxalic acid dihydrate [30]. Recrystallization from water gives fine colorless needles. The crystals are dried to constant weight over a drying agent in a desiccator:

$$2H_2C_2O_4{\cdot}2H_2O + 2N_2H_4{\cdot}H_2O \rightarrow N_2H_5HC_2O_4 + 2NH_3 + 6H_2O + 2CO_2 \quad (2.24)$$

Dihydrazinium oxalate is prepared by reacting hydrazine hydrate with ammonium oxalate and the reaction can be written as follows:

$$(NH_4)_2C_2O_4 + 2N_2H_4{\cdot}H_2O \rightarrow (N_2H_5)_2C_2O_4 + 2NH_3 + 2H_2O \quad (2.25)$$

The fact that only one hydrazine molecule is easily lost from $(N_2H_5)_2C_2O_4$ suggests that the two hydrazine moieties are held differently in this compound. This is evidenced from the infrared spectrum, which shows two different N–N stretching frequencies, at 960 and 975 cm^{-1}.

2.4.3.2 Thermal Properties

The available thermal data on dihydrazinium oxalate indicates that it melts at 148 °C and this melting is followed by another endotherm at 170 °C and an exothermic peak at 263 °C (Figure 2.15). The intermediate formed at 263 °C further decomposes exothermically at 494 °C.

The exothermic decomposition temperatures of dihydrazinium oxalate, $(N_2H_5)_2C_2O_4$, are almost the same as those of hydrazinium hydrogen oxalate ($N_2H_5HC_2O_4$). This strongly suggests that dihydrazinium oxalate might have been converted into hydrazinium hydrogen oxalate after melting by losing a hydrazine molecule. This transformation has been observed as an endothermic peak at 170 °C. Mass spectral analysis of the evolved gases obtained by decomposing both the oxalates at ~200 °C shows that the decomposition pattern is similar to the hydrazinium hydrogen oxalate case, except for an additional peak at $m/z = 32$ in the case of dihydrazinium oxalate. This suggests the loss of a N_2H_4 molecule, which fragments further to give the molecular ion of N_2H_4. The TG of this compound also shows a continuous weight loss. A small break at 43% weight loss suggests the formation of the same intermediate as in the case of hydrazinium hydrogen oxalate. This is further confirmed by infrared and X-ray powder pattern, which are identical with those obtained for the intermediate of $N_2H_6HC_2O_4$. Dihydrazinium oxalate

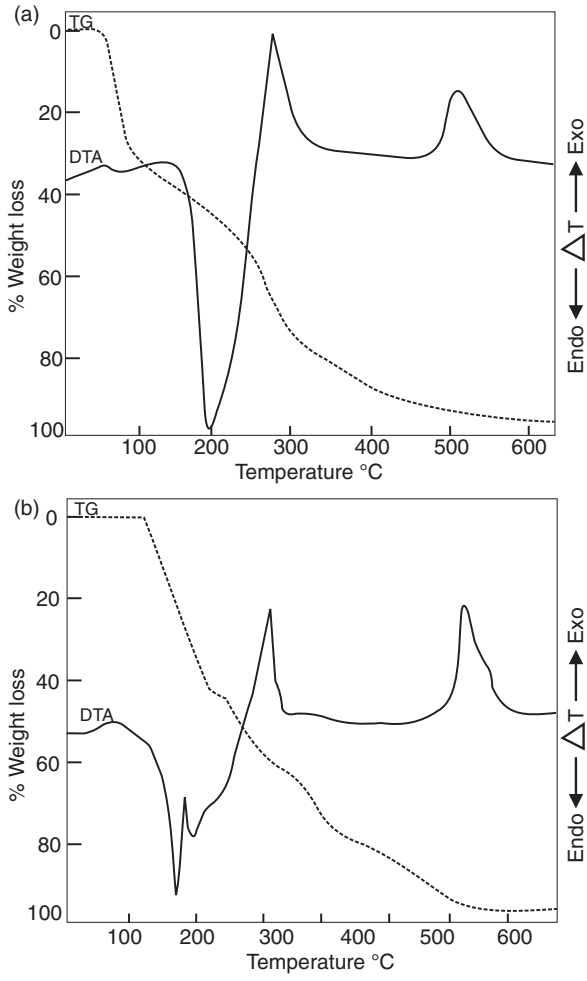

Figure 2.15 Simultaneous TG-DTA curves of (a) $N_2H_5HC_2O_4$ and (b) $(N_2H_5)_2C_2O_4$. Adapted from Ref [30] with permission from Elsevier © 1983.

on heating loses a molecule of N_2H_4 and is converted into hydrazinium hydrogen oxalate and hence the thermal analysis of the two compounds is similar.

The TG of hydrazinium hydrogen oxalate shows a continuous weight loss with a break at 31%. The product at this intermediate stage, when separately obtained and analyzed, is found to be insoluble in almost all common solvents, suggesting a polymeric nature of the compound. The weight loss and IR spectra of the intermediate suggests that it has a probable structure of $–(NH\text{-}CO\text{-}CO\text{-}NH)_n–$ instead of an oxamide.

2.4.4 Hydrazine Phosphates – Monohydrazinium Phosphate ($N_2H_5H_2PO_4$) and Dihydrazinium Phosphate [$(N_2H_5)_2HPO_4$]

Hydrazine forms two main salts with the hydrogen phosphate anions $H_2PO_4^-$ and HPO_4^{2-} as mono- and dihydrazinium salts.

2.4.4.1 Synthesis

Both monohydrazinium phosphate ($N_2H_5H_2PO_4$) and dihydrazinium phosphate, $(N_2H_5)_2HPO_4$, are prepared by the reaction of stoichiometric quantities of monobasic ammonium phosphate $NH_4H_2PO_4$ and diammonium phosphate, $(NH_4)_2HPO_4$, with hydrazine hydrate. Crystalline $N_2H_5H_2PO_4$ and $(N_2H_5)_2HPO_4$ are obtained by the removal of both ammonia gas and water, the former by suction and the latter by keeping the reaction product over P_2O_5 in a vacuum desiccator [10]:

$$NH_4H_2PO_4 + N_2H_4{\cdot}H_2O \rightarrow N_2H_5H_2PO_4 + H_2O + NH_3 \quad (2.26)$$

$$(NH_4)_2HPO_4 + 2N_2H_4{\cdot}H_2O \rightarrow (N_2H_5)_2HPO_4 + 2H_2O + 2NH_3 \quad (2.27)$$

The product has been characterized by chemical analysis and IR spectra (ν_{N-N} at 960 cm^{-1}). Table 2.7 lists the type of bond and the peak position for mono- and dihydrazinium phosphates. The very similar N–N stretching frequency characteristic of $N_2H_5^+$ in both these salts indicates the presence of the same hydrazinium cation.

Table 2.7 Infrared absorption frequencies (cm^{-1})[a] of hydrazine phosphates.

$N_2H_5H_2PO_4$	$(N_2H_5)_2HPO_4$	Assignment
—	3345m	Weakly H-bonded
1650m	1650w	N–H stretching frequency
—	1620w	NH_2 bending
—	1500w	NH_3^+ bending
1410s	1420w	$N_2H_5^+$ deformation
1250sh	1290w	NH_3^+ rocking
—	1135s	NH_2 rocking
967s	966s	N–N stretching
535s	560s	Torsional mode

[a] m = Medium, s = strong, sh = shoulder, w = weak.

2.4.4.2 *Thermal Properties*

Table 2.8 gives the TG and DTA results for monohydrazinium phosphate ($N_2H_5H_2PO_4$) and dihydrazinium phosphate, $(N_2H_5)_2HPO_4$, along with the associated products formed.

Figure 2.16a shows the TG and DTA curves of monohydrazinium phosphate. The first endotherm at 83 °C is due to melting of the salt. The endotherms at 107 and 119 °C are attributed to dehydration. On the basis of the TG weight loss the intermediate formed at the endotherm (107 °C) is proposed to be dihydrazinium pyrophosphate, $(N_2H_5)_2H_2P_2O_7$. Subsequently, this compound loses one molecule of water at the endotherm (119 °C) to form hydrazinium metaphosphate, $N_2H_5PO_3$. The weight loss observed (12.8%) in the TG curve is in fair agreement with the calculated weight loss of 13.8%. The corresponding ammonium salt, $NH_4H_2PO_4$, is reported to form a similar intermediate. The salt $N_2H_5PO_3$ further decomposes to $N_2H_4{\cdot}2HPO_3$ or $N_2H_6P_2O_6$ in the range 130–215 °C. This corresponds to a weak endotherm at 190 °C in the DTA curve. The exotherm at 266 °C in the DTA curve has been attributed to the formation of a syrupy liquid, metaphosphoric acid (HPO_3). The thermal decomposition of $N_2H_5H_2PO_4$ is similar to that of the ammonium salt, $NH_4H_2PO_4$.

In the TG and DTA curves of dihydrazinium phosphate (Figure 2.16b) the first endotherm, at 125 °C, is due to melting of $(N_2H_5)_2HPO_4$. The

Table 2.8 TG-DTA data of hydrazine phosphates.

Hydrazine salt	DTA peak temperature (°C)[a]	Thermogravimetry			Products
		Temperature range (°C)	% Weight loss		
			Obsd.	Calcd.	
$N_2H_5H_2PO_4$	83(−)	—	—	—	—
	107(−)	80–100	7.5	6.9	$(N_2H_5)_2H_2P_2O_7$
	119(−)	115–125	12.8	13.8	$N_2H_5PO_3 + H_2O$
	190(−)	130–215	25.5	26.2	$N_2H_5HP_2O_6 + N_2H_4$
	266(+)	220–320	42.0	39.4	$HPO_3 + NH_3$ and so on
$(N_2H_5)_2HPO_4$	125(−)	—	—	—	—
	156(−)	130–165	14.0	15.4	$(N_2H_5)_3HP_2O_7 + N_2H_4 + H_2O$
	187(−)	165–250	41.0	40.4	$N_2H_5HP_2O_6 + N_2H_4 + H_2O$
	266(+)	250–450	50.0	50.6	$HPO_3 + NH_3$ and so on

[a] (−) = Endotherm; (+) = exotherm.

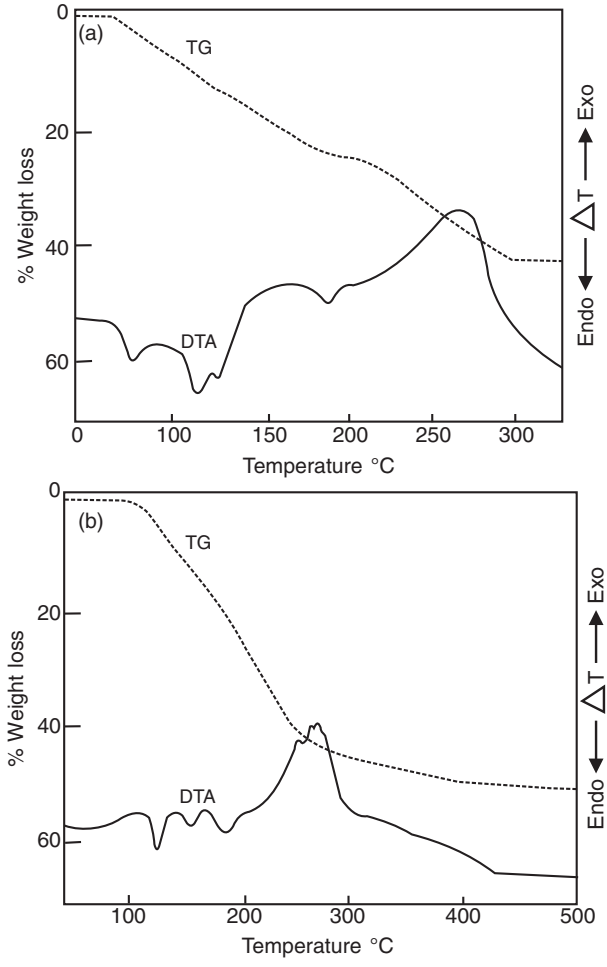

Figure 2.16 Simultaneous TG-DTA curves of (a) $N_2H_5H_2PO_4$ and (b) $(N_2H_5)_2HPO_4$. Adapted from Ref [10] with permission from Akademiai Kiado © 1983.

endotherms at 156 °C are attributed to dehydration and dehydrazination. The TG shows a weight loss of ~14% against the calculated weight loss of 15.4% for the formation of the intermediate $(N_2H_5)_3HP_2O_7$. Formation of the proposed intermediate is supported by the observed hydrazine content (34.1%) of the residue obtained after the endotherms at 156 °C (calculated 35.1%). The residue further loses weight continuously. The endotherm at 187 °C has been attributed to dehydration and dehydrazination with the formation of the compound $N_2H_6P_2O_6$ or $N_2H_4{\cdot}2HPO_3$.

The intermediate $N_2H_4{\cdot}2HPO_3$ is similar to that proposed for the endotherm at 190 °C during the thermal decomposition of $N_2H_5H_2PO_4$. The proposed intermediate finds support from the TG weight loss (observed 41.0% and calculated 40.7%) and the hydrazine content estimated for the residue obtained at 240 °C (observed 18.2% and calculated 16.6%). The exotherm at 266 °C in the DTA curve is attributed to the decomposition of $N_2H_4{\cdot}2HPO_3$ to metaphosphoric acid (HPO_3), which is a syrupy liquid. The TG curve also shows a weight loss of 50% required for the formation of HPO_3 (calculated 50.6%).

From the thermal decomposition of mono- and dihydrazinium phosphates it appears that both salts decompose through the intermediate formation of $N_2H_5HP_2O_6$ leading to metaphosphoric acid. Further, their decomposition patterns follow the corresponding decomposition pattern of ammonium salts. However, hydrazinium phosphate salts are of interest as superior flame retardants because of the hydrophilic nature or hygroscopic property of the hydrazinium ion. This supports dehydration more efficiently and limits the production of hydrocarbon gases, thereby promoting flame retardancy (see Chapter 6, Section 6.2.4).

2.4.5 Hydrazine Perchlorates – Hydrazinium Perchlorate ($N_2H_5ClO_4$), Hydrazinium Perchlorate Monohydrate ($N_2H_5ClO_4{\cdot}H_2O$), Hydrazinium Perchlorate Hemihydrate ($N_2H_5ClO_4{\cdot}0.5H_2O$), and Hydrazonium Perchlorate [$N_2H_6(ClO_4)_2$]

Hydrazine perchlorates are of interest due to their possible use as solid propellant oxidizers. Hydrazine forms two different perchlorates, depending on the degree of protonization. Hydrazinium (1+) perchlorate ($N_2H_5ClO_4$) forms $N_2H_5ClO_4$ monohydrate and hemihydrate. The divalent (2+) perchlorate forms hydrazonium perchlorate, $N_2H_6(ClO_4)_2$. Because both salts are high explosives, their preparation has to proceed with extreme precaution. Hydrazinium perchlorates can be sublimed under vacuum without decomposition.

2.4.5.1 Synthesis

The synthesis of anhydrous hydrazinium perchlorate ($N_2H_5ClO_4$), hydrazinium perchlorate monohydrate ($N_2H_5ClO_4{\cdot}H_2O$), and hydrazinium perchlorate hemihydrate ($N_2H_5ClO_4{\cdot}0.5H_2O$) has been discussed in Section 2.2.2.1.

Hydrazonium perchlorate is prepared by slowly adding a cooled solution of 85% hydrazine hydrate (54.4% N_2H_4) to a solution of 72% perchloric acid, providing a 10% excess of perchloric acid over the stoichiometrically required amount. Both solutions are precooled to 5 °C. Water is removed in a flash evaporator until hydrazonium perchlorate begins to precipitate. Its crystallization is permitted to proceed at temperatures slightly below room temperature for completion of the reaction. The precipitate is twice crystallized from 50% perchloric acid and dried in a vacuum drying pistol for 18 h at 80 °C. This salt is highly hygroscopic [31].

2.4.5.2 Infrared Spectra

Infrared spectra, thermal analysis, and conductivity studies of hydrazinium perchlorate hydrates indicate the presence of oxonium ion (H_3O^+) in these salts [32]. The IR spectrum of $N_2H_5ClO_4{\cdot}0.5H_2O$ shows absorption frequencies at 3400–3300, 1570, and 960 cm^{-1} (Figure 2.17a). Interestingly, additional bands occur at 3280, 2560, 2000, and 1570 cm^{-1}. These absorptions could be assigned by assuming the presence of oxonium (H_3O^+) ions or H-bonded water, since normal H_2O of hydration is not known to exhibit these absorptions. Table 2.9 lists the infrared spectral details of $N_2H_5ClO_4$.

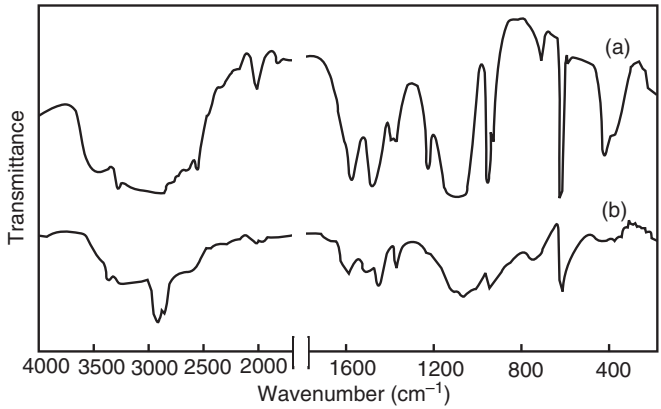

Figure 2.17 Infrared spectra of (a) $N_2H_5ClO_4{\cdot}0.5H_2O$ and (b) $N_2H_5ClO_4$. Reproduced from Ref [32] with permission of The Royal Society of Chemistry © 1983.

Table 2.9 Infrared absorption frequencies (cm^{-1})[a] of hydrazine perchlorates.

Assignment	$N_2H_5ClO_4$	$N_2H_5ClO_4 \cdot 0.5H_2O$	$N_2H_6(ClO_4)_2 \cdot 2H_2O$
ν(O–H) of H_2O		3600br, m	3600br
Hydrazine bands			
ν(N–H)	3380br, m	3400–3300br, m	3400–3300br, m
ν(N–N)	960m	960s	980s
Perchlorate bands			
ν_3	1100br, m	1100br, s	1100s
ν_4	620s	620s	620s
Oxonium bands (H_3O^+)			
ν_1		3280br	3240s
ν_3		2560br	2560m
ν_2		2000s	2060w, 1940w, 1810w
ν_4		1570br	1600s

[a] br = broad, m = medium, s = strong, w = weak.

2.4.5.3 Thermal Properties

The thermoanalytical data of hydrazine perchlorates are listed in Table 2.10.

The DTA of hydrazinium perchlorate hydrate shows an endotherm at 132 °C, which is attributed to its partial dehydration and melting. The second endothermic peak at 263 °C is due to decomposition. However, DTA in vacuum (Figure 2.18b) gives anhydrous hydrazinium perchlorate which further decomposes at 226 °C to ammonium perchlorate. The two endotherms at 240 and 290 °C have been assigned to ammonium perchlorate phase change and sublimation, respectively. This behavior is similar to that of hydrazonium perchlorate, which is known to decompose initially to hydrazinium perchlorate.

Table 2.10 Thermoanalytical data of hydrazine perchlorates.

Compound	DTA peak temperature (°C)[a]
$N_2H_5ClO_4 \cdot 0.5H_2O$	86(−), 224(+)
$N_2H_5ClO_4 \cdot H_2O$	132(−, m), 263(+), 132(−, m), 226(+), 240(−), 289(−)[b]
$N_2H_6(ClO_4)_2 \cdot 2H_2O$	100(−, m), 218(+)

[a] All DTA curves taken in air.
[b] In vacuum, m = melting, (−) = endotherm; (+) = exotherm.

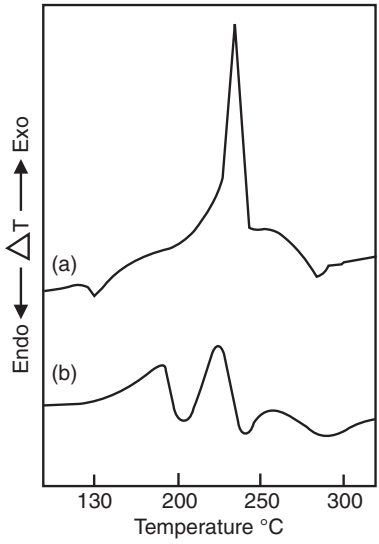

Figure 2.18 DTA curves of (a) $N_2H_5ClO_4{\cdot}H_2O$ and (b) $N_2H_6(ClO_4)_2$ in vacuum (below 20 Torr). Reproduced from Ref [34] with permission from Elsevier © 1980.

2.4.5.4 Nature of Water Present in Hydrazinium Perchlorate Hydrates, $N_2H_5ClO_4{\cdot}0.5H_2O$ and $N_2H_6(ClO_4)_2{\cdot}2H_2O$

It is evident from the literature that only a few hydrazine salts form hydrates, for example, $N_2H_5ClO_4{\cdot}0.5H_2O$, $N_2H_6(ClO_4)_2{\cdot}2H_2O$, $N_2H_6Br_2{\cdot}2H_2O$, $N_2H_6I_2{\cdot}2H_2O$, and so on. Very little work has been carried out to throw light on the nature of water present in hydrated hydrazine salts. The X-ray crystal structure of $N_2H_5ClO_4{\cdot}0.5H_2O$ has been investigated and, interestingly, the studies indicate that the water is H-bonded to $N_2H_5^+$ ions [33]. Surprisingly the IR spectra of hydrated hydrazine salts have not been documented, except for one article that reports the water bending frequency δH_2O at 1600 cm^{-1}. However, the nature of water present in $N_2H_5ClO_4{\cdot}0.5H_2O$ was not dealt with.

The nature of water in hydrazinium perchlorate was subsequently investigated and it is evident that that the band at 1570 cm^{-1} is due to both oxonium ion, $\delta(H_3O^+)$, and $\delta(NH_3^+)$ ion [32]. The inference that the oxonium ion is present in $N_2H_5ClO_4{\cdot}0.5H_2O$ is further substantiated by the reduced intensity of the band at 1570 cm^{-1}, and the absence of oxonium bands in anhydrous hydrazinium (1+) perchlorate, $N_2H_5ClO_4$. Although it is possible to dehydrate $N_2H_5ClO_4{\cdot}0.5H_2O$ by keeping the salt in an air oven at 100 °C for 5 h, the DTA results

show that only partial dehydration takes place at 71 °C (endotherm), where the weight loss is 1.72%. Complete dehydration would have resulted in a weight loss of 6.36%. This suggests that not all water is present as H_3O^+ ions, with some molecules being present as water of hydration. Since the chemical analysis corresponds to $N_2H_5ClO_4{\cdot}0.5H_2O$, the formula can be written as $(N_2H_5ClO_4)_2{\cdot}H_2O$ and $N_2H_5{}^+H_3O^+(ClO_4{}^-)_2{\cdot}N_2H_4$.

This formulation could explain all the observed infrared and thermal data. The concentration of oxonium ions appears to be small. Wide-line NMR (nuclear magnetic resonance) studies of this salt could not be used to establish this phenomenon since this spectrum showed a broad absorption at room temperature, making it is difficult to distinguish between N_2H_4 and H_3O^+ protons. In solution there is rapid exchange of these protons and only OH protons could be seen. Further evidence for the presence of H_3O^+ ions in $N_2H_5ClO_4{\cdot}0.5H_2O$ comes from conductivity experiments. The conductivity (σ) of $N_2H_5ClO_4{\cdot}0.5H_2O$ is found to be $4.8 \times 10^{-8}\,\Omega^{-1}\,cm^{-1}$, which is similar to that reported for hydronium alunite, $(H_3O, K)Al_3(SO_4)_2(OH)_6$, at 20 °C. The observed conductivity is attributed to the presence of oxonium ions. The conductivity of $H_3O^+ClO_4{}^-$ at 25 °C is $3 \times 10^{-4}\,\Omega^{-1}cm^{-1}$. Therefore, it appears that some of the water molecules are present as H_3O^+ ions in $N_2H_5ClO_4{\cdot}0.5H_2O$.

The assumption of H_3O^+ ion being present in hydrated hydrazine salts gains further support from infrared data of $N_2H_6(ClO_4)_2{\cdot}2H_2O$, which show IR absorptions at around $2000\,cm^{-1}$. This could be due to higher concentrations of H_3O^+ ions being present in these salts; they can be represented as:

$$N_2H_6(ClO_4)_2{\cdot}2H_2O \leftrightarrow (H_3O^+ClO_4{}^-)_2{\cdot}N_2H_4 \qquad (2.28)$$

Thermal analyses of the salts show that it is difficult to remove the water of hydration completely without decomposing the compound.

Accordingly, the TG-DTA studies (Table 2.11) of $N_2H_6(ClO_4)_2{\cdot}2H_2O$ show a partial weight loss of 5.33% at 100 °C; complete dehydration would have resulted in a weight loss of 15.65%. Therefore, infrared and DTA studies appear to indicate the presence of some oxonium ions in hydrazonium (2+) perchlorate dihydrate.

2.4.6 Hydrazine Perchlorate Ammoniates – $N_2H_5ClO_4{\cdot}NH_3$ and $N_2H_6(ClO_4)_2{\cdot}2NH_3$

The use of hydrazinium perchlorates as solid propellant oxidizers is greatly handicapped by their shock sensitivity, hygroscopic nature, and

Table 2.11 TG-DTA analysis of hydrazine perchlorates.

Salt	DTA peak temperature (°C)[a]	% Weight loss	Reaction
$N_2H_5ClO_4$	149(−, m)	—	Melting
—	263(+)	Explodes	Decomposition
—	353(+)	—	
$N_2H_5ClO_4{\cdot}0.5H_2O$	71(−)	1.72	Partial dehydration
—	263(+)	Explodes	Decomposition
—	353(+)	—	
$N_2H_6(ClO_4)_2{\cdot}2H_2O$	100(−)	5.33	Partial dehydration
—	273(+)	Explodes	Decomposition

[a] m = Melting, (−) = endotherm, (+) = exotherm.

incompatibility. Attempts were made to overcome such problems by stabilizing these compounds through the formation of adducts with ammonia. Hydrazine perchlorate-ammoniates behave like monopropellants having oxidizing (ClO_4^-) and reducing (N_2H_4, NH_3) groups in the same molecule.

2.4.6.1 Synthesis, Infrared Spectra, and Thermal Properties

The hydrazine perchlorate ammoniates $N_2H_5ClO_4{\cdot}NH_3$ and $N_2H_6(ClO_4)_2{\cdot}2NH_3$ are prepared by reaction of the respective hydrates with anhydrous NH_3 gas [34]. However, the products formed with liquid ammonia are mixtures of ammonium perchlorate and hydrazinium perchlorate. The reactions with ammonia gas can be written as follows:

$$N_2H_5ClO_4{\cdot}H_2O + NH_3 \rightarrow N_2H_5ClO_4{\cdot}NH_3 + H_2O + \text{heat} \qquad (2.29)$$

$$N_2H_6(ClO_4)_2{\cdot}2H_2O + 2NH_3 \rightarrow N_2H_6(ClO_4)_2{\cdot}2NH_3 + 2H_2O + \text{heat} \qquad (2.30)$$

The compositions of the ammoniates have been determined by hydrazine analysis. Hydrazinium perchlorate ammoniate is non-hygroscopic and can be stored without decomposition. It is also insensitive to shock and consequently preferred as a solid propellant.

Characteristic bands due to coordinated ammonia are observed at ~1400 and 750 cm^{-1} and are assigned to $\delta(NH_3)$ and $\rho_r(NH_3)$, respectively, in the IR spectrum. The spectrum shows an absorption at 3240 and 3380 cm^{-1} characteristic of ν_{N-H}, at 1400–1410 cm^{-1} corresponding to $\delta(NH_3)$, and at 750 cm^{-1} corresponding to $\rho_r(NH_3)$. All the perchlorate

bands corresponding to ν_3, ν_1, ν_4, and $\nu_{(N-N)}$ are observed at 1100, 945, 630, and 965 cm^{-1}, respectively.

Hydrazinium perchlorate ammoniate $N_2H_5ClO_4 \cdot NH_3$ exhibits an endotherm at 137 °C corresponding to melting, and an exothermic peak at 240 °C. The hydrazonium salt $N_2H_6(ClO_4)_2 \cdot 2NH_3$ melts at 100 °C and decomposes exothermically at 218 °C. The thermal properties of hydrazinium perchlorate ammoniate are quite different from those of the corresponding hydrate. The hydrazinium perchlorate ammoniate melts and decomposes exothermally and explosively; it is thermally less stable than the corresponding hydrate, as seen by the lower decomposition temperature in DTA. This is quite natural as $N_2H_5ClO_4 \cdot NH_3$ behaves like a monopropellant, having oxidizing (ClO_4^-) and reducing (N_2H_4, NH_3) groups in the same molecule.

2.5 HYDRAZINE SALTS OF ORGANIC ACIDS

In recent years, some new hydrazinium salts of organic acids have been prepared by neutralization of organic acids with hydrazine hydrate. The reaction of hydrazine hydrate and formic acid in an ice water bath has led to the isolation of a monoformate salt of hydrazine. This hydrazinium monoformate is reported to be a hydrogen donor with Raney nickel [35].

Hydrazinium salts with aromatic polycarboxylic acids such as hemimellitic (hml), trimellitic (tml), trimesic (tms), and pyromellitic (pml) acids have been prepared and their thermal behaviors studied [36]. Hydrazinium salts have been isolated of a) pyromellitic acid, such as $N_2H_5H_3$pml, $(N_2H_5)_2H_2$pml, $(N_2H_5)_3$Hpml, and $(N_2H_5)_4$pml$\cdot 3H_2O$, b) hemimellitic acid salts like $N_2H_5H_2$hml$\cdot 2H_2O$, c) trimellitic acid salts such as $N_2H_5H_2$tml$\cdot H_2O$, and d) trimesic acid salts like $N_2H_5H_2$tms$\cdot 2H_2O$. Hydrazinium hydrogen-trimellitate, hydrazinium trihydrogen-pyromellitate, hydrazinium dihydrogen pyromellitate, and hydrazinium hydrogen-pyromellitate are anhydrous salts whereas all other salts are hydrated. Each of these salts is water soluble. Significantly, hemimellitic acid forms only the monohydrazinium salt while trimellitic and trimesic acids form monohydrazinium and dihydrazinium salts.

The IR spectra of the hydrated salts of hydrazinium benzene tricarboxylates and hydrazinium pyromellitates display absorption bands due to O–H stretching of water, the carbonyl stretching frequencies of the carboxylate ion, and the N–N bond. The frequencies in the range 950–978 cm^{-1} due to N–N stretching are clear evidence of the presence of $N_2H_5^+$ ion in these salts.

Table 2.12 Infrared absorption frequencies (cm^{-1}) of [N_2H_5(Hoda)] and [$(N_2H_5)_2$oda] salts (Hoda = hydrogen-oxydiacetate and oda = oxydiacetate).

Assignment	N_2H_5(Hoda)	$(N_2H_5)_2$oda
ν(O–H)	3480, 3300	—
ν (N–H)	3210	3420, 3380, 3200
ν(C=O)	1751	—
ν_{asym}(COO)	1610	1585
ν_{sym}(COO)	1406	1410
ν(N–N)	953	960

Similarly, hydrazinium salts are reported with oxydiacetic acid, another class of dicarboxylic acid that also acts as a versatile complexing agent. Salts like hydrazinium hydrogen-oxydiacetate oxydiacetic acid, hydrazinium hydrogen-oxydiacetate [N_2H_5(Hoda)], and dihydrazinium oxydiacetate [$(N_2H_5)_2$oda] have been synthesized and their IR spectra and thermal data reported [37]. The infrared frequencies of the hydrazinium at 953 cm^{-1} and dihydrazinium salt at 960 cm^{-1} distinguish the two salts (Table 2.12).

Hydrazinium salts of 4,5-imidazole-dicarboxylic acid have also been prepared due to the attractive features of 4, 5-imidazole-dicarboxylic acid, which is sterically compact, planar, and has multi-donor coordination sites [38].

New hydrazinium salts arise from anions of 2-pyrazinecarboxylate (Hpc = 2-pyrazinecarboxylic acid) and 2,3-pyrazinedicarboxylate (H_2pdc = 2,3-pyrazinedicarboxylic acid) of the formulae N_2H_5pc, N_2H_5pc·H_2O, N_2H_5Hpdc, $(N_2H_5)_2$pdc·H_2O, and N_2H_5(Hpdc)·H_2pdc. Such salts are prepared by neutralization of aqueous hydrazine hydrate with the respective acids in appropriate molar ratios [39]. Interestingly, pyrazinedicarboxylic acid differs from simple aliphatic and aromatic dicarboxylic acids in terms of its salt-forming ability. Pyrazinedicarboxylic acid forms three types of hydrazinium salts in three different molar ratios. All the prepared salts undergo melting with decomposition. While hydrazinium salts of pyrazinecarboxylic acid show only endothermic decomposition, the salts of pyrazinedicarboxylic acid undergo both endothermic and exothermic decompositions. This is perhaps caused by one of the carboxylic groups being susceptible to decomposition due to the intramolecular hydrogen bond between the nitrogen atom and the carboxylic group in the ortho position.

Organic anion based hydrazinium salts have also been prepared by neutralization of aqueous hydrazine hydrate with 2,4-dichlorophenylacetic acid, phenoxyacetic acid, 2,4-dichlorophenoxyacetic acid,

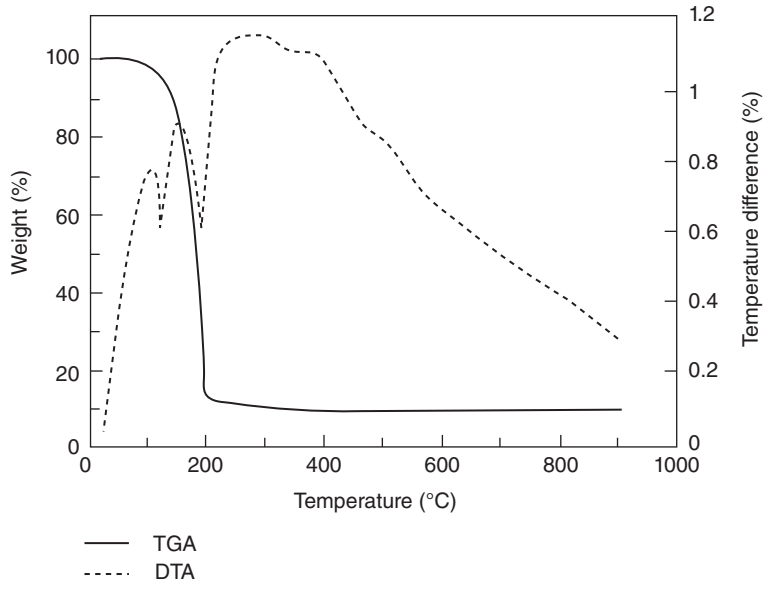

Figure 2.19 Simultaneous TG-DTA curves of hydrazinium picolinate.

diphenylacetic acid, and cinnamic acid. Similarly, hydrazonium salts of picolinic and nicotinic acids have also been prepared by neutralization of aqueous hydrazine hydrate with the respective acids [40].

Infrared spectra of all these salts register N–N stretching frequencies of $N_2H_5^+$ ion in the region 963–951 cm^{-1} and the frequencies of $N_2H_6^{2+}$ ion in the region 1047–1026 cm^{-1}. Thermal decomposition studies show that all compounds undergo melting with two- or three-step exothermic or endothermic decomposition through various intermediates and decompose completely into carbon residue as the final product. A typical thermogram of hydrazinium picolinate illustrates this (Figure 2.19).

2.6 SUMMARY

A novel simple method that exclusively gives N_2H_5A salts involves the reaction of solid ammonium salts with hydrazine hydrate. Several hydrazinium salts with the general formula N_2H_5A, where A = halide, sulfate, oxalate, sulfite, metavanadate, thiocyanate, acetate, sulfamate, picrate, nitrate, perchlorate, azide, organic carboxylates, and so on, have been prepared and characterized. Infrared spectra have been useful in identifying N_2H_4, $N_2H_5^+$, and $N_2H_6^{2+}$, which show characteristic absorptions of

Table 2.13 Melting points of hydrazine salts.

Hydrazine salt	Melting point (°C)
N_2H_5F	95
$N_2H_5HF_2$	184
$N_2H_6F_2$	184
N_2H_5Cl	89
$N_2H_6Cl_2$	155
N_2H_5Br	85
$N_2H_6Br_2$	195
N_2H_5I	127
$N_2H_6I_2{\cdot}2H_2O$	65
$N_2H_5ClO_4$	141
α-$N_2H_5NO_3$	62
β-$N_2H_5NO_3$	70
$N_2H_6(NO_3)_2$	103
$N_2H_5N_3$	82
$(N_2H_5)_2SO_4$	84
$(N_2H_5)_2SO_3$	71–73
$(N_2H_5)_2SO_4{\cdot}H_2O$	48–49
N_2H_5SCN	78–79
$N_2H_5C_6H_2(NO_2)_3O{\cdot}0.5H_2O$	160 (d)
$N_2H_5H_2PO_4$	83
$(N_2H_5)_2HPO_4$	114–116
$(N_2H_5)_2C_2O_4$	150
$N_2H_6SO_4$	265
$N_2H_6C_2O_4{\cdot}(N_2H_5HC_2O_4)$	200
$N_2H_5COOCH_3$	105
N_2H_5(Hoda)	130–153

ν_{N-N} at ~880, 960, and 1025 cm^{-1}, respectively. Most hydrazinium salts when heated decompose exothermically in air to the corresponding ammonium salts. Very few of these salts are stable at their melting points.

Some salient features of the present investigations of hydrazine salts are as follows:

- simple one-step preparation of hydrazinium bifluoride and bisulfite by the metathetical reaction of solid ammonium salts with hydrazine hydrate;
- an unusual solid-state rearrangement of N_2H_5SCN to $N_2H_3CSNH_2$ (thiosemicarbazide) when the former is isothermally heated at 100 °C for 9 h;
- new nitrogen-rich salts of hydrazine as potential green energetic oxidizers for use in solid propellant compositions;

- the nature of hydrogen bonding of water as oxonium ion (H_3O^+) in hydrazinium perchlorate hydrates as revealed by infrared and thermal measurements;
- formation of hydrazine perchlorate ammoniates to overcome the problems of hygroscopicity and incompatibility;
- synthesis of several new hydrazine salts with organic acids for the further formation of metal complexes.

Most of these hydrazinium salts melt below 200 °C, indicating they are ionic solids. Table 2.13 gives the melting points of some of the major salts.

REFERENCES

1. Audrieth, L.F. and Ogg, B.A. (1950) *The Chemistry of Hydrazine*, John Wiley, New York.
2. Soundararajan, R. (1979) The chemistry of hydrazine derivatives. Ph.D Thesis, Indian Institute of Science, Bangalore.
3. Vittal, J.J. (1981) Studies on hydrazinium salts. Ph.D Thesis, Indian Institute of Science, Bangalore.
4. Schmidt, E.W. (2001) *Hydrazine and its Derivatives: Preparation, Properties, Applications*, 2nd edn, John Wiley & Sons, Inc.
5. Milićev, S., Rahten, A., Borrmann, H., and Šiftar, J. (1997) Proton tunnelling in hydrazinium cations: vibrational spectra of $(N_2H_5)_2HGaF_6{\cdot}2H_2O$ and $(N_2H_5)_2HFeF_6{\cdot}2H_2O$ and crystal structure of $(N_2H_5)_2HFeF_6{\cdot}2H_2O$ at various temperatures. *Journal of Raman Spectroscopy*, **28**, 315–321.
6. Patil, K.C., Soundararajan, R., and Pai Verneker, V.R. (1978) Preparation and characterization of hydrazinium derivatives. *Proceedings of the Indian Academy of Sciences*, **87**, 281–284.
7. Hammerl, A., Klapotke, T.M., and Piotrowski, H. (2001) Synthesis and characterization of hydrazinium azide hydrazinate. *Propellants Explosives Pyrotechnics*, **26**, 161–164.
8. Patil, K.C., Vittal, J.P., and Patel, C.C. (1980) Preparation, characterization and thermal properties of hydrazinium derivatives Part III. *Proceedings of the Indian Academy of Sciences*, **89A**, 87–93.
9. Patil, K.C., Soundararajan, R., and Pai Verneker, V.R. (1979) Differential thermal analysis of hydrazinium derivatives. *Thermochimica Acta*, **31**, 259–261.
10. Patil, K.C., Vittal, J.P., and Patel, C.C. (1983) Syntheses and thermal decompositions of hydrazinium salts. *Journal of Thermal Analysis*, **26**, 191–198.
11. Fischer, N., Klapötke, T.M., Scheutzow, S., and Stierstorfer, J. (2008) Hydrazinium 5-aminotetrazolate: an insensitive energetic material containing 83.72% nitrogen. *Central European Journal of Energetic Materials*, **5**, 3–18.
12. Tao, G.H., Guo, Y., Joo., Y.H. *et al.* (2008) Energetic nitrogen-rich salts and ionic liquids: 5-aminotetrazole (AT) as a weak acid. *Journal of Materials Chemistry*, **18**, 5524–5530.
13. Fischer, N., Klapötke, T.M., and Stierstorfer, J. (2011) Hydrazinium nitriminotetrazolates. *Zeitschrift fur Anorganische und Allgemeine Chemie*, **637**, 1273–1276.

14. Dendage, P.S., Sarwade, D.B., Asthana, S.N., and Singh, H. (2001) Hydrazinium nitroformate (HNF) and HNF based propellants: A review. *Journal of Energetic Materials*, **19**, 41–78.
15. Kiselev, G.V. and Gritsan, P.N. (2009) Theoretical study of the primary processes in the thermal decomposition of hydrazinium nitroformate. *Journal of Physical Chemistry A*, **113**, 11067–11074.
16. Huang, H., Zhou, Z., Song, J. *et al.* (2011) Energetic salts based on dipicrylamine and its amino derivative. *Chemistry - A European Journal*, **17**, 13593–13602.
17. Manelis, G.B., Nazin, G.M., Yu.I. Rubstov, and Strunin, V.A. (2003) *Thermal Decomposition and Combustion of Explosives and Propellants*, CRC Press, Taylor and Francis, London.
18. Klapötke, T.M. (2011) *Chemistry of High-energy Materials*, Walter de Gruyter GmbH & Co. KG, Berlin/New York.
19. Göbel, M. and Klapötke, T.M. (2007) Potassium-, ammonium-, hydrazinium-, guanidinium-, aminoguanidinium-, diaminoguanidinium-, triaminoguanidinium- and melaminiumnitroformate - synthesis, characterization and energetic properties. *Zeitschrift fur Anorganische und Allgemeine Chemie*, **633**, 1006–1017.
20. Badgujar, D.M., Talawar, M.B., Asthana, S.N., and Mahulikar, P.P. (2008) Advances in science and technology of modern energetic materials: an overview. *Journal of Hazardous Materials*, **151**, 289–305.
21. Klapötke, T.M. (2007) New nitrogen rich explosives, in *High Energy Density Materials* (eds D.M.P. Mingos and T.M. Klapötke), Springer-Verlag, New York.
22. Hooper, J.B., Borodin, O., and Schneider, S. (2011) Insight into hydrazinium nitrates, azides, dicyanamide, and 5-azidotetrazolate ionic materials from simulations and experiments. *The Journal of Physical Chemistry, B*, **115**, 13578–13592.
23. Patil, K.C., Budkuley, J.S., and Pai Verneker, V.R. (1979) Thermoanalytical studies of hydrazidocarbonic acid derivatives. *Journal of Inorganic & Nuclear Chemistry*, **41**, 953–955.
24. Hammerl, A., Klapötke, T.M., Nöth, H. *et al.* (2001) $[N_2H_5]^{2+}[N_4C\text{-}N{=}N\text{-}CN_4]^{2-}$: A new high-nitrogen high-energetic material. *Inorganic Chemistry*, **40**, 3570–3575.
25. Ciezak-Jenkins, J. (2012) The high pressure characterization of energetic materials: dihydrazinium 5, 5′-azotetrazolate dihydrate. Shock Compression of Condensed Matter –2011 AIP Conference Proceedings. vol. 1426, 1425–1428.
26. Devipriya, S., Ranjithkumar, V., and Sundararajan, V. (2011) Hydrazine-1,2-diium bis(3-carboxy-4-hydroxybenzenesulfonate) tetrahydrate. *Acta Crystallographica, Section E*, **67**, o1236–o1237.
27. Patil, K.C., Soundararajan, R., and Pai Verneker, V.R. (1979) Synthesis and characterization of a new fluoride derivative of hydrazine, $N_2H_5HF_2$. *Inorganic Chemistry*, **18**, 1969–1971.
28. Patil, K.C. and Vittal, J.P. (1982) Synthesis and characterization of a new sulfate derivative of hydrazine, $N_2H_5HSO_4$. *Journal of the Chemical Society, Dalton Transactions*, **11**, 2291–2293.
29. Patil, K.C. and Vittal, J.P. (1982) DSC studies on the phase transformation of hydrazonium sulfate. *Materials Chemistry*, **7**, 577–586.
30. Gajapathy, D., Govindarajan, S., and Patil, K.C. (1983) Thermal decomposition of hydrazinium hydrogen oxalate and dihydrazinium oxalate. *Thermochimica Acta*, **60**, 87–92.

31. Nesamani, C. (1983) Studies on high energy hydrazine compounds. Ph.D Thesis, Indian Institute of Science, Bangalore.
32. Patil, K.C., Nesamani, C., and Pai Verneker, V.R. (1983) The nature of water in hydrazine salt hydrates. *Journal of the Chemical Society, Dalton Transactions*, 2047–2049.
33. Liminga, R. (1967) Hydrogen bond studies: the crystal structure of hydrazinium perchlorate hemihydrate, $N_2H_5ClO_4 \cdot (1/2)H_2O$. *Acta Chemica Scandinavica*, **21**, 1217–1228.
34. Patil, K.C., Nesamani, C., and Pai Verneker, V.R. (1980) Thermal analysis of hydrazine perchlorate hydrates and ammoniates. *Thermochimica Acta*, **36**, 91–95.
35. Gowda, S. and Channe Gowda, D. (2002) Application of hydrazinium monoformate as new hydrogen donor with Raney nickel: a facile reduction of nitro and nitrile moieties. *Tetrahedron*, **35**, 2211–2213.
36. Vairam, S. and Govindarajan, S. (2004) New hydrazinium salts of benzene tricarboxylic and tetracarboxylic acids–preparation and their thermal studies. *Thermochimica Acta*, **414**, 263–270.
37. Yasodhai, S. and Govindarajan, S. (2000) Hydrazinium oxydiacetates and oxydiacetate dianion complexes of some divalent metals with hydrazine. *Journal of Thermal Analysis and Calorimetry*, **62**, 737–745.
38. Premkumar, T. and Govindarajan, S. (2002) The chemistry of hydrazine derivatives-thermal behavior and characterization of hydrazinium salts and metal hydrazone complexes of 4,5-imidazoledicarboxylic acid. *Thermochimica Acta*, **386**, 35–42.
39. Premkumar, T., Govindarajan, S., and Wei-Ping, Pan. (2003) Preparation, spectral and thermal studies of pyrazinecarboxylic acids and their hydrazinium salts. *Proceedings of the Indian Academy of Sciences - Chemical Sciences*, **115**, 103–111.
40. Manimekalai, R., Sinduja, C.R., and Kalpanadevi, K. (2012) Preparation, analytical, IR spectral, and thermal studies of some new hydrazinium carboxylates. *International Journal of Inorganic Chemistry*. doi: 10.1155/2012/624374.

3

Metal Hydrazines

Dasaratharam Gajapathy[1] and Tanu Mimani Rattan[2]
[1]*K.M.G. College of Arts & Science, Gudiyathum, India*
[2]*Department of Physics, Sri Sathya Sai Institute of Higher Learning, Prasanthi Nilayam, India*

3.1 INTRODUCTION

Hydrazine, with its two lone pairs of electrons on nitrogen, can act as a good unidentate, bidentate, or bridged ligand in forming complexes with metal ions. However, in certain cases, it can also act as a solvated ligand similar to water, which is present as a hydrated molecule in many compounds. For instance, treating hydrated metal salts with alcoholic hydrazine hydrate results in metal salt hydrazines. Under such conditions, the addition of hydrazine as a solvated ligand is a readily reversible phenomena, as these salts can undergo hydrazination and dehydrazination cycles within temperatures as low as 130 °C, similar to that of water [1,2]. In addition, the synthesis of metal hydrazine complexes is straightforward; addition of alcoholic hydrazine hydrate to an aqueous solution of metal salts instantaneously yields such complexes. Literally, hundreds of metal hydrazine complexes have been prepared and investigated in the literature; Schmidt's book lists all of them in one of his longest cited tables [1].

Inorganic Hydrazine Derivatives: Synthesis, Properties and Applications, First Edition.
Edited by K. C. Patil and Tanu Mimani Rattan.

Of late, research activity in metal hydrazine chemistry has focused on increasing the range of various inorganic and organic anions that can coordinate to the metal atoms as well as be solvated by hydrazine. Such complexes are considered as precursors to nano-size metal powders, metal oxides, and mixed metal oxides or metal sulfides that form at relatively much lower temperatures [3–7]. This precursor technique supersedes the normally practiced ceramic method. The latter method is limited by its requirements of repeated grinding accompanied by high firing temperature, which may cause the loss of some materials, leading to non-stoichiometry in the final product. Details of investigations on applications of products prepared from such precursors are discussed in Chapter 6.

Common synthetic methods practiced for the preparation of metal hydrazines, and some single-crystal structures, are discussed briefly in Chapter 1. A direct method of synthesis of metal hydrazines has been developed that involves adding metal powders to hydrazine salts (preparation of salts discussed in Chapter 2). Details of the synthesis of several simple and mixed metal hydrazines by this and other methods, along with their spectral characterization and thermal reactivity, are now described.

3.2 METAL HYDRAZINES – $MX(N_2H_4)_n$, M = METAL, X = SO_4, SO_3, N_3, NCS, NO_3, ClO_4, RCOO, AND SO ON, ($n = 1$–3)

3.2.1 Metal Isothiocyanate Hydrazines $[M(NCS)_2(N_2H_4)_2]$

The synthesis of metal hydrazine complexes with thiocyanate or isothiocyanate as anions can be carried out by the following methods [8]. In the first case, stoichiometric quantities of metal(II) salts like chlorides or sulfates of Mn, Fe, Co, Ni, Zn, and Cd in an alcohol–water mixture (1 : 1 by volume) are added to hydrazinium thiocyanate. The latter is metathetically formed by the reaction of $NH_4SCN + N_2H_4{\cdot}H_2O$ (1 : 1 mole ratio) (Chapter 2):

$$MX_2 + 2N_2H_5SCN \rightarrow [M(NCS)_2(N_2H_4)_2] + 2HX \qquad (3.1)$$

where M = Mn, Fe, Co, Ni, Zn, Cd, and Mg.

Alternatively, the metal salt is mixed with ammonium thiocyanate and hydrazine hydrate in 1 : 2 : 2 mole ratio:

$$MX_2 + 2NH_4SCN + 2N_2H_4{\cdot}H_2O \rightarrow [M(NCS)_2(N_2H_4)_2] + 2NH_4X + 2H_2O \quad (3.2)$$

where M = Mn, Fe, Co, Ni, Zn, Cd, and Mg.

In another method, metal powders free from an oxide film are added directly to a solution of N_2H_5SCN in hydrazine hydrate. Owing to the high acidic nature of hydrazinium thiocyanate formed *in situ*, the metal powders dissolve instantaneously with the liberation of hydrogen gas, forming metal isothiocyanate hydrazines:

$$M^0 + 2NH_4SCN + N_2H_4{\cdot}H_2O \rightarrow [M(NCS)_2(N_2H_4)_2] + 2H_2 + H_2O \quad (3.3)$$

where M = Mn, Fe, Co, Ni, Zn, Cd, and Mg.

In reactions represented by (3.3), the metal powders exhibit different magnitudes of exothermicity. Magnesium reacts violently, while reactions with other metals such as Fe, Co, Ni, and Zn are hastened by magnetically stirring the solution and raising the temperature to 40–45 °C. The precipitated complexes are separated from the unreacted metal powders by centrifugation followed by filtration or by removing them through magnetic separation. The obtained complexes are washed with water and alcohol and allowed to dry over anhydrous calcium chloride in a desiccator. The reaction of N_2H_5SCN with copper salts results in the reduction of Cu(II) to Cu(I) or metallic copper, depending on the experimental conditions.

Interestingly, in all these synthesis methods, although one starts with the thiocyanate salt, with hydrazine as one of the ligands, the metal chelates to the N atom of the anion to form complexes of the rearranged isothiocyanate type. This formation of metal isothiocyanate hydrazines is confirmed by chemical analysis and infrared spectra (Table 3.1).

The IR spectral data show that the thiocyanate is bonded to the metal through nitrogen, as evidenced by the characteristic frequencies of ν_{C-N}, ν_{C-S}, and δ_{NCS}, at around 2075, 790, and 480 cm^{-1}, respectively (Figure 3.1). The N–N stretching frequency seen around 960 cm^{-1} indicates the bridging of N_2H_4 between the metal ions.

The metal–nitrogen frequencies ν_{M-N} of hydrazine and ν_{M-N} of isothiocyanate are observed at around 400 and 350 cm^{-1}, respectively. Since two different frequencies are observed, the two metal–nitrogen

Table 3.1 Infrared absorption frequencies (cm^{-1}) of $[M(NCS)_2(N_2H_4)_2]$.

Assignments	Mn	Fe	Co	Ni	Zn	Cd	Mg
N–H stretching	3215	3200	3200	3220	3212	3238	3224
C–N stretching	2088	2070	2068	2092	2075	2070	2084
NH_2 bending	1593	1590	1586	1593	1597	1587	1593
NH_2 wagging	1339	1340	1338	1342	1342	1342	1313
NH_2 twisting	1140	1150	1152	1164	1153	1140	1156
N–N stretching	951	960	965	975	958	960	963
C–S stretching	793	796	794	795	792	788	802
NH_2 asym rocking	569	582	595	619	600	580	586
NH_2 sym rocking	494	515	539	575	536	502	523
NCS bending	479	480	480	478	482	477	489
M–N (of N_2H_4) stretching	330	354	367	395	354	335	383
M–N (of NCS) stretching	312	331	342	362	315	300	343

bonds are clearly not of equal strength. It appears that the M–NCS bond is weaker than the M–N_2H_4 bond and so it is inferred that the geometry around the metal ion is not perfectly octahedral. The molecular symmetry around the metal ion is therefore D_{4h}. The IR assignment is in good agreement with the proposed polymeric structure shown in Figure 3.2.

The structural geometry of these complexes is further confirmed by Mössbauer spectroscopy conducted on the iron complex. The Mössbauer

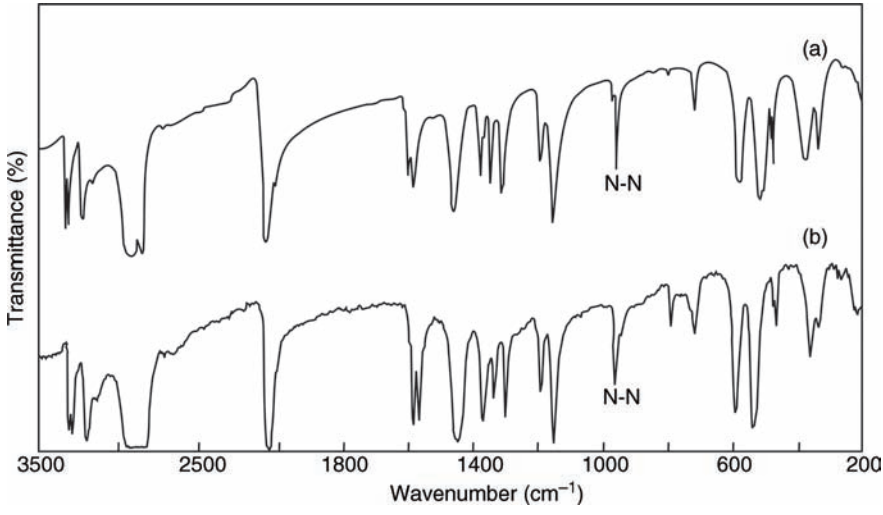

Figure 3.1 Infrared spectra of (a) $[Mg(NCS)_2(N_2H_4)_2]$ and (b) $[Co(NCS)_2(N_2H_4)_2]$. Ph.D Thesis of Vittal, J.J. under Prof. K. C. Patil at Indian Institute of Science.

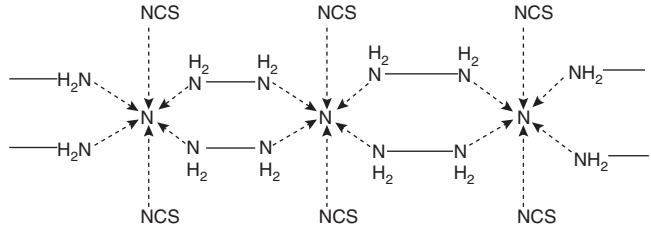

Figure 3.2 Polymeric structure of metal isothiocyanate hydrazine. Adapted from Ref. [8] with permission from the Indian Academy of Sciences © 1983.

spectrum of $[Fe(NCS)_2(N_2H_4)_2]$ (Figure 3.3) shows a two finger pattern with an isomer shift (IS) value of $1.03\,mm\,s^{-1}$ and a quadrupole splitting (QS) of $1.54\,mm\,s^{-1}$. The observed values indicate the presence of high-spin Fe^{2+} in a distorted octahedral environment and are comparable with those of $[Fe(IQ)_4(NCS)_2]$, where IQ = isoquinoline (IS = 1.37 and $QS = 1.50\,mm\,s^{-1}$).

The magnetic susceptibility of the complexes is measured by the standard Gouy method at room temperature. Table 3.2 gives the magnetic moment data.

Thermoanalytical data of the complexes $[M(NCS)_2(N_2H_4)_2]$ are listed in Table 3.3.

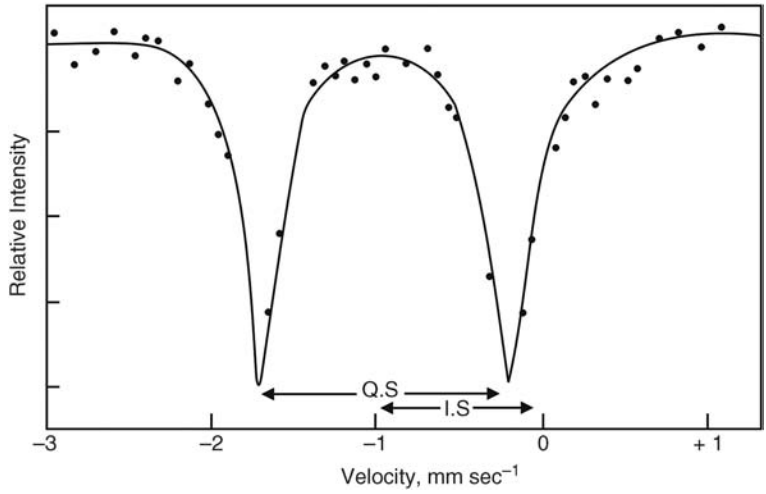

Figure 3.3 Mössbauer spectrum of $[Fe(NCS)_2(N_2H_4)_2]$. Ph.D Thesis of Vittal, J.J. under Prof. K. C. Patil at Indian Institute of Science.

Table 3.2 Color of metal isothiocyanate hydrazine complexes and magnetic moment data.

$[M(NCS)_2(N_2H_4)_2]$	Color	μ_{eff} (BM) 23 °C	
		Obsd.	Calcd. for spin only formula
M = Mn	White	5.87	5.91
M = Fe	White	4.91	4.89
M = Co	Pink	4.80	3.87
M = Ni	Blue	2.82	2.82
M = Zn	White	—	—
M = Cd	White	—	—
M = Mg	White	—	—

All the complexes initially lose hydrazine, forming the metal isothiocyanates:

$$3[M(NCS)_2(N_2H_4)_2] \xrightarrow{190-250°C} 3M(NCS)_2 + 8NH_3 + 2N_2 \qquad (3.4)$$

Table 3.3 Thermal analysis data of $[M(NCS)_2(N_2H_4)_2]$.

M	DTA peak temperature (°C)[a]	Thermogravimetry			Products
		TG temperature range (°C)	% Weight loss		
			Obsd.	Calcd.	
Mn	197 (+)	180–250	27.26	27.25	$Mn(NCS)_2$
	503 (+)	400–550	40.20	40.88	Mn(SCN)(CN)
	—	460–340	48.85	48.89	$2MnSO_4 \cdot Mn_2O_3$
Fe	173 (+)	150–180	39.30	40.72	Fe(NCS)(CN)
	450 (+)	350–500	—	66.18	Fe_2O_3
Co	190 (+)	180–220	40.60	40.20	Co(NCS)(CN)
	443 (+)	380–530	50.0	55.29	$CoSO_4 \cdot Co_2O_3$
Ni	226 (+)	220–280	39.20	40.29	Ni(NCS)(CN)
	485 (+)	410–550	54.82	55.00	$NiO + NiSO_4$
Zn	198 (+)	190–260	25.00	26.08	$Zn(NCS)_2$
	503 (+)	550–900	67.30	66.87	ZnO
Cd	203 (+)	190–270	29.30	32.85	Cd(NCS)(CN)
	485 (+)	450–650	49.00	50.60	CdS
Mg	261 (+)	230–360	47.00	47.00	Mg(NCS)(CN)
	—	360–500	72.50	72.44	MgS
	—	500–650	79.50	80.39	MgO

[a] (+) = Exotherm.

They further decompose to form the corresponding metal sulfides in the temperature range 450–620 °C, according to the reaction:

$$M(NCS)_2 \rightarrow MS + (CN)_2 + S \tag{3.5}$$

The metal sulfides are oxidized in air to the corresponding sulfates or oxides, depending on the metal ions. For example, $Zn(NCS)_2$ is oxidized directly to zinc oxide, whereas $Mn(NCS)_2$ decomposes to Mn(NCS)(CN) at 400–550 °C and finally to a mixture of $MnSO_4$ and Mn_2O_3 in the temperature range 560–640 °C. In the case of iron, cobalt, nickel, cadmium, and magnesium, the intermediates have been identified as M(NCS)(CN). These subsequently decompose to the respective metal sulfides slowly, at higher temperatures (~350–650 °C). In air, the intermediate Fe(NCS)(CN) is oxidized to Fe_2O_3, while Mg(NCS)(CN) and $Cd(NCS)_2$ decompose to the corresponding metal sulfides. In the magnesium case, magnesium sulfide is further oxidized to a mixture of the corresponding sulfate and oxide.

The thermal stability of the complexes is usually determined by the strength of the metal–ligand bonds. The IR frequencies of NH_2 twisting, symmetric, and asymmetric rocking, N–N stretching of N_2H_4, and M–N stretching of both M–NCS and M–N_2H_4 complexes are found to obey the Irving–Williams order for bivalent metal complexes, that is, $Mn^{2+} < Fe^{2+} < Co^{2+} < Ni^{2+} > Zn^{2+} > Cd^{2+}$.

The DTA (differential thermal analysis) peak temperature or the TG (thermogravimetry) inception temperature of decomposition in general can be taken as a measure of the thermal stability of the metal complexes. The order of thermal stability of $[M(NCS)_2(N_2H_4)_2]$ as indicated by the tabulated data is the following:

$$Mn^{2+} < Fe^{2+} < Co^{2+} < Ni^{2+} > Zn^{2+} > Cd^{2+}$$

Accordingly, there seems to be correlation between thermal stability and M–N bond strength of N_2H_4 or NCS.

3.2.2 Metal Sulfate Hydrazines [$MSO_4 \cdot xN_2H_4$]

Metal sulfate hydrazines $MSO_4 \cdot xN_2H_4$ (M = Mn, Co, Ni, Zn, and Cd; $x = 2$–3) are prepared by the addition of alcoholic hydrazine hydrate to an aqueous saturated solution of metal sulfates. The complexes precipitate instantaneously; they are then filtered, washed with alcohol, and dried

over P_2O_5 in a vacuum desiccator. For copper and iron, the reduction of Cu^{2+} to metallic copper, and the formation of $Fe(OH)_2$ with iron sulfate, hinder formation of the respective metal sulfate hydrazines by this method [9]. However, the dissolution of iron metal powder in a solution of $(N_2H_5)_2SO_4$ in $N_2H_4{\cdot}H_2O$ gives a solid, which presumably could be $FeSO_4{\cdot}xN_2H_4$ as it spontaneously ignites during suction filtration.

Chemical analysis revealed that all the metals form metal sulfate hydrazines except manganese, which forms a hydrated complex. Further, the number of hydrazine molecules in the complexes varies from two to three.

Infrared spectra of the complexes show a ν_{N-N} stretching frequency of N_2H_4 in the region 960–980 cm^{-1}, indicating the presence of bridged hydrazine. The sulfate ion appears to be free (ionic) as seen by the infrared absorption bands at 1100 (ν_3) and 600 cm^{-1} (ν_4). Coordination of the sulfate groups of the metal ion lowers the T_d symmetry of the SO_4^{2-} ion and, hence, the splitting of these bands occurs.

Table 3.4 summarizes the simultaneous TG (thermogravimetry)-DTG (differential thermogravimetry)-DTA (differential thermal analysis) results of the complexes. It can be seen that all the sulfate hydrazines lose their coordinated hydrazine exothermically in more than one step to yield the corresponding metal sulfates. Nickel and zinc complexes give a mixture of metal sulfide and sulfate. Figure 3.4 shows a typical thermogram of $MnSO_4{\cdot}2N_2H_4{\cdot}H_2O$.

Table 3.4 Thermal analysis data of $MSO_4{\cdot}xN_2H_4$.

Compound	Thermogravimetry			DTA peak temperature (°C)[a]	Product
	Temperature range (°C)	% Weight loss			
		Obsd.	Calcd.		
$MnSO_4{\cdot}2N_2H_4{\cdot}H_2O$	125–175	7.70	7.73	120 (+)	$MnSO_4{\cdot}2N_2H_4$
	175–245	21.20	21.46	180 (+)	$MnSO_4{\cdot}N_2H_4$
	245–360	35.20	35.60	300 (+)	$MnSO_4$
$CoSO_4\,2.75N_2H_4$	185–275	26.00	26.35	200 (+)	$CoSO_4\,0.75N_2H_4$
	275–385	36.00	36.22	325 (+)	$CoSO_4$
$NiSO_4\,2.5N_2H_4$	230–300	26.00	27.27	280 (+)	$NiSO_4\,0.5N_2H_4$
	300–485	41.50	40.91	455 (+)	NiS:$NiSO_4$ (1 : 3)
$ZnSO_4{\cdot}3N_2H_4$	100–165	19.00	18.65	110 (+)	$ZnSO_4\,1.5N_2H_4$.
	235–310	25.30	24.86	245 (+)	$ZnSO_4\,N_2H_4$
	310–425	45.00	45.50	350 (+)	ZnS:$ZnSO_4$ (1 : 2)
$CdSO_4{\cdot}3N_2H_4$	155–285	21.00	21.00	175 (+)	$CdSO_4\,N_2H_4$
	285–385	31.50	31.52	330 (+)	$CdSO_4$

[a] (+) = Exotherm.

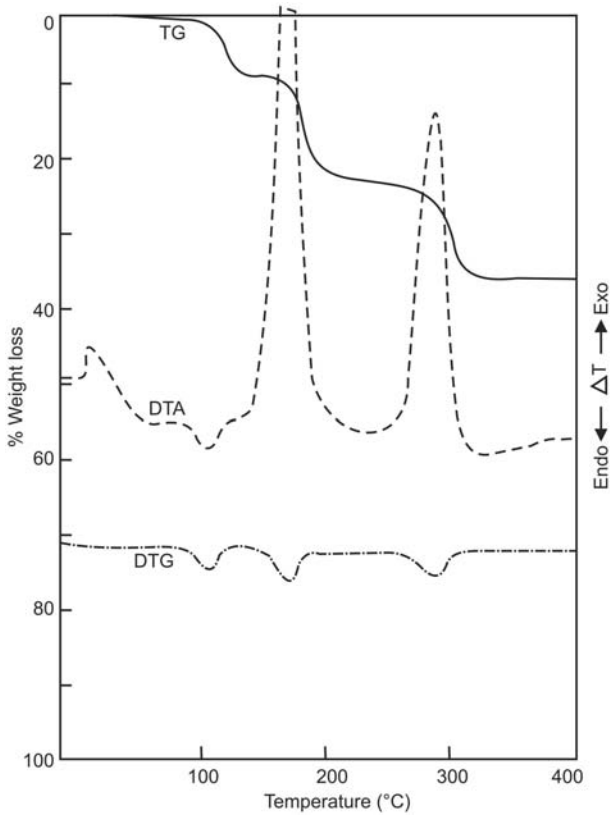

Figure 3.4 Simultaneous TG-DTG-DTA of $MnSO_4 \cdot 2N_2H_4 \cdot H_2O$. Adapted from Ref. [9] with permission from Elsevier © 1986.

3.2.3 Metal Formate Hydrazines [$M(HCOO)_2(N_2H_4)_2$]

Metal formate hydrazines $M(HCOO)_2(N_2H_4)_2$ (where M = Mn, Co, Ni, Zn, and Cd) are prepared by the addition of excess hydrazine hydrate to the corresponding metal formate hydrates [10]. The reaction is instantaneous with the evolution of heat:

$$M(HCOO)_2 \cdot (H_2O)_2 + 2N_2H_4 \cdot H_2O \rightarrow M(HCOO)_2(N_2H_4)_2 + 4H_2O \tag{3.6}$$

where M = Mn, Co, Ni, Zn, and Cd.

The complexes obtained are filtered off, washed with alcohol first and then with diethyl ether, and dried over phosphorus pentoxide.

Table 3.5 Infrared absorption frequencies (cm^{-1}) of $M(HCOO)_2(N_2H_4)_2$.

Assignment	Mn	Co	Ni	Zn	Cd
N–H stretching	3320, 3290	3340, 3310	3350, 3320	3340, 3320	3340, 3310
C–H stretching	2175	2820	2820	2750	2820
NH_2 bending	1620	1640	1650	1645	1620
COO asymmetric stretching	1570	1605	1615	1620	1600
C–H bending	1380	1405	1410	1410	1410
COO symmetric stretching	1290	1340	1350	1380	1380
NH_2 wagging	1190	1185	1190	1185	1160
N–N stretching	970	980	985	980	980
OCO bending	790	780	775	780	760
NH_2 asymmetric rocking	615	650	685	650	650
NH_2 symmetric rocking	525	580	625	580	550
M–N Stretching	328	382	410	318	335

Table 3.5 lists the infrared spectral data of these complexes.

The spectral data clearly show the presence of bridged hydrazine by the characteristic absorption at 980 cm^{-1}. Based on the absorption frequencies of symmetric and asymmetric stretching of –OCO– it has been concluded that M–O bonds in these complexes are essentially electrostatic. The formate ion is reported to be monodentate and the magnetic susceptibility values obtained are evidence for the bridging nature of hydrazine and the monodentate nature of the formate ion.

It is important to distinguish the decomposition of metal formates *vis-á-vis* metal hydrazine formates using thermogravimetry and differential thermal analysis. Metal formates are known to decompose exothermically in a single step, to the respective metal oxide or metal, depending upon the decomposition conditions. However, the thermal decomposition of metal hydrazine formate complexes in air occurs in two steps, with the exception of nickel. Initially, a loss of hydrazine takes place endothermically, followed by exothermic decomposition of the dehydrazinated metal formates to give the corresponding metal oxides. In the case of manganese, the weight loss observed for the first step corresponds to the loss of one hydrazine molecule, followed by decomposition to the respective oxides. However, the nickel complex decomposes in a single step to give a mixture of nickel oxide and nickel metal. Table 3.6 summarizes the results of TG and DTA studies of $M(HCOO)_2(N_2H_4)_2$.

Table 3.6 Thermal analysis data of $M(HCOO)_2(N_2H_4)_2$.

M	DTA peak temperature (°C)[a]	Thermogravimetry			Product
		Temperature range (°C)	% Weight loss		
			Obsd	Calcd	
Mn	170(−)	110–178	17.00	15.31	$Mn(HCOO)_2N_2H_4$
	192(−)	—	—	—	—
	272(+)	197–320	72.00	62.20	MnO, Mn_2O_3
Co	235(+)	210–400	44.00	43.00	CoC_2O_4
	254(+)	—	—	—	$CoCO_3$
	460(−)	250–400	60.65	60.03	CoO
Ni	275(+)	250–270	43.00	43.12	NiC_2O_4
	285(+)	—	—	—	$NiCO_3$
	650(−)	280–650	64.66	64.30	NiO + Ni
Cu	100(+)	90–105	—	—	CuC_2O_4
	120(+)	—	63.59	62.76	CuO
Zn	300(+)	240–260	57.60	—	ZnC_2O_4
	325(+)	—	—	—	$ZnCO_3$
	550(−)	300–550	63.17	61.50	ZnO

[a] (−) = Endotherm; (+) = exotherm.

Metal formate hydrazines exhibit autocatalytic combustion behavior when heated rapidly. Although TG/DTA shows endothermic decomposition in the beginning, combustion of these complexes is exothermic, since both hydrazine and formate undergo oxidation simultaneously.

3.2.4 Metal Acetate Hydrazines $[M(CH_3COO)_2(N_2H_4)_2]$

Metal acetate hydrazines $M(CH_3COO)_2(N_2H_4)_2$ (M = Mn, Co, Ni, Zn, and Cd) are synthesized by the reaction of freshly prepared metal acetate hydrates with excess hydrazine hydrate [11]. The reaction is instantaneous and yields hydrazine complexes as shown by (3.7):

$$M(CH_3COO)_2 \cdot xH_2O + 2N_2H_4 \cdot H_2O \rightarrow M(CH_3COO)_2(N_2H_4)_2 + (x+2)H_2O \quad (3.7)$$

where M = Mn, Co, Ni, Zn, or Cd.

The products of the reaction are filtered, washed with alcohol first and then with diethyl ether, and dried over P_2O_5 in a vacuum desiccator.

Table 3.7 lists infrared spectral data of these complexes.

Table 3.7 Infrared absorption frequencies (cm^{-1}) of $M(CH_3COO)_2(N_2H_4)_2$.

Assignment	Mn	Co	Ni	Zn	Cd
N–H stretching	3300	3300	3300	3320	3330
COO asymmetric stretching	1620	1625	1625	1625	—
COO symmetric stretching	1420	1420	1420	1420	1420
$\Delta\nu[\nu_{asym}(COO^-)\text{-}\nu_{sym}(COO^-)]$	(190)	(195)	(195)	(190)	(195)
C–O stretching	1535	1535	1535	1535	1535
CH_3 deformation	1295	1305	1305	1305	—
NH_2 twisting + wagging	1120	1145	1155	1140	1150
CH_3 rocking	1015	1015	1015	1010	1015
N–N stretching	965	975	980	975	970
C–C stretching	920	925	925	920	920
NH_2 rocking	645	655	655	650	650
COO rocking	620	620	615	—	620

The metal ion in these complexes has been reported to possess an octahedral coordination and the acetate group is coordinated to the metal through an oxygen atom as a monodentate ligand. The large separation of 190 cm^{-1} in the asymmetric and symmetric stretching frequencies of COO^- supports this argument.

Table 3.8 summarizes simultaneous TG-DTA data of the complexes.

Table 3.8 Thermal analysis data of $M(CH_3COO)_2(N_2H_4)_2$.

M	Thermogravimetry			DTA peak temperature (°C)[a]	Product
	Temperature range (°C)	% Weight loss			
		Obsd.	Calcd.		
Mn	130–170	21.00	20.26	150 (+)	$MnCH_3COO)_2$ 0·5N_2H_4
	170–205	27.00	27.01	190 (+)	$Mn(CH_3COO)_2$
	205–280	64.50	63.31	275 (+)	MnO_2
Co	160–190	20.00	19.92	180 (+)	$Co(CH_3COO)_2$ 0·5N_2H_4
	190–220	27.00	26.56	222 (+)	$Co(CH_3COO)_2$
	220–315	66.00	66.69	305 (+)	Co_3O_4
Ni	190–215	49.00	—	205 (+)	—
	215–245	52.00	51.10	230 (+)	$Ni + Ni(CH_3COO)_2$
	245–335	69.00	68.97	330 (+)	NiO
Zn	150–195	26.00	25.87	130 (+)	$Zn(CH_3COO)_2$
	195–310	46.00	46.49	280 (+)	$ZnO + Zn(CH_3COO)_2$
	310–450	69.00	67.10	410 (+)	ZnO
Cd	115–170	14.00	16.30	165 (+)	$Cd(CH_3COO)_2$ 0.5N_2H_4
	170–215	21.00	21.74	200 (+)	$Cd(CH_3COO)_2$
	215–395	57.00	56.38	385 (+)	CdO

[a] (+) = Exotherm.

The features of the thermal analysis data show that metal acetate hydrazines decompose exothermically, in three steps, to their respective metal oxides. Manganese, cobalt, zinc, and cadmium complexes decompose through the formation of their corresponding metal acetates, while the nickel complex decomposes through a mixture of nickel metal and nickel acetate (Figure 3.5). The zinc complex however, loses both hydrazine molecules in a single step, while Mn, Co, and Cd complexes lose hydrazine in two steps. The metal oxide formation temperatures from the decomposition of metal acetate hydrazine complexes occur at 275–385 °C. These are lower than those reported for metal acetate hydrates, which occur at 350–400 °C.

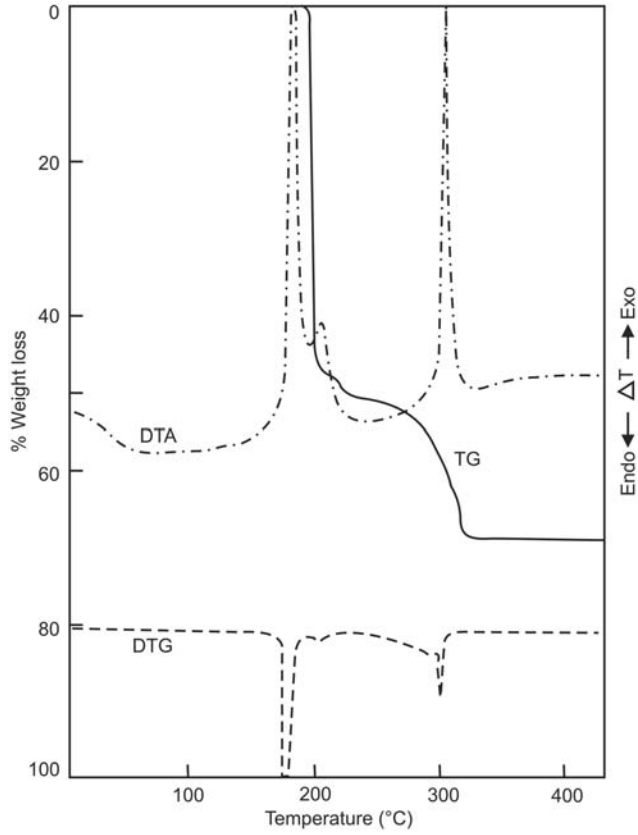

Figure 3.5 Simultaneous TG-DTG-DTA curves of $Ni(CH_3COO)_2(N_2H_4)_2$. Adapted from Ref. [11] with permission from Elsevier © 1986.

3.2.4.1 *Mixed Metal Acetate Hydrazines*

The procedure for synthesizing mixed metal acetate hydrazines is to add an excess of alcoholic hydrazine hydrate to a solution containing a mixture of the corresponding metal acetates, in the molar ratio of 1 : 2 [12]. The precipitated complexes are filtered, washed with ethanol and then diethyl ether, and stored in a vacuum desiccator over P_2O_5. This method has been used to prepare solid solutions of mixed metal acetate hydrazines of the type $M_{1/3}Co_{2/3}(CH_3COO)_2(N_2H_4)_2$ ($M = Ni^{2+}$ or Zn^{2+}), which are precursors to nickel and zinc cobaltites.

As the structure of metal acetate hydrazine complexes appears to be isomorphous, the formation of mixed metal hydrazines takes place easily. This is further confirmed by the identical infrared spectra of $Ni_{1/3}Co_{2/3}(CH_3COO)_2(N_2H_4)_2$ with the nickel and cobalt acetate hydrazine complexes (Figure 3.6).

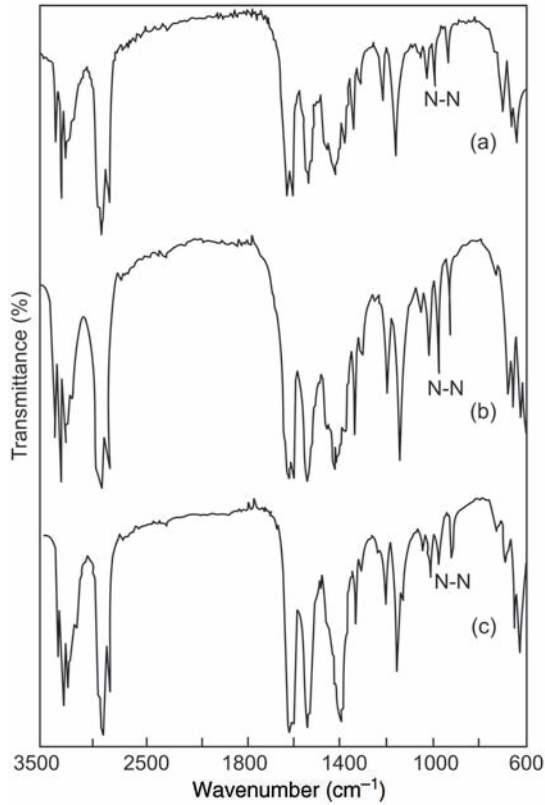

Figure 3.6 Infrared spectra of (a) $Ni(CH_3COO)_2(N_2H_4)_2$, (b) $Co(CH_3COO)_2(N_2H_4)_2$, and (c) $Ni_{1/3}Co_{2/3}(CH_3COO)_2(N_2H_4)_2$. Adapted from Ref. [12] with permission from Elsevier © 1987.

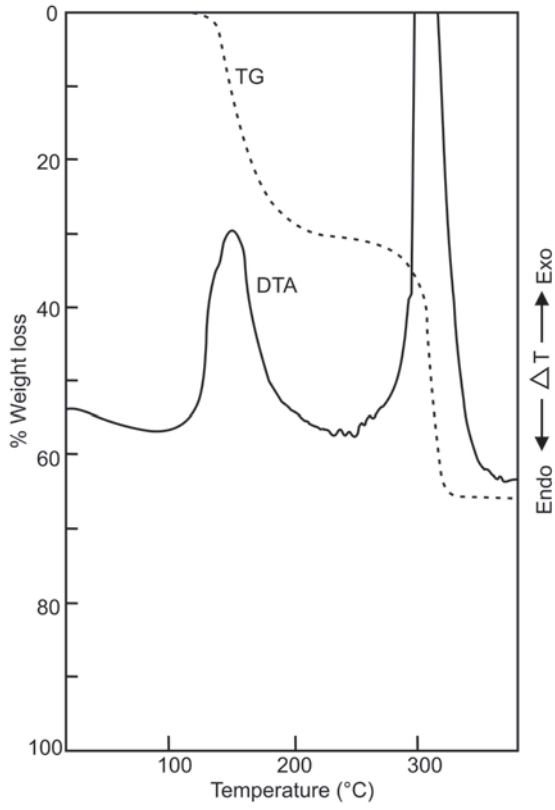

Figure 3.7 Simultaneous TG-DTA curves of $Zn_{1/3}Co_{2/3}(CH_3COO)_2(N_2H_4)_2$. Adapted from Ref. [12] with permission from Elsevier © 1987.

These precursors decompose exothermically in the temperature range 165–345 °C to yield the corresponding cobaltites, as depicted by the thermal analyses (Figure 3.7) [13]. Table 3.9 gives the thermal data of the mixed metal acetate hydrazines.

3.2.5 Metal Oxalate Hydrazines $[MC_2O_4(N_2H_4)_2]$

Metal oxalate hydrazines $MC_2O_4(N_2H_4)_2$ (M = Mg, Mn, Fe, Co, Ni, Cu, Zn, and Cd) are prepared by the following methods [13,14].

Table 3.9 Thermal analysis data of $M_{1/3}Co_{2/3}(CH_3COO)_2(N_2H_4)_2$.

Complex	Thermogravimetry	DTA peak temperature (° C)[a]	Product
	Temperature range (°C)		
$Ni_{1/3}Co_{2/3}(CH_3COO)_2(N_2H_4)_2$	180–205	190(+)	—
	205–220	210(+)	—
	220–325	325(+)	$NiCo_2O_4$
$Zn_{1/3}Co_{2/3}(CH_3COO)_2(N_2H_4)_2$	165–245	195(+)	$Zn_{1/3}Co_{2/3}(CH_3COO)_2$
	245–345	340(+)	$ZnCo_2O_4$

[a] (+) = Exotherm.

3.2.5.1 *Synthesis*

Reaction of Metal Oxalate Hydrates with Hydrazine Hydrate

Freshly prepared metal oxalate hydrates are treated with stoichiometric quantities of hydrazine hydrate. As the mixture is thoroughly stirred the reaction takes place instantaneously with the evolution of heat. In some cases, a change of color in the original salt is observed due to complex formation (Table 3.10).

Reaction of Aqueous Solutions of Metal Salts with Alcoholic Hydrazine Hydrate

The conventional procedure for preparing metal oxalate hydrazine complexes is to treat an aqueous solution of the metal salt with an alcoholic solution of hydrazine hydrate:

$$MC_2O_4{\cdot}2H_2O + 2N_2H_4{\cdot}H_2O\ (\text{alcoholic}) \rightarrow MC_2O_4(N_2H_4)_2 + 4H_2O \tag{3.8}$$

where M = Mn, Fe, Co, Ni, Zn, and Cd.

Table 3.10 Change of color due to hydrazine complex formation.

Metal	Hydrate	Hydrazine
Iron	Bright yellow	Light yellow
Cobalt	Light pink	Dark pink
Nickel	Light green	Blue

Reaction of Metal Powder with Ammonium Oxalate in Hydrazine Hydrate

When a metal powder M^0 is added to a solution of ammonium oxalate in hydrazine hydrate it dissolves with the evolution of gases like hydrogen and ammonia, together with liberation of heat. The product obtained is $MC_2O_4(N_2H_4)_2$:

$$M^0 + (NH_4)_2C_2O_4 + 2N_2H_4{\cdot}H_2O \rightarrow MC_2O_4(N_2H_4)_2 + 2H_2O + H_2 + 2NH_3 \quad (3.9)$$

where M = Mg, Mn, Fe, Co, Ni, Zn, Cu and so on.

When M^0 is copper, the complex $CuC_2O_4{\cdot}2N_2H_4$ forms but is highly unstable. It loses a molecule of hydrazine in air to form the monohydrazine ($CuC_2O_4{\cdot}N_2H_4$) as the stable product.

Reaction of Aqueous Solutions of Metal Salts with Ammonium Oxalate in Hydrazine Hydrate

When an aqueous solution of the metal salt of Fe, Co, and Ni is mixed with ammonium oxalate in hydrazine hydrate, the corresponding metal oxalate hydrazines are precipitated:

$$MX_2 + (NH_4)_2C_2O_4 + 2N_2H_4{\cdot}H_2O \rightarrow MC_2O_4(N_2H_4)_2 + 2H_2O + 2NH_4X \quad (3.10)$$

3.2.5.2 Spectral and Thermal Analysis

The main feature of the infrared data (Table 3.11) of these complexes is that hydrazine is present as a bridged ligand, as evidenced by the characteristic absorption at 960 cm^{-1}. The oxalate ion is bonded to the metal as bidentate ligand.

Table 3.11 Infrared absorption frequencies (cm^{-1}) of $MC_2O_4(N_2H_4)_2$.

Assignment	Mn	Fe	Co	Ni	Cu	Zn	Cd	Mg
N–H stretching	3330	3300	3300	3320	3480	3300	3310	3200
COO asym. stretching	1695	1660	1665	1635	1660	1660	1650	1610
COO sym. stretching	—	1305	—	1320	1370	1320	—	1320, 1280
NH_2 twisting + wagging	1310	1290	1300	1295	1345	1300	1310	1100
N–N stretching	965	980	960	980	990	960	960	955
C–C stretching	920	—	925	925	—	920	920	—
OCO bending	785	775	780	780	795	780	775	820

Single-step decomposition occurs in the case of Mn and Fe complexes, as the decomposition temperatures (T_d) of MnC_2O_4 ($T_d = 275\,°C$) and FeC_2O_4 ($T_d = 235\,°C$) coincide with the temperature at which N_2H_4 is lost from $M(N_2H_4)_2^{2+}$ complexes. However, as we go from Co ($T_d = 260\,°C$) to Ni ($T_d = 350\,°C$) to Cu ($T_d = 310\,°C$) the decomposition temperature of MC_2O_4 varies from 260–350 °C and the hydrazine molecules are lost successively without decomposition of the metal oxalates. The exothermic decomposition of hydrazine is enough to ignite the metal oxalates. On the other hand, the decomposition of Zn and Cd complexes appears to follow an entirely different path and is comparable to that of Mg. Unlike other transition metal ions, Zn and Cd have a completely filled d-shell and the decomposition of $ZnC_2O_4(N_2H_4)_2$ and $CdC_2O_4(N_2H_4)_2$ seems to be similar to $MgC_2O_4(N_2H_4)_2$. Thermal analysis data of the compounds are summarized in Table 3.12. Interestingly, Zn and Mg oxalate hydrazine decompose through a dinitrogen complex ($Zn/Mg\dot{C}O_2NH_2N_2$) intermediate, which has been identified by a characteristic N≡N frequency at 2200 cm^{-1} in the IR spectra. The observed difference in the

Table 3.12 Thermal analysis data of $MC_2O_4(N_2H_4)_2$.

M	Thermogravimetry			DTA peak temperature (°C)[a]	Product
	Temperature range (°C)	% Weight loss			
		Obsd	Calcd		
Mn	204–225	60.9	61.9	217(+)	Mn_2O_3
Fe	180–310	60.2	61.6	202(+)	Fe_2O_3
Co	204–258	16.1	15.2	209(+)	$CoC_2O_4{\cdot}N_2H_4$
	258–358	60.4	61.2	262(+)	Co_3O_4
Ni	226–258	14.0	15.2	219(+)	$NiC_2O_4{\cdot}N_2H_4$
	258–331	32.0	30.4	244(+)	NiC_2O_4
	331–419	63.0	64.6	290(+)	NiO
Cu	152–181	17.0	17.4	148(+)	CuC_2O_4
	181–370	58.0	56.6	274(+)	CuO
Zn	120–215	16.0	14.7	216(+)	$ZnC_2O_4{\cdot}N_2H_4$
	215–350	30.0	29.4	301(+)	$Zn\dot{C}O_2{\cdot}NH_2N_2$[b]
	350–466	64.0	62.6	406(+)	ZnO
Cd	169–181	11.0	12.1	182(+)	$CdC_2O_4{\cdot}N_2H_4$
				291(+)	—
	248–456	51.0	51.4	353(+)	CdO
Mg	32–215	19.0	18.2	205(+)	$MgC_2O_4{\cdot}N_2H_4$
	215–484	34.0	36.1	407(+)	$Mg\dot{C}O_2NH_2N_2$[b]
	484–688	78.0	77.1	530(+)	MgO

[a] (+) = Exotherm.
[b] Radical.

decomposition pattern and reactivity is due to the thermal stability of the anhydrous metal oxalates and the nature of $M-N_2H_4$ bonding in these complexes.

Transition metal oxalate hydrazines when touched with a glowing splinter undergo auto-combustion to yield the corresponding metal oxides. For example, when a strand of $FeC_2O_4(N_2H_4)_2$ is ignited in air, the maximum temperature of the condensed phase is 560 °C although the ignition temperature is only 180 °C. Another factor responsible for the autocatalytic behavior of these complexes can be attributed to the catalytic activity of the transition metal oxides formed *in situ*. This aspect is studied by carrying out temperature profile studies on one of the complexes like $FeC_2O_4(N_2H_4)_2$ and investigating the mechanism of its deflagration [15].

3.2.5.3 Temperature Profile Studies

When a system sustains self-combustion, temperature profile measurements provide an understanding of the chemical transformations occurring therein. The surface temperature of the material during the autocatalytic combustion process is determined by such measurements. The accuracy of these measurements depends upon the velocity of flame propagation and the fineness of the thermocouple bead. In the present investigation iron oxalate hydrazine is pelletized and cylindrical strands of 1 cm breadth and width were made. Small holes are drilled to accommodate the thermocouple beads (diameter 0.1 mm) and the thermocouple is embedded inside the strand such that the bead remains at the center. On heating, the solid front undergoes a linear regression and a mild flame is seen traveling across the vertical strand. A time (t) versus temperature (T) plot for four runs is obtained as shown in Figure 3.8.

The heat release rate (dq/dt) at any instance from the temperature profile curve is calculated using the following equation:

$$\frac{dq}{dt} = \overline{C}_p \frac{(T_2 - T_1)}{t_2 - t_1} \tag{3.11}$$

Here, T_2 and T_1 are the temperatures corresponding to time t_2 and t_1, respectively, and $\overline{C}_p$ is the average heat capacity of the solid. The points on the profile curve corresponding to T_1 and T_2 are chosen very closely so as to obtain an instantaneous rate at these points on the curve. The average data points from four temperature profile measurements are computed to

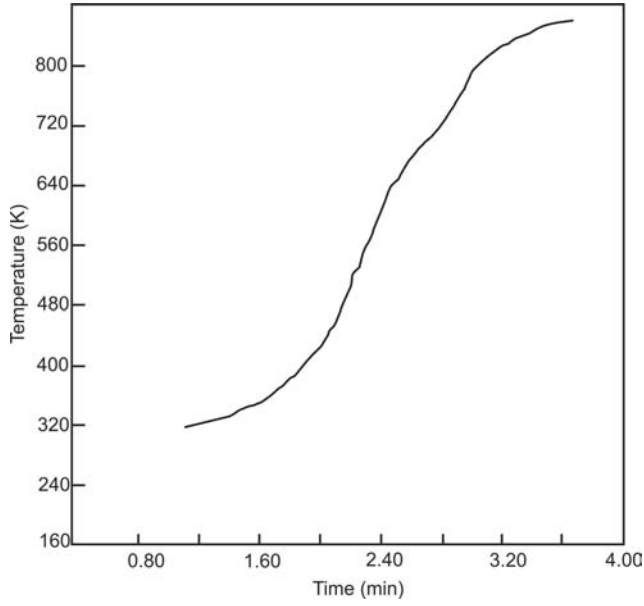

Figure 3.8 Temperature profile for the deflagration of $Fe(N_2H_4)_2C_2O_4$. Reproduced from Ref. [15] with permission from Elsevier © 1985.

obtain a plot of dq/dt versus "t" while $\overline{C}_p$ is determined from DSC. The value is found to be $1.824\,J\,g^{-1}$ for the temperature range 25–75 °C. The average dq/dt versus "t" plot for four measurements is shown along with DSC (differential scanning calorimetry) and DTA data for comparison in Figure 3.9. Although the DTA and TG show single-step decomposition, the temperature profile analysis establishes three steps of decomposition. These steps are successive loss of the hydrazine molecules followed by decomposition of the anhydrous oxalate. Although the decomposition temperature is around 200 °C, the temperature profile shows that the maximum temperature attained is ~600 °C.

From the temperature–time experimental curve, the adiabatic temperature (T_{ad}) at any instant of reaction can be calculated using the following equation:

$$T_{ad} = \frac{t_r}{t_d - t_r} T(t_1) + \frac{t_d}{t_d - t_r} T(t_2) + \frac{1}{t_d - t_r} \int_{t_1}^{t_2} T\,dt \qquad (3.12)$$

where t_r is the rise time of the rise zone and t_d is the decay time of the decay zone.

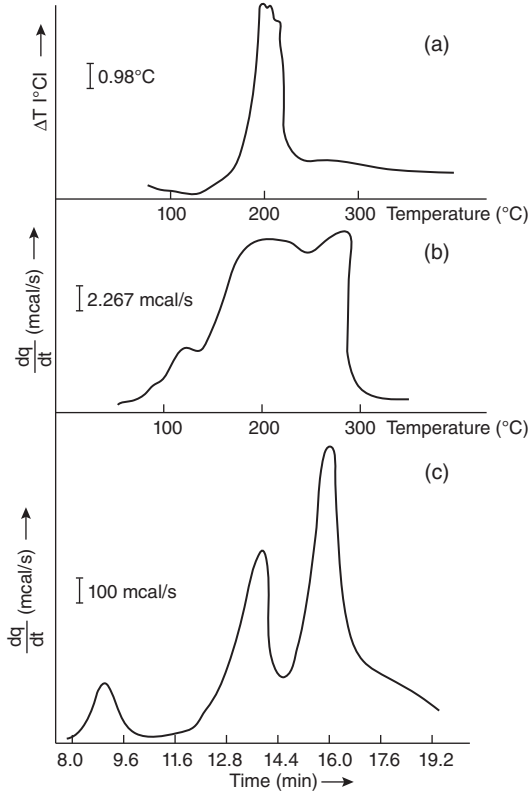

Figure 3.9 (a) DTA, (b) DSC, and (c) temperature profile traces for the decomposition of $Fe(N_2H_4)_2C_2O_4$. Adapted from Ref. [15] with permission from Elsevier © 1985.

The exothermicity for each stage is calculated using the expression $\Delta H = \overline{C}_p T_{ad}$. Table 3.13 presents the calculated values of ΔH at various break points in the temperature profile corresponding to various steps.

The enthalpy change for the steps involved has been calculated from the temperature profile data and is in agreement with the values obtained from DSC and combustion calorimetry.

3.2.6 Mixed Metal Oxalate Hydrazines

Mixed metal oxalate hydrazines containing iron as the common metal are prepared either from metal powders or metal salts. Stoichiometric quantities of the respective metal powders are dissolved in a solution of

Table 3.13 Heat of formation data.

Compound	ΔH_f^* (kJ mol^{-1})
FeC_2O_4 (s)	−870.3
Fe_2O_3 (s)	−821.3
CO_2 (g)	−393.5
H_2O (g)	−241.8
NH_3 (g)	−45.94
N_2H_4 (l)	+51.26
$FeC_2O_4(N_2H_4)_2$ (s)[a]	−319.1[a]
$FeC_2O_4(N_2H_4)$ (s)[a]	−523.2[a]

[a] From temperature profile study.

ammonium oxalate in hydrazine hydrate. After dissolution of the metal powders alcohol is added to precipitate out the complex. The precipitate is further washed with alcohol and diethyl ether:

$$M^0 + 2Fe^0 + 3(NH_4)_2C_2O_4(aq) + xN_2H_4{\cdot}H_2O \rightarrow MFe_2(C_2O_4)_3(N_2H_4)_x + 6NH_3 + xH_2O + 3H_2 \quad (3.13)$$

where M = Mn, Co, Ni, and Zn ($x = 6$) and M = Mg ($x = 5$).

Mixed metal oxalate hydrazines of Mg and Co can also be obtained by the reaction of mixed metal oxalate hydrates $MFe_2(C_2O_4)_3{\cdot}6H_2O$ with excess hydrazine hydrate [16,17].

Similar to the above, mixed metal oxalate hydrazines can be prepared with cobalt being the common metal. Stoichiometric quantities of the respective metal powders of magnesium and nickel are dissolved in a solution of ammonium oxalate in hydrazine hydrate. It takes a few hours for the metal powders to completely disperse into the solution. After their complete dissolution, alcohol is added to precipitate out the complex. The precipitate is further washed with alcohol and diethyl ether [18]:

$$Mg^0 + 2Co^0 + 3(NH_4)_2C_2O_4(aq) + 5N_2H_4{\cdot}H_2O \rightarrow MgCo_2(C_2O_4)_3(N_2H_4)_5 + 6NH_3 + 5H_2O + 3H_2 \quad (3.14)$$

$$Ni^0 + 2Co^0 + 3(NH_4)_2C_2O_4(aq) + 6N_2H_4{\cdot}H_2O \rightarrow NiCo_2(C_2O_4)_3(N_2H_4)_6 + 6NH_3 + 6H_2O + 3H_2 \quad (3.15)$$

The IR spectra of mixed metal oxalate hydrazines confirm the presence of coordinated oxalate and hydrazine groups. The spectra have characteristic absorptions of bidentate oxalate at 1650, 1320, 1300, and

Table 3.14 Infrared absorption frequencies (cm^{-1}) of $MCo_2(C_2O_4)_3(N_2H_4)_x$.

Assignment	Mg	Ni
N–H stretching	3320	3320
OCO asym. stretching	1650	1640
OCO asym. stretching	1320	1345
NH_2 twisting	1205	1205
N–N stretching	960	970
OCO bending	830	820
NH_2 rocking	650	660
M–O stretching	560	545
OCO bending + CCO bending	500	500
M–N stretching	365	350

780 cm^{-1} and bidentate bridging hydrazine at 3320, 3150, 1205, 1120, and 960 cm^{-1} (Table 3.14).

These complexes are crystalline solids with characteristic colors. As the reactions are carried out under reducing conditions, iron is present as Fe^{2+} in these complexes. The presence of Fe^{2+} makes them rather susceptible to atmospheric oxidation and they are unstable and decompose on storage, losing hydrazine. They need to be prepared and stored in an atmosphere of nitrogen. Table 3.15 gives the thermal decomposition temperatures of the complexes.

These complexes undergo a single-step decomposition, forming the corresponding ferrites (MFe_2O_4) (Figure 3.10). In the case of the magnesium complex only, a second exothermic peak at about ~350 °C is observed, which is attributed to the recrystallization of the $MgFe_2O_4$. All the other complexes result in ferrite formation at temperatures as low as 150–160 °C. On the other hand, mixed metal oxalate hydrates do not yield ferrites at such low temperatures. An example is magnesium oxalate

Table 3.15 Thermal analysis data of $MFe_2(C_2O_4)_3(N_2H_4)_x$.

Compound	TG temperature range (°C)	DTA peak temperature (°C)[a]	Product
$MgFe_2(C_2O_4)_3(N_2H_4)_5$	100–230	125 (+), 349 (+)	$MgFe_2O_4$
$MnFe_2(C_2O_4)_3(N_2H_4)_6$	110–204	128 (+)	$MnFe_2O_4$
$CoFe_2(C_2O_4)_3(N_2H_4)_6$	145–230	152 (+)	$CoFe_2O_4$
$NiFe_2(C_2O_4)_3(N_2H_4)_6$	149–240	164 (+)	$NiFe_2O_4$
$ZnFe_2(C_2O_4)_3(N_2H_4)_6$	147–250	157 (+)	$ZnFe_2O_4$

[a] (+) = Exotherm.

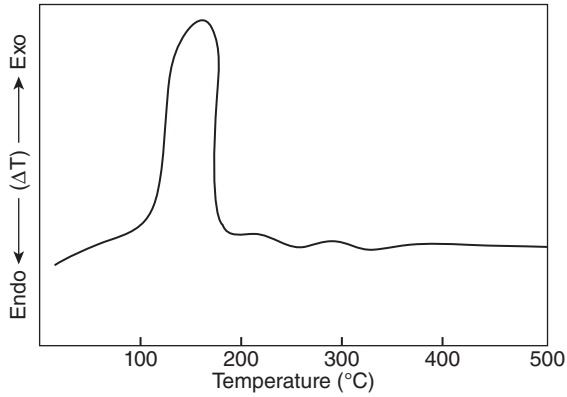

Figure 3.10 DTA of $CoFe_2(C_2O_4)_3(N_2H_4)_6$. Adapted from Ref. [16] with permission from Elsevier © 1983.

hexahydrate, which gives a mixture of α-Fe_2O_3, MgO, and magnesium ferrite ($MgFe_2O_4$) only above 1000 °C. Complex formation with hydrazine makes it possible to obtain ferrites from the oxalate precursors at low temperatures of ~150 °C. This shows that the exothermic decomposition of hydrazine is vital for the formation of ferrites at low temperatures.

The mixed metal oxalate hydrazines exhibit autocatalytic behavior, and the product of combustion is the spinel MFe_2O_4. Interestingly, the precursors ignite while undergoing suction filtration if allowed to dry.

Thermal analysis of the complexes $MgCo_2(C_2O_4)_3(N_2H_4)_5$ and $NiCo_2(C_2O_4)_3(N_2H_4)_6$ show that both decompose exothermically in air, with the peak temperatures being 272 and 223 °C, respectively. Thermogravimetric data confirm that in both cases decomposition occurs in a single step. Observed weight losses in TG are in agreement with the formation of cobaltites $MgCo_2O_4$ (observed weight loss is 62%; required loss is 63.7%) and $NiCo_2O_4$ (observed weight loss 63%; required loss is 61.9%). Once ignited, the combustion is self-sustained. The autocatalytic behavior and the low temperature decompositions are due to the exothermic decomposition of oxalate and hydrazine in air.

3.2.7 Metal Sulfite Hydrazine Complexes

The synthesis of metal sulfite hydrazine complexes involves two steps. Firstly, hydrazine hydrate (99–100%) is saturated with SO_2 gas and the resulting product, hydrazinium sulfite monohydrate $(N_2H_5)_2SO_3{\cdot}H_2O$, is

precipitated out by the addition of alcohol:

$$2N_2H_4{\cdot}H_2O + SO_2(g) \rightarrow (N_2H_5)_2SO_3{\cdot}H_2O \tag{3.16}$$

$$(N_2H_5)_2SO_3{\cdot}H_2O \rightleftarrows (N_2H_4)_2H_2SO_3{\cdot}H_2O \tag{3.17}$$

Secondly, metal sulfite hydrazines are obtained by the treatment of $(N_2H_5)_2SO_3{\cdot}H_2O$ with divalent metal ions (M^{2+} = Fe, Mn, Co, Ni, or Zn) [19].

3.2.7.1 *Metal Sulfite Hydrazines [$MSO_3{\cdot}xN_2H_4{\cdot}yH_2O$]*

Metal sulfite hydrazines are synthesized using hydrazinium sulfite monohydrate under different preparative conditions as mentioned below [20].

Method I: Reaction in Presence of $N_2H_4{\cdot}H_2O$
A calculated quantity of $(N_2H_5)_2SO_3{\cdot}H_2O$ is dissolved in $N_2H_4{\cdot}H_2O$ to obtain an alkaline solution of pH ~9. To this, a stoichiometric quantity of metal salt (M) solution ($M : SO_3 = 1 : 1$) in aqueous solution is added with constant stirring. The compound formed is initially washed with alcohol and then dried in vacuum desiccator over P_2O_5.

Method II: Reaction in the Absence of $N_2H_4{\cdot}H_2O$
To an aqueous solution of $(N_2H_5)_2SO_3{\cdot}H_2O$ (pH ~ 4) a stoichiometric quantity of $M : SO_3$ (1 : 1) is added with constant stirring. Alcohol is then added to the resulting solution to precipitate the product. The solid that separates is filtered off, washed with alcohol, and then dried in a vacuum desiccator over P_2O_5:

$$MCl_2 + (N_2H_4)_2H_2SO_3.H_2O(aq) + nH_2O \rightarrow MSO_3{\cdot}xN_2H_4{\cdot}yH_2O + 2HCl + (2-x)N_2H_4 + (n+1-y)H_2O \tag{3.18}$$

where M = Mn, Fe, Co, Ni, and Zn.

Spectral and Thermal Data
The composition of metal sulfite hydrazine hydrate complexes is established by chemical analysis. Infrared absorption spectra of the compounds are identical and show characteristic absorption frequencies of N_2H_4 and sulfite (Table 3.16).

Table 3.16 Infrared absorption frequencies (cm^{-1}) of $MSO_3 \cdot xN_2H_4 \cdot yH_2O$.

Assignment	Mn	Fe	Co	Ni	Zn
O–H stretching	3510	3530	3540	3530	3560
N–H stretching	3280	3300	3300	3340	3300
H_2O bending	1620	1630	1640	1650	1670
NH_2 bending	1600	1605	1595	1620	1600
NH_2 bending wagging	1195	1200	1188	1215	1190
NH_2 twisting	1150	1150	1150	1165	1152
S–O stretching	1000	1000	1000	980	1000
N–N stretching	960	900	900	900	960
S–O asym. stretching	900	900	900	900	900
NH_2 rocking	640	660	642	660	665
S–O sym. bending	630	623	600	620	605
S–O sym. bending	495	500	495	485	500
M–N stretching	355	370	370	370	370

Sulfite absorptions are observed at 1000, 620, and 495 cm^{-1}. The N–N stretching frequency observed at 960 cm^{-1} confirms the presence of bridged hydrazine.

Thermal data reveal that the decomposition of all the complexes is similar (Table 3.17). The steps involved are dehydration and dehydrazination, followed by disproportionation of the sulfites to form corresponding oxides/sulfides (Figure 3.11).

The complexes of Fe, Co, and Ni exhibit autocatalytic combustion, whereas those of Zn and Mn do not. Owing to exothermic decomposition of hydrazine, the disproportionation temperatures of the sulfites are relatively low. The combustion residue of the iron complex is a mixture of α- and γ-Fe_2O_3, as confirmed by X-ray studies, while in the case Co and Ni the residue is the corresponding oxide and sulfate; with Zn, a sulfide is formed.

3.2.7.2 Mixed Metal Sulfite Hydrazines

The synthesis of mixed metal sulfite hydrazines involves the use of hydrazinium sulfite monohydrate [$(N_2H_5)_2SO_3 \cdot H_2O$] as the starting material to generate the sulfite ions (Section 3.2.7). Stoichiometric quantities of metal sulfate hydrate, $MSO_4 \cdot xH_2O$, and $FeSO_4 \cdot 7H_2O$ in 1 : 2 molar ratio are dissolved in 15 ml of H_2O. The resultant solution is mixed with hydrazinium sulfite monohydrate, $(N_2H_5)_2 \cdot SO_3 \cdot H_2O$, in hydrazine hydrate.

Table 3.17 Thermal analysis data of $MSO_3 \cdot xN_2H_4 \cdot yH_2O$.

Compound	Thermogravimetry			DTA peak temperature (°C)[a]	Product
	Temperature range (°C)	% Weight loss			
		Obsd.	Calcd.		
$MnSO_3 \cdot 2N_2H_4 \cdot 2H_2O$[b]	120–158	15.00	15.32	158 (−)	$MnSO_3 \cdot 2N_2H_4$
	202–245	42.00	45.56	232.8 (+)	$MnSO_3$
$FeSO_3\ 2N_2H_4 \cdot H_2O$[b]	130–142	38.00	37.60	135 (+)	$FeSO_3$
	190–198	50.00	46.80	190 (+)	$Fe_2O_3 + FeSO_4$
$CoSO_3 \cdot 2N_2H_4 \cdot H_2O$[b]	88–121	8.00	8.15	105 (−)	$CoSO_3 \cdot 2N_2H_4$
	150–156	39.00	37.11	151 (+)	$CoSO_3$
	156–220	56.00	55.22	190 (+)	$CoS_3O_4 + CoSO_4$
$NiSO_3 \cdot 2N_2H_4 \cdot H_2O$[b]	72–140	8.00	7.12	98 (−)	$NiSO_3 \cdot 3N_2H_4$
	164–215	45.00	45.11	182 (+)	$NiSO_3$
	365–325	55.00	54.76	276 (+)	$NiO + NiSO_4$
$ZnSO_3 \cdot 2N_2H_4 \cdot 1.5H_2O$[b]	115–155	23.50	24.95	145 (−)	$ZnSO_3 \cdot N_2H_4$
	200–236	40.00	38.50	215 (+)	$ZnSO_3$
	370–400	49.00	48.65	400 (+)	$ZnS + ZnSO_4$
$CoSO_3 \cdot 1.5N_2H_4 \cdot H_2O$[c]	84–108	8.40	8.78	93 (−)	
	127–134	38.00	37.7	128 (+)	$CoSO_3$
	162–198	50.00		193 (+)	$Co_3O_4 + CoSO_4$
$NiSO_3 \cdot 2N_2H_4 \cdot H_2O$[c]	130–176	7.80	8.15	148 (−)	$NiSO_3 \cdot 2N_2H_4$
	220–256	24.00	22.65	251 (+)	$NiSO_3$
	272	58.5		272 (+)	$NiO + NiSO_4$

[a] (−) = Endotherm; (+) = exotherm.
[b] Method I.
[c] Method II.

A solid compound separates out initially, which is washed with 50% alcohol until free from sulfate; it is then washed with diethyl ether and dried in a vacuum desiccator over P_2O_5. Chemical analyses of the mixed metal sulfite hydrazine hydrates confirms a stoichiometry of $MFe_2(SO_3)_3 \cdot 6N_2H_4 \cdot 2H_2O$. The reaction can be written as follows:

$$MSO_4 + 2FeSO_4 + 3(N_2H_5)_2 \cdot SO_3 \cdot H_2O + 6N_2H_4 \cdot H_2O \rightarrow MFe_2(SO_3)_3 \cdot 6N_2H_4 \cdot 2H_2O + 3(N_2H_5)_2SO_4 + 4H_2O \quad (3.19)$$

where M = Mg, Mn, Co, Ni, and Zn.

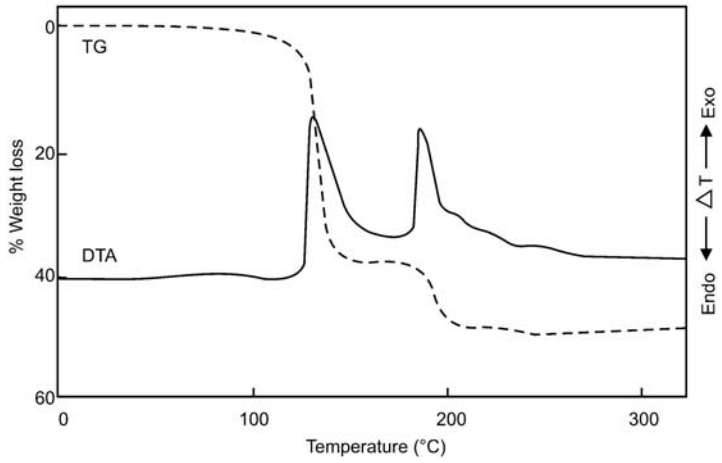

Figure 3.11 Simultaneous TG-DTA curves of $Fe(SO_3)_2{\cdot}2N_2H_4{\cdot}H_2O$. Adapted from Ref. [20] with permission from Akademiai Kiado © 1990.

Since the synthesis of these compounds is carried out in the presence of a strong reducing agent like hydrazine, iron remains in the ferrous state. Analytical data and qualitative tests support this observation. However, on long exposure to the atmosphere, Fe(II) in the compounds is oxidized to Fe(III).

The prepared mixed metal hydrazine hydrates are light in color and insoluble in water. From the chemical analysis it is evident that all mixed metal complexes, including magnesium, are present as sulfite [21]. However, when magnesium alone is used without $FeSO_4$, a bisulfate hydrazine is obtained under the same preparative conditions.

The combustion of mixed metal sulfite hydrazine complexes in the presence of air (~300 °C) gives homogenous ferrites (Table 3.18). This is confirmed by the observed weight loss and powder XRD.

Table 3.18 Combustion products of $MFe_2(SO_3)_3{\cdot}6N_2H_4{\cdot}2H_2O$.

Complex	% Weight loss		Product
	Obsd.	Calcd.	
$MgFe_2(SO_3)_3{\cdot}6N_2H_4{\cdot}2H_2O$	66.98	66.89	$MgFe_2O_4$
$MnFe_2(SO_3)_3{\cdot}6N_2H_4{\cdot}2H_2O$	64.70	63.66	$MnFe_2O_4$
$CoFe_2(SO_3)_3{\cdot}6N_2H_4{\cdot}2H_2O$	63.27	63.26	$CoFe_2O_4$
$NiFe_2(SO_3)_3{\cdot}6N_2H_4{\cdot}2H_2O$	63.70	63.28	$NiFe_2O_4$
$ZnFe_2(SO_3)_3{\cdot}6N_2H_4{\cdot}2H_2O$	62.90	62.63	$ZnFe_2O_4$

3.2.7.3 *Magnesium Bisulfite Hydrazine Hydrate*

For the synthesis of magnesium bisulfite complex, an aqueous solution of $MgCl_2$ is mixed with aqueous $(N_2H_5)_2SO_3{\cdot}H_2O$ or $(N_2H_4)_2{\cdot}H_2SO_3{\cdot}H_2O$ stoichiometrically in a $Mg:SO_3$ ratio of 1 : 2. The compound is precipitated out by addition of alcohol. It is further washed with alcohol, then diethyl ether and dried in vacuum desiccator [22]:

$$MgCl_2 + 2(N_2H_4)_2{\cdot}H_2SO_3{\cdot}H_2O \rightarrow Mg(HSO_3)_2{\cdot}N_2H_4{\cdot}H_2O + HCl + N_2H_5Cl + H_2O + 2N_2H_4 \quad (3.20)$$

Interestingly, the same compound is obtained when synthesis is carried out with $(N_2H_5)_2SO_3{\cdot}H_2O$ in hydrazine hydrate instead of aqueous solution.

Thermal studies of this highly hygroscopic, colorless compound show three steps in the TG on heating up to 600 °C (Figure 3.12). The first step, with 16% weight loss, is due to the loss of two water molecules, which is observed in the temperature range 133–160 °C. The bisulfite appears to dissociate into H_2O and $S_2O_5^{2-}$, accounting for the formation of the two H_2O molecules:

$$Mg(HSO_3)_2{\cdot}N_2H_4{\cdot}H_2O \rightarrow MgS_2O_5{\cdot}N_2H_4 + 2H_2O\uparrow \quad (3.21)$$

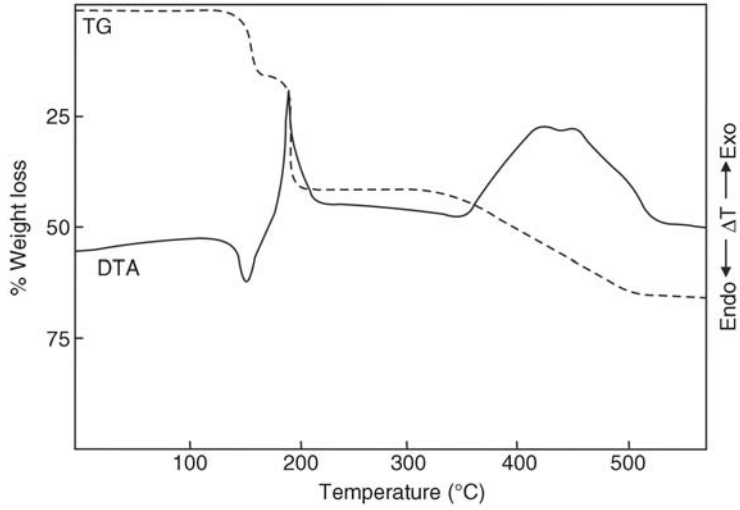

Figure 3.12 Simultaneous TG-DTA curves of $Mg(HSO_3)_2{\cdot}N_2H_4{\cdot}H_2O$. Adapted from Ref. [22] with permission from Elsevier © 1989.

Subsequently, hydrazine decomposes at around 190 °C with the evolution of N_2 and NH_3 gases, with a 41.5% weight loss observed in the TG curve for this step:

$$3MgS_2O_5{\cdot}N_2H_4 \rightarrow 3MgS_2O_3 + 3O_2\uparrow + 4NH_3\uparrow + N_2\uparrow \qquad (3.22)$$

The TG profile further shows decomposition of the intermediate MgS_2O_3, magnesium thiosulfite, with a weight loss of 67.5% between 335 and 580 °C due to the formation of MgO and $MgSO_4$ by disproportionation as follows:

$$MgS_2O_3 \rightleftharpoons MgSO_3 + S \qquad (3.23)$$

$$MgSO_3 \rightarrow MgO + SO_2 \qquad (3.24)$$

$$SO_2 + 2MgSO_3 \rightarrow 2MgSO_4 + S \qquad (3.25)$$

Mass spectrometry carried out on the evolved gases after decomposition of the compound at 240 °C shows the presence of gases like N_2 (*m/z* 14, 28), NH_3 (*m/z* 17), S (*m/z* 16), and H_2O (*m/z* 18). The detection of these gases support the proposed decomposition pattern represented in (3.21)–(3.25).

Magnesium thiosulfite, MgS_2O_3, appears to form $MgSO_3$ before it undergoes disproportionation to oxide and sulfate (3.24 and (3.25)). On heating in air, this compound exhibits a change of color from blue to violet, which is typical of the reaction:

$$MgSO_3 + S \rightleftharpoons MgS_2O_3 \qquad (3.26)$$

DTA shows an endotherm at 152 °C corresponding to the loss of H_2O. The two exotherms at 190 and 446 °C are complementary to the decomposition as seen in the TG. The exotherm at 446 °C is broad and is probably due to the three reactions shown in (3.24)–(3.26).

3.2.8 Metal Azide Hydrazines $[M(N_3)_2(N_2H_4)_2]$

3.2.8.1 Synthesis

Metal azide hydrazines are prepared by three different methods.

Method I

Metal azide hydrazines of the type $M(N_3)_2(N_2H_4)_2$, where M = Co, Ni, and Zn, are prepared by the conventional method of adding alcoholic

hydrazine hydrate to a mixture of aqueous solutions of metal nitrate and sodium azide. For example, $Zn(N_3)_2(N_2H_4)_2$ is prepared by the addition of hydrazine hydrate to an aqueous mixture of zinc nitrate hexahydrate and sodium azide in the ratio 2 : 1 : 2, respectively, at room temperature. The product is obtained by the addition of alcohol (97% yield) [23,24]:

$$M(NO_3)_2 \cdot 6H_2O + 2NaN_3 + 2N_2H_4 \cdot H_2O \text{ (alcoholic)} \rightarrow M(N_3)_2(N_2H_4)_2 + 2NaNO_3 + 8H_2O \quad (3.27)$$

where M = Co, Ni, or Zn.

The azide complexes of Co, Ni, Zn, and Cd are also synthesized using metal chloride salts, forming $[M(N_2H_4)(H_2O)(N_3)Cl]_n$ and $[M(N_2H_4)(N_3)_2]_n$ type complexes. Here the azide group and hydrazine molecule both act as bidentate bridging ligands [25]. The complexes of Co(II), Ni(II), and Zn(II) explode on heating but Cd(II) complexes decompose above 250 °C.

Method II

Metal azide hydrazines where M = Mn, Co, Ni, and Zn are prepared by dissolving the corresponding metal powders in a solution of ammonium azide in hydrazine hydrate. A solid product is obtained in 95% yield by the addition of alcohol:

$$M^0 + 2NH_4N_3 + 2N_2H_4 \cdot H_2O \rightarrow M(N_3)_2(N_2H_4)_2 + 2NH_3 + H_2 + 2H_2O \quad (3.28)$$

where M = Mn, Co, Ni, or Zn.

The results of chemical analysis of all metal azide hydrazines show that metal azides form dihydrazine complexes of the type $M(N_3)_2(N_2H_4)_2$.

Method III

Hydrazine complexes of alkaline earth azides, $Mg(N_3)_2(N_2H_4)_2$ and $Ca(N_3)_2 \cdot 1.5N_2H_4$, are prepared by the solid-state reaction of the corresponding alkaline earth metal oxides with hydrazinium azide (1 : 2) at 120 °C for 5 h. Barium forms non-solvated azide $[Ba(N_3)_2]$:

$$MgO + 2N_2H_5N_3 \xrightarrow{\Delta} Mg(N_3)_2(N_2H_4)_2 + H_2O \quad (3.29)$$

$$CaO + 2N_2H_5N_3 \xrightarrow{\Delta} Ca(N_3)_2 \cdot 1.5N_2H_4 + 0.5NH_3 + H_2O + 0.25N_2 + 0.25H_2 \quad (3.30)$$

$$BaO + 2N_2H_5N_3 \xrightarrow{\Delta} Ba(N_3)_2 + 2NH_3 + H_2O + N_2 + H_2 \qquad (3.31)$$

3.2.8.2 *Spectral, Structural, and Thermal Data*

The infrared ν_{N-N} frequency of N_2H_4 of metal azide hydrazines is observed at $\sim 960\,cm^{-1}$, indicating the presence of bridged hydrazine in these complexes. The characteristic infrared absorption frequencies of the azide observed at 2080, 1310, and $640\,cm^{-1}$ are assigned as shown in Table 3.19.

The IR spectrum of $Ca(N_3)_2 \cdot 1.5N_2H_4$ shows characteristic azide absorptions at 2080, 1310, and $640\,cm^{-1}$ while the absorptions at 3400, 3350, 1655, 1600, 880, 820, and $600\,cm^{-1}$ are due to hydrazine. The ν_{N-N} frequency of N_2H_4 appearing at $880\,cm^{-1}$ indicates the presence of hydrazine as an adduct. The absence of a ν_{N-N} frequency around $970\,cm^{-1}$ proves that N_2H_4 is not coordinated. The IR spectrum of $Ba(N_3)_2$ shows characteristic azide absorptions at 2080, 1310, and $640\,cm^{-1}$.

The structure of $M(N_3)_2(N_2H_4)_2$ is expected to be similar to the halide complexes, exhibiting octahedral coordination of the metal ion, which is surrounded by 4N atoms of N_2H_4 and 2N atoms of the azide [23]. The observed M–N stretching frequencies of $M-N_3$ and $M-N_2H_4$ support the above argument.

Recently, the crystal structure of polymeric zinc(II) azide hydrazine $[Zn(N_3)_2(N_2H_4)_2]n$, synthesized by the above method, was determined (Figure 3.13) [26].

Table 3.19 Infrared absorption frequencies (cm^{-1}) of $M(N_3)_2(N_2H_4)_2$.

Assignments	Mg	Co	Ni	Zn
NH_2 asym. stretching	3400	3360	3280	3380
NH_2 sym. stretching	3300	3300, 3260	3220, 3170	3310, 3280
N_3^- asym. stretching	2080	2060	2070	2060
NH_2 bending	1600	1620	1610, 1580	1610, 1580
N_3^- sym. stretching	1310	1300	1320	1310
NH_2 twisting	1170, 1080	1180, 1140	1180	1170
N–N stretching of N_2H_4	965	970	970	970
NH_2 rocking	820, 350	560	820, 550	560
N_3^- bending	640	640	640	640
N–N stretching of metal azide	400	370	390	370
N–N stretching of $M - N_2H_4$	350	270	280	270

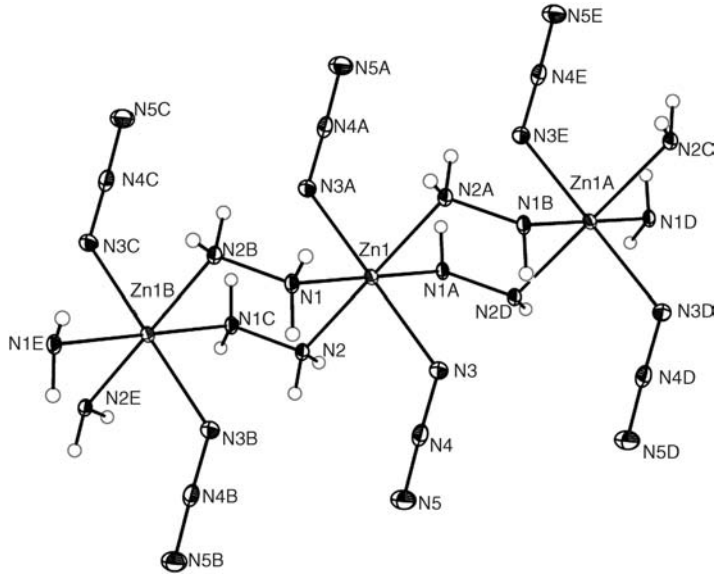

Figure 3.13 Molecular structure of $[Zn(N_3)_2(N_2H_4)_2]n$. Reproduced from Ref. [26] Copyright © 2011 WILEY-VCH Verlag GmbH & Co. KGaA, Weinheim.

The DTA data of the azide complexes are tabulated in Table 3.20. DTA curves of $Ca(N_3)_2 \cdot 1.5N_2H_4$ and $Ba(N_3)_2$ are shown in Figure 3.14a & b. All the metal azide hydrazine complexes decompose violently and exothermically, without leaving any residue in the platinum cup. As expected, unlike transition metal azide hydrazines, magnesium azide hydrazine is non-explosive.

The DTA of calcium azide hydrazine shows two exotherms. The first exotherm at 168 °C corresponds to the loss of hydrazine, yielding anhydrous calcium azide. The second exotherm at 286 °C corresponds to the explosion temperature of $Ca(N_3)_2$. The DTA of $Ba(N_3)_2$ shows an exotherm at 236 °C, which corresponds to the explosion temperature of $Ba(N_3)_2$.

Table 3.20 DTA data of $M(N_3)_2(N_2H_4)_2$.

Compound	DTA peak temperature (° C)[a]
$Mg(N_3)_2(N_2H_4)_2$	217 (+), 350(−)
$Co(N_3)_2(N_2H_4)_2$	223 (+)
$Ni(N_3)_2(N_2H_4)_2$	196 (+)
$Zn(N_3)_2(N_2H_4)_2$	212 (+)
$Ca(N_3)_2\ 1.5N_2H_4$	168 (+), 286 (+)
$Ba(N_3)_2$	236 (+)

[a] (−) = Endotherm; (+) = exotherm.

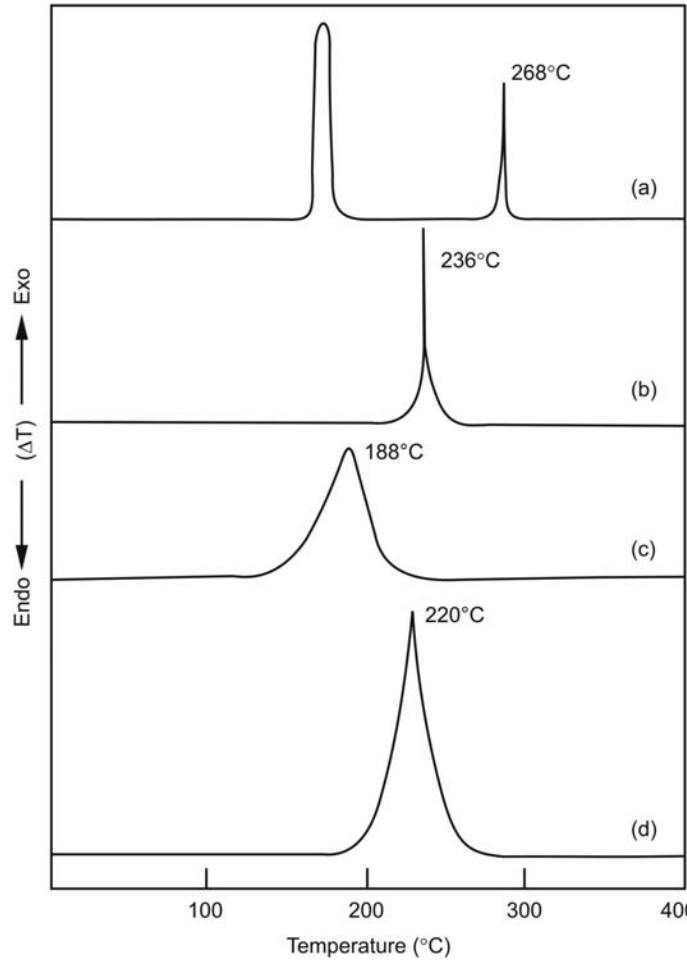

Figure 3.14 DTA curves of (a) $Ca(N_3)_2 \cdot 1.5N_2H_4$, (b) $Ba(N_3)_2$, (c) $[Co(NO_3)_2(N_2H_4)_3]$, and (d) $[Ni(NO_3)_2(N_2H_4)_3]$. Ph.D Thesis of Nesamani, C. under Prof K. C. Patil at Indian Institute of Science.

3.2.8.3 Dinitrogen Compound

Nitrogen is of paramount importance to all forms of life. Yet plants and animals cannot make use of elemental nitrogen and rely on certain bacteria and algae to "fix" nitrogen in a combined form to use as a nutrient. Nitrogen assimilation, which takes place in the presence of an enzyme, is not yet fully understood, but coordinate bonding of N_2 to

heavy metals (iron, molybdenum, etc.) present in all nitrogen assimilating microorganisms forms the first step. This hypothesis has gained credibility after the synthesis of the first dinitrogen complex of ruthenium. Molecular dinitrogen complexes are generally formed by transition metals. The dinitrogen complexes of calcium, strontium, and barium are formed during the incomplete solvolysis of the corresponding metal pernitrides (M_3N_4) with water, acetic acid, and hydrazine. An indirect route to dinitrogen complexes involves the oxidation of hydrazine, thermolysis, or acid-catalyzed decomposition of an azide complex [27].

Apparently, the source of molecular nitrogen appears to be either azide or hydrazine. It is therefore interesting to investigate the thermolysis of hydrazine complexes of metal azides, $M(N_3)_2(N_2H_4)_2$. As these molecules contain both hydrazine and azide they are expected to give rise to a dinitrogen complex. Since, transition metal azide hydrazine complexes are highly explosive, alkaline earth metal complexes were chosen for this study. Thermolysis of calcium azide hydrazine, $Ca(N_3)_2(N_2H_4)_2$, and barium azide hydrazine, $Ba(N_3)_2(N_2H_4)$, does not yield any dinitrogen complex. This is probably because the hydrazine is lost initially, giving anhydrous metal azides that explode violently. Consequently, the magnesium azide hydrazine complex prepared by the reaction of magnesium metal powder with ammonium azide dissolved in hydrazine hydrate (Section 3.2.8.1) is considered for this study.

The focal point of this investigation is the intermediate obtained during the thermal decomposition of $Mg(N_3)_2(N_2H_4)_2$ (Figure 3.15). TG-DTA data shows an initial exotherm followed by an endotherm. The decomposition product after the exotherm at 217 °C is blue and sensitive to moisture and air. The observed weight loss of 51% is in good agreement with the formula $Mg(N_2)(NH_2)_2$. On further heating $Mg(N_2)(NH_2)_2$ it decomposes endothermically at 350 °C with the evolution of nitrogen and ammonia to give MgNH (Table 3.21).

The infrared spectrum of the intermediate shows characteristic amide absorptions at 3660, 3300, 3200, 1630, 1200, 1080, and 600 cm^{-1}, which have been assigned similarly to those reported for $Mg(N_2)(NH_2)_2$. The absorptions at 2160 and 2040 cm^{-1} and 400 cm^{-1} have been assigned to $\nu_{N\equiv N}$ and ν_{Mg-N2}, respectively (Table 3.22). The presence of N_3^- in the residue, which is known to show $\nu_{N=N}$ at 2100 cm^{-1} as in the parent compound, was ruled out by qualitative analysis of the residue (negative test with $FeCl_3$ solution, no blood red color). In addition, the absence of N_3^- bands at 1310 and 640 cm^{-1} supports this fact. Chemical analysis of the residue shows the presence of Mg^{2+} (obsd 28.59%; calcd 28.84%) and amide. Acid hydrolysis of the residue yields

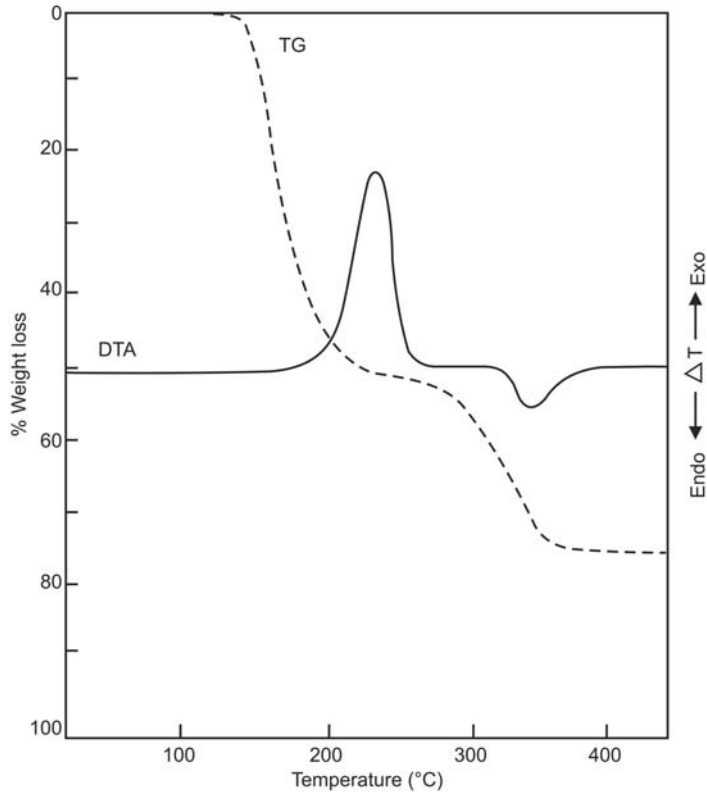

Figure 3.15 Simultaneous TG-DTA of $Mg(N_3)_2(N_2H_4)_2$. Ph.D Thesis of Nesamani, C. under Prof. K. C. Patil at Indian Institute of Science.

an ammonium salt that gives a positive test with Nessler's reagent. The blue colored compound shows absorption at 240 nm in the UV (ultraviolet) spectrum.

Figure 3.16 shows the infrared spectra of $Mg(N_3)_2(N_2H_4)_2$ and $Mg(N_2)(NH_2)_2$.

Table 3.21 Thermal analysis data of $Mg(N_3)_2(N_2H_4)_2$.

Thermogravimetry			DTA peak temperature[a]	Product
Temperature range (°C)	% Weight loss			
	Obsd.	Calcd.		
125–217	51.0	51.06	217 (+)	$Mg(N_2)(NH_2)_2$
217–350	77.0	77.18	350 (−)	MgNH

[a] (−) = Endotherm; (+) = exotherm.

Table 3.22 Infrared absorption frequencies (cm^{-1}) of $Mg(N_2)(NH_2)_2$.

Assignments	Wavenumber[a]
NH_2 asym. stretching	3300 (w)
NH_2 sym. Stretching	3200 (m)
N≡N stretching	2160 (s), 2040 (sh)
NH_2 bending	1630 (s)
NH_2 wagging	1200 (s)
NH_2 rocking	600 (vb)
N−N stretching of Mg−N_2	400 (s)

[a] m = Medium, s = strong, sh = shoulder, w = weak, vb = very broad.

The evolution of N_2 and NH_3 gases during thermolysis is confirmed by mass spectrometric analysis of the evolved gases at above 350 °C, which shows peaks at *m/z* 14, 15, 16, 17, and 28. The peaks at 28 and 14 are characteristic of N_2 species and those at 17, 16, 15, and 14 are the characteristic fragmentation pattern of NH_3. It is not surprising that the thermolysis of $Mg(N_3)_2(N_2H_4)_2$ yields $Mg(N_2)(NH_2)_2$ since the hydrazine moiety is known to disproportionate to amide and coordinated nitrogen. The occurrence of this blue colored compound, which shows strong infrared absorption at ~2100 cm^{-1}, indicates the formation of a dinitrogen complex. This investigation presents a new route for the formation of dinitrogen complexes by the solid-state decomposition of metal azide hydrazine complexes.

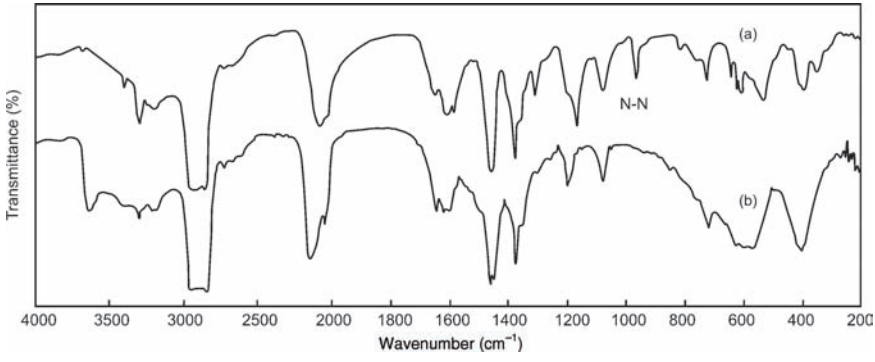

Figure 3.16 Infrared spectra of (a) $Mg(N_3)_2(N_2H_4)_2$ and (b) $Mg(N_2)(NH_2)_2$. Ph.D Thesis of Nesamani, C. under Prof. K. C. Patil at Indian Institute of Science.

3.2.9 Metal Nitrate Hydrazines [$M(NO_3)_2(N_2H_4)_n$]

3.2.9.1 Synthesis

Metal nitrate hydrazines are prepared by two different methods [23].

Method I

Metal nitrate hydrazines of the type $M(NO_3)_2(N_2H_4)_n$ are prepared by the conventional route, which involves the addition of alcoholic hydrazine hydrate to an aqueous solution of metal nitrate. Cobalt nitrate hydrazine, $[Co(NO_3)_2(N_2H_4)_3]$, is prepared in a reaction mixture containing an aqueous solution of cobalt nitrate hexahydrate and hydrazine hydrate (1 : 3), at room temperature. The product is precipitated instantaneously in 96% yield by the addition of alcohol:

$$M(NO_3)_2 \cdot 6H_2O + nN_2H_4 \cdot H_2O(\text{alcoholic}) \rightarrow M(NO_3)_2(N_2H_4)_n \cdot (n+6)H_2O \tag{3.32}$$

where M = Mg then $n = 2$; M = Mn, Co, Ni, Zn, or Cd, $n = 3$.

Method II

Metal nitrate hydrazines can also be prepared by dissolving the respective metal powders in a solution of ammonium nitrate in hydrazine hydrate:

$$M^0 + 2NH_4NO_3 + nN_2H_4 \cdot H_2O \rightarrow M(NO_3)_2(N_2H_4)_n + 2NH_3 + H_2 + nH_2O \tag{3.33}$$

where M = Mg ($n = 2$); M = Mn, Fe, Co, Ni, Zn, and Cd ($n = 3$).

In the preparation of nickel nitrate hydrazine $[Ni(NO_3)_2(N_2H_4)_3]$ stoichiometric amounts of ammonium nitrate in hydrazine hydrate and nickel metal powder are allowed to react in the ratio of 2 : 3 : 1, respectively, at room temperature. The nickel metal dissolves exothermically with the evolution of hydrogen. The solid compound is obtained in 97% yield by the addition of alcohol.

An attempt to prepare $Cu(NO_3)_2(N_2H_4)_3$ by the reaction of copper metal powder with ammonium nitrate dissolved in hydrazine hydrate failed, due to explosion. The product is not isolated because of the high exothermicity of the reaction.

The results of chemical analysis of most of the metal nitrate hydrazine complexes reveal that they form trihydrazine complexes of the type $M(NO_3)_2(N_2H_4)_3$.

Zhu *et al*. have modified the synthesis procedure for nickel nitrate hydrazine so as to make it viable for industrial manufacture [28]. Detailed investigations on physical and thermochemical properties, stability test, explosive performance test, and safety tests have been made to evaluate the performance of nickel hydrazine nitrate (NiHN) and cobalt hydrazine nitrate (CoHN) as primary explosives [29].

Cadmium Nitrate Dihydrazine

Cadmium nitrate dihydrazine, $[Cd(NO_3)_2(N_2H_4)_2]$, is prepared by the addition of $N_2H_4{\cdot}H_2O$ to an aqueous mixture of cadmium acetate and ammonium nitrate (2 : 1 : 2 ratio, respectively). The reaction is quantitative and the product is precipitated by the addition of alcohol (96% yield):

$$\begin{aligned} Cd(OAc)_2 + 2NH_4NO_3 + 2N_2H_4{\cdot}H_2O(\text{alcoholic}) \\ \rightarrow Cd(NO_3)_2(N_2H_4)_2 + 2NH_4OAc + 2H_2O \end{aligned} \tag{3.34}$$

The infrared spectra of all metal nitrate hydrazines are identical. The probable assignments of frequencies are made on the basis of earlier studies on hydrazine and ionic nitrate as reported in Table 3.23. The ν_{N-N} of N_2H_4 is observed at 960 cm^{-1}, indicating the presence of hydrazine bridging between two metal ions. The characteristic infrared absorption frequencies observed at 1390, 1050, and 820 cm^{-1} show the presence of ionic NO_3^-. The probable structure of the metal ion is an octahedral coordination with all 6N atoms contributed by N_2H_4 groups.

The DTA curves of $[Co(NO_3)_2(N_2H_4)_3]$ and $[Ni(NO_3)_2(N_2H_4)_3]$ are shown in Figure 3.14c and d. All the metal nitrate hydrazines decompose violently on heating, giving metal oxides (Table 3.24). An interesting observation in the decomposition of $Fe(NO_3)_2(N_2H_4)_n$ is that this iron complex is quite unstable and ignites at room temperature itself during suction filtering. The product of decomposition is magnetic in nature and has been identified by X-ray powder diffraction to be a mixture of α- and γ-Fe_2O_3.

3.2.10 Metal Perchlorate Hydrazines $[M(ClO_4)_2(N_2H_4)_2]$

3.2.10.1 Synthesis and Properties

The synthesis and properties of Li, Mg, Al, and Cr perchlorate hydrazines are discussed here [24,30].

Table 3.23 Infrared absorption frequencies (cm^{-1}) of $M(NO_3)_2(N_2H_4)_n$.

Assignments	M						
	Mn	Fe	Co	Ni	Zn	Cd	Mg
NH_2 asym. stretching	3320	—	3330	3300	3320	3320	3320
NH_2 sym. stretching	3240, 3180	3260	3260	3240, 3180	3240, 3180	3240, 3180	3260, 3180
NH_2 -bonding	1620, 1590	1600	1620, 1590	1630	1620, 1590	1620, 1590	1620, 1590
NH_2. twisting	1180	1180	1170	1180	1180	1150	1180
N—N stretching of H_2H_4	970	950	970	970	970	960	965
NH_2 rocking	540	600, 540	540	550	540	540	520
ν_3	1400	1390	1400	1400	1400	1400	1390
ν_1	1050	1075	1050	1050	1050	1050	1050
ν_2	820	820	820	820	820	820	820

Table 3.24 DTA data of $M(NO_3)_2(N_2H_4)_n$.

Compound	DTA peak temperature (°C)[a]
$Mn(NO_3)_2(N_2H_4)_3$	141 (+), 212 (+)
$Fe(NO_3)_2(N_2H_4)_3$	140 (+)
$Co(NO_3)_2(N_2H_4)_3$	188 (+)
$Ni(NO_3)_2(N_2H_4)_3$	220 (+)
$Zn(NO_3)_2(N_2H_4)_3$	212 (+)
$Cd(NO_3)_2(N_2H_4)_3$	145 (+), 243 (+)
$Mg(NO_3)_2(N_2H_4)_2$	241 (+)

[a] (+) = Exotherm.

$Li_3Al(ClO_4)_6{\cdot}5N_2H_4$

In the synthesis of $Li_3Al(ClO_4)_6{\cdot}5N_2H_4$ a hydrolyzed sample of $LiAlH_4$ is dissolved in hot (70%) perchloric acid, which on crystallization gives the complex perchlorate hydrate. When this complex is treated with $N_2H_4{\cdot}H_2O$ under suitable conditions (*caution*) it gives a non-crystalline solid that chemical analysis revealed as $Li_3Al(ClO_4)_6{\cdot}5N_2H_4$.

$Mg(ClO_4)_2(N_2H_4)_2$

Method I Magnesium perchlorate hydrazine, $Mg(ClO_4)_2(N_2H_4)_2$ is prepared by the addition of hydrazine hydrate to an aqueous solution of magnesium perchlorate hexahydrate (2 : 1 ratio, respectively) at room temperature. The reaction is almost instantaneous and the solid compound is precipitated by the addition of alcohol (90% product yield):

$$Mg(ClO_4)_2{\cdot}6H_2O + 2N_2H_4{\cdot}H_2O\ (\text{alcoholic}) \rightarrow Mg(ClO_4)_2(N_2H_4)_2 + 8H_2O \tag{3.35}$$

Method II Magnesium perchlorate hydrazine can also be prepared by the reaction of stoichiometric quantities of magnesium powder with ammonium perchlorate dissolved in hydrazine hydrate (1 : 2 : 2 ratio, respectively) at room temperature. Magnesium metal dissolves exothermically with the evolution of hydrogen. The solid compound is obtained by the addition of alcohol (~96% yield):

$$Mg^0 + 2NH_4ClO_4 + 2N_2H_4{\cdot}H_2O \rightarrow Mg(ClO_4)_2(N_2H_4)_2 + 2NH_3 + H_2 + 2H_2O \tag{3.36}$$

$Al(ClO_4)_3 \cdot 3N_2H_4$

Freshly prepared $Al(OH)_3$ is treated with aqueous perchloric acid; the resulting solution is concentrated carefully. Highly hygroscopic crystals of $Al(ClO_4)_3 \cdot xH_2O$ so-obtained are treated with $N_2H_4 \cdot H_2O$ under highly specific conditions (*danger*) to give a non-hygroscopic crystalline solid, which chemical analysis showed to be $Al(ClO_4)_3 \cdot 3N_2H_4$ [31].

Diperchlorate Dihydrazine Chromium(III) Perchlorate

Diperchlorate dihydrazine chromium(III) perchlorate, $[Cr(ClO_4)_2(N_2H_4)_2]ClO_4$, is prepared by the addition of alcoholic hydrazine hydrate to an aqueous solution of chromium(III) perchlorate. The reaction is instantaneous with the formation of a crystalline violet compound [32].

The IR spectrum of $Mg(ClO_4)_2(N_2H_4)_2$ shows characteristic absorptions of coordinated hydrazine at 3385, 3260, 1600, 1520, 965, and 735 cm^{-1} and of ionic perchlorate at 1085 and 630 cm^{-1} (Table 3.25). The N–N stretching frequency of hydrazine is observed at 965 cm^{-1}, indicating the presence of bridged hydrazine (Figure 3.17a). Since hydrazine is bridged and perchlorate is not coordinated to the metal ion, as seen by the observed frequencies (no splitting in the infrared spectrum in the region of ν_3 and ν_4), the probable structure of $Mg(ClO_4)_2(N_2H_4)_2$ is square planar with Mg^{2+} surrounded by N atoms of N_2H_4.

The IR spectrum of $Cr(ClO_4)_2(N_2H_4)_2 \cdot ClO_4$ shows characteristic absorptions of coordinated hydrazine as well as of covalently bound perchlorate groups (Figure 3.17b). Hydrazine appears to be present as a monodentate ligand, as seen by the ν_{N-N} absorption of N_2H_4 at 950 cm^{-1}. The observed splitting of the perchlorate bands at ~1100 cm^{-1} (ν_3) and 630 cm^{-1} (ν_4) is indicative of the presence of perchlorate ion of lower symmetry C_{2v}. The weak IR absorption band at 370 cm^{-1} could be assigned to ν_{Cr-N} on the basis of earlier studies on similar compounds.

Table 3.25 Infrared frequencies (cm^{-1}) of $M(ClO_4)_2(N_2H_4)_2$.

Types of vibrations	$Mg(ClO_4)_2(N_2H_4)_2$	$Cr(ClO_4)_2(N_2H_4)_2 \cdot ClO_4$
$\gamma N-N$	3385, 3260	3260
ζNH_2	1600, 1520	1640, 1460
$\gamma N-N$	965	950
NH_2	735	800
ν_3	1085	1110, 1090, 990
ν_4	630	640, 630

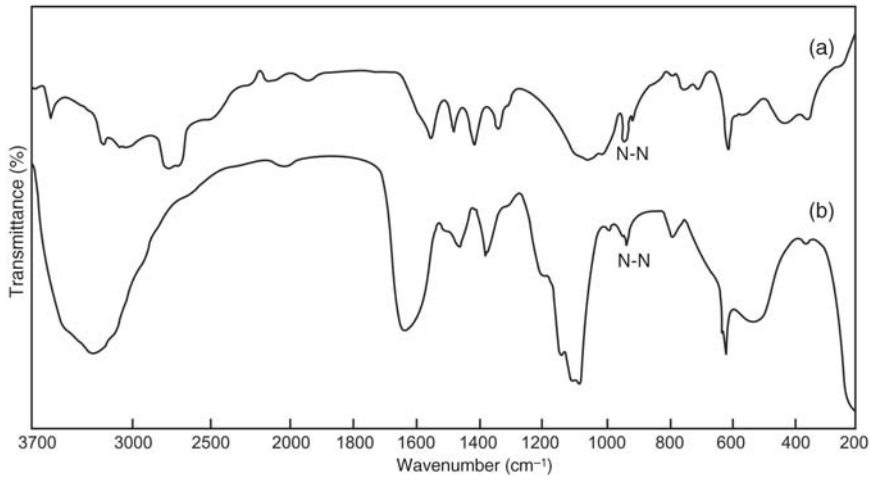

Figure 3.17 Infrared spectrum of (a) $[Mg(ClO_4)_2(N_2H_4)_2]$ and (b) $[Cr(ClO_4)_2(N_2H_4)_2]ClO_4$. Ph.D Thesis of Nesamani, C. under Prof. K. C. Patil at Indian Institute of Science.

The probable structure of $Cr(ClO_4)_2(N_2H_4)_2{\cdot}ClO_4$ has an octahedral chromium bonded to two nitrogen atoms of hydrazine and four oxygen atoms of two perchlorate groups (Figure 3.18).

Figure 3.19 shows the DTA curves of $Mg(ClO_4)_2(N_2H_4)_2$ and $Cr(ClO_4)_2(N_2H_4)_2{\cdot}ClO_4$. The complexes decompose exothermically at 267 and 240 °C to give MgO and Cr_2O_3, respectively.

The synthesis and crystal structure of nickel perchlorate hydrazine, a purple compound, has been reported (Figure 3.20). However, this compound is hazardous; it is explosive and needs to be handled carefully [33,34].

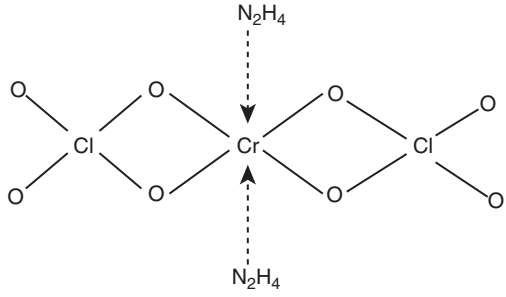

Figure 3.18 Structure of diperchlorate dihydrazine chromium(III) perchlorate. Ph.D Thesis of Nesamani, C. under Prof. K. C. Patil at Indian Institute of Science.

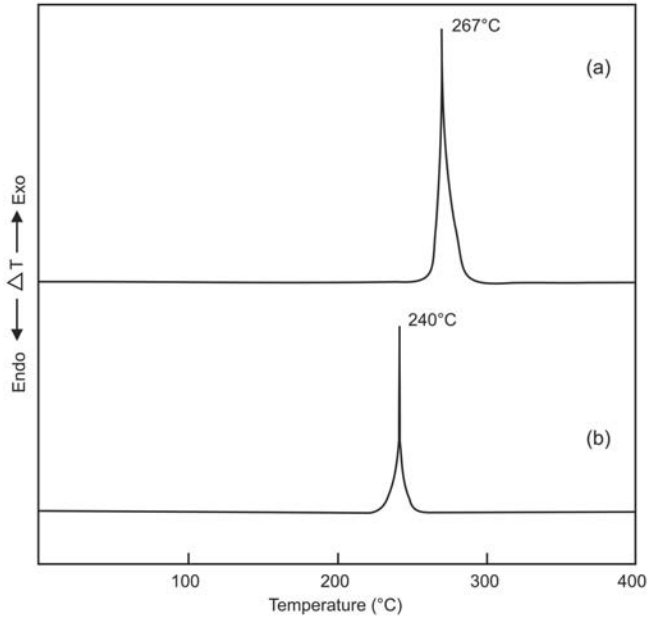

Figure 3.19 DTA curves of (a) $Mg(ClO_4)_2(N_2H_4)_2$ and (b) $Cr(ClO_4)_2(N_2H_4)_2{\cdot}ClO_4$. Ph.D Thesis of Nesamani, C. under Prof. K. C. Patil at Indian Institute of Science.

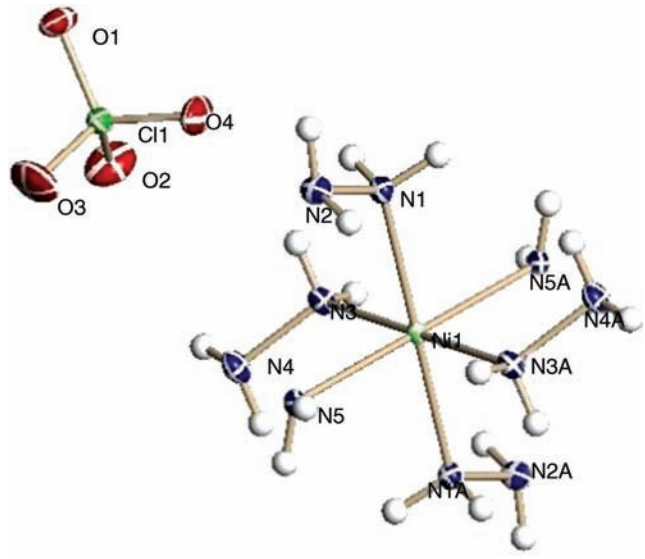

Figure 3.20 Monomeric unit of nickel perchlorate hydrazine polymer. Reproduced from Ref. [33] © 2011 WILEY-VCH Verlag GmbH & Co. KGaA, Weinheim.

New perchlorate salts $[Cr(ClO_4)_3](N_2H_4)_3$ and $[Cd(ClO_4)_2](N_2H_4)_3$ have been synthesized and their energetic characteristics evaluated by applying underwater detonation tests [35].

3.2.11 Metal Hydrazines of Organic Acids

Hydrazine reacts with several organic anions to form salts as discussed in Chapter 2, and these salts in turn react with metal ions to form complexes. Several such complexes of metal hydrazines investigated recently are briefly discussed in this section.

Hydrazine hydrate reacts with 4,5-imidazoledicarboxylic acid (imdc) to form hemihydrate metal complexes of the type $M(imdc)\cdot 0.5N_2H_4\cdot H_2O$, where M = Mn, Co, and Cd. On the other hand, Ni and Zn form monohydrazine metal complexes $M(imdc)N_2H_4\cdot H_2O$. The complexes of Co and Ni are high-spin complexes as indicated by their electronic spectra. They all undergo two-step decomposition with intermediate formation of imidazoledicarboxylate ion, which further gives rise to the corresponding oxides [36]. Similarly, hydrazine complexes with pyridine-2,*n*-dicarboxylic acid as the main class have been prepared. Complexes of the type $M(L)N_2H_4\cdot xH_2O$, where L = pyridine-2,*n*-dicarboxylate dianion, $x = 1$–3, and $n = 3$–6, have been synthesized and their properties investigated [37].

Rare earth based lanthanide complexes with 3-acetoxybenzoic acid (3-abH) of formula $[Ln(3\text{-}ab)_3(N_2H_4)_2]\cdot xH_2O$ (Ln = La, Ce, Pr, and Gd and $x = 0$; Ln = Nd and Sm and $x = 1$) and monohydrazine complexes with 4-acetoxybenzoic acid (4-abH) of formula $[Ln(4\text{-}ab)_3(N_2H_4)]\cdot H_2O$ (Ln = La, Ce, Pr, Nd, Sm, and Gd) have been prepared. These complexes undergo exothermic decomposition to form their respective metal oxides [38].

Glyoxylic acid reacts with transition metals in the presence of excess hydrazine hydrate to yield metal glyoxylate hydrazines of the formula $M(OOCCHO)_2(N_2H_4)_2$, where M = Mg, Mn, Co, Ni, Cu, Zn, and Cd. As these complexes are found to be isomorphous, this method is exploited for the preparation of mixed metal hydrazines of the formula $M^{1}_{/3}Co^{2}_{/3}(OOCCHO)_2(N_2H_4)_2$, where M = Mg, Mn, Ni, Zn, and Cd. On thermal decomposition the mixed metal complexes form the respective metal cobaltites (MCo_2O_4) below 290 °C [39]. In a similar fashion, nanoparticles of $NiCo_2O_4$ are prepared from a precipitate of the complex containing a solution of diphenylacetic acid together with hydrazine hydrate and nickel salt [40]. Mixed fumerate hydrazine with zinc ferrous

fumerato-hydrazinate is prepared by adding hydrazine hydrate to sodium fumerate taken in an aqueous medium. The whole solution is stirred in an inert atmosphere, while a metal ion solution containing metal salts in stoichiometric amount is added dropwise to it. The fumerato hydrazine complex has been used to prepare nano-sized nickel ferrite and mixed-metal ferrite $Co_{0.5}Zn_{0.5}Fe_2O_4$ [41].

3.3 REACTIVITY OF METAL SALT HYDRAZINES (FROM DETONATION TO DEFLAGRATION TO DECOMPOSITION)

The complexing of N_2H_4 with metal salts has the advantage of controlling the explosive characteristic of hydrazine. Coordination of hydrazine with a metal ion appears to alter the explosivity depending upon the nature of metal ion, that is, transition or non-transition metal. Transition metal ions like iron catalyze the decomposition of N_2H_4 readily to explosion. In contrast, non-transition metal ions like Mg and Al decrease the explosivity. Similarly, the nature of the anion also plays an important role. For example, oxidizing anions like ClO_4^-, NO_3^-, N_3^- enhance the decomposition of N_2H_4 and lead to explosion. Interestingly, Mg and Al perchlorates do not explode but deflagrate instead. Transition metal hydrazine complexes containing reducing anions like formate, oxalate, sulfite, and hydrazine carboxylates undergo combustion or deflagration once ignited.

Based on the thermal reactivity, three distinct groups of metal salt hydrazines have been distinguished (Table 3.26):

Table 3.26 Thermal reactivity of metal salt hydrazines.

$M(N_2H_4)_n^{2+}$	Anion		
	ClO_4^-, NO_3^-, N_3^-	$N_2H_3COO^-$, $C_2O_4^{2-}$ $HCOO^-$, CH_3COO^-, SO_3^{2-},	SO_4^{2-}, SCN^-, X^- (X = halogens)
M = (Cr, Mn, Fe, Co Ni, Zn, Cu, Cd)	Detonation	Deflagration (precursor to fine oxide)	Decomposition
M = (Mg, Al)	Deflagration (precursor to fine oxide)	—	—

1. metal salt hydrazines that detonate (detonators);
2. metal salt hydrazines that exhibit self-sustained but controlled combustion (combustibles);
3. metal salt hydrazines that undergo dehydrazination exothermically, followed by decomposition of the metal salts.

3.3.1 Precautions in Handling Explosive Materials

Transition metal hydrazine perchlorate, nitrate, and azide complexes are explosive in nature, as indicated by DTA experiments and impact sensitivity measurements. Special precautions have to be taken during the synthesis and characterization of these materials. Small quantities of up to 1 g can be prepared without any explosion. Special mention should be made of the nickel hydrazine azide complex, which is prepared from $NiCl_2 + NaN_3 + 2N_2H_4{\cdot}H_2O$. The product is highly friction sensitive, especially in dry state, and so samples are to be handled with a Teflon spatula. A few milligrams are used for DTA and impact sensitivity tests.

3.4 SUMMARY

A new method for the preparation of simple metal isothiocyanate, oxalate, azide, nitrate, and perchlorate hydrazine complexes has been developed by dissolving metal powders into a solution of ammonium or hydrazinium salts in hydrazine hydrate. Mixed metal salt hydrazines are also prepared by a similar method. These complexes have been investigated as precursors for the preparation of technologically important oxide materials like ferrites and cobaltites and energetic compounds like metal perchlorate, azide, and nitrate hydrazines. Interestingly, only magnesium azide hydrazine, $Mg(N_3)_2(N_2H_4)_2$, and magnesium oxalate hydrazine, $MgC_2O_4(N_2H_4)_2$, complexes, prepared by dissolving magnesium metal in ammonium azide/ammonium oxalate in hydrazine hydrate, give dinitrogen compounds on pyrolysis.

REFERENCES

1. Schmidt, E.W. (2001) *Hydrazine and its Derivatives: Preparation, Properties, Applications*, 2nd edn, John Wiley & Sons, Inc.
2. Bottomley, F. (1970) Reactions of hydrazine with transition-metal complexes. *Quarterly Reviews, Chemical Society*, **24**, 617–638.

3. Manimekalai, R., Sinduja, C.R., and Thrivikraman, K. (2012) Synthesis and characterization of nickel ferrite nanoparticles from 2,4-dichlorophenoxy acetate hydrazinate precursors. *International Journal of NanoScience and Nanotechnology*, **3**, 105–110.
4. Park, J.W., Chae, E.H., Kim, S.H. *et al.* (2006) Preparation of fine Ni powders from nickel hydrazine complex. *Materials Chemistry and Physics*, **97**, 371–378.
5. Gingasu, D., Mindru, I., Patron, L.A. *et al.* (2011) Investigation of magnetite formation in the presence of hydrazine dihydrochloride. *Digest Journal of Nanomaterials and Biostructures*, **6**, 1065–1072.
6. Gawas, U.B., Verenkar, V.M.S., and Mojumdar, S.C. (2012) Nano-crystalline $Mn_{0.3}Ni_{0.3}Zn_{0.4}Fe_2O_4$ obtained by novel fumarato-hydrazinate precursor method. *Journal of Thermal Analysis and Calorimetry*, **108**, 865–870.
7. Krishna Bhat, D. (2008) Facile synthesis of ZnO nanorods by microwave irradiation of zinc–hydrazine hydrate complex. *Nanoscale Research Letters*, **3**, 31–35.
8. Patil, K.C., Vittal, J.J., and Patel, C.C. (1983) Preparation, characterization and thermal properties of di-N-isothiocyanato dihydrazine metal (II). *Proceedings of the Indian Academy of Sciences-Chemical Sciences*, **92**, 83–89.
9. Govindarajan, S., Babu, P.J., and Patil, K.C. (1986) Thermal analysis of metal sulfate hydrazinates and hydrazinium metal sulfates. *Thermochimica Acta*, **97**, 287–293.
10. Ravindranathan, P. and Patil, K.C. (1983) Thermal reactivity of metal formate hydrazinates. *Thermochimica Acta*, **71**, 53–57.
11. Mahesh, G.V. and Patil, K.C. (1986) Thermal reactivity of metal acetate hydrazinates. *Thermochimica Acta*, **99**, 153–158.
12. Mahesh, G.V. and Patil, K.C. (1987) Low temperature preparation of nickel and zinc cobaltites. *Reactivity of Solids*, **4**, 117–123.
13. Patil, K.C., Gajapathy, D., and Kishore, K. (1982) Thermal reactivity of metal oxalate hydrazinates. *Thermochimica Acta*, **52**, 113–120.
14. Gajapathy, D. (1983) *Studies on metal–hydrazine system*, Ph.D Thesis, Indian Institute of Science, Bangalore.
15. Kishore, K., Patil, K.C., and Gajapathy, D. (1985) Mechanistic studies on self deflagrating solids from temperature profile analysis. *Propellants Explosives Pyrotechnics*, **10**, 187–191.
16. Gajapathy, D. and Patil, K.C. (1983) Mixed metal oxalate hydrazinates as compound precursors to spinel ferrites. *Materials Chemistry and Physics*, **9**, 423–438.
17. Patil, K.C., Gajapathy, D., and Pai Verneker, V.R. (1982) Low temperature ferrite formation using metal oxalate hydrazinate precursor. *Materials Research Bulletin*, **17**, 29–32.
18. Patil, K.C., Gajapathy, D., and Pai Verneker, V.R. (1983) Low temperature cobaltite formation using mixed metal oxalate hydrazine precursor. *Journal of Materials Science Letters*, **2**, 272–274.
19. Budukuley, J.S. (1984) *Studies on hydrazine hydrate sulphur-oxide transition metal ion system*, Ph.D thesis, University of Bombay.
20. Budukuley, J.S. and Patil, K.C. (1990) Synthesis, infrared spectra and thermoanalytical properties of transition metal sulphite hydrazine hydrates. *Journal of Thermal Analysis*, **36**, 2583–2592.
21. Budukuley, J.S. and Patil, K.C. (1989) Synthesis and thermoanalytical properties of mixed metal sulphite hydrazinate hydrates-I. *Synthesis and Reactivity in Inorganic and Metal-Organic Chemistry*, **19**, 909–922.

22. Budukuley, J.S. and Patil, K.C. (1989) Thermal properties of magnesium bisulphite hydrazinate hydrate. *Thermochimica Acta*, **153**, 419–422.
23. Nesamani, C. (1983) *Studies on high energy hydrazine compound*, Ph.D Thesis, Indian Institute of Science, Bangalore.
24. Patil, K.C., Nesamani, C., and Pai Verneker, V.R. (1982) Synthesis and characterization of metal hydrazine nitrate, azide and perchlorate complexes. *Synthesis and Reactivity in Inorganic and Metal-Organic Chemistry*, **12**, 383–395.
25. Singh, V.P., Singh, K.B., and Narang, K.K. (2009) Synthesis, electronic and IR spectral studies of some polymeric cobalt(II), nickel(II), zinc(II) and cadmium(II) azido complexes with hydrazine. *Journal of Macromolecular Science, Part A. Pure and Applied Chemistry*, **46**, 110–115.
26. Wu, B.D., Yang, L., Wang, S.W. *et al.* (2011) Preparation, crystal structure, thermal decomposition, and explosive properties of a novel energetic compound [Zn $(N_2H_4)_2(N_3)_2]n$: a new high-nitrogen material (N = 65.60%). *Zeitschrift fur Anorganische und Allgemeine Chemie*, **637**, 450–455.
27. Patil, K.C., Nesamani, C., and Pai Verneker, V.R. (1982) Dinitrogen complex of magnesium. *Polyhedron*, **1**, 421–422.
28. Zhu, S.G., Wu, Y.C., Zhang, W.Y., and Mu, J.G. (1997) Evaluation of a new primary explosive: nickel hydrazine nitrate (NHN). *Propellants Explosives Pyrotechnics*, **22**, 317–320.
29. Chhabra, J.S., Talawar, M.B., Makashir, P.S. *et al.* (2003) Synthesis, characterization and thermal studies of (Ni/Co) metal salts of hydrazine: potential initiatory compounds. *Journal of Hazardous Materials*, **A99**, 225–239.
30. Soundararajan, R. (1979) *The chemistry of hydrazine derivatives*, PhD Thesis, Indian Institute of Science, Bangalore.
31. Patil, K.C., Soundararajan, R., and Pai Verneker, V.R. (1980) A Process for the synthesis of aluminium perchlorate trihydrazinate. Indian Patent, No. 150422.
32. Patil, K.C., Nesamani, C., and Pai Verneker, V.R. (1979) Synthesis and characterization of diperchlorate dihydrazine chromium(III) perchlorate. *Chemistry & Industry (London)*, 901–902.
33. Bushuyev, O. and Hope-Weeks, L.J. (2011) *Structure of transition metal hydrazine perchlorate primary explosives and the ways to work with them*. Texas Tech University Poster.
34. Jyllian, K. (2010) Texas tech lessons. *C&EN News*, **88**, 34–37.
35. Wojewodka, A., Bełzowski, J., Wilk, Z., and Stas, J. (2009) Energetic characteristics of transition metal complexes. *Journal of Hazardous Materials*, **171**, 1175–1177.
36. Premkumar, T. and Govindrajan, S. (2002) The chemistry of hydrazine derivatives – thermal behaviour of hydrazinium salts and metal hydrazine complexes of 4,5-imidazole dicarboxylic acid. *Thermochimica Acta*, **386**, 35–42.
37. Saravanan, K., Govindarajan, S., and Chellappa, D. (2004) Preparation, characterization, and thermal reactivity of divalent transition metal hydrazine pyridine-2, n-dicarboxylates (n *5* 3, 4, 5, and 6). *Synthesis and Reactivity in Inorganic and Metal-Organic Chemistry*, **34**, 353–369.
38. Pricilla Bai, E.H. and Vairam, S. (2013) Hydrazine complexes of lanthanides with 3-acetoxy- and 4-acetoxybenzoic acids: spectroscopic, thermal, and XRD Studies. *Journal of Chemistry*, doi: 10.1155/2013/717618.

39. Vikram, L. and Sivasankar, B.N. (2007) Spectral, thermal and X-ray studies on some new bis-hydrazine metal glyoxylates and bis-hydrazine mixed metal glyoxylates. *Thermochimica Acta*, **452**, 20–27.
40. More, A., Verenkar, V.M.S., and Mojumdar, S.C. (2008) Nickel ferrite nanoparticles synthesis from novel fumarato-hydrazinate precursor. *Journal of Thermal Analysis and Calorimetry*, **94**, 63–67.
41. Gonsalves, L.R., Verenkar, V.M.S., and Mojumdar, S.C. (2009) Preparation and characterization of $Co_{0.5}Zn_{0.5}Fe_2(C_4H_2O_4)_3{\cdot}6N_2H_4$, A precursor to prepare $Co_{0.5}Zn_{0.5}Fe_2O_4$ nanoparticles. *Journal of Thermal Analysis and Calorimetry*, **96**, 53–57.

4

Metal Hydrazine Carboxylates

K. C. Patil[1] and Tanu Mimani Rattan[2]
[1]*Department of Inorganic and Physical Chemistry, Indian Institute of Science, Bangalore, India*
[2]*Department of Physics, Sri Sathya Sai Institute of Higher Learning, Prasanthi Nilayam, India*

4.1 INTRODUCTION

Hydrazine hydrate reacts with carbon dioxide gas and H^+ cation to form hydrazine carboxylate anion ($N_2H_3COO^-$) or the zwitterion $NH_3{}^+NHCOO^-$. This anion is a bidentate ligand that coordinates with a metal ion through N and O atoms to form metal hydrazine carboxylate complexes of various types [1–4]. The synthesis and single-crystal structures of many hydrazine carboxylate based complexes are summarized in Chapter 1 (Section 1.2.3). The complexes have so far been prepared from solutions containing the corresponding metal ions in hydrazine hydrate saturated with CO_2 gas. The reactions of metal ions in hydrazine hydrate with CO_2 are heterogeneous (liquid–gas, solid–gas) in nature and the time required for completion of the reaction varies from days to weeks. It is also difficult to control the kinetics of these reactions and obtain the desired product. Therefore, a new method of synthesis by homogeneous reactions is attractive. In these reactions metal ions are

Inorganic Hydrazine Derivatives: Synthesis, Properties and Applications, First Edition.
Edited by K. C. Patil and Tanu Mimani Rattan.

homogenously mixed in a solution of hydrazinium hydrazine carboxylate ($N_2H_5COON_2H_3$), which is prepared by dissolving ammonium carbonate in hydrazine hydrate (discussed in Chapter 2):

$$\begin{aligned} NH_4HCO_3{\cdot}NH_2COONH_4 + 2N_2H_4{\cdot}H_2O \rightarrow N_2H_5HCO_3{\cdot}NH_2COON_2H_5 + 2NH_4OH \\ \downarrow \\ N_2H_5COON_2H_3 + NH_3 + CO_2 + H_2O \end{aligned} \tag{4.1}$$

The complexes crystallize in a few hours to a few days. Interestingly, as the products are formed from the process of crystallization, they are single crystals of high purity. This chapter describes the synthesis, infrared spectra, electronic spectra, and thermal reactivity of several simple and mixed metal hydrazine carboxylate complexes prepared by this method.

4.2 METAL HYDRAZINE CARBOXYLATES – $M(N_2H_3COO)_2$

Metal hydrazine carboxylates are formed by reaction of the respective metal ions with a saturated solution of ammonium carbonate in hydrazine hydrate [5]. The products precipitate instantaneously. The formation of metal hydrazine carboxylates by the reaction of metal ions with the ligand $N_2H_3COO^-$ (1.23) can be represented by the following general equation:

$$M^{2+}(aq) + 2N_2H_3COO^-(aq) \rightarrow M(N_2H_3COO)_2(s) \tag{4.2}$$

where M = Mn, Co, Ni, Cu, and Zn.

In all these complexes, the metal ion is coordinated to the ligand through N and O atoms, forming a five-membered ring. The coordination number of the metal atom varies from five to seven.

The formation of metal hydrazine carboxylates is confirmed by chemical analysis and infrared spectroscopy. Table 4.1 summarizes the infrared absorption frequencies of these complexes and their assignments.

The assignments of infrared absorption bands are based on those observed for metal glycinates, since the structure of metal hydrazine carboxylates is reported to be similar to that of metal glycinates [6]. As the hydrazine carboxylate anion acts as a bidentate ligand, characteristic absorptions due to COO^- and N_2H_3 groups are observed and

Table 4.1 Infrared absorption frequencies (cm^{-1}) of $M(N_2H_3COO)_2$.

Assignment	Mn	Co	Ni	Cu	Zn
$\nu_{as}(COO^-)$	1608	1615	1615	1625	1615
$\nu_s(COO^-)$	1375	1390	1385	1375	1385
$\delta(N_2H_3)$	1590, 1484	1590, 1510	1580, 1475	1580, 1475	1580, 1510
$\rho_r(N_2H_3)$	1208	1210	1225	1210	1210
ν(N-N)	1000	980	985	992	982
ν(O-C-O) or $\rho_w NH_2$	820	820	820	808	820
$\rho_w(COO^-)$	660	660	650	658	660
$\rho_r NH_2$ or $\delta(COO^-)$	620	616	615	625	610
υM-N	430	438	415	445	438

assigned as shown in Table 4.1. The ν_{N-N} of N_2H_3 appears in the region 980–1000 cm^{-1} as expected [7].

Thermal analysis data of metal hydrazine carboxylates, given in Table 4.2, reveal that the compounds decompose exothermically. The two exotherms observed in all cases are due to the decomposition of hydrazine carboxylate complex. These complexes decompose to the corresponding metal oxalate first, and later to form the carbonate salt. Formation of the oxalate intermediate is confirmed by interrupting the DTA

Table 4.2 Thermal analysis data of $M(N_2H_3COO)_2$.

M	DTA peak temperature (°C)[a]	Thermogravimetry			
		Temperature range (°C)	% Weight loss		
			Obsd.	Calcd.	Product
Mn	205(+)	190–200	52.00	—	MnC_2O_4
	230(+)	—	—	—	$MnCO_3$
	460(−)	230–400	66.25	65.40	MnO
Co	235(+)	210–400	44.00	43.00	CoC_2O_4
	254(+)	—	—	—	$CoCO_3$
	460(−)	250–400	60.65	60.03	CoO
Ni	275(+)	250–270	43.00	43.12	NiC_2O_4
	285(+)	—	—	—	$NiCO_3$
	650(−)	280–400	64.66	64.30	NiO
Cu	100(+)	90–105	—	—	CuC_2O_4
	120(+)	—	63.59	62.76	CuO
Zn	300(+)	240–260	57.60	—	ZnC_2O_4
	325(+)	—	—	—	$ZnCO_3$
	550(−)	300–500	63.17	61.50	ZnO

[a] (−) = Endotherm; (+) = exotherm.

(differential thermal analysis) runs after the first exotherms and testing the residue for oxalate. The residue sample shows a positive test for $C_2O_4^{2-}$, while no effervescence is observed with an acid test, indicating the absence of CO_3^{2-}. The residue after the second exotherm shows a positive test for carbonate alone and no oxalate is found. On further heating, the metal carbonates decompose endothermically to metal oxides.

Thermogravimetric results of metal hydrazine carboxylates show one or two steps. For cobalt and nickel complexes, the observed weight loss after the first step corresponds to the formation of a carbonate compound. Manganese and zinc complexes show weight losses that correspond to the formation of neither a carbonate compound nor an oxide, but somewhere in-between. The residue, however, gives a positive test for CO_3^{2-}, indicating incomplete decomposition. Thus, it appears that intermediates like oxalate and carbonates are formed metathetically. It is not surprising that TG (thermogravimetry) results do not agree with DTA peaks, since TG is more dynamic in nature than DTA, which is static.

The final weight losses in all the metal complexes agree with the formation of respective metal oxides MO, with cobalt complex giving Co_2O_3. The various steps of decomposition are represented as follows:

$$M(N_2H_3COO)_2(s) \rightarrow MC_2O_4(s) + N_2(g) + 2NH_3(g) \qquad (4.3)$$

$$MC_2O_4(s) \xrightarrow{\text{Air}} MCO_3(s) + CO_2(g) \qquad (4.4)$$

$$MCO_3(s) \rightarrow MO(s) + CO_2(g) \qquad (4.5)$$

where M = Mn, Co, Ni, Cu, and Zn.

The thermal analysis results of these complexes are at variance with those reported in earlier literature. Previous studies indicated the formation of corresponding metals as the end product, when DTA was carried out in an argon atmosphere. The formation of intermediates was not identified then. However, in this thermal analysis, metal oxides are obtained as the products of decomposition of metal hydrazine carboxylates, even when the decompositions are carried out in a nitrogen atmosphere.

4.3 METAL HYDRAZINE CARBOXYLATE HYDRATES – $M(N_2H_3COO)_n \cdot xH_2O$; $n = 2, 3$

Some metals ions react with hydrazine carboxylate anion to form metal hydrazine carboxylate hydrates. When metal salts in solution are added to

dilute solutions of 5% of N_2H_3COOH in $N_2H_4{\cdot}H_2O$, they initially form a precipitate that dissolves in excess reagent. The clear solution so-obtained, when kept in an open atmosphere, crystallizes to give a solid product within a couple of days. On chemical analysis, these crystals were found to be metal hydrazine carboxylate hydrates [8,9]. The formation of various hydrazine carboxylate hydrates by the reaction of metal ions with $N_2H_3COON_2H_5$ can be represented by the following equations:

$$MX_2(aq) + 2N_2H_3COON_2H_5(aq) + xH_2O(l) \rightarrow$$
$$M(N_2H_3COO)_2{\cdot}xH_2O(s) + 2N_2H_5X(aq) \qquad (4.6)$$

where M = Mg, Ca, Cr, Mn, Cu, TiO, and ZrO; X = anion.

The formation of hydrazine carboxylate hydrates of copper(II) and chromium(II) takes place under different conditions [10,11]. For the copper complex, an optimum concentration of $N_2H_3COO^-$ is required to avoid the reduction of Cu^{2+} ions to copper metal. The addition of solid N_2H_3COOH to a saturated solution containing Cu^{2+} ions facilitates the ready precipitation of the blue $Cu(N_2H_3COO)_2{\cdot}H_2O$ complex. Similarly, the lilac colored Cr(II) complex requires a freshly prepared chromous chloride solution obtained by passing a Cr(III) solution through a zinc amalgam column with N_2H_3COOH under nitrogen atmosphere.

Red chromium(III) hydrazine carboxylate trihydrate complex is prepared by treating aqueous chromium(III) chloride with a solution of $N_2H_3COON_2H_5$:

$$CrCl_3(aq) + 3N_2H_3COON_2H_5(aq)$$
$$\rightarrow Cr(N_2H_3COO)_3{\cdot}3H_2O(s) + 3N_2H_5Cl(aq) \qquad (4.7)$$

All the metal hydrazine carboxylates hydrates of Mg, Ca, Cr, Mn, Cu, TiO, and ZrO show characteristic infrared absorptions at 3500 (ν_{OH}), 2980 (ν_{N-H}), 1655 ($\nu_{asy\ COO^-}$), 1495 ($\nu_{sym\ COO^-}$), 1010 (ν_{N-N}), 805 (ν_{N-N}), and 755 cm^{-1} (δ_{O-C-O}), which are characteristic of $N_2H_3COO^-$ anion. In the case of titanyl/zirconyl hydrazine carboxylates, an additional peak at 930–960 cm^{-1} is seen due to the stretching frequency of Ti/Zr = O (Figure 4.1).

The structure and bonding in these complexes are evaluated by their electronic spectra and magnetic moment. Typical cases of the $Cu(N_2H_3COO)_2{\cdot}H_2O$ and $Cr(N_2H_3COO)_2{\cdot}H_2O$, show an absorption at 625 and 550 nm, respectively. This absorption has been assigned, respectively, to the $^2T_{2g} \rightarrow {}^2E_g$ transition of Cu^{2+} and the $^5E_g \rightarrow {}^5T_{2g}$

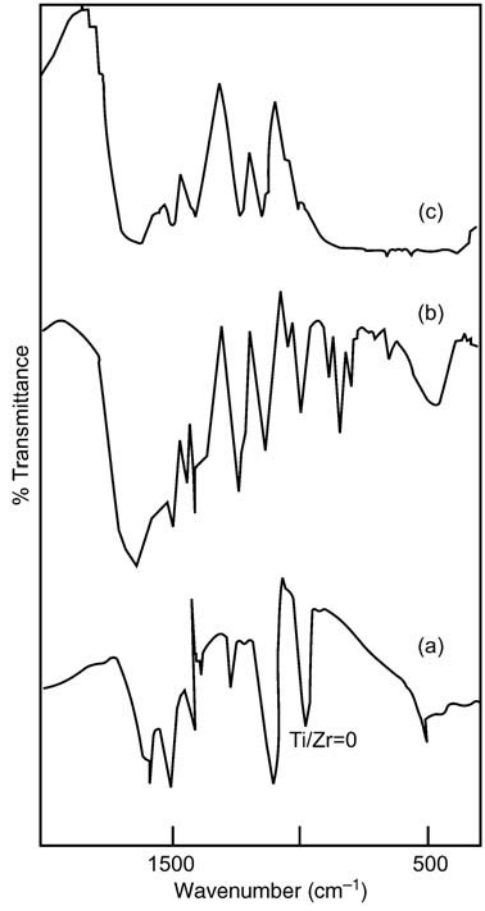

Figure 4.1 Infrared spectra of (a) $TiO(N_2H_3COO)_2 \cdot 2H_2O$, (b) $ZrO(N_2H_3COO)_2 \cdot 2H_2O$, and (c) $ZrTiO_2(N_2H_3COO)_2 \cdot 4H_2O$. Reproduced from Ref. [12] with permission from Elsevier © 1993.

transition of Cr^{2+} in an octahedral field. The spin-only magnetic moment value at 298 K for Cu^{2+} is 1.52 BM as against the expected value of 1.73 BM; the corresponding high-spin value of Cr^{2+} is 2.79 as against 4.95 BM. The reduction in the magnetic moment of these complexes is attributed to magnetic exchange of an antiferromagnetic nature. This is a consequence of a weak bond between two or more metal atoms or a super-exchange process via intervening oxygen or other atoms. Both copper and chromium(II) show a similar structural trend as per their magnetic moment, which is further confirmed by their identical XRD patterns (Figure 4.2).

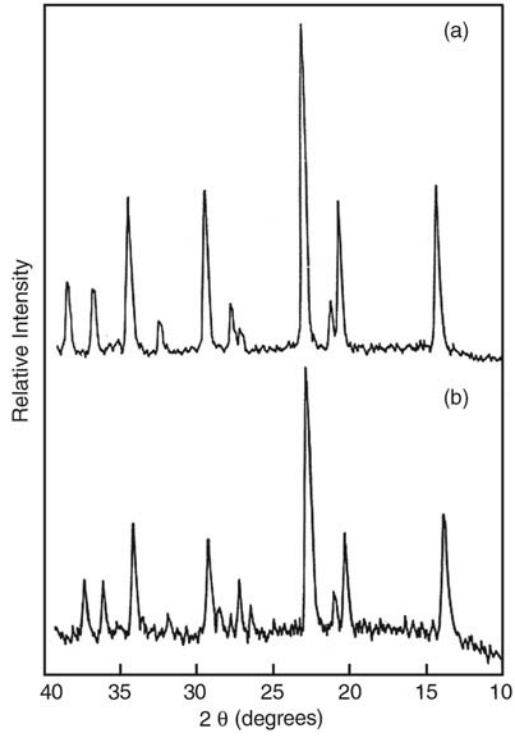

Figure 4.2 XRD pattern of (a) $Cu(N_2H_3COO)_2{\cdot}H_2O$ and (b) $Cr(N_2H_3COO)_2{\cdot}H_2O$. Reproduced with permission from [11] © 1989 The Indian Academy of Sciences.

The electronic spectra of Cr^{3+} shows three absorption bands, at 700, 515, and 397 nm, corresponding to $^4A_{2g} \rightarrow {}^2E_g$, $^4T_{2g} \rightarrow {}^4T_{1g}$ transitions; this confirms its octahedral field provided by the coordination of its three bidentate $N_2H_3COO^-$ ligands, while the three water molecules remain un-coordinated.

Thermal analysis of metal hydrazine carboxylate hydrate complexes, $M(N_2H_3COO)_2{\cdot}xH_2O$, initially shows an endotherm due to the loss of water of hydration. This is followed by exothermic decomposition of the anhydrous salts through carbonate intermediates to the corresponding oxides, similar to anhydrous metal hydrazine carboxylates (Figure 4.3). The TG (thermogravimetry) and DTA data of some of metal hydrazine carboxylate hydrates are summarized in Table 4.3.

TG-DTA curves of the titanyl/zirconyl hydrazine carboxylate complexes show their decomposition below 300 °C in more than one step [12].

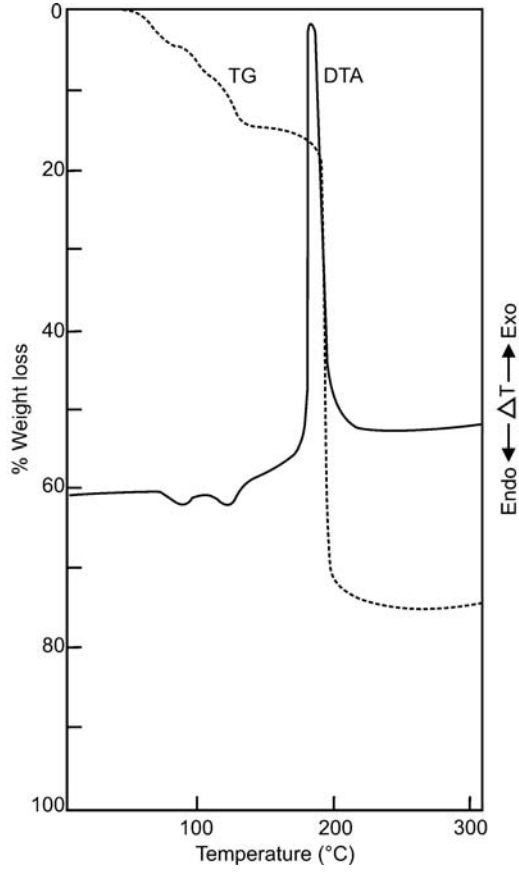

Figure 4.3 Simultaneous TG-DTA curves of $Cr(N_2H_3COO)_2{\cdot}3H_2O$. Ph.D Thesis of Ravindranathan, P. under Prof. K. C. Patil at Indian Institute of Science.

The TG plots show two-step decomposition whereas DTA curves show four peaks. The two steps observed in TG correspond to the formation of titanyl/zirconyl oxalate hydrazine and TiO_2/ZrO_2 respectively. The DTA peaks are assigned to dehydration, dehydrazination, and decomposition reactions that can be written as follows:

$$MO(N_2H_3COO)_2{\cdot}2H_2O \xrightarrow{\text{endo}} MO(N_2H_3COO)_2 + 2H_2O \qquad (4.8)$$

$$MO(N_2H_3COO)_2 \xrightarrow{\text{exo}} MOC_2O_4{\cdot}N_2H_4 + N_2 + H_2 \qquad (4.9)$$

$$MOC_2O_4{\cdot}N_2H_4 \xrightarrow{\text{air}} MOCO_3 + CO_2 + N_2H_4 \qquad (4.10)$$

Table 4.3 Thermal analysis data of $M(N_2H_3COO)_n \cdot xH_2O$.

M	DTA peak temperature (°C)[a]	Thermogravimetry			
		Temperature range (°C)	% Weight loss		
			Obsd.	Calcd.	Products
Mg	170(−)	150–180	18.00	17.11	$Mg(N_2H_3COO)_2$
	325(+)	—	—	—	—
	380(+)	180–485	81.00	80.83	MgO
Ca	135(−)	115–152	8.60	8.65	$Ca(N_2H_3COO)_2$
	281(+)	—	—	—	—
	308(+), 345(+)	152–310	38.20	38.44	CaC_2O_4
	420(+)	310–700	51.80	51.90	$CaCO_3$
	720(−)	700–930	73.00	73.04	CaO
Mn	130(−)	110–170	25.80	14.94	$Mn(N_2H_3COO)_2$
	170, 180(+)	170–205	29.50	27.39	$MnC_2O_4 \cdot N_2H_4$
	205(+)	205–300	69.90	70.55	MnO
Cu	70(−)	60–90	7.0	7.8	$Cu(N_2H_3COO)_2$
	115(+)	90–130	70.50	70.20	Cu, CuO
Cr(II)	90(−)	80–110	9.0	8.2	$Cr(N_2H_3COO)_2$
	180(+)	110-250	65.0	65.40	Cr_2O_3
Cr(III)	90(−)	80–100	8.0	8.0	$Cr(N_2H_3COO)_2 \cdot 1.5H_2O$
	120(−)	100–130	15.0	16.0	$Cr(N_2H_3COO)_2$
	190(+)	130–240	76.0	77.0	Cr_2O_3
TiO	65(−)	50–110	—	—	$TiO(N_2H_3COO)_2$
	90(+)	—	26.5	27.0	$TiOC_2O_4 \cdot N_2H_4$
	150(+)	110–270	—	—	$TiOCO_3$
	260(−)	—	67.0	68.0	TiO_2
ZrO	75(−)	65–130	—	—	$ZrO(N_2H_3COO)_2$
	120(+)	—	22.0	22.5	$ZrOC_2O_4 \cdot N_2H_4$
	210(+)	130–300	—	—	$ZrOCO_3$
	295(−)	—	58.0	58.0	ZrO_2
$ZrTiO_2$	95(−)	85–230	—	—	$ZrTiO_2(N_2H_3COO)_4$
	220(+)	—	24.0	24.3	$ZrTiO_2(C_2O_4)_2 \cdot N_2H_4$
	240(+)	230–300	—	—	$ZrTiO_2(CO_3)_2$
	285(−)	—	61.5	62.0	$ZrTiO_4$

[a] (−) = Endotherm; (+) = exotherm.

$$MOCO_3 \xrightarrow{\text{endo}} MO_2 + CO_2 \tag{4.11}$$

where M = Ti, Zr.

Titanyl and zirconyl hydrazine carboxylates and their solid solutions decompose below 300 °C to yield fine particle, large surface area TiO_2, ZrO_2, and $ZrTiO_4$, respectively. Fine particle TiO_2 may be useful as a catalyst for photodecomposition of water into H_2 and O_2.

4.3.1 Lead Hydroxy Metal Hydrazine Carboxylate Hydrates – $[PbMO(OH)_2(N_2H_3COO)_2{\cdot}xH_2O]$

When solutions containing isomorphous (identical crystal structures and sizes) metal ions undergo crystallization they form a new solid, resulting in solid solutions. Metal hydrazine carboxylate hydrates combine with lead to form a solid solution of lead hydroxy hydrazine carboxylate complex. Lead hydroxy metal hydrazine carboxylate hydrates of the type $PbMO(OH)_2(N_2H_3COO)_2{\cdot}xH_2O$, where M = Zr and Ti, are prepared by the reaction of the corresponding ions in aqueous solutions with hydrazine carboxylic acid and ammonia [13,14]:

$$\begin{aligned} &Pb(Zr,Ti)O(OH)_2{}^{2+}(aq) + 2N_2H_3COO^-(aq) + xH_2O(l) \rightarrow \\ &Pb(Zr,Ti)O(OH)_2(N_2H_3COO)_2{\cdot}H_2O(s) \end{aligned} \tag{4.12}$$

In similar complexes, when lanthanum substitutes lead, it gives rise to a complex of the type $[Pb/LaMO(OH)_2(N_2H_3COO)_2{\cdot}xH_2O]$.

All these complexes form as a curdy white precipitate, which is filtered off, washed, and dried over P_2O_5 in a vacuum desiccator. The composition of the precursors has been determined by chemical and TG-DTA analysis (Table 4.4).

Infrared spectra of these lead/lanthanum based hydrazine carboxylates show characteristic absorptions at 3340–3360 (ν_{OH}), 3295–3325 (ν_{N-H}), 1730–1740 (δ_{COO}), and 996–1005 cm^{-1} (ν_{N-N}). The stretching frequency of Ti=O is seen at 930–960 cm^{-1}.

Lead hydroxy metal hydrazine carboxylate hydrates decompose exothermically to carbonate hydrazine intermediate, followed by an exotherm to form respective oxides such as lead zirconium titanate (PZT) and lead lanthanum zirconium titanate PLZT, as one can see from Figure 4.4.

The decomposition/combustion reaction of the redox precursors (oxidizing and reducing groups in same molecule) can be written as:

$$\begin{aligned} &PbMO(OH)_2(N_2H_3COO)_2{\cdot}H_2O(s) \xrightarrow[350\,^\circ C]{2O_2} PbMO_3(s) \\ &+ 2CO_2(g) + 5H_2O(g) + 2N_2(g) \end{aligned} \tag{4.13}$$

where M = Ti, Zr, or TiZr.

Combustion of the redox compound yields a single-phase (100%) perovskite $PbMO_3$, that is, $PbTiO_3$, $PbZrO_3$, and $PbZrTiO_3$.

Table 4.4 Thermal analysis data of lead/lanthanum hydroxy metal hydrazine carboxylate hydrates.

Precursors	DTA peak temperature (°C)[a]	Thermogravimetry % Weight loss		Product
		Obsd.	Calcd.	
$PbTiO(OH)_2(N_2H_3COO)_2{\cdot}H_2O$	105 (−)	16.10	16.48	$PbTiO(OH)_2CO_3N_2H_4$
	160 (+), 245 (+)	35.10	35.92	$PbTiO_3$
$PbZrO(OH)_2(N_2H_3COO)_2{\cdot}H_2O$	115 (−)	13.82	14.69	$PbZrO(OH)_2CO_3N_2H_4$
	160 (+), 225 (+)	33.20	34.30	$PbZrO_3$
$Pb(Zr_{0.53}Ti_{0.47})O(OH)_2(N_2H_3COO)_2{\cdot}H_2O$	140 (−), 205 (+)	16.00	15.32	$Pb(Zr_{0.53}Ti_{0.47})O(OH)_2CO_3N_2H_4$
	250 (+)	35.00	34.30	$Pb(Zr_{0.53}Ti_{0.47})O_3$
$Pb_{0.92}La_{0.08}(Zr_{0.65}Ti_{0.35})O(OH)_2(N_2H_3COO)_2{\cdot}5H_2O$	120 (−)	27.80	26.30	$Pb_{0.92}La_{0.08}(Zr_{0.53}Ti_{0.47})O(OH)_2CO_3N_2H_4$
	200 (+), 245 (+)	42.50	42.70	$Pb_{0.92}La_{0.08}(Zr_{0.53}Ti_{0.47})O_3$

[a] (−) = Endotherm; (+) = exotherm.

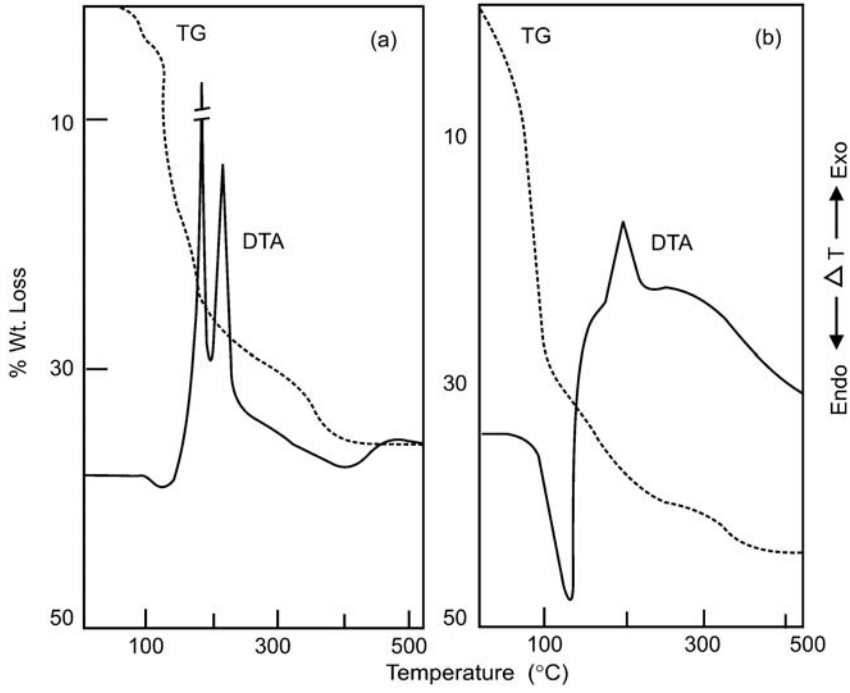

Figure 4.4 Simultaneous TG-DTA curves of (a) $Pb(Zr,Ti)O(OH)_2(N_2H_3COO)_2{\cdot}H_2O$ and (b) $(Pb,La)(Zr,Ti)O(OH)_2(N_2H_3COO)_2{\cdot}H_2O$. Adapted from [13] with permission from Allerton Press © 1994.

4.3.2 Rare Earth Metal Hydrazine Carboxylate Hydrates – $Ln(N_2H_3COO)_3{\cdot}3H_2O$

When aqueous solutions of rare earth salts are treated with solutions of ammonium carbonate in hydrazine hydrate ($N_2H_5COON_2H_3$), rare earth metal hydrazine carboxylate hydrate complexes are formed [15]. Initially, a precipitate forms that dissolves with the addition of excess reagent. On keeping the solution for a couple of days crystalline solids separate. The crystals are washed with alcohol and then diethyl ether and stored in a vacuum desiccator. The composition of the crystals determined by chemical analysis and infrared spectra has been found to be $Ln(N_2H_3COO)_3{\cdot}3H_2O$:

$$LnX_3(aq) + 3N_2H_5COON_2H_3 + 3H_2O \rightarrow$$
$$Ln(N_2H_3COO)_3{\cdot}3H_2O + 3N_2H_5X \qquad (4.14)$$

where Ln = rare earth metal ion; X = anion.

As expected, the IR absorption spectra of $Ln(N_2H_3COO)_3{\cdot}3H_2O$ type complexes are all identical. They show the characteristic N–N stretching frequency of $N_2H_3COO^-$ in the region 990–l000 cm^{-1}. Other infrared absorption frequencies of $N_2H_3COO^-$ are similar to those reported for $M(N_2H_3COO)_2{\cdot}xH_2O$.

Thermal analysis of the complexes $Ln(N_2H_3COO)_3{\cdot}3H_2O$ shows the loss of water of hydration initially, in a single step, to yield the corresponding metal hydrazine carboxylates (Table 4.5). The dehydration

Table 4.5 Thermal analysis data of $Ln(N_2H_3COO)_3{\cdot}xH_2O$.

Ln	DTA peak temperature (°C)[a]	Thermogravimetry			
		Temperature range (°C)	% Weight loss		
			Obsd.	Calcd.	Products
Ce	145(−)	100–160	13.00	12.88	$Ce(N_2H_3COO)_3$
	240(+)	160–280	59.00	58.93	CeO_2
Pr	150(−)	120–160	13.00	12.86	$Pr(N_2H_3COO)_3$
	275(+)	160–290	22.00	23.57	$Pr_2(C_2O_4)_3{\cdot}3N_2H_4$
	310(+)	290–335	42.00	45.01	$Pr_2(CO_3)_3$
		335–450	53.00	55.48	$Pr_2O_2CO_3$
	475(−)	450–510	60.00	59.45	Pr_6O_{11}
Nd	150(−)	135–170	13.00	12.75	$Nd(N_2H_3COO)_3$
	255(+)	170–290	23.00	23.39	$Nd_2(C_2O_4)_3{\cdot}3N_2H_4$
	310(+)	290–330	39.00	36.56	$Nd_2(CO_3)_3$
	380(−)	330–560	57.00	55.05	$Nd_2O_2CO_3$
	560(−)	560–600	61.00	60.24	Nd_2O_3
Sm	150(−)	120–160	13.00	12.57	$Sm(N_2H_3COO)_3$
	260, 350(+)	160–310	45.00	44.02	$Sm_2(CO_3)_3$
	455(−)	310–550	57.00	54.26	$Sm_2O_2CO_3$
	575(−)	550–590	61.00	59.39	Sm_2O_3
Eu	165(−)	135–175	13.00	12.53	$Eu(N_2H_3COO)_3$
	245, 265(+)	175–275	43.00	43.85	$Eu_2(CO_3)_3$
	420(−)	275–515	56.00	54.06	$Eu_2O_2CO_3$
	560(−)	515–575	60.00	59.17	Eu_2O_3
Gd	185(−)	150–195	13.00	12.73	$Gd(N_2H_3COO)_3$
	280(+)	195–305	23.00	22.69	$Gd_2(C_2O_4)_3{\cdot}3N_2H_4$
	335(+)	305–370	40.00	43.32	$Gd_2(CO_3)_3$
	650(−)	370–670	58.50	58.45	Gd_2O_3
Tb	160(−)	130–170	13.00	12.33	$Tb(N_2H_3COO)_3$
	260, 300(+)	170–310	44.00	43.16	$Tb_2(CO_3)_3$
	435(−)	310–480	54.50	53.20	$Tb_2O_2CO_3$
	610(−)	480–610	58.00	57.31	Tb_4O_7
Dy	165(−)	130–170	13.00	12.23	$Dy(N_2H_3COO)_3$
	250, 305(+)	170–310	45.00	42.80	$Dy_2(CO_3)_3$
	425(−)	310–575	55.00	52.77	$Dy_2O_2CO_3$

Table 4.5 (*Continued*)

Ln	DTA peak temperature (°C)[a]	Thermogravimetry			
		Temperature range (°C)	% Weight loss		
			Obsd.	Calcd.	Products
	590(−)	575–610	59.00	57.75	Dy_2O_3
Ho	175(−)	130–180	12.50	12.16	$Ho(N_2H_3COO)_3$
	270, 310(+)	180–315	46.00	42.57	$Ho_2(CO_3)_3$
	630(−)	315–655	59.00	57.44	Ho_2O_3
Er	175(−)	130–175	13.00	12.10	$Er(N_2H_3COO)_3$
	260, 305(+)	175–310	45.00	42.35	$Er_2(CO_3)_3$
	615(−)	310–620	57.00	57.14	Er_2O_3
Yb	175(−)	120–170	12.00	11.94	$Yb(N_2H_3COO)_3$
	260, 305(+)	170–305	45.00	41.81	$Yb_2(CO_3)_3$
	615(−)	305–655	58.00	56.41	Yb_2O_3
Y	170(−)	135–175	16.00	14.67	$Y(N_2H_3COO)_3$
	260, 310(+)	175–315	56.00	51.37	$Y_2(CO_3)_3$
	415, 615(−)	315–640	72.00	69.31	Y_2O_3

[a] (−) = Endotherm; (+) = exotherm.

takes place at fairly high temperatures (120–200 °C), indicating the coordination of water molecules to the metal.

The hydrazine carboxylates obtained after dehydration decompose exothermically to their respective metal carbonates, $Ln_2(CO_3)_3$. The DTA curve shows two exotherms, while the TG curve shows a single step for the decomposition that leads to the formation of $Ln_2(CO_3)_3$. In certain cases, like Pr, Nd, and Gd complexes, the TG shows a break indicating decomposition (~22% weight loss) through a very unstable intermediate. The observed weight loss appears to suggest the formation of an intermediate of the type $Ln_2(CO_3)_3 \cdot 3N_2H_4$. This intermediate could not be isolated as the TG curve shows a continuous reaction in this region (Figure 4.5).

In the case of lighter rare earths, the respective carbonates decompose through the oxy carbonates $Ln_2O_2CO_3$ (as indicated by TG), which then decompose endothermically to their respective oxides. However, this step is not observed in the heavier rare earth complexes, which give the oxide directly. The oxide formation temperatures do not alter significantly in the series. The decomposition sequences can be represented as follows:

$$Ln(N_2H_3COO)_3 \cdot 3H_2O \xrightarrow{\text{endo}} Ln(N_2H_3COO)_3 + 3H_2O \qquad (4.15)$$

$$2Ln(N_2H_3COO)_3 \xrightarrow{\text{exo}} Ln_2(C_2O_4)_3 \cdot 3N_2H_4 + 3N_2 + 3H_2 \qquad (4.16)$$

$$Ln_2(C_2O_4)_3 \cdot 3N_2H_4 \xrightarrow{\text{Air}} Ln_2(CO_3)_3 + 3CO_2 + 3N_2 + 6H_2 \qquad (4.17)$$

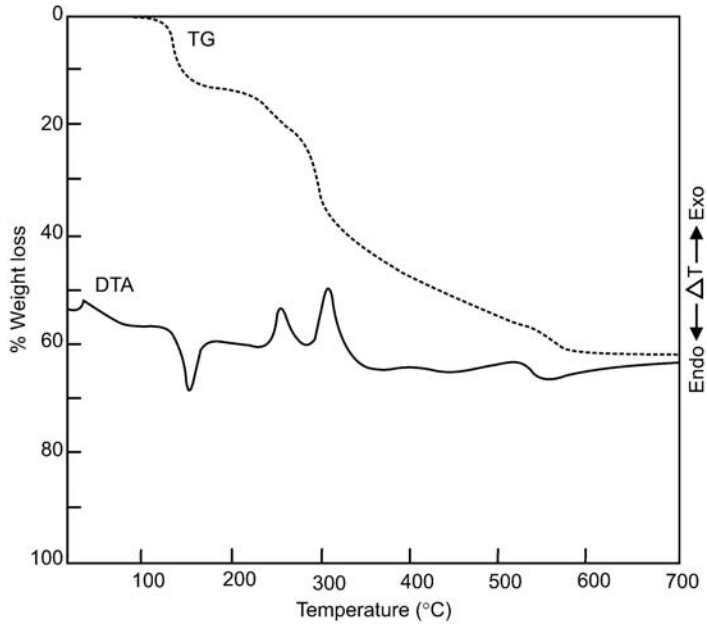

Figure 4.5 Simultaneous TG-DTA curves of $Nd(N_2H_3COO)_3{\cdot}3H_2O$. Adapted with permission from [15] © 1986 The Indian Academy of Sciences.

$$Ln_2(CO_3)_3 \xrightarrow{\text{endo}} Ln_2O_2CO_3 + 2CO_2 \tag{4.18}$$

$$Ln_2O_2CO_3 \xrightarrow{\text{endo}} Ln_2O_3 + CO_2 \tag{4.19}$$

where Ln = La, Ce, Pr, Nd, Tm, Sm, Eu, Pm, Gd, Tb, Dy, Ho, Er, Yb, and Y.

The cerium complex $Ce(N_2H_3COO)_3{\cdot}3H_2O$ behaves differently to the other rare earth complexes. It loses its water of hydration in the region 100–160 °C to form $Ce(N_2H_3COO)_3$, which then decomposes exothermically in a single step to the oxide CeO_2. The decomposition behavior of rare earth hydrazine carboxylates is quite interesting. The decomposition of these complexes is autocatalytic and is accompanied by swelling due to the evolution of large volumes of gases like NH_3, H_2O, N_2, and CO_2.

4.3.3 Metal Ion Doped Metal Hydrazine Carboxylate Hydrates – $M^{x+}/M(N_2H_3COO)_2{\cdot}xH_2O$

The formation of single crystals of metal hydrazine carboxylates from aqueous solutions containing metal ions and hydrazine carboxylate ligand facilitates the incorporation of desired impurity ions in the host. The slow

crystallization process simply allows atomic level substitution of the impurity ions homogenously. This ionic doping is one of the significant features of metal hydrazine carboxylate complexes. Therefore, these compounds act as ideal precursors for the preparation of metal ion substituted oxide materials with interesting magnetic, catalytic, and electronic properties.

4.3.3.1 *Manganese-Substituted Calcium Hydrazine Carboxylate Hydrate*

The electrical conductivity of simple oxides can be varied by doping with an appropriate transition metal. In this regard manganese-doped calcium hydrazine carboxylate hydrate has been investigated as a precursor to $Mn_xCa_{1-x}O$. The precursor is prepared by treating an aqueous solution containing Mn^{2+} and Ca^{2+} ions in the required amounts with $N_2H_5COON_2H_3$. Pale pink crystals separate after a few days, indicating the presence of Mn^{2+} in $Ca(N_2H_3COO)_2{\cdot}H_2O$ [16]. Doping of Mn^{2+} is possible in the calcium hydrazine carboxylate complex due to the comparable ionic sizes of Ca^{2+} (0.99 Å) and Mn^{2+} (0.8 Å), and the isomorphic crystal structures of $Ca(N_2H_3COO)_2{\cdot}H_2O$ and $Mn(N_2H_3COO)_2{\cdot}H_2O$.

Single crystals of Mn^{2+} doped calcium hydrazine carboxylate monohydrate has been studied by ESR of Mn in the calcium sites. The X-band ESR indicates a large crystal field splitting necessitating experiments at Q band (Figure 4.6a and b). The analysis shows two magnetically inequivalent, but chemically equivalent, sites with values of the principal components of the three tensors "*g*," "*D*," and "*A*" being at variance along the three directions in the crystal structure. One of the principal components of the crystal field, (D_{zz}) is found to be along the $Ca \leftrightarrow Ca$ direction; a second one (D_{xx}) is found to be along the perpendicular to the plane of the triangle formed by three neighboring calcium ions. The "*A*" tensor is found to have an orientation different from that of the "*g*" and "*D*" tensors, reflecting low symmetry of the Ca^{2+} sites.

4.3.3.2 *Praseodymium-Substituted Cerium Hydrazine Carboxylate Hydrate*

Red ceramic pigments are normally based on cadmium sulfoselenide, which being toxic is banned or restricted in its use in many countries. A need exists, therefore, to prepare an environmental friendly red pigment. Praseodymium doped/substituted ceria is known to be a substitute for cadmium sulfoselenide as red ceramic pigments. Conventionally,

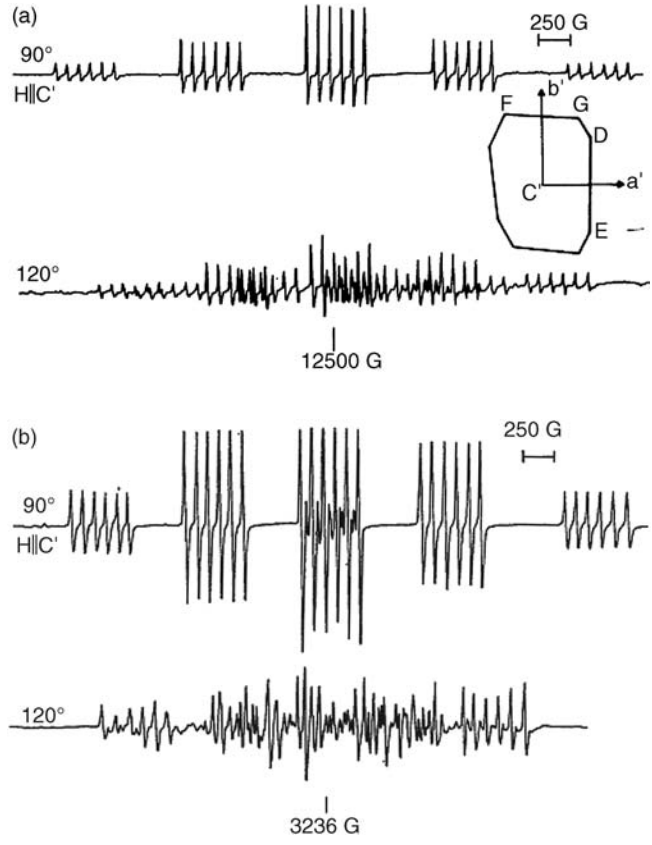

Figure 4.6 ESR spectra of $Mn_xCa_{1-x}(N_2H_3COO)_2{\cdot}H_2O$ at (a) X band ($\nu =$ 9.15 GHz) and (b) Q band ($\nu = 34.45$ GHz). Reproduced with permission from [16] © 1994 The Indian Academy of Sciences.

praseodymium doped/substituted ceria pigments are prepared by a solid-state reaction between ceria and praseodymium oxide at high temperatures. A low temperature method for the preparation of praseodymium-doped ceria is possible by synthesis of hydrazine carboxylate complexes that act as precursors [17].

As the crystal structures of all the rare earth metal hydrazine carboxylates are isomorphous, it is possible to prepare solid solutions of Pr-Ce hydrazine carboxylates. The complexes $Ce_{1-x}Pr_x(N_2H_3COO)_3{\cdot}3H_2O$, with $x = 0$–0.5, are prepared by the same procedure used in preparing rare earth metal hydrazine carboxylates as mentioned in Section 4.3.2. Stoichiometric amounts of cerium nitrate and praseodymium nitrate are dissolved in doubly distilled water, and to this a solution of hydrazine carboxylate in hydrazine is added slowly. The mixture is allowed to

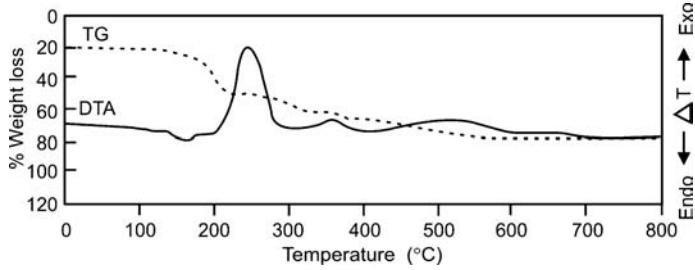

Figure 4.7 Simultaneous TG-DTA curves of $Ce_{0.5}Pr_{0.5}(N_2H_3COO)_3{\cdot}3H_2O$. Adapted from Ref. [17] with permission from Elsevier © 2001.

crystallize in air at room temperature, and light green color crystals appear within two days. The crystals are washed in ethanol and dried in a vacuum desiccator. With increasing Pr content, the color of the complexes obtained vary from colorless ($x \leq 0.10$ Pr) to light green ($x = 0.5$ Pr). The composition of the complexes is determined by chemical analysis.

Thermograms of $Ce_{0.99}Pr_{0.01}(N_2H_3COO)_3{\cdot}3H_2O$ and $Ce_{0.5}Pr_{0.5}(N_2H_3COO)_3{\cdot}3H_2O$ are similar to those reported for $Ce(N_2H_3COO)_3{\cdot}3H_2O$ or $Pr(N_2H_3COO)_3{\cdot}3H_2O$ (Figure 4.7). All the complexes lose water of hydration initially to yield the corresponding metal hydrazine carboxylates at approximately 120–200 °C. The high temperature required for the dehydration step indicates that the water molecules are coordinated to the metals. These complexes decompose exothermally with a swelling at ~250 °C to give the respective oxides. With increasing Pr substitution, the thermograms of the complexes resemble $Pr(N_2H_3COO)_3{\cdot}3H_2O$. The DTA of $Ce_{0.5}Pr_{0.5}(N_2H_3COO)_3{\cdot}3H_2O$ shows an endothermic peak (180 °C) corresponding to its dehydration. Three other exothermic peaks at 230, 310, and 500 °C correspond to the formation of a carbonate. In the last step, the carbonate decomposes to give the red colored oxide:

$$Ce_{1-x}Pr_x(N_2H_3COO)_3{\cdot}3H_2O(s) \xrightarrow{\text{air}/300^\circ C} Ce_{1-x}Pr_xO_{2-\delta}(s) + 3N_2(g) + 3CO_2(g) + 7.5H_2O(g) \quad (4.20)$$

4.3.3.3 Europium-Substituted Yttrium Hydrazine Carboxylate Hydrate

Nowadays, there is a widespread use of compact fluorescent lamps (CFLs) for lighting purposes. CFL technology uses a combination of three phosphor materials: red $Y_2O_3{:}Eu^{3+}$ (60%), green $CeMgAl_{11}O_{19}{:}Tb^{3+}$ (30%), and

blue $BaMgAl_{10}O_{17}:Eu^{2+}$ (10%). This has resulted in a great demand for rare earth activator based phosphor materials. Of these, europium substituted yttria ($Y_{1-x}Eu_xO_{2-\delta}$) – the red phosphor – is a major component required for CFL manufacturing. The synthesis of this phosphor by the pyrolysis of hydrazine carboxylate hydrate precursor is described here.

As mentioned in Section 4.3.2, yttrium hydrazine carboxylate hydrate and europium hydrazine carboxylate hydrate are isomorphous, and therefore it is possible to prepare homogenously substituted Eu^{3+} in $Y(N_2H_3COO)_3{\cdot}3H_2O$. Yttrium(III) chloride and europium(III) chloride are treated with hydrazine carboxylate $N_2H_3COON_2H_5$ at room temperature. This reaction yields the yttrium europium hydrazine carboxylate precursor $Y_{0.99}Eu_{0.01}(N_2H_3COO)_3{\cdot}3H_2O$ [18]. Powder XRD patterns (Figure 4.8) of these complexes show them to be similar to each other and hence they easily form solid solutions.

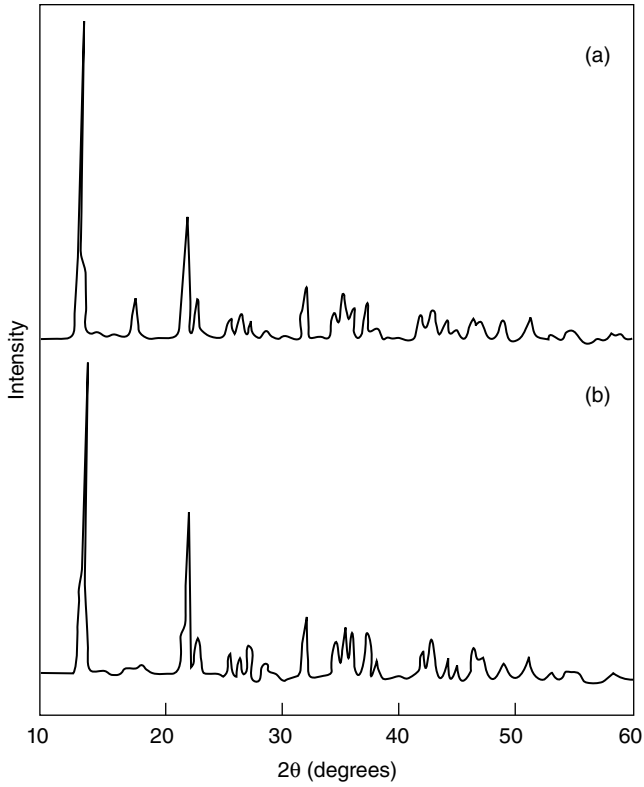

Figure 4.8 Powder XRD patterns of (a) $Y(N_2H_3COO)_3{\cdot}3H_2O$ and (b) $Eu(N_2H_3COO)_3{\cdot}3H_2O$. Adapted from Ref. [18] with permission from Elsevier © 2005.

The complex $Y_{0.99}Eu_{0.01}(N_2H_3COO)_3{\cdot}3H_2O$ decomposes in air at 600 °C to form the corresponding europium-doped yttrium oxide. The decomposition temperature can be reduced, however, by mixing the redox compound with a calculated amount of either ammonium nitrate (1 : 6) or ammonium perchlorate (1 : 2.4) and rapidly heating the mixture at 300 °C to obtain Eu^{3+}-substituted Y_2O_3 – the red phosphor.

Fluorescence spectra of $Y_2O_3{:}Eu^{3+}$ prepared from $Y_{0.99}Eu_{0.01}(N_2H_3COO)_3{\cdot}3H_2O$ show an intense emission at 611 nm (excitation wavelength = 254 nm), which is attributed to the electric dipole transition $^5D_0 \rightarrow {}^7F_2$ of Eu^{3+}.

4.4 METAL HYDRAZINE CARBOXYLATE HYDRAZINES – $M(N_2H_3COO)_2{\cdot}(N_2H_4)_2$

Metal hydrazine carboxylate hydrazine complexes are prepared by treating an aqueous solution containing metal ions like Mg^{2+}, Ca^{2+}, Mn^{2+}, Fe^{2+}, Co^{2+}, Ni^{2+}, and Zn^{2+} with a 5% solution of N_2H_3COOH in $N_2H_4{\cdot}H_2O$. Initially, a precipitate is formed that dissolves as more $N_2H_3COON_2H_5$ is added [9]. The clear solution obtained is kept open to the atmosphere and within a couple of days crystalline solids separate from it:

$$M^{2+} + 2N_2H_3COO^- + 2N_2H_4{\cdot}H_2O \rightarrow M(N_2H_3COO)_2(N_2H_4)_2 + 2H_2O \quad (4.21)$$

where M = Fe, Co, Ni, and Zn.

Manganese hydrazine carboxylate hydrazine, $Mn(N_2H_3COO)_2{\cdot}(N_2H_4)_2$, is obtained by treating a fine powder of $Mn(N_2H_3COO)_2{\cdot}2H_2O$ with $N_2H_4{\cdot}H_2O$:

$$Mn(N_2H_3COO)_2{\cdot}2H_2O + 2N_2H_4{\cdot}H_2O \rightarrow Mn(N_2H_3COO)_2{\cdot}(N_2H_4)_2 + 4H_2O \quad (4.22)$$

Infrared spectra of metal hydrazine carboxylate hydrazines show the characteristic N–N stretching frequency of bidentate $N_2H_3COO^-$ in the region 990–1015 cm^{-1}. The metal ions in all these complexes have an octahedral coordination. The octahedron is completed by the two monodentate N_2H_4 groups. Infrared spectra of such hydrazine complexes clearly show the stretching frequencies of ν_{N-N} monodentate N_2H_4 at ~925 cm^{-1}, and ν_{N-N} of $N_2H_3COO^-$ at 1000 cm^{-1}.

Table 4.6 Thermal analysis data of $M(N_2H_3COO)_2{\cdot}(N_2H_4)_2$.

M	DTA peak temperature (°C)[a]	Thermogravimetry			
		Temperature range (° C)	% Weight loss		
			Obsd.	Calcd.	Products
Mn	175(+), 195(+)	130–290	72.80	73.80	MnO
Fe	135(+), 175(+)	130–205	70.10	70.41	Fe_2O_3
Co	190(+), 200(+)	210–269	70.00	70.59	Co_3O_4
Ni	195(+), 228(+)	187–200	72.00	72.60	NiO
Zn	200(+)	155–250	32.00	33.64	$ZnC_2O_4{\cdot}N_2H_4$
	310(+)	250–325	71.90	70.87	ZnO

[a] (+) = Exotherm.

The thermal analysis of metal hydrazine carboxylate hydrazines $M(N_2H_3COO)_2{\cdot}(N_2H_4)_2$, where M = Mn, Fe, Co, Ni, Zn, and Mg, shows single-step decomposition in TG-DTG (differential thermogravimetry), except for Zn (Table 4.6). However, DTA shows two exotherms: the first corresponding to the decomposition of coordinated hydrazine followed by the decomposition of metal hydrazine carboxylates to their respective metal oxides. The zinc complex appears to decompose through $ZnC_2O_4{\cdot}N_2H_4$. Figure 4.9 shows the decomposition steps of $Co(N_2H_3COO)_2(N_2H_4)_2$.

Metal hydrazine carboxylate hydrazines containing strong reducing groups like $N_2H_3COO^-$ and N_2H_4 undergo combustion in the presence of air. This occurs autocatalytically, at low ignition temperatures of 120–300 °C, with the evolution of NH_3, H_2O, N_2, and CO_2, to yield technologically useful nano-size oxide materials. These decomposition products (metal oxides) are identified by their X-ray powder diffraction patterns. For example, $Fe(N_2H_3COO)_2{\cdot}(N_2H_4)_2$ when ignited at 120 °C catches fire and burns autocatalytically to yield nano-size magnetic oxide γ-Fe_2O_3 [19].

The fine particle nature of the combustion derived powders is ascribed to the low exothermicity of the combustion reaction. It is also attributed to the evolution of large amount of gases like NH_3, N_2, H_2O, and CO_2, which help to dissipate the heat, thereby preventing oxides from sintering. The formation of γ-Fe_2O_3 is confirmed by powder XRD; it shows characteristic line broadening with a cell constant "*a*" of 0.837 nm and crystallite size of 18 nm. The surface area of this oxide is $38\ m^2\ g^{-1}$ while its coercivity is 180 Oe:

$$2Fe(N_2H_3COO)_2{\cdot}(N_2H_4)_2 + 2.5O_2 \xrightarrow{\text{air}} Fe_2O_3 + 4CO_2 + 8NH_3 + 4N_2 + 2H_2O \quad (4.23)$$

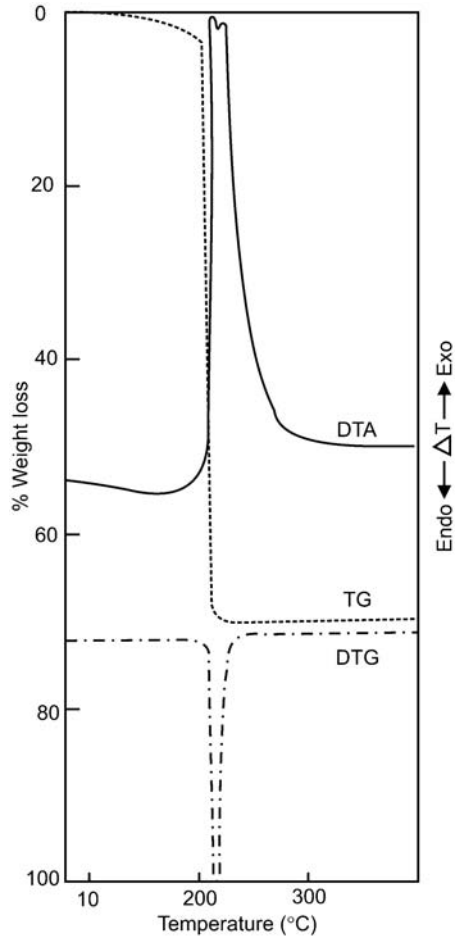

Figure 4.9 Simultaneous TG-DTG-DTA of $Co(N_2H_3COO)_2(N_2H_4)_2$. Adapted with permission from [9] © 1985 The Indian Academy of Sciences.

Additionally, these preparative methods have been extended to make mixed metal hydrazine carboxylate hydrazines of the formula $M_{1/3}Fe_{2/3}(N_2H_3COO)_2.(N_2H_4)_2$, where M = Mg, Mn, Co, Ni, and Zn. These complexes are prepared by the reaction of solutions containing metal and iron in a 1 : 2 mole ratio, with hydrazine carboxylate as the ligand. These precursors decompose at lower temperatures, of about 125–150 °C, with the evolution of large amounts of gases to yield corresponding ferrites. Formation of ferrites is confirmed by their characteristic XRD patterns. The crystallite sizes of the ferrites calculated from the X-ray line

broadening are in the range 13–25 nm, while their surface areas range from 75 to 120 $m^2 g^{-1}$ [20].

4.5 HYDRAZINIUM METAL HYDRAZINE CARBOXYLATE HYDRATES – $N_2H_5M(N_2H_3COO)_3 \cdot H_2O$

When an aqueous solution containing metal ions like Mg^{2+}, Fe^{2+}, Co^{2+}, Ni^{2+}, and Zn^{2+} is treated with a higher concentration of 15% solution of N_2H_3COOH in $N_2H_4 \cdot H_2O$ it results in hydrazinium metal hydrazine carboxylate hydrates [21]. The initially formed precipitate simply dissolves, giving a clear solution. When kept open to the atmosphere for three to four days, crystalline solids begin to separate from the solution. The crystals are washed with alcohol and diethyl ether and then stored in a vacuum desiccator. The composition of the crystals found by chemical analysis is $N_2H_5M(N_2H_3COO)_3 \cdot H_2O$:

$$MX_2 + 3N_2H_5COON_2H_3 + H_2O \rightarrow N_2H_5M(N_2H_3COO)_3 \cdot H_2O + 2N_2H_5X \quad (4.24)$$

where M = Mg, Fe, Co, Ni, and Zn; X = anion.

Interestingly, manganese does not readily form the hydrazinium complex although manganese hydrazine carboxylate hydrate and hydrazine complexes are formed.

All these complexes show the characteristic N–N stretching frequency of the bidentate $N_2H_3COO^-$ in their infrared spectra, observed in the region 990–1015 cm^{-1}, and of ionic $N_2H_5^+$ at 965 cm^{-1}.

More recently, detailed investigations on the crystal and molecular structure of the Co and Zn complexes by X-ray crystallography, vibrational spectroscopy, and quantum chemical study have been made [22]. Figure 4.10 shows the crystal structure of $N_2H_5Co(N_2H_3COO)_3 \cdot H_2O$ determined in this study.

The crystal structures of $N_2H_5M(N_2H_3COO)_3 \cdot H_2O$, where M = Fe, Co, and Zn, are found to be isomorphous. Under these conditions the metal ions are in the same crystal lattice and substitute one another in the concentration range $x = 0.1$–1.0 to form solid solutions.

Table 4.7 gives thermal decomposition data of $N_2H_5M(N_2H_3COO)_3 \cdot H_2O$. The iron complex shows a single step in TG-DTG and two exotherms in DTA, while both cobalt and nickel complexes show two-step decomposition in TG-DTG and two exotherms in DTA. The observed weight loss after the first step corresponds to the formation of metal oxalate hydrazine

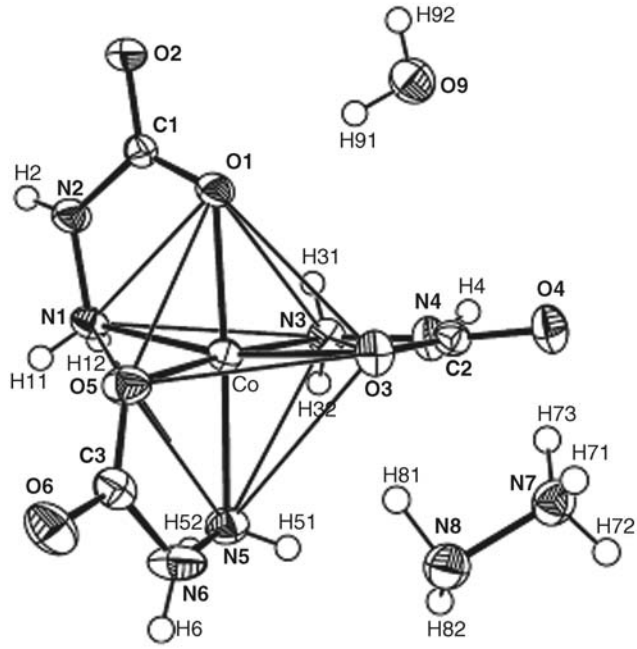

Figure 4.10 Crystal structure of $N_2H_5Co(N_2H_3COO)_3{\cdot}H_2O$. Reproduced from Ref. [22] with permission from Elsevier © 2004.

Table 4.7 Thermal analysis data of $N_2H_5M(N_2H_3COO)_3{\cdot}H_2O$.

M	DTA peak temperature (°C)[a]	Thermogravimetry			
		Temperature range (°C)	% Weight loss		
			Obsd.	Calcd.	Products
Mg	122(−), 140(+)	130–160	7.00	5.99	$N_2H_5Mg(N_2H_3COO)_3$
	190(+)	160–230	51.50	51.94	$MgC_2O_4{\cdot}N_2H_4$
	360(+)	230–415	86.20	86.5	MgO
Fe	165(+), 180(+)	145–220	76.00	75.93	Fe_2O_3
Co	175(+)	170–245	36.50	37.61	$CoC_2O_4{\cdot}N_2H_4$
	245(+)	245–280	76.10	76.03	Co_3O_4
Ni	182(+), 193(+)	170–210	48.00	46.60	$NiC_2O_4{\cdot}N_2H_4$
	220(+)	210–385	76.00	77.67	NiO
Zn	145(−)	70–165	18.00	18.16	$Zn(N_2H_3COO)_2(N_2H_4)_2$
	195(+)	165–215	53.00	55.07	ZnC_2O_4
	240(+)	215–390	76.00	76.17	ZnO

[a] (−) = Endotherm; (+) = exotherm.

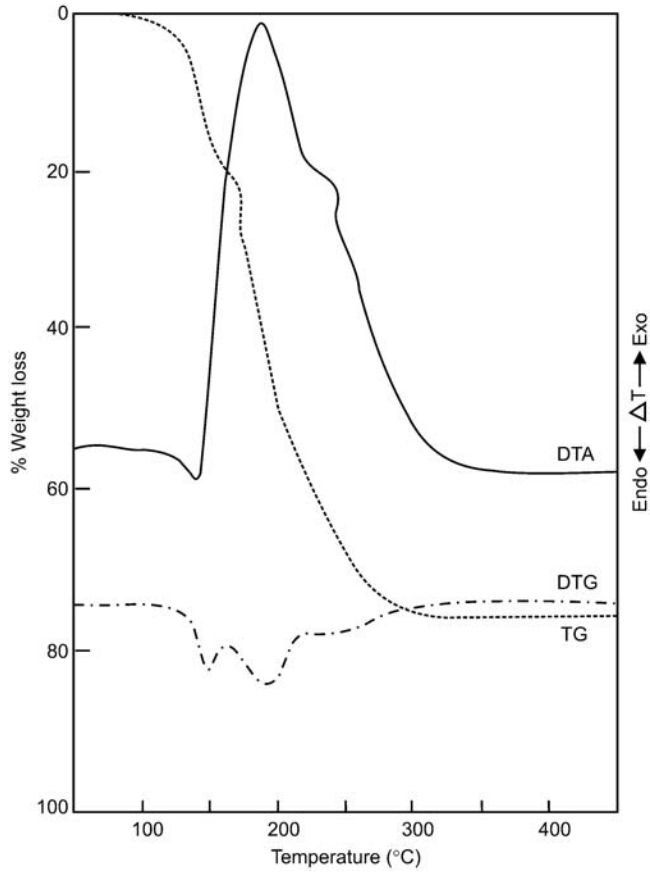

Figure 4.11 Simultaneous TG-DTG-DTA of $N_2H_5Zn(N_2H_3COO)_3{\cdot}H_2O$. Ph.D Thesis of Ravindranathan, P. under Prof. K. C. Patil at Indian Institute of Science.

($MC_2O_4{\cdot}N_2H_4$) intermediate. The decomposition of zinc (Figure 4.11) and magnesium complexes involves three steps each. Possible intermediates could be $M(N_2H_3COO)_2(N_2H_4)_2$, $MC_2O_4{\cdot}N_2H_4$, MC_2O_4, and so on. The final residue after decomposition corresponds to the formation of the respective metal oxides, as observed by TG weight loss:

$$2N_2H_5Fe(N_2H_3COO)_3{\cdot}H_2O + 2.5O_2 \rightarrow Fe_2O_3 + 6CO_2 + 8NH_3 + 4H_2O + 4N_2 \quad (4.25)$$

Similar to iron hydrazine carboxylate hydrazine ($Fe(N_2H_3COO)_2{\cdot}(N_2H_4)_2$), the iron hydrazinium complex ($N_2H_5Fe(N_2H_3COO)_3{\cdot}H_2O$)

also undergoes autocatalytic combustion to yield γ-Fe_2O_3 as confirmed by its XRD pattern. The crystallite size of γ-Fe_2O_3 is 13 nm with a cell constant "*a*" of 0.835 nm. The surface area of the oxide is 75 $m^2 g^{-1}$, while its coercivity is 130 Oe [23].

The hydrazinium nickel hydrazine carboxylate complex, $(N_2H_5)Ni(N_2H_3COO)_3 \cdot H_2O$, is also used as precursor for the synthesis of metallic Ni in the sonochemical preparation of Ni-Mo-S/Al_2O_3, since volatile Ni precursors such as $Ni(CO)_4$ are exceptionally toxic and dangerous to use [24]. Similarly, copper hydrazine carboxylate is used to prepare nanoparticles of copper by the sonication method [25]. The presence of a zwitterionic surfactant in the synthesis procedure causes the formation of elongated nanoparticles of aspect ratio 10, which is of significance for electrical applications. In the absence of the zwitterionic surfactant only spherical particles result [26].

4.5.1 Cobalt-Substituted Hydrazinium Iron Hydrazine Carboxylate Hydrate

The spinel γ-Fe_2O_3 is the most widely used material for recording in magnetic tapes and discs. However, it has its limitation because of its coercivity. For a given magnetic material the coercivity can be increased by reducing the particle size of magnetic single domains, thereby enhancing its shape anisotropy and increasing the magnetocrystalline anisotropy, either in bulk or at the surface. In γ-Fe_2O_3 ($M_s = 84$ emu g^{-1}) the magentocrystalline anisotropy can be increased by dopants like Co(II) either by substitution in the lattice or by diffusion on the surface.

Doping of Co in γ-Fe_2O_3 is performed by substituting Co in the complex $N_2H_5Fe(N_2H_3COO)_3 \cdot H_2O$. For this synthesis an aqueous solution containing iron(II) sulfate and cobalt(II) sulfate in the required ratio is treated with a solution of N_2H_3COOH in hydrazine hydrate until the precipitate formed just dissolves. On keeping this solution exposed to air, rose red crystals separate out in about a week. The crystals are washed with alcohol and dried over P_2O_5 in a vacuum desiccator. Chemical analysis of these crystals determined the composition to be $N_2H_5Co_xFe_{1-x}(N_2H_3COO)_3 \cdot H_2O$ where $x = 1$, 2, 3, 4, and 10 atom % [27].

Similar to preparation of nano-size γ-Fe_2O_3 described in Section 4.6, cobalt-substituted γ-Fe_2O_3 can be synthesized by thermal decomposition of the precursor containing cobalt(II) ions, that is, $N_2H_5Co_xFe_{1-x}(N_2H_3COO)_3 \cdot H_2O$. The formation of solid solutions of the corresponding metal salts with atomic level substitution of Fe^{2+} (0.92 Å) by Co^{2+} (0.885 Å) ions is possible due to their comparable ionic sizes. The TG-DTG-DTA

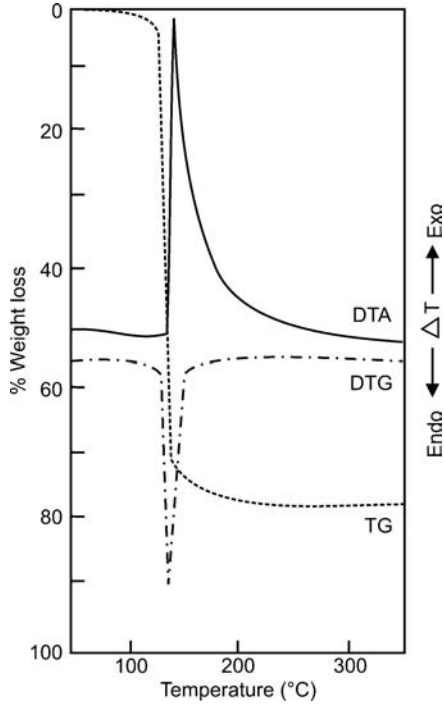

Figure 4.12 Simultaneous TG-DTG-DTA of $N_2H_5Co_xFe_{1-x}(N_2H_3COO)_3{\cdot}H_2O$, $x = 1$ atom %. Reproduced from Ref [37] with permission from Akademiai Kiado © 1989.

data of this complex shows it to decompose in a single step at ~170 °C to give the oxide cobalt-doped γ-Fe_2O_3. The DTA curve shows a small doublet corresponding to the single TG step (Figure 4.12). The doublet has been attributed to the decomposition of the metathetically formed iron oxalate hydrazine intermediate. These crystals when ignited at around 225 °C in air decompose with the evolution of large amounts of gases like N_2, NH_3, H_2O, and CO_2 to yield voluminous nano-size magnetic oxide γ-Fe_2O_3 particles.

4.5.2 Manganese-Substituted Hydrazinium Zinc Hydrazine Carboxylate Hydrate

Single crystals of Mn-doped hydrazinium zinc hydrazine carboxylate hydrate $[N_2H_5Mn_{0.02}Zn_{0.98}(N_2H_3COO)_3{\cdot}H_2O]$ are prepared by the method described in Section 4.5. Pale pink crystals of the complex are obtained in a couple of days, and the presence of Mn^{2+} is confirmed by

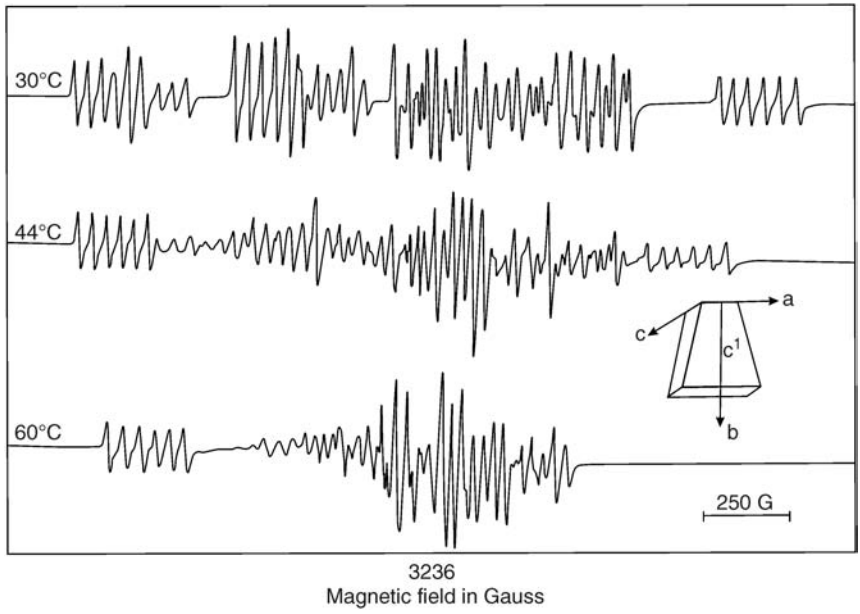

Figure 4.13 The X-band ($\nu = 9.15$ G Hz) ESR spectra of Mn^{2+}-doped $N_2H_5Zn(N_2H_3COO)_3{\cdot}H_2O$ when the magnetic field (H) makes an angle of 10°, 20°, and 26° (top to bottom, respectively) with the a-axis in the ab plane.

ESR spectra. The ESR spectrum of the complex shows two equivalent paramagnetic sites [28]. The spectrum in three mutually orthogonal planes (ab, bc', $c'a$) reveals the unusual character of the Mn^{2+} spectrum with angle orientation. Figure 4.13 shows the ESR spectrum in the $c'a$ plane for three different orientations with respect to magnetic field. This precursor, on decomposition in a controlled atmosphere, gives a useful spintronic material, $Zn_{1-x}Mn_xO$. The preparation of uniformly doped transition metal ions in ZnO is a challenge, as the dopant concentration is low. The process of preparing single-crystal zinc hydrazine carboxylate by crystallization has consequently become useful in doping trace amounts of Mn, Co, Ni, and so on in the host crystal.

4.6 SOLID SOLUTIONS OF HYDRAZINIUM METAL HYDRAZINE CARBOXYLATE HYDRATES – $N_2H_5M_{1/3}(Co/Fe/Mn)_{2/3}(N_2H_3COO)_3{\cdot}H_2O$

Hydrazinium cobalt and iron complexes form solid solutions in the entire range $N_2H_5Co_xFe_{1-x}(N_2H_3COO)_3{\cdot}H_2O$, where $x = 0.1$–0.9, and the

lattice parameters vary with x. The solid solution precursors of the type $N_2H_5M_{1/3}(Co/Fe/Mn)_{2/3}(N_2H_3COO)_3{\cdot}H_2O$ (where M = Mg, Mn, Co, Ni, and Zn) are synthesized as follows:

4.6.1 Synthesis

Solid solutions of hydrazinium metal hydrazine carboxylate hydrates of the type $N_2H_5M_{1/3}Co_{2/3}(N_2H_3COO)_3{\cdot}H_2O$, $N_2H_5M_{1/3}Fe_{2/3}(N_2H_3COO)_3{\cdot}H_2O$ (where M = Mg, Mn, Fe, Co, Ni, and Zn), and $N_2H_5M_{1/3}Mn_{2/3}(N_2H_3COO)_3{\cdot}H_2O$ (where M = Co and Ni) are prepared by the reaction of an aqueous solution of metal sulfates containing M^{2+}, $Co/Fe/Mn^{2+}$ ions in the mole ratio 1:2, with $N_2H_3COON_2H_5$ or N_2H_3COOH in $N_2H_4{\cdot}H_2O$ [20,21,30,31]. Crystalline solids separate from the solution in a couple of days. The crystals are washed with alcohol and dried over P_2O_5 in a vacuum desiccator. Chemical analysis of the complexes confirms the desired composition of $N_2H_5M_{1/3}Co_{2/3}(N_2H_3COO)_3{\cdot}H_2O$, $N_2H_5M_{1/3}Fe_{2/3}(N_2H_3COO)_3{\cdot}H_2O$, and $N_2H_5M_{1/3}Mn_{2/3}(N_2H_3COO)_3{\cdot}H_2O$ (where M = Mg, Mn, Fe, Co, Ni, and Zn), showing that the atomic ratio of M^{2+}/Co^{2+} or Fe^{2+} or Mn^{2+} is 1:2 within experimental error.

Similar to the above, solid solutions of hydrazinium metal hydrazine carboxylate hydrates of the formula $N_2H_5M'_{1/3}Fe_{2/3}(N_2H_3COO)_3{\cdot}H_2O$ (where $M'_{1/3} = Mg_xMn_{1-x}$, Ni_xZn_{1-x}, Mn_xZn_{1-x}) are prepared by the reaction of aqueous solution containing corresponding metal ions in the required mole ratio, with N_2H_3COOH in $N_2H_4{\cdot}H_2O$ [32–37]. Bluish pink crystals of the complex separate from the solution in a couple of days when kept exposed to air. The crystals are washed with alcohol and then diethyl ether and dried over P_2O_5 in a vacuum desiccator. The composition of the crystals determined by chemical analysis was found to be $N_2H_5(Ni_xZn_{1-x})_{1/3}Fe_{2/3}(N_2H_3COO)_3{\cdot}H_2O$, $N_2H_5(Mn_xZn_{1-x})_{1/3}Fe_{2/3}(N_2H_3COO)_3{\cdot}H_2O$, where $x = 0.2$–0.8, and $N_2H_5(Mg_xMn_{1-x})_{1/3}Fe_{2/3}(N_2H_3COO)_3{\cdot}H_2O$, where $x = 0.5$ and 0.62.

Infrared spectra of the complexes are similar to those of $N_2H_5M_{1/3}Fe_{2/3}(N_2H_3COO)_3{\cdot}H_2O$. All these complexes show characteristic absorption frequencies of $N_2H_3COO^-$ at 3200, 3260, 3300 (ν_{N-H}), 1590 (NH_2 band), 1650 (ν_{COO^-}), 1100 (ν_{N-C}), 900 (ν_{N-N} of $N_2H_3^+$), and 960 cm^{-1} (ν_{N-N} of $N_2H_5^+$). Formation of solid solution is evident by the similarity of infrared spectra of the mixed metal complexes with that of the Fe complex.

4.6.2 XRD Data

The single-crystal Weissenberg photograph recorded for $N_2H_5Ni_{1/3}Fe_{2/3}(N_2H_3COO)_3{\cdot}H_2O$ shows that the crystal data is in good agreement with that of the reported nickel complex ($N_2H_5Ni(N_2H_3COO)_3{\cdot}H_2O$) [38]. Table 4.8 gives the cell parameters and unit cell volumes of the complexes calculated from XRD data. X-Ray powder diffraction patterns of the solid solution precursors, $N_2H_5M_{1/3}Co_{2/3}(N_2H_3COO)_3{\cdot}H_2O$ (M = Mg, Mn. Fe, Ni, and Zn), are identical to that of $N_2H_5Ni(N_2H_3COO)_3{\cdot}H_2O$, indicating the formation of solid solutions. Although $N_2H_5Mn(N_2H_3COO)_3{\cdot}H_2O$ is not formed readily, a solid solution containing Mn is formed due to its comparable ionic radii with that of Fe^{2+} ion ($Mn^{2+} = 0.080$ nm, and $Fe^{2+} = 0.075$ nm).

X-Ray powder diffraction patterns of the precursors reveal that the complexes are isostructural, possessing the monoclinic structure of $N_2H_5Fe(N_2H_3COO)_3{\cdot}H_2O$. The unit cell dimensions (Table 4.9) clearly reveal that solid solutions of the type $N_2H_5(Ni_xZn_{1-x})_{1/3}Fe_{2/3}(N_2H_3COO)_3{\cdot}H_2O$ are formed in the entire range of $x = 0.2$–0.8.

Figure 4.14 shows typical XRD powder patterns of $N_2H_5Mg_{1/3}Fe_{2/3}(N_2H_3COO)_3{\cdot}H_2O$, $N_2H_5Mn_{1/3}Fe_{2/3}(N_2H_3COO)_3{\cdot}H_2O$, and $N_2H_5(Mg_xMn_{1-x})_{1/3}Fe_{2/3}(N_2H_3COO)_3{\cdot}H_2O$.

Table 4.8 Unit cell dimensions for the monoclinic hydrazinium metal hydrazine carboxylate hydrates and their solid solutions.

Complex	a (nm)	b (nm)	c (nm)	β (°)	V (nm^3)
$N_2H_5Co(N_2H_3COO)_3{\cdot}H_2O$[a]	1.2139	1.0916	1.0261	120.92	1.1166
$N_2H_5Zn(N_2H_3COO)_3{\cdot}H_2O$[a]	1.2127	1.0914	1.0301	120.94	1.1169
$N_2H_5Ni(N_2H_3COO)_3{\cdot}H_2O$[b]	1.2129	1.0858	1.0255	121.10	1.1564
$N_2H_5Fe(N_2H_3COO)_3{\cdot}H_2O$	1.2106	1.0944	1.0286	120.68	1.1720
$N_2H_5Co(N_2H_3COO)_3{\cdot}H_2O$	1.2106	1.0873	1.0252	121.10	1.155
$N_2H_5Mg_{1/3}Fe_{2/3}(N_2H_3COO)_3{\cdot}H_2O$	1.2151	1.1007	1.0282	120.68	1.1826
$N_2H_5Mn_{1/3}Fe_{2/3}(N_2H_3COO)_3{\cdot}H_2O$	1.2165	1.1029	1.0272	121.69	1.1726
$N_2H_5Co_{1/3}Fe_{2/3}(N_2H_3COO)_3{\cdot}H_2O$	1.2207	1.1016	1.0268	121.09	1.1824
$N_2H_5Ni_{1/3}Fe_{2/3}(N_2H_3COO)_3{\cdot}H_2O$	1.2111	1.1016	1.0268	121.53	1.1677
$N_2H_5Ni_{1/3}Fe_{2/3}(N_2H_3COO)_3{\cdot}H_2O$[b]	1.1850	1.0960	1.0260	118.21	1.1742
$N_2H_5Zn_{1/3}Fe_{2/3}(N_2H_3COO)_3{\cdot}H_2O$	1.2130	1.1006	1.0279	120.73	1.1795
$N_2H_5Mg_{1/3}Co_{2/3}(N_2H_3COO)_3{\cdot}H_2O$	1.2133	1.0892	1.0229	121.09	1.157
$N_2H_5Mn_{1/3}Co_{2/3}(N_2H_3COO)_3{\cdot}H_2O$	1.2147	1.0941	1.0245	121.09	1.166
$N_2H_5Ni_{1/3}Co_{2/3}(N_2H_3COO)_3{\cdot}H_2O$	1.2138	1.0979	1.0283	121.08	1.173
$N_2H_5Zn_{1/3}Co_{2/3}(N_2H_3COO)_3{\cdot}H_2O$	1.2128	1.0916	1.0279	121.09	1.165

[a] Single-crystal data, Reference [23].
[b] Single-crystal data, Reference [38].

Table 4.9 Unit cell dimensions for the monoclinic $N_2H_5(Ni_xZn_{1-x})_{1/3}Fe_{2/3}(N_2H_3COO)_3{\cdot}H_2O$.

x	a (nm)	b (nm)	c (nm)	β (°)
0.0	1.2130	1.1006	1.0279	120.73
0.2	1.2140	1.1043	1.0280	121.09
0.4	1.2146	1.0971	1.0267	121.09
0.5	1.2155	1.1012	1.0271	121.09
0.6	1.3151	1.1916	1.1116	121.03
0.8	1.2174	1.0949	1.0275	121.03
1.0	1.2111	1.1016	1.0268	121.53

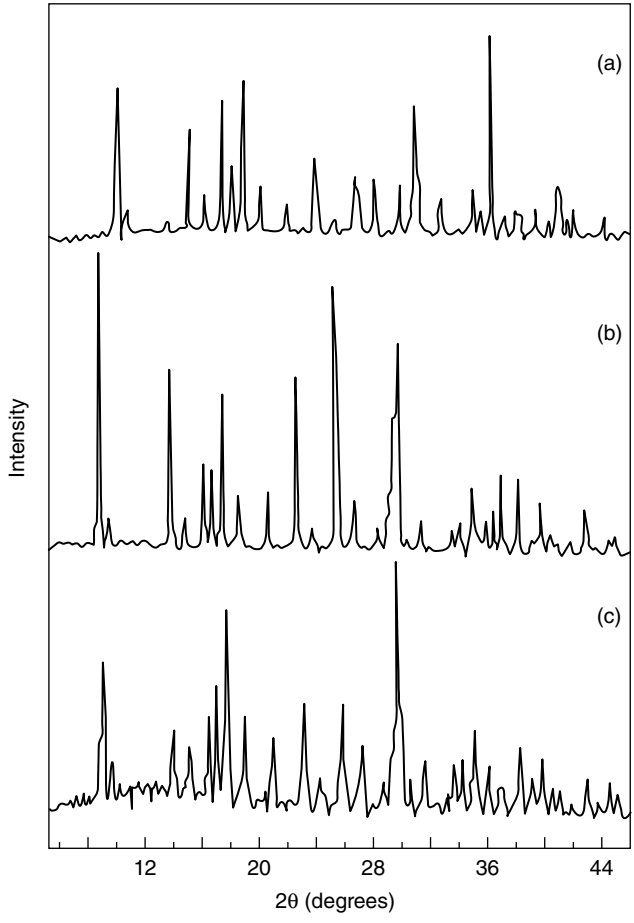

Figure 4.14 XRD powder patterns of (a) $N_2H_5Mg_{1/3}Fe_{2/3}(N_2H_3COO)_3{\cdot}H_2O$, (b) $N_2H_5Mn_{1/3}Fe_{2/3}(N_2H_3COO)_3{\cdot}H_2O$, and (c) $N_2H_5(Mg_xMn_{1-x})_{1/3}Fe_{2/3}(N_2H_3COO)_3{\cdot}H_2O$. Reproduced with permission from [35] © 1989 Sundar, Manoharan, S. and Patil, K.C.

The IR spectra of all these complexes show the characteristic N–N stretching frequency of $N_2H_3COO^-$ in the region 900–1010 cm^{-1} and that of $N_2H_5^+$ at 965 cm^{-1}.

4.6.3 Thermal Properties

Table 4.10 summarizes the TG-DTA data of cobalt-based complexes. Figure 4.15a shows a typical thermogram of $N_2H_5Mg_{1/3}Co_{2/3}(N_2H_3COO)_3 \cdot H_2O$. It is seen that all the complexes decompose in more than one step to yield corresponding metal cobaltites (MCo_2O_4) as the final product. The observed weight loss in TG corresponds to the expected theoretical value. Although DTA of the complexes shows three distinct exotherms, the corresponding steps in TG are not well defined. The breaks in TG may correspond to $M_{1/3}Co_{2/3}(N_2H_3COO)_2(N_2H_4)_x$, where $x = 1$–2. Formation of such intermediates has been reported during the decomposition of $N_2H_5M(N_2H_3COO)_3 \cdot H_2O$ where M = Co and Zn. However, isolation of these intermediates is not possible as the decomposition of the complexes is autocatalytic, going to completion very quickly.

Table 4.10 Thermal analysis data of $N_2H_5M_{1/3}(Co/Fe/Mn)_{2/3}(N_2H_3COO)_3 \cdot H_2O$.

Compound	DTA peak temperature (°C)[a]	Thermogravimetry			
		Temperature range (°C)	% Weight loss		
			Obsd.	Calcd.	Products
	$N_2H_5M_{1/3}Co_{2/3}(N_2H_3COO)_3 \cdot H_2O$, M = Mg, Mn, Fe, Co, Ni, and Zn				
Mg	132(+), 215(+), 245(+)	125–265	76.00	78.70	$MgCo_2O_4$
Mn	150(+), 230(+)	115–240	75.50	76.30	$MnCo_2O_4$
Fe	125(+), 160(+) 205(+)	120–235	77.00	76.26	$FeCo_2O_4$
Co	165(+), 190(+), 205(+), 240(+)	145–245	75.50	76.03	Co_3O_4
Ni	160(+), 225(+)	140–245	77.00	76.05	$NiCo_2O_4$
Zn	175(+), 205(+)	145–220	75.00	75.55	$ZnCo_2O_4$
	$N_2H_5M_{1/3}Fe_{2/3}(N_2H_3COO)_3 \cdot H_2O$, M = Mg, Mn, Fe, Co, Ni, and Zn				
Mg	132(+)	117–170	79.35	79.24	$MgFe_2O_4$
Mn	130(+)	75–120	76.90	76.81	$MnFe_2O_4$
Fe	165(+), 180(+)	145–220	76.00	75.93	Fe_2O_3
Co	170(+)	147–200	76.65	76.50	$CoFe_2O_4$
Ni	160(+)	130–185	76.85	76.52	$NiFe_2O_4$
Zn	135(+)	105–185	76.20	76.01	$ZnFe_2O_4$
	$N_2H_5M_{1/3}Mn_{2/3}(N_2H_3COO)_3 \cdot H_2O$, M = Co, Ni				
Co	205(+)	147–200	78.50	78.65	$CoMn_2O_4$
Ni	210(+)	130–185	77.00	76.67	$NiMn_2O_4$

[a] (+) = Exotherm.

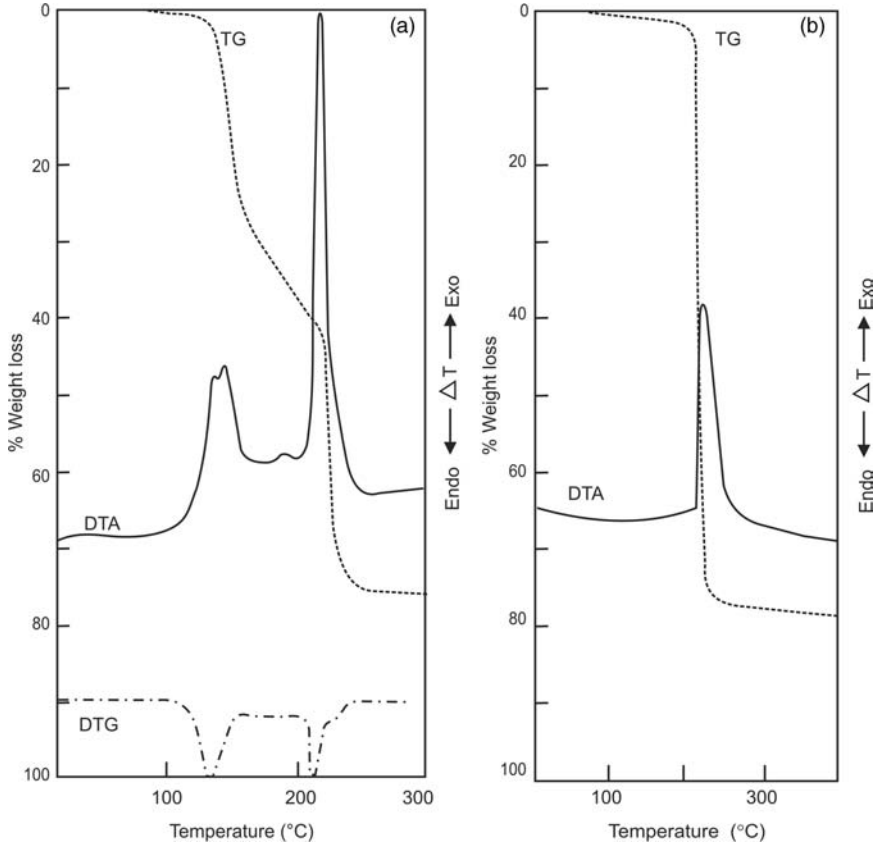

Figure 4.15 Simultaneous TG-DTG-DTA of (a) $N_2H_5Mg_{1/3}Co_{2/3}(N_2H_3COO)_3{\cdot}H_2O$ Adapted from Ref. [30] with permission from Elsevier © 1987. (b) $N_2H_5Ni_{1/3}Mn_{2/3}(N_2H_3COO)_3{\cdot}H_2O$. Reproduced from Ref. [31] with permission from Elsevier © 1993.

The TG-DTA data of the iron-based complexes are also summarized in Table 4.10. It can be seen that all the precursors decompose in a single step to the corresponding metal ferrites at 75–200 °C. The exothermic DTA peak temperatures of the precursors are lower than that of iron complex reported in the literature. The observed weight loss measured by TG corresponds to the formation of corresponding ferrites (MFe_2O_4).

Figure 4.15b shows a representative thermogram of mixed metal complex (manganese based) $N_2H_5Ni_{1/3}Mn_{2/3}(N_2H_3COO)_3{\cdot}H_2O$. The TG-DTA data summarized in Table 4.10 show single-step decomposition. The exothermic peak (200–240 °C) is attributed to the oxidation of $N_2H_3COO^-$ by atmospheric oxygen. The TG weight loss is in good

Table 4.11 Thermal analysis data of $N_2H_5(Ni_xZn_{1-x})_{1/3}Fe_{2/3}(N_2H_3COO)_3{\cdot}H_2O$.

x	DTA peak temperature (°C)[a]	Thermogravimetry			
		Temperature range (°C)	% Weight loss		
			Obsd.	Calcd.	Products
0.2	150(+)	130–170	76.05	76.12	$Ni_{0.2}Zn_{0.8}Fe_2O_4$
0.4	150, 210(+)	140–220	76.20	76.22	$Ni_{0.4}Zn_{0.6}Fe_2O_4$
0.5	155(+)	120–165	76.10	76.27	$Ni_{0.5}Zn_{0.5}Fe_2O_4$
0.6	145(+)	140–165	76.25	76.32	$Ni_{0.6}Zn_{0.4}Fe_2O_4$
0.8	143(+)	140–170	76.30	76.42	$Ni_{0.8}Zn_{0.2}Fe_2O_4$

[a] (+) = Exotherm.

agreement with the formation of spinel manganites from the decomposition of the hydrazinium precursors.

The thermal decomposition studies of the precursors hydrazinium metal hydrazine carboxylate hydrates of the formula $N_2H_5M'_{1/3}Fe_{2/3}(N_2H_3COO)_3{\cdot}H_2O$ (where $M'_{1/3} = Mg_xMn_{1-x}$, Ni_xZn_{1-x}) further show that all these complexes decompose exothermically, in a single step, in the temperature range 120–220 °C. Table 4.11 summarizes the results of TG-DTA of the complex $N_2H_5(Ni_{0.5}Zn_{0.5})_{1/3}Fe_{2/3}(N_2H_3COO)_3{\cdot}H_2O$; Figure 4.16 shows a typical thermogram. It can be observed that the weight loss in TG corresponds to the formation of the corresponding Ni-Zn ferrite.

The combustion of mixed metal iron complexes is similar to that observed for hydrazinium metal iron hydrazine carboxylates. The combustion is autocatalytic, once ignited, and leaves behind voluminous mixed ferrites. The particulate properties of these oxides such as cobaltites, ferrites and mixed ferrites have been investigated [32].

The thermal reactivity of all these solid solutions of the type $N_2H_5M_{1/3}(Co/Fe/Mn)_{2/3}(N_2H_3COO)_3{\cdot}H_2O$ indicates their exothermic decomposition at very low temperatures, due to the oxidation of highly reducing groups like $N_2H_3COO^-$ and $N_2H_5^+$. The reactivity is particularly enhanced in the presence of Fe, which is known to catalyze hydrazine decomposition/combustion. This fact has been confirmed by the combustion behavior of all these solid solutions on yielding the corresponding cobaltites, ferrites, and manganites. The combustion is accompanied by evolution of large amounts of cold gases like CO_2, H_2O, and N_2, resulting in nanocrystalline oxide materials of technological importance.

Quite recently, a solid solution of hydrazinium mixed metal hydrazine carboxylate complex of the type $(N_2H_5)Ni_{0.5}Co_{0.5}(N_2H_3COO)_3{\cdot}H_2O$ has been prepared by mixing the respective metal solutions in a molar ratio of 1 : 1 [4]. To this solution hydrazine carboxylic acid is added until

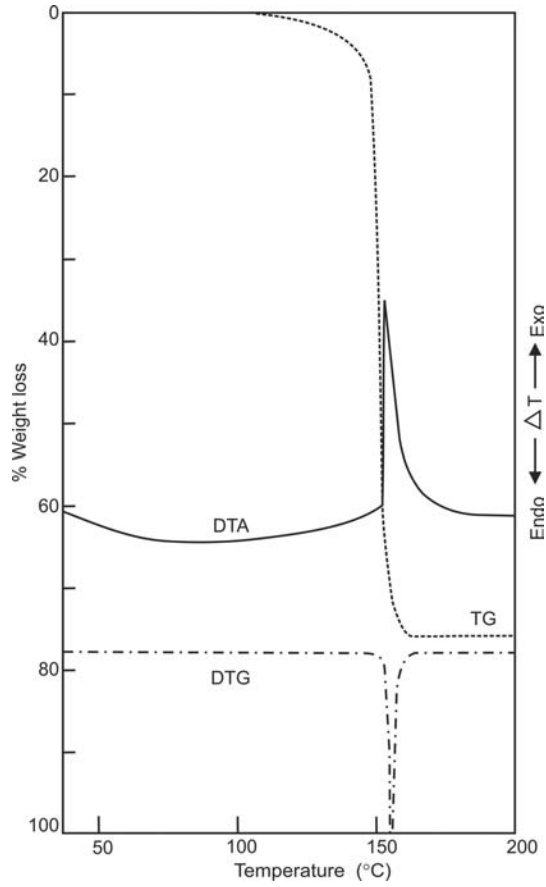

Figure 4.16 Simultaneous TG-DTG-DTA of $N_2H_5(Ni_{0.5}Zn_{0.5})_{1/3}Fe_{2/3}(N_2H_3COO)_3 \cdot H_2O$. Adapted from Ref. [33]. With kind permission from Springer Science and Business Media © 1987.

the molar ratio of 1 : 15 metal to hydrazine is reached. After a day, colored crystals are obtained, which are filtered, washed with water and then alcohol, and then dried.

The thermal decompositions reactions of these complexes are indicated below:

$$N_2H_5M(N_2H_3COO)_3 \cdot H_2O \rightarrow M(N_2H_3COO)_3 \cdot N_2H_4 + N_2H_4 + CO_2 + H_2O \tag{4.26}$$

$$M(N_2H_3COO)_3 \cdot N_2H_4 \rightarrow 2M + 6NH_3 + 3N_2 + H_2 + CO_2 \tag{4.27}$$

where M = Ni and Co.

Hydrazinium mixed metal hydrazine carboxylate complexes of Ni and Co act as a precursor to a bimetallic nano-size powder of $Ni_{0.5}Co_{0.5}$. Overall, it is inferred that metal hydrazine carboxylate derivatives are potential precursors for generating nanocrystalline structures.

4.7 SUMMARY

This chapter on metal hydrazine carboxylates has dealt with investigations of the coordination of hydrazine carboxylate anion ($N_2H_3COO^-$) as a bidentate ligand, forming numerous metal complexes. Four types of metal hydrazine carboxylates have been prepared and characterized. Since all of them form single crystals, several X-ray crystallographic structures have been determined. The formation of single-crystal complexes is useful in incorporating atomic level impurities in the host compounds. It has also been useful in preparing several solid solutions due to the isomorphous structures of both transition and rare earth hydrazine carboxylates. The thermal reactivity of these metal hydrazine carboxylates is of importance as most of them undergo combustion when rapidly heated, to yield oxides or metals. Metal hydrazine carboxylates may also serve as useful model compounds for conversion and storage of the greenhouse gas CO_2. Nonetheless, investigations indicate that the metal hydrazine carboxylate precursor route is promising for the synthesis of a wide variety of useful nanocrystalline metal powders and oxides that could be scaled up for industrial application.

REFERENCES

1. Audrieth, L.F. and Ogg, B.A. (1950) *The Chemistry of Hydrazine*, John Wiley, New York.
2. Schmidt, E.W. (2001) *Hydrazine and its Derivatives: Preparation, Properties, Applications*, 2nd edn, John Wiley & Sons, Inc.
3. Lee, B., Kang, S.H., Kang, D. *et al.* (2011) Isolation and structural characterization of the elusive 1:1 adduct of hydrazine and carbon dioxide. *Chemical Communications*, **47**, 11219–11221.
4. Maeck, J., Zaloznik, B., Novosel, B., and Marinsek, M. (2001) Preparation of cobalt and nickel nanopowders by the thermal decomposition of hydrazidocarbonates. *Acta Chimica Slovenica*, **48**, 127–135.
5. Patil, K.C., Budkuley, J.S., and Pai Verneker, V.R. (1979) Thermoanalytical studies of hydrazidocarbonic acid derivatives. *Journal of Inorganic & Nuclear Chemistry*, **41**, 953–995.

6. Nakamato, K. (2009) *Infrared and Raman Spectra of Inorganic and Coordination Compounds*, John Wiley & Sons, Inc., Hoboken.
7. Braibanti, A., Dallavalle, F., Pellinghelli, M.A., and Leporati, E. (1968) The nitrogen-nitrogen stretching band in hydrazine derivatives and complexes. *Inorganic Chemistry*, **7**, 1430–1433.
8. Ravindranathan, P. (1986) *Studies on metal hydrazine carboxylates: precursors to fine particle oxide materials*, Ph.D Thesis, Indian Institute of Science, Bangalore.
9. Ravindranathan, P. and Patil, K.C. (1985) Preparation, characterization and thermal analysis of metal hydrazine carboxylate derivatives. *Proceedings of the Indian Academy of Sciences – Chemical Sciences*, **95**, 345–356.
10. Sundar, Manoharan, S. (1991) *Combustion synthesis and properties of fine particle spinel, perovskite and K_2NiF_4 type oxides*. Ph.D Thesis, Indian Institute of Science, Bangalore.
11. Sundar, Manoharan, S. and Patil, K.C. (1989) Synthesis, characterization and thermal analysis of copper and chromium hydrazine carboxylates. *Proceedings of the Indian Academy of Sciences – Chemical Sciences*, **101**, 377–381.
12. Sekar, M.M.A. and Patil, K.C. (1993) Hydrazine carboxylate precursors to fine particle TiO_2, ZrO and $ZrTiO_4$. *Materials Research Bulletin*, **28**, 485–492.
13. Sekar, M.M.A. and Patil, K.C. (1994) Combustion synthesis of lead based dielectrics: a comparative study of redox compounds and mixtures. *International Journal of Self-Propagating High-Temperature Synthesis*, **3**, 27–38.
14. Sekar, M.M.A. (1994) *Combustion synthesis and properties of ferroelectrics, relaxor ferroelectrics and microwave resonator materials*, PhD Thesis, Indian Institute of Science, Bangalore.
15. Mahesh, G.V., Ravindranathan, P., and Patil, K.C. (1986) Preparation, characterization and thermal analysis of rare earth and uranyl hydrazine carboxylate derivatives. *Proceedings of the Indian Academy of Sciences – Chemical Sciences*, **97**, 117–123.
16. Adbel Gawad, M.M., Mahesh, G.V., Patil, K.C., and Bhat, S.V. (1994) An electron spin resonance study of Mn^{2+} doped calcium hydrazine carboxylate monohydrate. *Bulletin of Material Science*, **17**, 1131–1141.
17. Aruna, S.T., Ghosh, S., and Patil, K.C. (2001) Combustion synthesis and properties of $Ce_{1-x}Pr_xO_{2-\delta}$ red ceramic pigments. *International Journal of Inorganic Materials*, **3**, 387–392.
18. Ekambaram, S., Patil, K.C., and Maaza, M. (2005) Synthesis of lamp phosphors: facile combustion approach. *Journal of Alloys and Compounds*, **393**, 81–92.
19. Patil, K.C. and Pai Verneker, V.R. (1980) A novel method of preparing γ-Fe_2O_3. *Magnetic Society of India Transactions*, **4**, 8–10.
20. Patil, K.C. (1986) Metal hydrazine complexes as precursors to oxide materials. *Proceedings of the Indian Academy of Sciences – Chemical Sciences*, **96**, 459–464.
21. Ravindranathan, P. and Patil, K.C. (1987) A low temperature path to ultrafine ferrites. *American Ceramic Society Bulletin*, **66**, 688–692.
22. Patil, K.C., Soundararajan, R., and Goldberg, E.P. (1983) Reactions of hydrazinium hydrazido carboxylate salts of Mg, Mn, Fe, Co, Ni and Zn. *Synthesis and Reactivity in Inorganic, Metal-Organic, and Nano-Metal Chemistry*, **13**, 29–43.
23. Jesih, A., Rahten, A., Benkic, P. *et al.* (2004) The crystal and molecular structure of $N_2H_5[M(N_2H_3COO)_3]\cdot H_2O$ ($M\in${Co, Zn}) isomorphic compounds-an X-ray crystallographic, vibrational spectroscopic and quantum-chemical study. *Journal of Solid State Chemistry*, **177**, 4482–4493.

24. Ravindranathan, P. and Patil, K.C. (1986) A one-step process for the preparation of γ-Fe_2O_3. *Journal of Materials Science Letters*, **5**, 221–222.
25. Arul Dhas, N., Arash, E., and Kenneth, S.S. (2001) Sonochemical preparation of supported hydrodesulfurization catalysts. *Journal of the American Chemical Society*, **123**, 8310–8316.
26. Mastai, Y. and Gedankan, A. (2004) Sonochemistry and other novel methods developed for the synthesis of nanoparticles, in *The Chemistry of Nanomaterials*, vol. 1 (eds C.N.R. Rao, A. Müller, and A.K. Cheetham), Wiley-VCH Verlag GmbH, Weinheim, ch 6, p. 116.
27. Salkar, R.A., Jeevanandam, P., Kataby, G. *et al.* (2000) Elongated copper nanoparticles coated with a zwitterionic surfactant. *The Journal of Physical Chemistry B*, **104**, 893–897.
28. Suresh, K., Mahesh, G.V., and Patil, K.C. (1989) Preparation of cobalt doped γ-Fe_2O_3, in *Advances in Ferrites*, vol. 2 (eds C.M. Srivastava and M.J. Patni), Oxford & IBH Pub. Co. Pvt. Ltd., New Delhi, pp. 893–897.
29. Adbel Gawad, M.M., Mahesh, G.V., and Bhat, S.V. (1987) An ESR study of Mn^{2+} doped hydrazinium tris (hydrazinecarboxylato-N′O) zincate (II) monohydrate. *Hydrazine Centenary Abstracts*, Indian Institute of Science, Bangalore, pp. 5–7.
30. Ravindranathan, P., Mahesh, G.V., and Patil, K.C. (1987) Low temperature preparation of fine particle cobaltites. *Journal of Solid State Chemistry*, **66**, 20–25.
31. Arul Dhas, N. and Patil, K.C. (1993) Combustion synthesis and properties of fine particle spinel manganites. *Journal of Solid State Chemistry*, **102**, 440–445.
32. Patil, K.C. and Sekar, M.M.A. (1994) Synthesis, structure and reactivity of metal hydrazine carboxylates: combustible precursors to fine particle oxide materials. *International Journal of Self-Propagating High-Temperature Synthesis*, **3**, 181–196.
33. Ravindranathan, P. and Patil, K.C. (1987) Novel solid solution precursor method to the preparation of fine particle Ni-Zn ferrites. *Journal of Materials Science*, **22**, 3261–3264.
34. Srinivasan, T.T., Ravindranathan, P., Cross, L.E. *et al.* (1988) Studies on high density nickel-zinc ferrites and its magnetic properties using novel hydrazine precursors. *Journal of Applied Physics*, **63**, 3789–3791.
35. Sundar, Manoharan, S. and Patil, K.C. (1989) Preparation and properties of fine particle Mg-Mn ferrites, in *Advances in Ferrites*, vol. 1 (eds C.M. Srivastava and M.J. Patni), Oxford & IBH Pub. Co. Pvt. Ltd., New Delhi, pp. 43–47.
36. Suresh, K. and Patil, K.C. (1989) Preparation of high density Mn-Zn ferrite, in *Advances in Ferrites*, vol. 1 (eds C.M. Srivastava and M.J. Patni), Oxford & IBH Pub. Co. Pvt. Ltd., New Delhi, pp. 103–107.
37. Suresh, K., Mahesh, G.V., and Patil, K.C. (1989) Preparation of cobalt doped γ-Fe_2O_3 and Mn-Zn ferrites by the thermal decomposition of the hydrazine precursors. *Journal of Thermal Analysis and Calorimetry*, **35**, 1137–1143.
38. Braibanti, A., Manotti Lanfredi, A.M., and Tiripicchio, A. (1967) The crystal and molecular structure of hydrazinium tris(hydrazinecarboxylate-N′,O) niccolate(II) monohydrate. *Zeitschrift für Kristallographie*, **124**, 248–254.

5

Hydrazinium Metal Complexes

Subbiah Govindrajan[1] and Singanahally T. Aruna[2]
[1]*Department of Chemistry, Bharathiar University, Coimbatore, India*
[2]*Surface Engineering Division, CSIR-National Aerospace Laboratories, Bangalore, India*

5.1 INTRODUCTION

Monoprotonated hydrazine ($N_2H_5^+$) possesses a lone pair of electrons and is capable of coordinating to metal ions to form complexes. Single-crystal X-ray studies of hydrazinium metal sulfate and hydrazine carboxylates have proved the presence of hydrazinium cation as a ligand [1]. The synthesis and crystal structure of several hydrazinium metal complexes reported in the literature are discussed in Chapter 1 [1,2]. This chapter presents investigations on the synthesis, spectra, and single-crystal structure of several hydrazinium metal sulfates, oxalates, halides (chloride, bromide), and thiocyanate complexes of transition and rare earth metals. Continued interest in hydrazinium metal complexes persists, as evidenced by recent publications, not only in terms of the nature of bonding of hydrazinium cation but also their use as precursors to nanostructured metals, metal oxides, and metal chalcogenides [3–12].

Inorganic Hydrazine Derivatives: Synthesis, Properties and Applications, First Edition.
Edited by K. C. Patil and Tanu Mimani Rattan.

5.2 HYDRAZINIUM METAL SULFATES

The sulfate ion (SO_4^{2-}), though a simple dianionic ligand, exhibits a rather flexible symmetry and variable mode of binding with metal ions in the crystalline state. Interest in metal sulfate interactions with the hydrazinium cation arises from the fact that these compounds exhibit one- and three-dimensional magnetic interactions of a linear-chain antiferromagnet. Dihydrazinium sulfate forms a series of double sulfates with divalent and trivalent cation that are well crystallized and, in a few instances, are even less soluble than hydrazinium sulfate itself. The most easily prepared double sulfates are those of Cr, Mn, Fe, Co, Ni, Cu, Zn, Cd, Li, Mg, Al, La, Ce, Pr, Nd, and Sm. These salts are similar to the ammonium "alums" obtained with some metal sulfates. In contrast to the ammonium double salts, the hydrazinium metal sulfates of first row transition elements and lithium crystallize without water, whereas the lighter lanthanides and aluminum form hydrated salts.

5.2.1 Hydrazinium Metal Sulfates – $(N_2H_5)_2M(SO_4)_2$

5.2.1.1 Synthesis, Spectra, and Thermal Analysis

Hydrazinium metal sulfates, $(N_2H_5)_2M(SO_4)_2$ (where M = Cr, Mn, Fe, Co, Ni, Cu, Zn, Cd, and Mg), are prepared by adding aqueous solutions of corresponding metal sulfate hydrates to a warm solution of either $(N_2H_5)_2SO_4$ or $N_2H_6SO_4$ in dilute sulfuric acid [13]. The hydrazinium metal sulfates separate instantaneously to give the solid product, except in the case of Mn where the mixture first has to be cooled to 10 °C. Double sulfates invariably result in polycrystalline powders and attempts to obtain single crystals are largely unsuccessful; however, the reaction of aqueous $MSO_4 \cdot nH_2O$ (where M = Mn, Fe, and Cd) with ethyl bromoacetate and hydrazine hydrate in dry ethanol yields single crystals suitable for X-ray study.

Hydrazinium metal sulfate hydrazines of the formula $(N_2H_5)_2M(SO_4)_2 \cdot 3N_2H_4$ are prepared by reaction of the corresponding ammonium metal sulfate hexahydrates with stoichiometric amounts of hydrazine hydrate:

$$(NH_4)_2M(SO_4)_2 \cdot 6H_2O + 5N_2H_4 \cdot H_2O \rightarrow (N_2H_5)_2M(SO_4)_2 \cdot 3N_2H_4 + 2NH_3 + 11H_2O \quad (5.1)$$

where M = Fe, Co, Ni, Zn, and Cd.

The reaction is instantaneous with the evolution of ammonia and color change. After complete removal of ammonia, the products are washed with ethanol and diethyl ether, and dried over P_2O_5. However, the above reaction with Mn gives only the hydrazinium metal sulfate $(N_2H_5)_2Mn(SO_4)_2$ and not the hydrazinium metal sulfate hydrazine as expected. The corresponding hydrazinium metal sulfate hydrazine of copper is also not obtained because of its instant reduction to copper metal on addition of hydrazine hydrate.

Hydrazinium aluminum sulfate dihydrazine, $N_2H_5Al(SO_4)_2{\cdot}2N_2H_4$, is prepared by treating ammonium aluminum sulfate dodecahydrate, $NH_4Al(SO_4)_2{\cdot}2H_2O$, with excess hydrazine hydrate [14]. The hexahydrazine $N_2H_5Al(SO_4)_2{\cdot}6N_2H_4$ formed initially is unstable and loses four hydrazine molecules at room temperature to give a stable dihydrazine.

Hydrazinium zinc and cadmium sulfates can also be prepared by dehydrazination of the corresponding hydrazine complexes:

$$(N_2H_5)_2M(SO_4)_2{\cdot}3N_2H_4 \xrightarrow{80-250\,^{\circ}C} (N_2H_5)_2M(SO_4)_2 + 3N_2H_4 \qquad (5.2)$$

Hydrazinium metal sulfate complexes show IR (infrared) absorption at around 990–1005 cm^{-1}, characteristic of ν_{N-N} of the coordinated $N_2H_5^+$ cation and splitting of ν_3 (1100 cm^{-1}) and ν_4 (600 cm^{-1}) bands of SO_4^{2-} indicating the presence of bidentate sulfate groups (Table 5.1)

Table 5.1 Infrared absorption frequencies (cm^{-1})[a] of hydrazinium metal sulfates and hydrazinium metal sulfate hydrazines.

$(N_2H_5)_2M(SO_4)_2$	$(N_2H_5)_2M(SO_4)_3{\cdot}3N_2H_4$	Assignment
3290m, 3080w	3410, 3300, 3180w	N–H stretching
2720w, 2650w	2370s	N–H stretching of NH_3^+ (N^+–H···O
1630s, 1605m, 1575s, 1495s, 1310s	1690, 1640, 1610, 1350, 1310, 1250, 1230, 1200	NH_2 bending and wagging
1030–1170s,b	1120, 1100	S–O stretching of SO_4^{2-}
995w, 1005m	1008, 995	N–N stretching of $N_2H_5^+$/ N_2H_4
645s, 630m, 610s, 575s	610	Asymmetric bending and N–H deformation
490m	645, 625	Symmetric bending of SO_4^{2-}
410s	480	M–O stretching

[a] b = Broad, m = medium, s = sharp, w = weak.

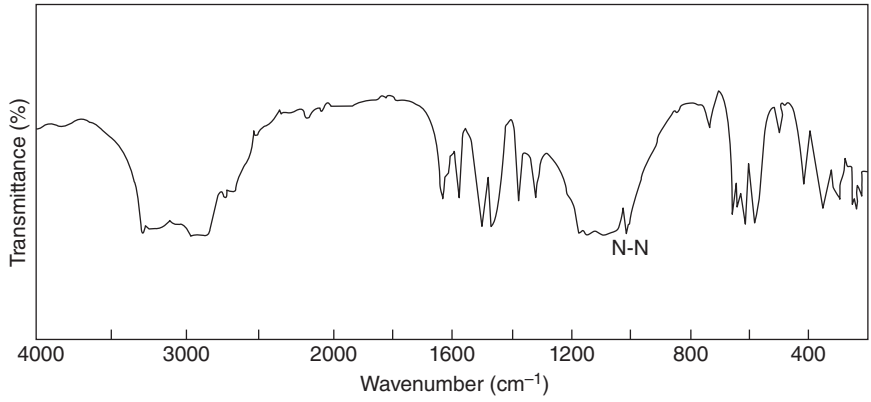

Figure 5.1 Infrared spectra of $(N_2H_5)_2Mg(SO_4)_2$. Ph.D Thesis of Govindrajan, S. under Prof. K. C. Patil at Indian Institute of Science.

A typical infrared spectrum of the hydrazinium complex shows the presence of a band at 980 cm^{-1}, characteristic of the ν_{N-N} stretching frequency of $N_2H_5^+$ (Figure 5.1).

The magnetic moments of the double sulfates $(N_2H_5)_2M(SO_4)_2$ reported in the literature correspond to an octahedral high-spin complex. The magnetic moments of $(N_2H_5)_2M(SO_4)_2{\cdot}3N_2H_4$ where M = Fe, Co, and Ni are 5.20, 4.83, and 2.97 BM, respectively, at 25 °C, corresponding to the high-spin octahedral complexes. The Mössbauer spectrum of $(N_2H_5)_2Fe(SO_4)_2{\cdot}3N_2H_4$ shows a two-finger pattern with an isomer shift (IS) of 1.24 mm s^{-1} and quadrupole splitting of 3.89 mm s^{-1} (Figure 5.2). These values are in good agreement for an octahedral Fe(II) high-spin complex. Owing to the $3d^6(t_{2g}^4,e_g^2)$ electronic configuration of Fe(II) ions, the Mossbauer spectra of compounds containing such ions show the largest quadrupole splitting (1.6–3.9 mm s^{-1}). The observed quadrupole splitting confirms the $3d^6(t_{2g}^4,e_g^2)$ electronic configurations. These values are similar to those reported earlier for $(N_2H_5)_2Fe(SO_4)_2$ ($\delta = 1.46$ mm s^{-1} and $\Delta Eq = 3.16$ mm s^{-1}) containing Fe(II) ions in a high-spin state with octahedral geometry [15]. Notably, the freshly prepared sample exhibits a two-line spectrum with satellite peaks at the sides. On aging, the intensity of the central peaks decreases and the satellite peaks grow in size until the intensities of all four peaks are equal. This observation clearly shows the presence of Fe^{2+} nuclei in two different environments. The species present initially undergoes a structural transformation that is in equilibrium with the new structure.

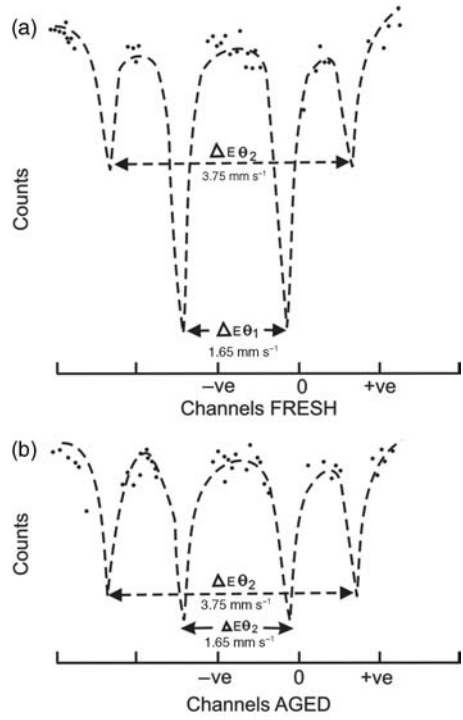

Figure 5.2 Mössbauer spectrum of (a) fresh and (b) aged $(N_2H_5)_2Fe(SO_4)_2{\cdot}3N_2H_4$. Ph.D Thesis of Soundararajan, R. under Prof. K. C. Patil at Indian Institute of Science.

Table 5.2 gives the TG (thermogravimetry) and DTA (differential thermal analysis) data of $(N_2H_5)_2M(SO_4)_2$ where M = Mn, Fe, Co, Ni, Cu, Zn, Cd, and Mg.

Thermogravimetry data shows that all the compounds decompose in two steps. The final product in all cases is the respective metal oxide. However, the intermediate is different in each case; for instance, for the iron complex the intermediate is a mixture of Fe(II) and Fe(III) sulfate and the cobalt complex gives cobalt sulfate, whereas the nickel complex gives a mixture of nickel sulfate and nickel sulfide. The formation of these intermediates has been confirmed by observed weight losses in TG as well as chemical analysis of the TG residues after the first step. For the iron complex, the residue obtained at 310 °C is gray and hygroscopic. It gives positive tests for both Fe(II) and Fe(III) in addition to sulfate.

Table 5.3 summarizes the TG and DTA data of $(N_2H_5)_2M(SO_4)_2{\cdot}3N_2H_4$ where M = Fe, Co, Ni, Zn, and Cd. All the complexes lose solvated hydrazine initially, yielding their hydrazinium complex. The

Table 5.2 Thermal analysis data of $(N_2H_5)_2M(SO_4)_2$.

M	Thermogravimetry			DTA peak temperature (°C)[a]	Product
	Temperature range (°C)	% Weight loss			
		Obsd.	Calcd.		
Mn	305–382	49.90	51.80	314(+)	$MnSO_4$
Fe	305–392	41.30	41.41	310(+)	$FeSO_4 + Fe_2(SO_4)_3$
Co	310–399	50.40	51.12	322(+)	$CoSO_4$
Ni	318–466	56.60	56.15	365(+)	$NiSO_4 + NiS$
Zn	320–455	57.80	59.92	328(+)	$ZnSO_4$
	—	—	—	368(+)	ZnS
Cd	324–425	53.80	52.38	330(+)	$CdSO_4$
	—	—	—	356(+)	CdS
Cu	245–315	74.50	75.27	252(+), 285(+)	CuO
Mg	300–504	45.80	46.05	302(+)	$MgSO_4 \cdot N_2H_4$
	—	56.90	57.38	504(−)	$MgSO_4$

[a] (−) = Endotherm, (+) = exotherm.

Table 5.3 Thermal analysis data of $(N_2H_5)_2M(SO_4)_2 \cdot 3N_2H_4$.

M	Thermogravimetry			DTA peak temperature (°C)[a]	Product
	Temperature range (°C)	% Weight loss			
		Obsd.	Calcd.		
Fe	35–215	15.40	15.61	130(−), 192(−)	—
	215–285	23.10	23.42	254(+)	—
	285–350	54.50	55.14	292(+)	$FeSO_4 + Fe_2(SO_4)_3$
	637–763	77.10	80.50	688(−)	—
Co	37–280	23.00	23.24	139(−), 205(−), 260(+)	—
	290–419	62.50	62.48	298(+)	$CoSO_4$
	826–975	79.90	80.57	890(+)	$Co_3O_4 + SO_3 + SO_2$
Ni	35–269	23.30	23.25	110(−), 232(−), 259(+)	—
	310–462	66.50	66.39	356(+)	$NiSO_4 + NiS$
	728–941	82.00	81.90	841(−)	NiO
Zn	85–275	22.30	22.88	148(−), 242(+)	—
	275–460	70.10	69.15	320(+)	$ZnSO_4$
	—	—	—	362(+)	ZnS
Cd	80–295	20.20	20.58	142(−)	—
	295–435	61.00	62.18	255(+)	—
	—	—	—	322(+)	$CdSO_4$
	—	—	—	350(+)	CdS

[a] (−) = Endotherm, (+) = exotherm.

fact that the loss of hydrazine commences at temperatures as low as 35 °C clearly shows that the hydrazine moiety is not coordinated in these complexes. The hydrazinium complexes obtained by the dehydrazination process decompose to $(N_2H_5)_2M(SO_4)_2$. However, they decompose at lower temperatures than the chemically prepared double sulfates.

Thermogravimetry shows two-step decomposition, namely, the loss of hydrazine (5.2) and decomposition of the hydrazinium double sulfate (5.3) in almost all cases:

$$(N_2H_5)_2M(SO_4)_2 \longrightarrow MSO_4 + (N_2H_5)_2SO_4 \qquad (5.3)$$

The weight losses observed are in total agreement with the proposed steps of decomposition. However, DTA of the complexes shows a complex pattern, though the temperature range in which decomposition occurs is same as found in TG. Figure 5.3 shows a typical thermogram of fresh and aged $(N_2H_5)_2Fe(SO_4)_2{\cdot}3N_2H_4$, showing several intermediate steps for a fresh sample while an aged sample shows two-step decomposition.

The DTA curve of $N_2H_5Al(SO_4)_2{\cdot}2N_2H_4$ shows two exothermic peaks, at 200 °C and 270 °C, and an endothermic peak at 870 °C. The exothermic reaction centered around 200 °C is due to its dehydrazination resulting in

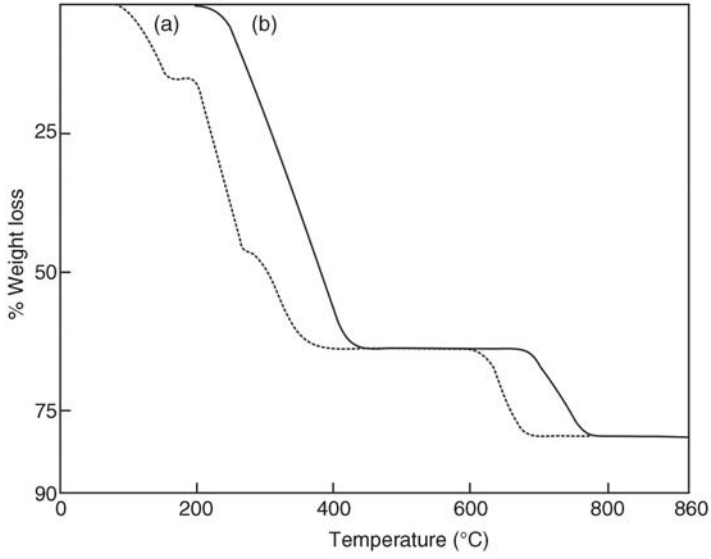

Figure 5.3 Thermogravimetric curves of fresh (a) and aged (b) $(N_2H_5)_2Fe(SO_4)_2{\cdot}3N_2H_4$. Adapted from Ref. [15] with permission from Elsevier © 1986.

$N_2H_5Al(SO_4)_2$, which further decomposes to alumina. The reaction can be written as:

$$N_2H_5Al(SO_4)_2 \cdot 2N_2H_4 \xrightarrow{110-260\,^{\circ}C} (N_2H_5Al(SO_4)_2 + 2N_2H_4 \qquad (5.4)$$

$$2N_2H_5Al(SO_4)_2 \xrightarrow{255-495\,^{\circ}C} Al_2(SO_4)_3 + (N_2H_5)_2SO_4 \qquad (5.5)$$

$$Al_2(SO_4)_3 \xrightarrow{740-965\,^{\circ}C} Al_2O_3 + 3SO_2 + \tfrac{3}{2}O_2 \qquad (5.6)$$

The weight loss observed during TG is in good agreement with the expected value for the various steps of decomposition for the compound.

5.2.1.2 *Single-Crystal Structures of $(N_2H_5)_2M(SO_4)_2$, M = Transition Metal*

Hydrazinium metal sulfates of first row transition metals (Cr, Mn, Fe, Co, Ni, Cu, Zn, and Cd) have essentially similar structures [16–18]. Single-crystal structures of hydrazinium cadmium sulfate (Figure 5.4) shows it to be a chain of metal ions linked by bridging bidentate sulfate groups, with $N_2H_5^+$ ligands in the *trans* position completing a distorted octahedron. These complexes exhibit one- and three-dimensional magnetic interactions of a linear chain antiferromagnet. Table 5.4 gives the crystallographic data of some of these double sulfates.

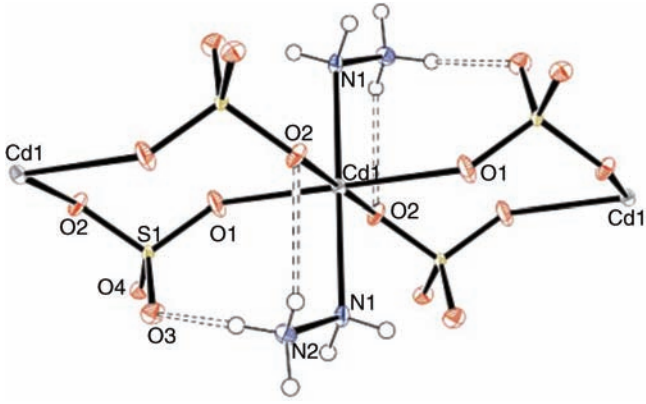

Figure 5.4 Molecular structure of $(N_2H_5)_2Cd(SO_4)_2$. Reproduced from Ref. [17] with permission from the International Union of Crystallography © 2006.

Table 5.4 Crystallographic data of hydrazinium metal sulfates.

Compound	Crystal data (*a*, *b*, and *c* are in Å and α, β, and γ in °)	N–N bond length (Å)
$(N_2H_5)_2Mn(SO_4)_2$	P-1 triclinic $a = 5.391(1)$, $b = 5.8678(11)$, $c = 7.3954$ (14); $\alpha = 92.651(2)\beta = 104.332(2)$, $\gamma = 99.249(2)$	1.447(3)
$(N_2H_5)_2Fe(SO_4)_2$	P-1 triclinic $a = 5.3306(3)$, $b = 5.8205(3)$, $c = 7.3835(4)$; $\alpha = 92.034(3)$, $\beta = 103.313(3)$, $\gamma = 99.237(3)$	1.446(4)
$(N_2H_5)_2Cd(SO_4)_2$	P-1 triclinic $a = 5.4835(2)$, $b = 5.9034(1)$, $c = 7.3624(2)$; $\alpha = 92.116(2)$, $\beta = 103.5206(16)$, $\gamma = 96.7984(18)$	1.450(2)

5.2.2 Hydrazinium Rare Earth Metal Sulfate Hydrates– $N_2H_5Ln(SO_4)_2{\cdot}H_2O$

5.2.2.1 Synthesis, Spectra, and Thermal Analysis

A hot aqueous solution of lanthanide sulfate hydrate, $Ln_2(SO_4)_3{\cdot}nH_2O$ (where Ln = La, Ce, Pr, Nd, or Sm), taken in H_2SO_4 is mixed with $(N_2H_5)_2SO_4$ or $N_2H_6SO_4$. The resulting solution when left to stand in air affords the respective hydrazinium rare earth metal sulfate [19]. Small crystals suitable for X-ray studies are obtained in a few days. They exhibit the characteristic color of the lanthanide ions:

$$(N_2H_5)_2SO_4 + Ln_2(SO_4)_3{\cdot}nH_2O \rightarrow 2N_2H_5Ln(SO_4)_2{\cdot}H_2O + (n-2)H_2O \tag{5.7}$$

$$2N_2H_6SO_4 + Ln_2(SO_4)_3{\cdot}nH_2O \rightarrow 2N_2H_5Ln(SO_4)_2{\cdot}H_2O + H_2SO_4 + (n-2)H_2O \tag{5.8}$$

where $n = 9$ for La or Ce and $n = 8$ for Pr, Nd, or Sm.

The compound $N_2H_5Nd(SO_4)_2{\cdot}H_2O$ is also prepared by isothermal evaporation (~50 °C) of an aqueous solution containing neodymium sulfate and hydrazinium sulfate in a molar ratio of 1 : 3. Efforts to readily prepare the corresponding sulfates of heavier elements (Eu to Lu) by this method have been unsuccessful due to the separation of starting materials.

The products have been characterized by chemical analysis and infrared and electronic spectra. The observed infrared absorption frequencies of $N_2H_5Ln(SO_4)_2{\cdot}H_2O$ are similar to those reported for $(N_2H_5)_2M(SO_4)_2$ complexes. The main features of the spectra are:

1. The ν_{N-N} of $N_2H_5^+$ is seen in the region 995–1000 cm^{-1}, indicating coordination of $N_2H_5^+$ to Ln^{3+}.
2. The splitting of ν_3 and ν_4 of SO_4^{2-} into three or four bands points to the presence of bidentate or bridging sulfate groups.

Table 5.5 summarizes data obtained on the thermal decomposition of hydrazinium rare earth sulfates using TG/DTA analysis. All the compounds distinctly show three similar steps of decomposition according to the following reaction sequence:

$$N_2H_5Ln(SO_4)_2{\cdot}H_2O \xrightarrow{255-305^\circ C} N_2H_5Ln(SO_4)_2 + H_2O \qquad (5.9)$$

$$2N_2H_5Ln(SO_4)_2 \xrightarrow{300-445^\circ C} N_2H_6SO_4{\cdot}Ln_2(SO_4)_3 + NH_3 + \tfrac{1}{2}N_2 + \tfrac{1}{2}H_2 \qquad (5.10)$$

Table 5.5 Thermal analysis data of $N_2H_5Ln(SO_4)_2{\cdot}H_2O$.

Ln	Thermogravimetry				DTA peak temperature (°C)[a]	Product
	Step number	Temperature range (°C)	% Weight loss			
			Obsd.	Calcd.		
La	1	260–300	4.80	4.71	280(−)	$N_2H_5La(SO_4)_2$
	2	205–240	77.0	76.0	301(+)	$N_2H_6(SO_4){\cdot}La_2(SO_4)_3$
	3	240–360	34.0	33.6	320–440(+)	$La_2(SO_4)_3$
Ce	1	270–305	4.90	4.7	290(−)	$N_2H_5Ce(SO_4)_2$
	2	305–435	24.90	25.84	305(+)	$N_2H_6(SO_4){\cdot}Ce_2(SO_4)_3$
	3	435–540	9.0	8.87	325–370(+)	$Ce_2(SO_4)_3$
Pr	1	256–305	5.0	4.69	283(−)	$N_2H_5Pr(SO_4)_2$
	2	305–430	26.0	25.79	300(+)	$N_2H_6(SO_4){\cdot}Pr_2(SO_4)_3$
	3	430–535	9.10	8.86	305–410(+)	$Pr_2(SO_4)_3$
Nd	1	260–302	4.5	4.65	284(−)	$N_2H_5Nd(SO_4)_2$
	2	302–440	25.50	25.57	303(+)	$N_2H_6(SO_4){\cdot}Nd_2(SO_4)_3$
	3	440–560	9.0	8.78	310–395(+)	$Nd_2(SO_4)_3$
Sm	1	255–305	4.8	4.85	285(−)	$N_2H_5Sm(SO_4)_2$
	2	305–427	25.0	25.17	308 (+)	$N_2H_6(SO_4){\cdot}Sm_2(SO_4)_3$
	3	427–545	8.9	8.64	315–380(+)	$Sm_2(SO_4)_3$

[a] (−) = Endotherm, (+) = exotherm.

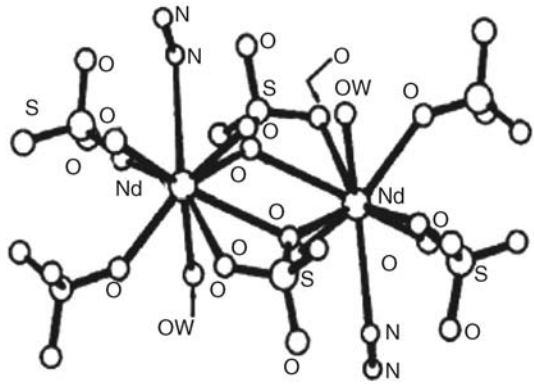

Figure 5.5 Molecular structure of $N_2H_5Nd(SO_4)_2{\cdot}H_2O$. Reproduced from Ref. [19] with permission of The Royal Society of Chemistry © 1986.

$$2N_2H_6SO_4{\cdot}Ln_2(SO_4)_3 \xrightarrow{425-560^{\circ}C} 2Ln_2(SO_4)_3 + 2NH_3 + N_2 + 3H_2O + 2SO_2 + \tfrac{1}{2}O_2 \quad (5.11)$$

The first step shows an endothermic peak due to dehydration occurring at a fairly high temperature (~250 °C), indicating the presence of coordinated water. The second and third steps of decomposition, involving dissociation of hydrazine, are both exothermic. Owing to the close similarity in the structure of rare-earth-metal complexes, the observed decomposition temperatures are identical.

5.2.2.2 Single-Crystal Structure of $N_2H_5Nd(SO_4)_2{\cdot}H_2O$

The structure of $N_2H_5Nd(SO_4)_2{\cdot}H_2O$ is polymeric with two crystallographically independent neodymium atoms in the asymmetric unit having similar coordination. The asymmetric part of the structure shown in Figure 5.5 has an amazingly accurate local center of inversion at 0.125, 0.25, and 0.02, which is repeated at 0.375, 0.25, 0.52, 0.625, 0.75, 0.02, and 0.875, 0.75, 0.52. This is a fascinating feature of the structure. Each neodymium atom is coordinated to seven oxygen atoms from six sulfate groups, one oxygen atom from water, and one nitrogen atom of $N_2H_5^+$. The Nd1 . . . Nd2 distance of 4.53 Å confirms the absence of metal–metal interaction, a conclusion that is supported by the magnetic moment values of 2.30 BM for Ce, 3.37 BM for Pr, 3.43 BM for Nd, and 1.48 BM for Sm.

Table 5.6 Unit cell dimensions for the isomorphic $N_2H_5Ln(SO_4)_2{\cdot}H_2O$.

$N_2H_5Ln(SO_4)_2{\cdot}H_2O$	Lattice parameters (Å)	U (Å^3)
La	$a = 11.05(3)$, $b = 9.63(3)$, $c = 15.93(4)$	1695.4
Ce	$a = 11.02(3)$, $b = 9.60(3)$, $c = 15.87(5)$	1680.0
Pr	$a = 10.98(3)$, $b = 9.57(2)$, $c = 15.82(4)$	1662.3
Nd[a]	$a = 10.96(3)$, $b = 9.55(3)$, $c = 15.79(4)$	1653.4
	$a = 10.951(3)$, $b = 9.554(3)$, $c = 15.762(3)$	1649.1
Sm	$a = 10.90(3)$, $b = 9.50(2)$, $c = 15.71(4)$	1628.1

[a] Single-crystal data.

There are four crystallographically non-equivalent sulfate groups present in the structure, all acting as bridging ligands. In all the sulfates, three oxygen atoms take part in metal coordination, with the fourth being free. The bridging mode for the S(1) and S(2) sulfate groups is different from the other two, in that while the former links two dimers, the latter links three. Interestingly, O(1) of the S(1) sulfate group and O(5) of the S(2) sulfate group coordinate to both Nd(1) and Nd(2) atoms. This type of bonding with two bridging oxygen atoms has not been previously observed in lanthanide sulfate complexes, except in $CsLa(SO_4)_2$, where one of the oxygen atoms is coordinated to two lanthanum atoms of adjacent molecules.

The structure is built up of neodymium atoms linked by sulfate groups forming sheets parallel to the (001) plane. The sheets are held together by N–H···O (sulfate) type hydrogen bonds. Water molecules are also involved in hydrogen bonding with the oxygen of the sulfate group, and van der Waals interactions between sheets appear to further stabilize the structure.

Table 5.6 summarizes the unit-cell dimensions for the series lanthanum to samarium obtained from XRD powder patterns. These values and the observed intensities of the diffraction lines confirm the expected isomorphism in the rare earth complexes.

5.3 HYDRAZINIUM METAL OXALATES

Among the organic oxy-ligands, the oxalate anion $C_2O_4^{2-}$, because of its great versatility, has attracted a great deal of interest. It can act as a monodentate, bidentate, tetradentate chelating ligand and form several types of arrangements: discrete anions, chains, and layers of three-dimensional networks with metallic cations. Metal oxalate complexes containing the coordinated oxalate ligand are quite well known. As compared to

other double salts, the double oxalates of metals with monocation like NH_4^+, alkali metal, and so on, are somewhat rare since oxalate anion precipitates metals as insoluble metal oxalates. Hence, special methods are needed to synthesize double oxalates.

5.3.1 Hydrazinium Metal Oxalates – $(N_2H_5)_2M(C_2O_4)_2{\cdot}nH_2O$, M = Co, Ni, Cu, and so on

5.3.1.1 Synthesis, Spectra, and Thermal Analysis

Hydrazinium transition metal oxalates of Co, Ni, and Cu are prepared by mixing aqueous solutions of respective metal nitrate hydrates and hydrazinium oxalate $(N_2H_5)_2C_2O_4$ (mole ratio of 1 : 4) and keeping the mixture at 5 °C for a couple of days. The rate of product formation increases in the order Co < Ni < Cu. The cobalt compound is somewhat unstable and it decomposes in air. Efforts to prepare the corresponding Mn, Fe, and Zn compounds using a similar procedure yielded only the simple metal oxalates [20]:

$$2(N_2H_5)_2C_2O_4 + M(NO_3)_2{\cdot}nH_2O \rightarrow$$
$$(N_2H_5)_2M(C_2O_4)_2{\cdot}nH_2O + 2N_2H_5NO_3 \qquad (5.12)$$

where M = Co, Ni, and Cu.

All these complexes have been investigated by infrared, electronic, and ESR spectroscopy. Magnetic studies were carried out using a Gouy balance at room temperature. Tables 5.7 and 5.8 list, respectively, the IR absorption frequencies and the electronic spectral details and magnetic data of hydrazinium metal oxalates.

Infrared absorption of ν_{N-N} at 965 cm^{-1} clearly shows that $N_2H_5^+$ is outside the coordination sphere. Among the complexes only the nickel complex specifically shows a N−N stretching frequency at around 1000, 1010 cm^{-1}, indicating coordination of N_2H_5 to the metal. Supporting evidence for an octahedral environment around Ni(II) is furnished by the reflectance spectrum. The bands at 16,600 and 26,300 cm^{-1} can be assigned to $^3A_{2g} \rightarrow {}^3T_{1g}(F)$ and $^3A_{2g} \rightarrow {}^3T_{1g}(P)$ transitions, respectively, which are characteristic of an octahedral geometry around Ni(II). The magnetic susceptibility value (μ_{eff}) of 3.1 BM is in accordance with that of a high-spin complex of nickel.

The IR spectrum of $(N_2H_5)_2Cu(C_2O_4)_2{\cdot}H_2O$ does not offer conclusive evidence about the coordination of $N_2H_5^+$ to the metal. The spectrum

Table 5.7 Infrared absorption frequencies (cm^{-1}) of $(N_2H_5)_2M(C_2O_4)_2{\cdot}xH_2O$.

$(N_2H_5)_2$ $Co(C_2O_4)_2{\cdot}3H_2O$	$(N_2H_5)_2$ $Ni(C_2O_4)_2{\cdot}2H_2O$	$(N_2H_5)_2$ $Cu(C_2O_4)_2{\cdot}H_2O$	Assignment
3500b	3500b	3620b	Asym. CH stretching
3315s	3380s	3330m	Asym. NH stretching
—	3260m	3265w	Sym. NH stretching
2660w	2660w	2650w	NH stretching of NH_3^+
1725s	1720b	1710w	Asym OCO stretching
1625b	1650b	1690s, 1650b	NH_2 and OH bending
1550w	—	1510w	Bending of NH_3^+
1300m	1310s	—	Sym. OCO stretch
—	1290s	1280s	NH_2 wagging
1150s	1150s	1125m	NH_2 twisting
965s	1010s	980s	N–N stretching
—	895w	895w	OCO bending
805s	800s	800s	OCO deformation
615w	630s	—	NH_2 rocking
465m	495s	495m	M–O stretching
370m	390w	—	M–N stretching

exhibits two absorptions, at 975 and 980 cm^{-1}. The assignment of these absorptions is rather difficult since the observed frequency is too high for ionic $N_2H_5^+$ ($\nu_{N-N} = 965\,cm^{-1}$) and too low for coordinated $N_2H_5^+$ ($\nu_{N-N} = 1005\,cm^{-1}$). The magnetic susceptibility value of 1.86 BM shows that the complex is high spin and could have octahedral or tetrahedral geometry. The ESR spectrum of the copper complex shows a "*g*" value of 2.11, which is in agreement to its square-planar geometry (Figure 5.6).

It has been shown that orbital contributions in tetrahedral Co(II) complexes decrease as the ligand varies from I^- towards CN^- in the spectrochemical series. Hence tetracoordinated Co(II) complexes have tetrahedral structures only if the magnetic moments are in the range 4.2–4.7 BM (Table 5.8). The observed magnetic moment of 5 BM for the present cobalt complex thus rules out the possibility of it having a tetrahedral geometry.

The nickel complex decomposes in three steps ((5.13)–(5.15)). In the first step water is lost endothermically at 124 °C. Thereafter, the anhydrous complex further decomposes to give nickel oxalate monohydrazine. This is observed as an endotherm with a peak temperature of 280 °C. The final step corresponds to the decomposition of nickel oxalate monohydrazine to nickel oxide (NiO). This decomposition is exothermic at 342 °C (Figure 5.7a):

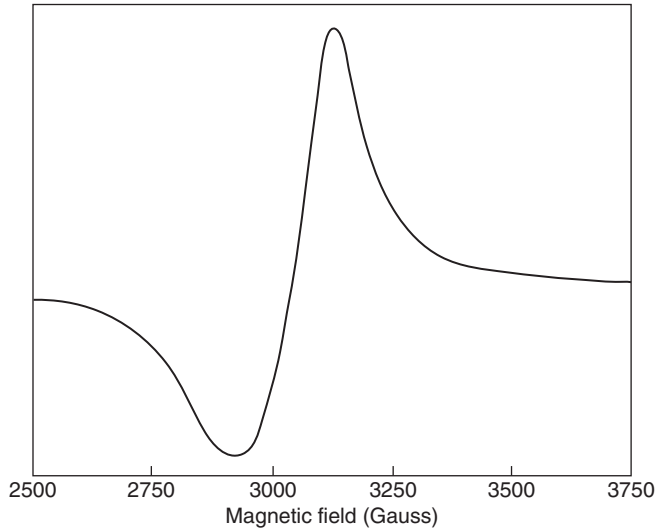

Figure 5.6 ESR spectrum of $(N_2H_5)_2Cu(C_2O_4)_2{\cdot}H_2O$. Reproduced from Ref. [20] with permission from Elsevier © 1983.

Table 5.8 Electronic spectral and magnetic data.

Compound	Electronic spectra		μ_{eff} (26 °C) (BM)
	Wavelength (nm)	Assignment	
$(N_2H_5)_2Cu(C_2O_4)_2{\cdot}H_2O$	662	$^2B_{1g} \rightarrow {}^2E_g$	1.86
	332	Charge transfer	
$(N_2H_5)_2Ni(C_2O_4)_2{\cdot}2H_2O$	602	$^3A_{2g} \rightarrow {}^3T_{1g}(F)$	3.10
	380	$^3A_{2g} \rightarrow {}^3T_{1g}(P)$	
	326	Charge transfer	
$(N_2H_5)_2Co(C_2O_4)_2{\cdot}3H_2O$	521, 465	$^4T_{1g}(F) \rightarrow {}^4T_{1g}(P)$	5.00
	340	Charge transfer	

$$(N_2H_5)_2Ni(C_2O_4)_2{\cdot}2H_2O \xrightarrow{124^\circ C} (N_2H_5)_2Ni(C_2O_4)_2 + 2H_2O \quad (5.13)$$

$$(N_2H_5)_2Ni(C_2O_4)_2 \xrightarrow{280^\circ C(\text{endo})} NiC_2O_4{\cdot}N_2H_4 + 2NH_3 + 2CO_2 \quad (5.14)$$

$$NiC_2O_4{\cdot}N_2H_4 + \tfrac{3}{2}O_2 \xrightarrow{342^\circ C(\text{exo})} NiO + 2CO_2 + N_2 + 2H_2O \quad (5.15)$$

The TG curve shows three distinct steps with percentage weight losses of 10.5%, 47%, and 77% corresponding to the formation of the

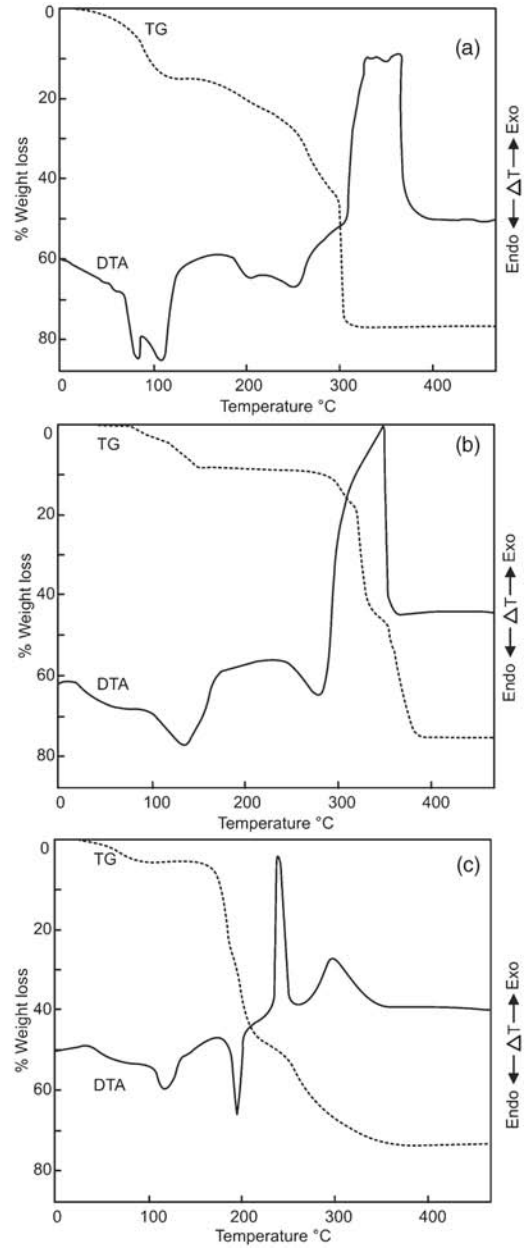

Figure 5.7 Simultaneous TG-DTA curves of (a) $(N_2H_5)_2Ni(C_2O_4)_2{\cdot}2H_2O$, (b) $(N_2H_5)_2Co(C_2O_4)_2{\cdot}3H_2O$, and (c) $(N_2H_5)_2Cu(C_2O_4)_2{\cdot}H_2O$. Adapted from Ref. [20] with permission from Elsevier © 1983.

anhydrous compound, $NiC_2O_4{\cdot}N_2H_4$, and NiO respectively. The theoretically calculated percentage weight losses for these steps are 10.7%, 46.9%, and 77.8%, respectively.

Hydrazinium cobalt oxalate trihydrate decomposes in a manner similar to the nickel compound, giving rise to Co_3O_4 (Figure 5.7b). The DTA curve of hydrazinium copper oxalate (Figure 5.7c) first shows an endotherm at 119 °C corresponding to dehydration. The next endotherm at 198 °C is where the anhydrous compound melts sharply. Lastly, an exotherm at 238 °C is due to the decomposition of anhydrous hydrazinium copper oxalate, which further decomposes exothermically at 305 °C to give CuO. The decomposition scheme for $(N_2H_5)_2Cu(C_2O_4)_2{\cdot}H_2O$ in air can be represented as follows:

$$(N_2H_5)_2Cu(C_2O_4)_2{\cdot}H_2O \xrightarrow{119\,^{\circ}C\,(endo)} (N_2H_5)_2Cu(C_2O_4)_2 + H_2O \quad (5.16)$$

$$(N_2H_5)_2Cu(C_2O_4)_2 \xrightarrow{238\,^{\circ}C\,(exo)} CuC_2O_4 + N_2 + H_2O + 2NH_3 + 2CO_2 \quad (5.17)$$

$$CuC_2O_4 + \tfrac{1}{2}O_2 \xrightarrow{305\,^{\circ}C\,(exo)} CuO + 2CO_2 \quad (5.18)$$

The percentage weight losses observed in TG for these steps are 5.5%, 52.0%, and 75%, respectively. The theoretically calculated percentage weight losses of 5.6%, 53.2%, and 75.4%, respectively, for these steps are in good agreement with the observed values.

5.3.1.2 *Single-Crystal Structure of $(N_2H_5)_2Cu(C_2O_4)_2{\cdot}nH_2O$*

The reflectance spectrum of the complex shows the d–d transition at $15,100\,cm^{-1}$, which favors square-planar stereochemistry for Cu(II). However, unequivocal proof about the coordination environment of the metal, comes from a single-crystal X-ray study of the complex. The crystal contains discrete $N_2H_5^+$ ions, $Cu(C_2O_4)_2^{2-}$ ions, and water molecules. The copper atom lies on a center of symmetry, with square-planar coordination of oxygen from two bidentate (chelate) oxalate groups (Figure 5.8a and b) . The $N_2H_5^+$ ion is not coordinated to the metal (Table 5.9).

The Cu–O(1) distance of 1.944 (2) Å is slightly longer than Cu–O(2) distance of 1.926 (2) Å. The bite angle of the bidentate ligand [O(1)–Cu–O(2)] is 85.5°. The oxalate group is planar and Cu(II) is out of this plane by

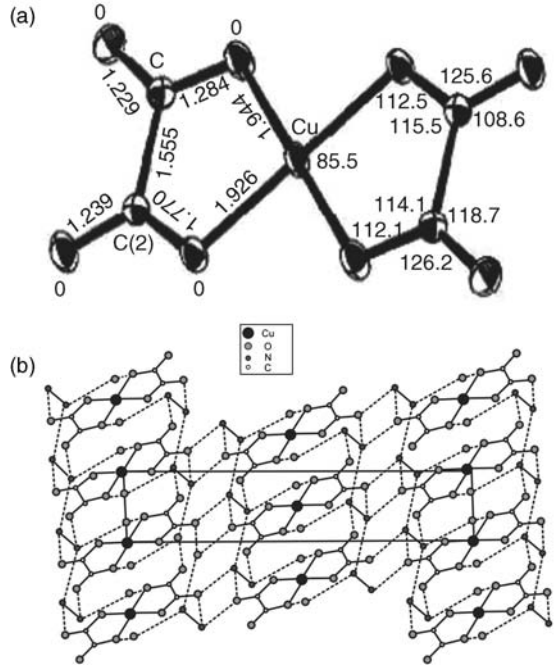

Figure 5.8 (a) Molecular structure of $Cu(C_2O_4)_2^{2-}$ in $(N_2H_5)_2Cu(C_2O_4)_2{\cdot}H_2O$ and (b) packing diagram of $(N_2H_5)_2Cu(C_2O_4)_2{\cdot}H_2O$. Reproduced from Ref. [20] with permission from Elsevier © 1983.

Table 5.9 Crystal structure data of $(N_2H_5)_2Cu(C_2O_4)_2{\cdot}H_2O$.

Space group	Lattice parameters: a, b, and c (Å) and angle β (°)	N–N bond length (Å)
Monoclinic, $P2_1/n$	$a = 3.592(1)$, $b = 7.855(2)$, $\beta = 94.3(3)$, $c = 19.143(3)$	1.429(4)

0.1 Å. As expected, coordinated C–O distances (1.284 and 1.270 Å) are slightly longer than the free C–O distances (1.229 and 1.239 Å).

The C–C–O bond angle of 114.1–115.5° is due to the steric restrictions on the planar five-membered chelate ring. In the $N_2H_5^+$ ion, the NH_3 group is staggered with respect to the NH_2 group and its lone pair. In the crystal structure there is a network of hydrogen bonds involving the $N_2H_5^+$ ion, lattice water, and oxalate oxygen. The hydrogen bond lengths are in the range 2.84–3.10 Å. The molecules are stacked one above the other, along the "*a*" axis having a separation of 3.6 Å, with the unit cell translation being *a*.

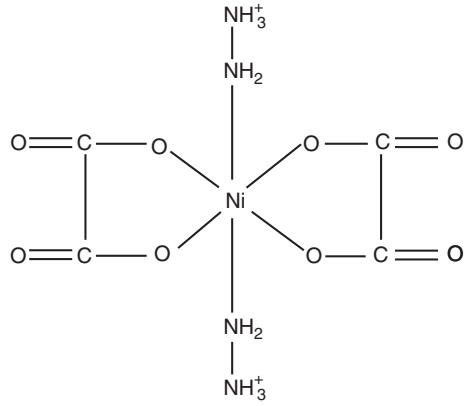

Figure 5.9 Structure of hydrazinium nickel oxalate dihydrate. Adapted from Ref. [20] with permission from Elsevier © 1983.

A single-crystal X-ray study of the hydrazinium nickel oxalate dihydrate complex could not be carried out as the crystal shows twinning, rendering the X-ray investigation difficult. Therefore, based upon IR, UV spectra, and magnetic susceptibility data, the proposed structure of hydrazinium nickel oxalate dihydrate is represented as shown in Figure 5.9. In this case, apart from two bidentate (chelate), oxalate groups occupy the equatorial plane, while the axial positions are filled by hydrazinium cations. As a whole the nickel atom displays octahedral coordination.

Supporting evidence for an octahedral environment around Ni(II) is furnished by the reflectance spectrum. The bands at 16 600 and 26 300 cm^{-1} can be assigned to $^3A_{2g} \rightarrow {}^3T_{1g}(F)$ and $^3A_{2g} \rightarrow {}^3T_{1g}(P)$ transitions, respectively, which are characteristic of octahedral geometry around Ni(II). A magnetic susceptibility of 3.1 BM is in accordance with that of a high-spin complex of nickel.

The fact that hydrazinium cobalt oxalate trihydrate is not isomorphic with either the copper or nickel analog suggests that the geometry around Co^{2+} is different from that of Cu^{2+} and Ni^{2+}. All known tetrahedral cobaltous complexes exhibit a characteristic intense multicomponent band in the 13, 300–16, 600 cm^{-1} region associated with the $^4A_2 \rightarrow {}^4T_1(P)$ transition in tetrahedral geometry, whereas no band is observed in this specified region in the reflectance spectrum of the cobalt complex. The electronic spectrum of hydrazinium cobalt oxalate trihydrate shows bands at 21 500 and 19 200 cm^{-1} assigned to $^4T_{1g}(F) \rightarrow {}^4T_{1g}(P)$, which is usually split due to spin–orbit coupling in the $^4T_{1g}(P)$ state. The electronic spectrum

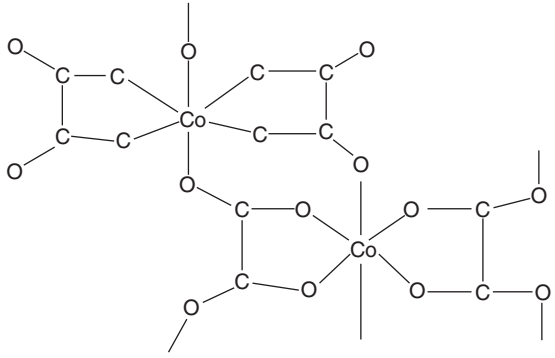

Figure 5.10 Structure of hydrazinium cobalt oxalate trihydrate. Reproduced from Ref. [20] with permission from Elsevier © 1983.

is comparable with the spectrum of octahedral Co(II) complexes as reported in the literature, with a double band having a center of gravity at $\sim$20,000 cm^{-1}. The pink color of the complex is also indicative of octahedrally coordinated Co(II). From coordination chemistry it is well known that planar spin-free complexes are possible if the four donor atoms provide a weak enough ligand field for Co(II) in a ligand field of D_{4h} symmetry. Thus, it is concluded that the cobalt complex may have planar $Co(C_2O_4)_2^{2-}$ anions that aggregate to form a chain structure with pairs of long Co–O bonds between anions, making it octahedral. The structure could be represented as shown in Figure 5.10.

5.3.2 Hydrazinium Uranyl Oxalates

Among uranium compounds, the uranyl ion (UO_2^{2+}) is the most stable species present in nature and has a linear structure. In uranyl complexes, the ligands coordinate to the metal center in a plane nearly perpendicular to the O–U–O axis, as shown by the structures of uranyl systems containing various ligands. In the coordination chemistry of UO_2^{2+}, the oxalate chelating ligand has, in particular, attracted special attention because different types of complexes are formed depending upon the UO_2^{2+}:$C_2O_4^{2-}$ mole ratio and the nature of oxalate coordination. An additional interesting feature of the ligand is that it has an unusually large bite distance of 2.7 Å.

The following complexes of hydrazinium uranyl oxalates are discussed: $(N_2H_5)_2[UO_2(C_2O_4)_2(H_2O)]$ and $(N_2H_5)_6[(UO_2)_2(C_2O_4)_5]\cdot 2H_2O$.

5.3.2.1 Synthesis, Spectra, and Thermal Analysis

The complex $(N_2H_5)_2[UO_2(C_2O_4)_2(H_2O)]$ is prepared by mixing aqueous solutions of uranyl nitrate hexahydrate and hydrazinium oxalate in a molar ratio of 1 : 2, at room temperature [21]. Yellow tabular crystals appear on slow evaporation. The composition of the crystals has been determined by conventional analysis of hydrazine, oxalate, and uranyl groups. The hexahydrazinium diuranyl pentaoxalate dihydrate complex, $(N_2H_5)_6[(UO_2)_2(C_2O_4)_5]\cdot 2H_2O$, is obtained by the reaction of uranyl nitrate hexahydrate and hydrazinium oxalate (1 : 4 mol ratio) at 5 °C [22]:

$$2UO_2(NO_3)_2\cdot 6H_2O + 5(N_2H_5)_2C_2O_4 \rightarrow$$
$$(N_2H_5)_6(UO_2)_2(C_2O_4)_5\cdot 2H_2O + 4N_2H_5NO_3 + 10H_2O \qquad (5.19)$$

The IR spectrum of $(N_2H_5)_6[(UO_2)_2(C_2O_4)_5]\cdot 2H_2O$ shows characteristic absorption of the uranyl ion, ν_3 (O=U=O) at 910 cm^{-1}, and an absorption at 960 cm^{-1}, which is assigned to ν_{N-N} of ionic $N_2H_5^+$. The ν_{N-N} of coordinated $N_2H_5^+$ is known to occur in the region 990–1005 cm^{-1}. The absence of absorptions in this region indicates the absence of bonding of $N_2H_5^+$ groups to the uranyl ion. An absorption at 3530 cm^{-1} has been attributed to ν_{O-H} of free water molecules. The infrared spectral results clearly show the presence of bidentate coordination of oxalate groups to the uranyl ion.

The visible absorption spectrum of the complex shows sharp absorption at 385, 395, 407, 418, 428, 439, 453, 468, and 490 nm (Figure 5.11). The absorption at 439 nm is assigned to the $^1\Sigma_{g+} \rightarrow {}^3\Pi_u$ transition of the uranyl ion.

The complex $(N_2H_5)_6[(UO_2)_2(C_2O_4)_5]\cdot 2H_2O$ shows three steps of decomposition in TG and four peaks in DTA (Figure 5.12). The first TG step corresponds to the loss of water; the second step to the decomposition of the anhydrous complex to $UO_2C_2O_4\cdot 2N_2H_4$; finally, the hydrazine intermediate decomposes to U_3O_8. The DTA peaks are generally in agreement with the TG steps. The overall decomposition sequence of this complex can be written as follows:

$$(N_2H_5)_6(UO_2)_2(C_2O_4)_5\cdot 2H_2O \xrightarrow{148\ ^\circ C(endo)} (N_2H_5)_6(UO_2)_2(C_2O_4)_5 + 2H_2O \qquad (5.20)$$

$$(N_2H_5)_6(UO_2)_2(C_2O_4)_5 \xrightarrow{200\ ^\circ C(endo)} 2[UO_2(C_2O_4)_2\cdot 2N_2H_4] + 4NH_3 + 2CO_2 + H_2 \qquad (5.21)$$

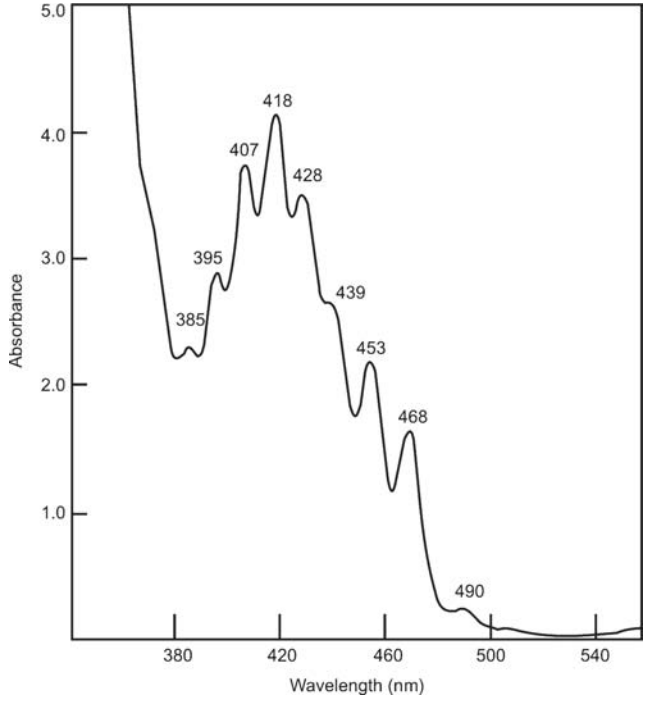

Figure 5.11 Electronic spectrum of $(N_2H_5)_6[(UO_2)_2(C_2O_4)_5]\cdot 2H_2O$. Adapted from Ref. [22] with permission from Elsevier © 1986.

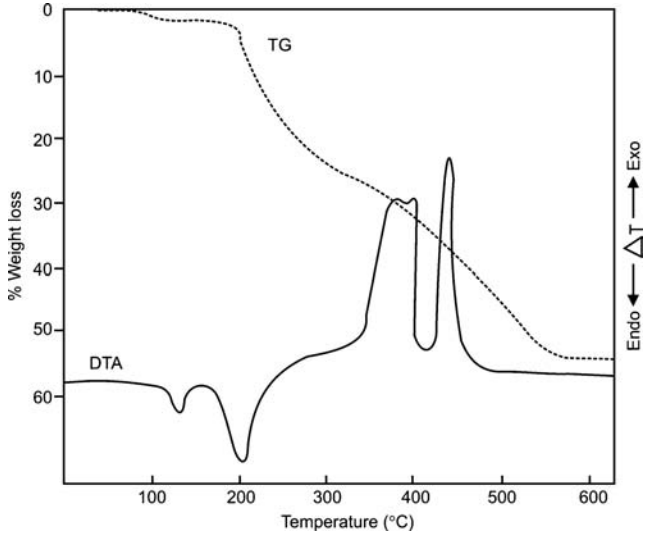

Figure 5.12 Simultaneous TG-DTA of $(N_2H_5)_6[(UO_2)_2(C_2O_4)_5]\cdot 2H_2O$. Adapted from Ref. [22] with permission from Elsevier © 1986.

$$UO_2(C_2O_4)_2 \cdot 2N_2H_4 \xrightarrow{350-390\,^{\circ}C(\text{exo})} UO_2C_2O_4 + 2NH_3 + N_2 + H_2 + 2CO_2 \quad (5.22)$$

$$3UO_2C_2O_4 + O_2 \xrightarrow{430\,^{\circ}C(\text{exo})} U_3O_8 + 6CO_2 \quad (5.23)$$

The spectral and thermal results for $(N_2H_5)_6[(UO_2)_2(C_2O_4)_5]\cdot 2H_2O$ indicate the presence of free $N_2H_5^+$ and H_2O groups in the complex.

5.3.2.2 *Single-Crystal Structures of $(N_2H_5)_6[(UO_2)_2(C_2O_4)_5]\cdot 2H_2O$ and $(N_2H_5)_2(UO_2)(C_2O_4)_2\cdot H_2O$*

$(N_2H_5)_6[(UO_2)_2(C_2O_4)_5]\cdot 2H_2O$

In the crystal structure of $(N_2H_5)_6[(UO_2)_2(C_2O_4)_5]\cdot 2H_2O$, the $N_2H_5^+$ ions and water molecules are not involved in coordination (Table 5.10). Figure 5.13 shows the arrangement of the $[UO_2(C_2O_4)_2(H_2O)]^{2-}$ anion.

The uranyl group is coordinated by four oxygen atoms of two chelating bidentate oxalate groups and an oxygen atom from water. The coordination polyhedron is an approximate pentagonal bipyramid, with the metal being virtually in the plane of the pentagon. The uranyl ion is linear with an O–U–O angle of 178.0 (4) Å, with the two U–O distances of 1.770(8) and 1.773(8) Å. In the equatorial plane, the U–O(water) bond length is 2.395(9) Å, and the U–O (oxalate) distances vary from 2.359(8) to 2.400(9) Å, with an average value of 2.375 Å. Both the oxalate groups, which bind the metal through 1,4 coordination, are virtually planar. The N–N distances of 1.44(2) and 1.46(2) Å in the two crystallographically independent $N_2H_5^+$ ions are comparable to those found in other complexes.

Table 5.10 Crystal structure data of hydrazinium uranyl oxalates.

Compound	Space group	Lattice parameters: a, b, and c (Å) and angle β (°)	N–N bond length(Å)
$(N_2H_5)_6[(UO_2)_2(C_2O_4)_5]\cdot 2H_2O$	Orthorhombic, Pbca	$a = 10.979(3)$, $b = 26.708(5)$, $c = 10.704(3)$	1.39(5), 1.28(6), 1.59(8)
$(N_2H_5)_2[UO_2(C_2O_4)_2(H_2O)]$	Monoclinic, $P2_1/n$	$a = 7.850(2)$, $b = 10.893(3)$, $\beta = 100.96(2)$, $c = 15.051(4)$	1.444(16), 1.461(16)

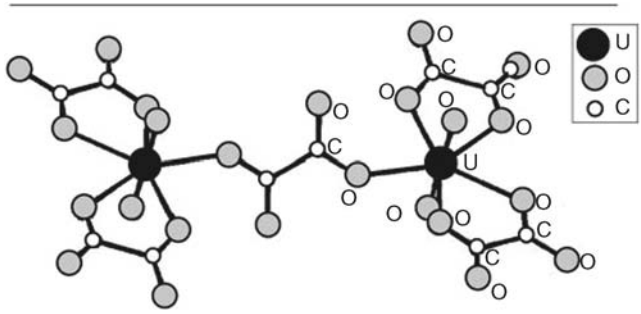

Figure 5.13 Molecular structure of $[UO_2(C_2O_4)_2(H_2O)]^{2-}$. Reproduced from Ref. [22] with permission from Elsevier © 1986.

$(N_2H_5)_2(UO_2)(C_2O_4)_2 \cdot H_2O$

The structure of the other uranyl compound, that is, $(N_2H_5)_2[UO_2(C_2O_4)_2 \cdot (H_2O)]$, consists of $N_2H_5^+$ cations and complex $[UO_2(C_2O_4)_2(H_2O)]^{2-}$ anions (Figure 5.14). In the crystal, the discrete $[UO_2(C_2O_4)_2(H_2O)]^{2-}$ ions are linked by hydrogen bonds. Both the free and coordinated oxygen atoms of $C_2O_4^{2-}$ act as acceptors. The coordinated water donates both its protons to the oxygen atoms of $C_2O_4^{2-}$ belonging to a neighboring $[UO_2(C_2O_4)_2(H_2O)]^{2-}$ moiety. The nitrogen atoms of the $N_2H_5^+$ ions are also involved in hydrogen bonds with the oxygen of oxalate groups. Two oxalate groups chelate in bidentate fashion (1,4-coordination), while the third lies on a center of symmetry, acting as bridging bidentate (1,4-coordination), thus resulting in a dimeric structure.

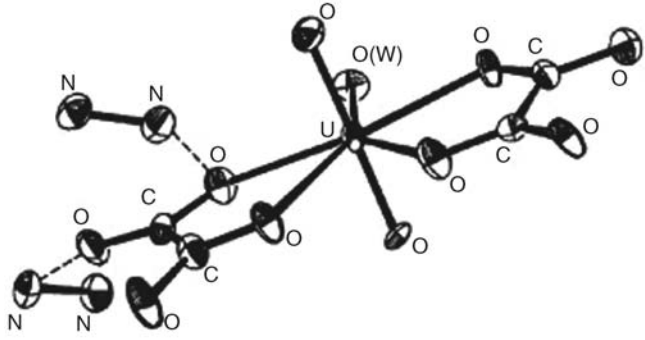

Figure 5.14 Molecular structure of $(N_2H_5)_2(UO_2)(C_2O_4)_2 \cdot H_2O$. Reproduced from Ref. [21] with permission from the Indian Academy of Sciences © 1987.

Depending upon the uranyl-oxalate ratio (1 : 1, 1 : 1.5, 1 : 2 or 1 : 3) complexes of the type $UO_2C_2O_4$, $[(UO_2)(C_2O_4)_2]^{2-}$, or $[(UO_2)(C_2O_4)_3]^{4-}$ are formed. The uranyl oxalate complexes with UO_2^{2+}:$C_2O_4^{2-}$ mol ratios of 1 : 1, 1 : 1.5, and 1 : 2 containing NH_4^+ cation have five-coordinate uranyl groups.

5.4 HYDRAZINIUM METAL HALIDES

Hydrazinium metal halide complexes are of two types: anhydrous and hydrated. The hydrazinium chloride complexes, which are the most prevalent, are discussed here.

5.4.1 Hydrazinium Metal Chloride Hydrates – $(N_2H_5)_2MCl_4 \cdot 2H_2O$, M = Transition Metal

5.4.1.1 Synthesis, Spectra, and Thermal Analysis

Hydrazinium metal chloride hydrate complexes are generally prepared by the reaction of aqueous solutions of metal chlorides with N_2H_5Cl or $N_2H_6Cl_2$ in dilute HCl. Preparative methods for individual complexes vary mainly with the mole ratios of the reagents employed [23].

The iron complex $(N_2H_5)_2FeCl_4 \cdot 2H_2O$ is synthesized by refluxing an aqueous solution of $FeCl_3 \cdot 6H_2O$ and N_2H_5Cl in water for 30 min. The resulting colorless solution is concentrated on a water bath and allowed to crystallize in a vacuum desiccator. Colorless plates appear after a week and are removed from the solution. They are then dried by pressing between filter paper and stored in an airtight bottle.

The cobalt complex $(N_2H_5)_2CoCl_4 \cdot 2H_2O$ is prepared by mixing an aqueous saturated solution of $CoCl_2 \cdot 6H_2O$ with a saturated solution of N_2H_5Cl (1 : 2 mole ratio). The precipitate that forms initially is filtered off and the solution is left exposed to air for slow evaporation. Dark pink crystals separate out from the solution. These are filtered off, washed with alcohol and diethyl ether, and stored in a desiccator. Alternatively, the complex can be prepared by decomposing solid $N_2H_5Co(N_2H_3COO)_3 \cdot H_2O$ in dilute HCl (6N) and allowing the solution to slowly evaporate.

The nickel complex $(N_2H_5)_2NiCl_4 \cdot 2H_2O$ is prepared in a similar way, either from aqueous solutions of nickel chloride and hydrogen chloride or by decomposing $N_2H_5Ni(N_2H_3COO)_3 \cdot H_2O$ in dilute HCl. A green

crystalline product is obtained, which is found to be a hydrazine adduct, $(N_2H_5)_2NiCl_4{\cdot}2H_2O{\cdot}0.5N_2H_4$. This green product is removed from the solution as and when it is formed, and, later, the hydrazinium nickel chloride complex separates out from the solution as a greenish-blue solid in small amounts.

The copper complex of formula $(N_2H_5)_2CuCl_4{\cdot}2H_2O$ is prepared by mixing a saturated solution of $CuCl_2{\cdot}4H_2O$ with a saturated solution of $N_2H_4{\cdot}2HCl$ (1 : 2 mole ratio), with vigorous stirring. The copper complex precipitates out as a blue crystalline mass in a couple of minutes. It is filtered off from the solution instantly, and then air-dried.

The platinum complex $(N_2H_5)_2PtCl_4{\cdot}2H_2O$ is obtained by adding K_2PtCl_4 (or H_2PtCl_6) solution to a saturated solution of $N_2H_6Cl_2$ or N_2H_5Cl. Golden yellow crystals of the complex are formed in a day. The crystals are filtered off from the solution and air-dried. Likewise, the Pd complex $(N_2H_5)_2PdCl_4(H_2O)_2$ is prepared by starting with either Na_2PdCl_4 or $PdCl_2$ in HCl, and then adding N_2H_5Cl or $N_2H_6Cl_2$ [24].

In the reaction between aqueous solutions of metal chlorides and $N_2H_6Cl_2$ or N_2H_5Cl to yield the complexes of $(N_2H_5)_2MCl_4{\cdot}2H_2O$, the solution needs to be heated in the case of iron for complete reduction of iron(III) to iron(II). However, for copper, platinum, and palladium reduction to metals can be prevented by employing $N_2H_6Cl_2$, which is known to dissociate into $N_2H_5^+$, H_3O^+, and Cl^- ions in water, providing the required acidic medium.

The IR spectra of all the $(N_2H_5)_2MCl_4.2H_2O$ complexes are similar, showing characteristic absorption bands at $\sim 2650\,cm^{-1}$ ($\nu_{(N-H)}$ of $-NH_3^+$) and $\sim 1100\,cm^{-1}$ ($\omega_{(N-H)}$ of NH_3^+). When $\nu_{(N-N)}$ frequencies occur in the region 990–1015 cm^{-1} it indicates the presence of coordinated $N_2H_5^+$ in these complexes.

The electronic spectral and magnetic moment values of hydrazinium metal chloride hydrates are comparable to those reported for octahedral complexes of Co(II), Ni(II), and Cu(II) and square-planar complexes of Pt(II) and Pd(II) (Table 5.11). The magnetic moment values correspond to spin-only values for cobalt(II), nickel(II), and copper(II) ions.

Table 5.12 summarizes the results of the thermal studies of the series $(N_2H_5)_2MCl_4{\cdot}2H_2O$, where M = Fe, Co, Ni, and Cu. The composition of the proposed intermediate best fit the observed weight loss data. Figure 5.15 shows a typical TG-DTA curve of $(N_2H_5)_2CuCl_4{\cdot}2H_2O$. The first step in the decomposition sequence corresponds to the loss of water molecules. The temperature range at which this decomposition occurs (60–80 °C) indicates the possibility of non-coordinated water molecules to the metal. In the second step, the anhydrous compound decomposes,

Table 5.11 Infrared absorption frequency and electronic spectra data for $(N_2H_5)_2MCl_4{\cdot}2H_2O$.

M	$\nu_{(N-N)}$ (cm^{-1})	Electronic spectra		μ_{298} (BM)
		Wavelength (nm)	Assignment	
Fe	1000	—	—	—
Co	995	495	$[^4T_{1g}(F) \rightarrow {}^4T_{1g}(P)]$	4.96
	—	532	$[^4T_{1g}(F) \rightarrow {}^4A_{2g}(F)]$	—
Ni	1000	407	$[^3A_{2g}(F) \rightarrow {}^3T_{1g}(P)]$	2.95
	—	671	$[^3A_{2g}(F) \rightarrow {}^3T_{1g}(F)]$	—
Cu	1015	758	$[^2E_g \rightarrow {}^2T_{2g}]$	1.93
Pd	1000	403	$[^1A_{1g} \rightarrow {}^1B_{1g}]$	—
Pt	1010	379	$[^1A_{1g} \rightarrow {}^1B_{1g}]$	—

Table 5.12 Thermal analysis data for $(N_2H_5)_2MCl_4{\cdot}2H_2O$.

M	Thermogravimetry			DTA peak temperature (° C)[a]	Product
	Temperature range (° C)	% Weight loss			
		Obsd.	Calcd.		
Fe	60–120	12.0	12.0	75(−)	$(N_2H_5)_2FeCl_4$
	205–240	34.0	33.6	206(−)	$FeCl_2.2N_2H_4$
	240–360	77.0	76.0	260(+), 266(−)	—
	—	—	—	350(+)	FeO
Co	90–110	12.0	11.9	95(−), 105(+)	$(N_2H_5)_2CoCl_4$
	170–270	42.0	40.9	210(−), 250(+)	$CoCl_2.1.5N_2H_4$
	270–290	51.0	51.5	280(+)	$CoCl_2.0.5N_2H_4$
	290–385	57.0	57.1	350(−)	$CoCl_2$
	390–530	73.0	73.5	Broad(−)	Co_3O_4
Ni	100–140	5.5	5.9	125(−)	$(N_2H_5)_2NiCl_4{\cdot}H_2O$
	140–175	22.0	23.9	140(−)	$N_2H_5NiCl_3{\cdot}N_2H_4$
	180–250	42.0	41.0	235(−)	$NiCl_2.1.5N_2H_4$
	275–350	58.5	57.2	325(+)	$NiCl_2$
	370–555	75.0	75.3	Broad(−)	NiO
Cu	60–85	11.0	11.7	75(−)	$(N_2H_5)CuCl_4$
	100–195	28.0	28.8	130(−) 140(−)	$N_2H_5CuCl_3.0.5N_2H_4$
	200–350	68.0	67.8	235(+) 260(−)	Cu_2Cl_2
	—	—	—	410(−)	—
	415–560	77.5	76.7	Broad(−)	Cu_2O

[a] (−) = Endotherm, (+) = exotherm.

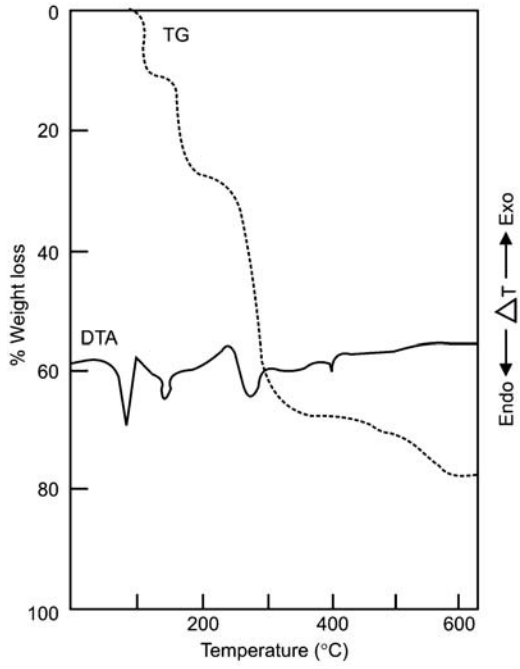

Figure 5.15 Simultaneous TG-DTA of $(N_2H_5)_2CuCl_4{\cdot}2H_2O$. Reproduced from Ref. [23] with permission from Elsevier © 1991.

losing HCl and forming a hydrazine adduct. Evolution of HCl in this step has been confirmed by testing the evolved gas qualitatively. Interestingly, this intermediate further decomposes to form cuprous chloride, as evidenced by an endothermic DTA peak at 410 °C, which corresponds to the melting of Cu_2Cl_2. The formed chloride further decomposes to cuprous oxide at higher temperatures.

The results of the other complexes show more or less, a similar trend. They lose water in the first step followed by HCl and then form N_2H_4 adducts of different compositions. The temperature range (90–130 °C) at which the loss of water occurs does not indicate conclusively whether water is bonded to the metal or not. All the complexes decompose to their respective metal oxides via the formation of metal chlorides.

5.4.1.2 Single-Crystal Structures of $(N_2H_5)_2FeCl_4{\cdot}2H_2O$ and $(N_2H_5)_2PtCl_4{\cdot}2H_2O$

The structure of $(N_2H_5)_2FeCl_4{\cdot}2H_2O$ consists of chloride ions and the aqua complex cation, $[Fe(N_2H_5)_2(H_2O)_2Cl_2]^{2+}$. Figure 5.16 presents a

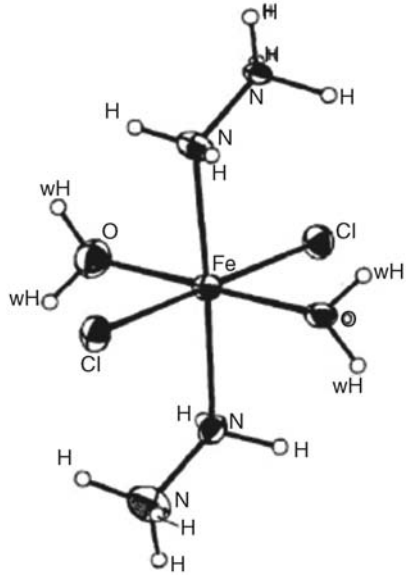

Figure 5.16 ORTEP diagram of $[Fe(N_2H_5)_2(H_2O)_2Cl_2]^{2+}$. Reproduced from Ref. [23] with permission from Elsevier © 1991.

perspective view of this complex cation. The metal coordination site in the molecule is a distorted octahedron made up of two nitrogen atoms (one from each $N_2H_5^+$ ion), two oxygen atoms from water, and two chlorine atoms (Table 5.13). The complex cation $[Fe(N_2H_5)_2(H_2O)_2Cl_2]^{2+}$ possesses a pseudo-inversion centre as the coordinated atoms are *trans* to each other.

Table 5.13 Crystallographic data of hydrazinium chlorometallates.

Compound	Space group	Lattice parameters: *a*, *b*, and *c* (Å) and angle β (°)	N–N bond length (Å)
$(N_2H_5)_2FeCl_4{\cdot}2H_2O$	Monoclinic, *P*c	$a = 8.027(1)$, $b = 5.725(2)$, $c = 11.430(2)$, $\beta = 97.08$	1.480(4), 1.424(3)
$(N_2H_5)_2PtCl_4{\cdot}(H_2O)_2$	Monoclinic, $P2_1/c$	$a = 7.427(1)$, $b = 7.717(1)$, $c = 9.629(1)$, $\beta = 101.40(1)$	1.443(7)

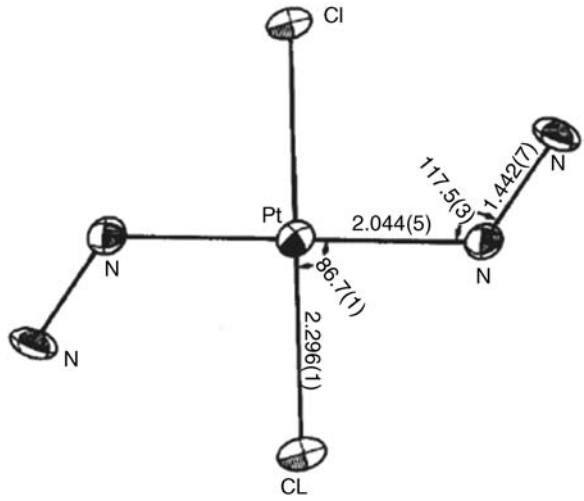

Figure 5.17 ORTEP diagram of $[Pt(N_2H_5)_2Cl_2]^{2+}$. Reproduced from Ref. [24] with permission from Elsevier © 1991.

The structure of $(N_2H_5)_2PtCl_4(H_2O)_2$ consists of $[Pt(N_2H_5)_2Cl_2]^{2+}$, Cl^- ions, and water molecules. Though the platinum compound has an identical composition to that of iron, the Pt atom has square-planar coordination, bonded by two chlorine atoms, and two nitrogen atoms from the $N_2H_5^+$ ions. Both the chlorine and nitrogen atoms are *trans* to each other, making the molecule centric.

Figure 5.17 illustrates the structure of the cation, $[Pt(N_2H_5)_2Cl_2]^{2+}$. The Pt–Cl distance [2.296(1) Å] is equivalent to the value of 2.30(2) Å found in *trans*-$[Pt(NH_3)_2Cl_2]$ and also in various other chloroplatinum (II) complexes. The Pt–N bond length [2.044(5) Å] observed in the present structure is unusually shorter than in the corresponding ammine complexes, for example, 2.17(4) Å in *trans*-$[Pt(NH_3)_2Cl_2]$.

The observed short metal–nitrogen distance in the present case is surprising, as $N_2H_5^+$ is a poorer σ-donor than NH_3 and is known to form weak metal–nitrogen bonds. The N–N bond length (1.443(7) Å) in the present structure is not significantly different from the one observed in N_2H_5Cl (1.45 Å). The Pt–N(1)–N(2) angle is 117.5(3)°, which is larger than the value of 110° observed in $(N_2H_5)_2Zn(SO_4)_2$ but is comparable to the 119.1(3)° found in $N_2H_5CuCl_3$. The N(2) atom is 0.476 Å away from the plane of Pt–N(1)–Cl(1). The water molecules are in the vicinity of $-NH_3^+$ of $N_2H_5^+$, bonded by N–H···O type hydrogen bonds. The distance of 2.755(1) Å observed for N(2)–O(w) indicates strong hydrogen bonding. The angle observed for N(1)–N(2)–O(w) is 104.5(1)°.

5.4.2 Hydrazinium Metal Bromide Hydrates – $(N_2H_5)_2MBr_4 \cdot 4H_2O$, M = Transition Metal

5.4.2.1 Synthesis, Spectra, and Thermal Analysis

The reaction of dilute hydrobromic acid with solid hydrazine carboxylate complexes, $N_2H_5M(N_2H_3COO)_3 \cdot H_2O$ (discussed in Chapter 4) where M is Co and Ni, has been investigated. These cobalt and nickel complexes are obtained by treating freshly prepared solid complexes of $N_2H_5M(N_2H_3COO)_3 \cdot H_2O$, M = Co and Ni, with dilute HBr and therein allowing them to decompose [25]. The resulting solutions are kept in a desiccator over P_2O_5 for slow concentration. The solid products obtained, dark crimson for cobalt and green for nickel, are removed from the solution. They are dried by pressing between filter paper and stored. The products are air sensitive and decompose even on slight exposure to the atmosphere and therefore have to be stored in airtight bottles. This method of preparation is simple compared to the one involving the reaction of corresponding metal bromides with the hydrazinium bromides.

Table 5.14 gives the N–N stretching frequencies for the two complexes. The values, 1000 and 995 cm^{-1} for cobalt and nickel, respectively, indicate the presence of coordinated $N_2H_5^+$ ion in the complexes.

Electronic spectral data show octahedral coordination around the metals in both the complexes, similar to that of chloride complexes.

Table 5.15 summarizes thermal data of the $(N_2H_5)_2MBr_4 \cdot 4H_2O$ complexes. The data show that both complexes lose water in the first step. In case of cobalt this step commences at the very low temperature of 40 °C. The corresponding temperature for nickel is twice that, that is, 80 °C. The cobalt complex then decomposes in a continuous step, forming a hydrazine adduct, $CoBr_2 \cdot N_2H_4$. This intermediate is stable up to 380 °C and thereafter decomposes to cobalt oxide. This second step shows a

Table 5.14 Infrared absorption frequency and electronic spectra data for $(N_2H_5)_2MBr_4 \cdot 4H_2O$.

M	$\nu_{(N-N)}$ (cm^{-1})	Electronic spectra	
		Wavelength (nm)	Assignment
Co	1000	455	$[^4T_{1g}(F) \rightarrow {}^4T_{1g}(P)]$
	—	520	$[^4T_{1g}(F) \rightarrow {}^4A_{2g}(F)]$
Ni	995	400	$[^3A_{2g}(F) \rightarrow {}^3T_{1g}(P)]$
	—	660	$[^3A_{2g}(F) \rightarrow {}^3T_{1g}(F)]$

Table 5.15 Thermal data for $(N_2H_5)_2MBr_4{\cdot}4H_2O$.

M	Thermogravimetry			DTA peak temperature (°C)[a]	Product
	Temperature range (°C)	% Weight loss			
		Obsd.	Calcd.		
Co	40–95	14.0	13.9	70(−), 80 (−)	$(N_2H_5)_2CoBr_4$
	200–345	51.5	51.5	210(+), 240(+)	$CoBr_2{\cdot}N_2H_4$
	380–465	58.0	57.7	Broad(+)	$CoBr_2$
	465–560	86.0	84.5	Broad(−)	Co_3O_4
Ni	80–120	13.9	13.9	100(−)	$(N_2H_5)_2NiBr_4$
	200–305	55.0	54.6	280(−), 290(+)	$NiBr_2{\cdot}0.5N_2H_4$
	320–360	57.0	57.7	335(+)	$NiBr_2$
	420–625	84.0	85.5	Broad(−)	NiO

[a] (−) = Endotherm, (+) = exotherm.

deflection at 465 °C and the weight loss corresponds to the formation of $CoBr_2$. The decomposition of the nickel complex shows a similar trend.

5.4.3 Anhydrous Hydrazinium Metal Chlorides – $N_2H_5CuCl_3$, $(N_2H_5)_2ZnCl_4$, $(N_2H_5)_3MnCl_5$, and $(N_2H_5)_4FeCl_6$

The reaction of copper, zinc, manganese, and iron chlorides with hydrazinium chloride ($N_2H_5^+$ or $N_2H_6^+$) yields anhydrous hydrazinium metal chlorides of different compositions [25,26]. All the complexes are hygroscopic and air sensitive. The zinc complex in particular is deliquescent in nature.

5.4.3.1 Synthesis, Spectra, and Thermal Analysis

An interesting antiferromagnetic compound that has a coordinated $N_2H_5^+$ ion is $N_2H_5CuCl_3$. This copper complex is prepared by adding solid $N_2H_6Cl_2$ to an aqueous solution of $CuCl_2{\cdot}2H_2O$ in HCl. A light green precipitate forms immediately, which is subsequently filtered off from the solution and air-dried.

The complex $(N_2H_5)_2ZnCl_4$ is prepared by mixing saturated aqueous solutions of $ZnCl_2$ and N_2H_5Cl in a 1 : 2 mole ratio. Any precipitate formed is removed from the solution by filtration and the solution is concentrated in a desiccator over P_2O_5. A white solid appears in a week,

which is removed from the solution and dried by pressing between filter papers. It is stored in an airtight bottle. Alternatively, the complex can be prepared by decomposing $Zn(N_2H_3COO)_2(N_2H_4)_2$ or $N_2H_5Zn(N_2H_3COO)_3{\cdot}H_2O$ in dilute HCl. The zinc complex in particular is deliquescent. Further isolation of the zinc complex in pure form is difficult owing to the simultaneous solidification of unreacted N_2H_5Cl.

The hydrazinium complex of manganese $(N_2H_5)_3MnCl_5$ is prepared in similar fashion. Saturated aqueous solutions of $MnCl_2{\cdot}2H_2O$ and $N_2H_4{\cdot}HCl$ are mixed in a 1 : 3 mole ratio. The resulting solution is kept in a desiccator over P_2O_5. Light pink crystals form after a week and are removed from the solution. They are dried by pressing between filter papers and stored in an airtight bottle. Alternatively, the complex can be prepared by decomposing the solid hydrazine carboxylate complex $Mn(N_2H_3COO)_2{\cdot}(H_2O)_2$ in dilute HCl. The reaction, which is exothermic, can be represented as follows:

$$Mn(N_2H_3COO)_2(H_2O)_2(s) + 4HX(aq) \rightarrow$$
$$Mn^{2+}(aq) + 2N_2H_5{}^+(aq) + 4X^-(aq) + 2CO_2(g) \qquad (5.24)$$

Irrespective of the reactants mole ratios, the product obtained is of the same composition.

The iron(II) complex $(N_2H_5)_4FeCl_6$ is prepared from $FeCl_3{\cdot}6H_2O$ and N_2H_5Cl. The reaction is achieved by taking ferric chloride in ethanol and adding solid N_2H_5Cl (1 : 6 mole ratio). The mixture is then boiled under reflux for half an hour. A white solid forms immediately and is filtered off from the solution; it is washed with hot ethanol three to four times and finally with diethyl ether. The solid product is stored in a desiccator over P_2O_5.

The IR spectra of the $(N_2H_5)_3MnCl_5$ and $(N_2H_5)_4FeCl_6$ complexes exhibit two sharp bands at 995 and 985 cm^{-1}, respectively, corresponding to $\nu_{(N-N)}$ of $N_2H_5{}^+$ ions. The values indicate the presence of both coordinated and non-coordinated $N_2H_5{}^+$ ions in these complexes. The IR spectrum of $N_2H_5CuCl_3$ shows $\nu_{(N-N)}$ at 1015 cm^{-1}, indicating the coordination of $N_2H_5{}^+$ ion to metal; this value agrees well with the literature value.

Table 5.16 gives reflectance spectral data for the $(N_2H_5)_3MnCl_5$ complex. The assignments are made on the basis of literature values that correspond to the octahedral Mn(II) ion.

Figure 5.18 shows the Mössbauer spectrum recorded for $(N_2H_5)_4FeCl_6$. The observed isomer shift and quadrupole splitting values

Table 5.16 Electronic spectral data for $[(N_2H_5)_3MnCl_5]$.

Wavelength (nm)	Assignment
529	$^6A_{1g} \rightarrow {}^4T_{1g}(G)$
442	$^6A_{1g} \rightarrow {}^4T_{2g}(G)$
419	$^6A_{1g} \rightarrow {}^4E_g(G)$
390	$^6A_{1g} \rightarrow {}^4A_{1g}(G)$
372	$^6A_{1g} \rightarrow {}^4T_{2g}(D)$
357	$^6A_{1g} \rightarrow {}^4E_g(D)$

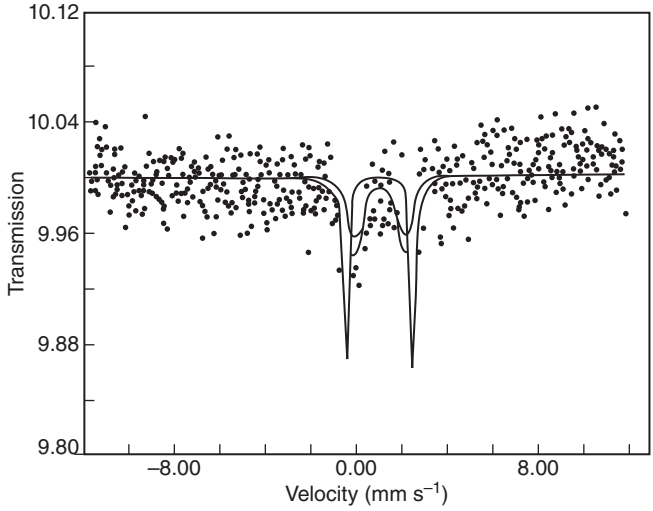

Figure 5.18 Mössbauer spectrum of $(N_2H_5)_4FeCl_6$. Ph.D Thesis of Kumar, N.R.S. under Prof. K. C. Patil at Indian Institute of Science.

are given in Table 5.17. The Mössbauer spectrum of $(N_2H_5)_4FeCl_6$ can be resolved into two quadrupole doublets of different line widths. This indicates that there are two types of iron sites in this complex, suggesting the structure is complicated.

Table 5.17 Mössbauer data[a] for $(N_2H_5)_4FeCl_6$.

Site	Isomer shift (mm s^{-1})	Quadrupole splitting (mm s^{-1})
1	1.0453	2.888
2	1.1081	2.128

[a] Values are with respect to Fe metal.

The isomer shift values of both components are indicative of iron in the high-spin ferrous state (the ferric state has values between 0.3 and 0.6 mm s^{-1}). Typical values of 1.0–1.4 mm s^{-1} have been observed for similar halide complexes. The tetrahedral iron(II) halide complexes generally have lower isomer shift values of around 1.01 mm s^{-1}, when compared to octahedrally coordinated complexes where the isomer shift is about 1.35 mm s^{-1}. One can therefore tentatively conclude that the Fe(II) ions at both sites are in tetrahedral coordination. The large quadrupole splitting observed indicate a very low symmetry of the environments, but offers no further proof regarding the coordination.

The complex $(N_2H_5)_4FeCl_6$ and anhydrous intermediate $(N_2H_5)_2FeCl_4$ formed from $(N_2H_5)_2FeCl_4{\cdot}2H_2O$ are structurally related, as indicated by thermal analysis. The structure of $(N_2H_5)_2FeCl_4{\cdot}2H_2O$ is octahedral and the metal is bonded by two hydrazinium cations, two chlorides, and two water molecules; the pairs of coordinated groups are *trans* to each other. After losing two *trans* water molecules, it is probable that the $(N_2H_5)_4FeCl_6$ molecule rearranges itself from O_h symmetry to lower symmetry, or might have rearranged to a polymeric structure involving chloride bridges in which the iron atoms are in two different environments. Thus, the structure of $(N_2H_5)_4FeCl_6$, the composition of which can be written as $[Fe(N_2H_5)_2Cl_4] \cdot 2N_2H_5Cl$, can be thought of as consisting of a polymeric structure where the iron(II) ions are in two different environments. In such a case, the symmetry around the metals is very much distorted from O_h symmetry. Single crystals of iron complex are not obtainable but spectral, thermal, and Mössbauer studies on the complex indicate that its structure is not simple.

All these complexes have been characterized by thermal analysis, the data of which is summarized in Table 5.18.

Simultaneous TG-DTA curves for the $N_2H_5CuCl_3$ complex show a three-step decomposition. The compound starts to decompose at 95 °C endothermically, forming the hydrazine intermediate $CuCl_2{\cdot}0.5N_2H_4$. Evolution of HCl gas and the formation of hydrazine adduct is confirmed by qualitative tests. This hydrazine adduct decomposes exothermically to cuprous chloride. The formation of cuprous chloride at 410 °C is evident from DTA, which shows an endothermic peak due to its melting. Cuprous chloride, at higher temperatures, decomposes to metallic copper.

Interestingly, thermal decomposition of $N_2H_5CuCl_3$ gives metallic copper as the end product, unlike $(N_2H_5)_2CuCl_4{\cdot}2H_2O$, which gives copper oxide, even though both complexes decompose through cuprous chloride. This difference in decomposition mode can be attributed to the static conditions employed in the thermal analysis experiments, which

Table 5.18 Thermal data of $N_2H_5CuCl_3$, $(N_2H_5)_2ZnCl_4$, $(N_2H_5)_3MnCl_5$, and $(N_2H_5)_4FeCl_6$.

Compound	Thermogravimetry			DTA peak temperature (°C)[a]	Product
	Temperature range (°C)	% Weight loss			
		Obsd.	Calcd.		
$N_2H_5CuCl_3$	95–140	25.0	25.8	130(−), 135(−)	$CuCl_2{\cdot}0.5N_2H_4$
	170–350	51.0	51.2	230(+), 275(−)	Cu_2Cl_2
	—	—	—	410(−)	—
	420–535	68.0	68.7	Broad(−)	Cu
$(N_2H_5)_2ZnCl_4$	—	—	—	140(−)	—
	210–365	51.0	50.1	215(+), 315(−)	$ZnCl_2$
	410–555	72.0	70.2	Broad(−)	ZnO
$(N_2H_5)_3MnCl_5$	—	—		165(−)	—
	175–330	62.5	62.0	225(+), 260(−), 320(−)	$MnCl_2$
	410–555	72.0	70.2	Broad(−)	MnO
$(N_2H_5)_4FeCl_6$	—	—	—	88(−)	—
	205–250	62.5	62.0	206(−)	$FeCl_2(N_2H_4)_2{\cdot}N_2H_5Cl$
	250–310	68.0	68.0	258(+)	$FeCl_2$
	315–360	82.0	82.1	Broad(−)	FeO

[a] (−) = Endotherm, (+) = exotherm.

force the evolving gases to remain in the vicinity of the decomposing solid. Thus, formation of Cu_2O from $(N_2H_5)_2CuCl_4{\cdot}2H_2O$ can be attributed to the presence of water molecules in the complex; accordingly, Cu_2Cl_2 oxidizes to Cu_2O, whereas the absence of water molecules causes $N_2H_5CuCl_3$ to decompose to metallic copper.

The thermal data for the zinc complex $(N_2H_5)_2ZnCl_4$ show that it melts at 140 °C. This value indicates that the zinc complex is not a simple adduct of $ZnCl_2$ and N_2H_5Cl, as the latter melts at 89 °C. The compound begins to decompose at 210 °C exothermically, followed by an endotherm in a single continuous step, to $ZnCl_2$. At higher temperatures $ZnCl_2$ forms ZnO.

Thermal data for the $(N_2H_5)_3MnCl_5$ reveals that the complex melts at 165 °C. This temperature is much higher than the melting point of N_2H_5Cl (89 °C), indicating the absence of any free N_2H_5Cl in the complex. The melting of the manganese complex is immediately followed by its decomposition, and TG shows a single, continuous step corresponding to the formation of $MnCl_2$. At higher temperatures, $MnCl_2$ decomposes to MnO.

Thermal data for the $(N_2H_5)_4FeCl_6$ complex shows an endotherm at 88 °C due to the melting of N_2H_5Cl. This suggests that there is free N_2H_5Cl present in the complex. DTA shows another endotherm at 206 °C, which corresponds to the melting of the iron complex. The compound simultaneously starts decomposing and TG shows a deflection leading to the formation of $FeCl_2$, which at higher temperatures forms iron oxide. There is remarkable coincidence in the first step observed for $(N_2H_5)_4FeCl_6$ with the second step observed for $(N_2H_5)_2FeCl_4{\cdot}2H_2O$. In both cases the DTA peaks are exactly at 206 °C with the endotherms starting at 195 °C. This is immediately followed by exotherms as the compounds begin to decompose. These observations indicate that the intermediate formed in the first step for $(N_2H_5)_2FeCl_4{\cdot}2H_2O$, namely, the anhydrous $(N_2H_5)_2FeCl_4$, truly matches the complex formulated as $(N_2H_5)_2FeCl_4{\cdot}2N_2H_5Cl$. This is also consistent with the IR data, which indicates the presence of free N_2H_5Cl in the compound.

5.4.3.2 *Single-Crystal Structure of $(N_2H_5)_3MnCl_5$*

Details of the X-ray analysis for $(N_2H_5)_3MnCl_5$ indicates a monoclinic system with a space group of $P2_1/n$ with $a = 8.988(3)$ Å, $b = 10.974(2)$ Å, $c = 11.788(4)$ Å, $\beta = 94.33(3)$, $V = 1159.3$ Å^3, and $Z = 4$. In contrast to other chloride complexes, $(N_2H_5)_3MnCl_5$ is a rare example of having both coordinated and uncoordinated $N_2H_5^+$ ions. The structure of $(N_2H_5)_3MnCl_5$ consists of complex anions $[Mn(N_2H_5)Cl_5]^{2-}$ and $N_2H_5^+$ ions. The manganese atom is surrounded by five chlorine atoms and one nitrogen atom of $N_2H_5^+$ ion. The coordinated atoms are arranged at the corners of a slightly distorted octahedron. Figure 5.19 illustrates the structure of $[Mn(N_2H_5)Cl_5]^{2-}$.

The metal–chlorine distances in the complex anion vary from 2.491(2) to 2.579(1) Å, with an average of 2.537 Å. These distances are comparable to the values found in the anion $[MnCl_5(H_2O)]^{3-}$, in which the average Mn−Cl distance is 2.545 Å. The anion $[MnCl_5(N_2H_5)]^{2-}$ has an essentially octahedral geometry, the cis angles differing from 90° by only 3°. The Mn−N bond length of 2.369(3) Å is longer than the usual Mn−N distances found in $Mn(N_2H_3COO)_2(H_2O)$, which are 2.19(2) and 2.21(2) Å; this indicates a weak Mn−N interaction.

The N−N bond length in the coordinated $N_2H_5^+$ cation is 1.441(4) Å, similar to those found in iron and platinum complexes. The N−N bond lengths in non-coordinated $N_2H_5^+$ ions are 1.419(5) and 1.424(6) Å and these bonds are slightly shorter than the coordinated one. The Mn−N(1)−N(2) angle in the complex is 122.7(4)°, which is comparable to those

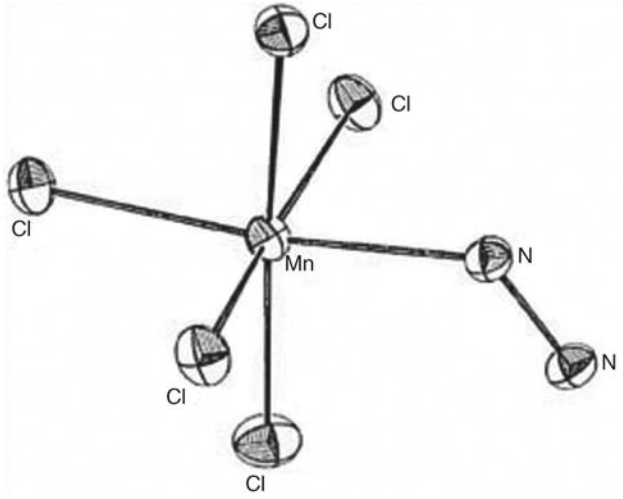

Figure 5.19 Molecular structure of anion $[Mn(N_2H_5)Cl_5]^{2-}$. Reprinted from [25] by permission of the publisher Taylor & Francis Ltd, © 1991 http://www.tandf.co.uk/journals.

found in the iron and platinum complexes. The manganese atom more or less lies in the planes formed by the coordinated atoms. The maximum deviation of 0.12 Å is found in the plane formed by Cl(1), Cl(3), Cl(4), and N(1). The atom N(2), that is, the non-bonded nitrogen of the coordinated $N_2H_5^+$, lies exactly in the plane formed by the atoms N(1), Cl(2), Cl(3), Cl (5), and Mn (plane IV), and the deviation is only 0.04 Å. In the crystal, the free hydrazinium cations and the complex anions are held together by a network of N–H···Cl hydrogen bonds.

5.5 HYDRAZINIUM METAL THIOCYANATES – $(N_2H_5)_2M(NCS)_4{\cdot}2H_2O$, M = Co AND Ni

Although thiocyanate with neutral amines (bases) has been investigated intensively with transition metals, knowledge of the respective thiocyanates with cationic amines is very limited and, in particular, with the hydrazinium cation is almost unknown. The absence of reports on the hydrazinium metal complexes of thiocyanates is not surprising as the usual method of preparation from aqueous solutions of the metal thiocyanates and hydrazinium thiocyanate always yields metal thiocyanate hydrazines. The first examples in which the hydrazinium cations are coordinated to the metal in the *cis*

positions are in the hydrazinium metal thiocyanate complexes of cobalt(II) and nickel(II). These are prepared from the respective hydrazine carboxylates and thiocyanic acid. Another unique feature of these complexes is that the two canonical forms of metal−NCS linkage, that is, the angular and linear ones, are present in the same molecule.

5.5.1 Synthesis, Spectra, and Thermal Analysis

The reaction between metal thiocyanates and hydrazinium thiocyanates cannot be used to prepare hydrazinium metal thiocyanate complexes. Consequently, an alternate method is employed, namely, the decomposition of hydrazinium metal hydrazine carboxylates with dilute thiocyanic acid (<5%) [27,28]. Hydrazinium metal hydrazine carboxylates complexes $N_2H_5M(N_2H_3COO)_3{\cdot}H_2O$, where M = Co and Ni, are prepared from metal nitrates, sulfates, or chlorides and hydrazine hydrate saturated with carbon dioxide. The dilute thiocyanic acid is prepared by adding barium thiocyanate trihydrate to dilute sulfuric acid.

The complex $(N_2H_5)_2Co(NCS)_4{\cdot}2H_2O$ is prepared by adding freshly prepared solid hydrazinium cobalt hydrazine carboxylate complex to dilute thiocyanic acid in small portions, while maintaining the reaction temperature at around 0 °C. The solid decomposes with the evolution of carbon dioxide to give a purple solution. The addition of solid is continued till the solution becomes neutral. The resulting solution is allowed to stand open to atmosphere at room temperature. Dark purple crystals separate from the solution in 6–8 weeks. The crystals are removed from the solution and dried by pressing between filter papers and stored in an airtight bottle. The reaction is exothermic and is accompanied by the decomposition of carboxylate and the evolution of carbon dioxide.

$$N_2H_5M(N_2H_3COO)_3{\cdot}H_2O + 6HSCN \rightarrow (N_2H_5)_2M(SCN)_4{\cdot}2H_2O + M(SCN)_2 + 6CO_2 + 6NH_3 + 3N_2 \quad (5.25)$$

To prepare $(N_2H_5)_2Ni(NCS)_4{\cdot}2H_2O$, the reaction between solid $N_2H_5Ni(N_2H_3COO)_3{\cdot}H_2O$ and dilute thiocyanic acid is carried out under similar conditions as those for the cobalt complex. When the resulting green solution is kept for slow evaporation, a dark blue crystalline solid appears in a few days. This product is found to be the thiosemicarbazide complex $Ni(NCS)_2(N_2H_3{\cdot}CS.NH_2)_2$, the single-crystal structure of which has been accurately determined. The solution later gives a light blue crystalline solid, $(N_2H_5)_2Ni(NCS)_4{\cdot}2H_2O$, in small

quantities. This solid is dried with filter paper and stored in an airtight bottle. The anomaly in this reaction can be attributed to the rearrangement of hydrazinium thiocyanate to thiosemicarbazide both in solid state and in aqueous solutions:

$$N_2H_5SCN \rightarrow N_2H_3{-}CS{-}NH_2 \tag{5.26}$$

While carrying out the reaction at room temperature, the formation of thiosemicarbazide takes place during the addition of $N_2H_5M(N_2H_3COO)_3 \cdot H_2O$ to thiocyanic acid. This occurs due to the exothermic nature of the reaction. Carrying out the reaction at low temperatures prevents the formation of thiosemicarbazide at the stage of addition. However, when the solution is left open to air at room temperature for slow evaporation, conversion of hydrazinium thiocyanate into thiosemicarbazide takes place. In the case of cobalt, a cobalt thiosemicarbazide complex is not isolated, which may be ascribed to the low stability of Co(II) thiosemicarbazide complexes. With nickel, the reaction gives $Ni(NCS)_2(N_2H_3 \cdot CS \cdot NH_2)_2$ as a major product, since nickel(II) is known to form very stable complexes with thiosemicarbazide. Although the conversion of hydrazinium thiocyanate into thiosemicarbazide at room temperature is known to take place very slowly, the role of metal ion in this conversion cannot be ruled out. This is because the reaction in case of nickel gives the thiosemicarbazide complex in a few days.

Hydrazinium and thiosemicarbazide complexes of nickel can be distinguished very easily by their color, solubility, and stability. The thiosemicarbazide complex is a dark blue crystalline compound, which is not readily soluble in water and is stable indefinitely even when exposed to air. The hydrazinium complex, on the other hand, is a light blue compound, which is readily soluble in water, is hygroscopic, and decomposes when exposed to air.

The complexes $(N_2H_5)_2M(NCS)_4 \cdot 2H_2O$ (M = Co or Ni) are very hygroscopic, readily soluble in water, and decompose when exposed to air. Infrared spectra of both complexes show absorption bands in the region 990–1010 cm^{-1} (995 cm^{-1} for cobalt and 1000 cm^{-1} for nickel). These bands clearly indicate the presence of coordinated $N_2H_5^+$ ions. The spectra also show strong bands (doublet) near 2100 cm^{-1} (2100 and 2130 cm^{-1} for cobalt; 2105 and 2135 cm^{-1} for nickel) assigned to N–C stretching of the NCS group. The N–C stretching frequency of thiocyanate, when it is terminal N-bonded, is known to occur in the region 2050–2100 cm^{-1} and there is some overlap with the corresponding region for the terminal S-bonded form

[$\nu_{(C-N)}$ 2083–2130 cm^{-1}]. Thiocyanate complexes of nickel(II) and cobalt(II) are found to contain the NCS ligand either terminal N- or N,S-bridge bonded. Interestingly, the IR spectra of both complexes exhibit two sharp peaks (a doublet) indicating the presence of two non-equivalent NCS groups. For the cobalt complex, these peaks are seen at 2130 and 2100 cm^{-1}, and for nickel, at 2135 and 2105 cm^{-1}.

The solid-state electronic spectral data for the complexes along with their assignments are as follows: cobalt, 513 nm [$^4T_{1g}(F) \rightarrow {}^4A_{2g}(F)$] and 490 nm [$^4T_{1g}(F) \rightarrow {}^4T_{1g}(P)$]; nickel, 578 nm [$^3A_{2g}(F) \rightarrow {}^3T_{1g}(F)$] and 435 nm [$^3A_{2g}(F) \rightarrow {}^3T_{1g}(P)$]. These data indicate octahedral coordination around the metal ions as the above bands are characteristic of octahedral cobalt(II) and nickel(II) complexes.

Figure 5.20 shows simultaneous TG-DTA curves for nickel complex. The first step in the TG corresponds to the loss of water. The temperature at which this occurs is below 100 °C, indicating the possibility of non-coordination of water molecules to the metal. At higher temperatures,

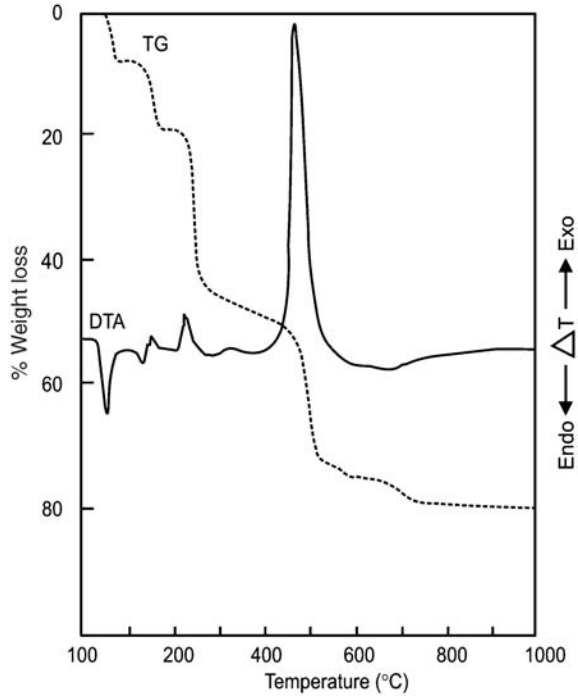

Figure 5.20 Simultaneous TG-DTA of $(N_2H_5)_2Ni(NCS)_4 \cdot 2H_2O$. Ph.D Thesis of Kumar, N.R.S. under Prof. K. C. Patil at Indian Institute of Science.

both complexes decompose to metal oxide through metal sulfides via several steps. As the decomposition pattern is found to be very complex, the composition of the intermediates is difficult to ascertain. The cobalt complex shows more or less similar characteristics of decomposition.

While it is possible to suggest that the metal ions are surrounded by two hydrazinium cations and four terminal N-bonded NCS ion from these data, it is difficult to perceive the presence of two different kinds of thiocyanate groups. Further, it is not possible to predict from these results alone the relative positions of the $N_2H_5^+$ and NCS ligands. To resolve these issues, single-crystal X-ray structural analysis of $(N_2H_5)_2Co(NCS)_4{\cdot}2H_2O$ has been carried out.

5.5.2 Single-Crystal Structure of $(N_2H_5)_2Co(NCS)_4{\cdot}2H_2O$

The crystal structure of $(N_2H_5)_2Co(NCS)_4{\cdot}2H_2O$ contains discrete $(N_2H_5)_2Co(NCS)_4$ and H_2O molecules. The coordination around the cobalt atom is essentially octahedral with the cobalt atoms lying on the twofold axes. The structure with the atom numbering scheme is shown in Figure 5.21, with the symmetry-related atoms indicated by primes.

The cobalt atom is hexacoordinated by two hydrazinium ions and four thiocyanate ions. All four thiocyanate groups are terminal N-bonded. The most interesting feature of the structure is the presence of two kinds of NCS groups: two of the four have angular Co–NCS linkages and the other two have linear linkages (Figure 5.22). The linear Co–NCS groups are cis to each other, and the angular ones are *trans*. The presence of two kinds of Co–NCS groups can be understood as the M–NCS linkage is known to occur in both linear and bent forms.

From the above structure it is obvious that the N–C bond distance in linear form should be smaller than in the bent form, whereas the C–S bond distance in linear form should be larger than in the angular form. The Co–N bond distances of 2.091(6) Å in the linear and 2.098(7) Å in the angular Co–NCS linkages are equal; these are comparable to the similar bond lengths observed in many cobalt thiocyanate complexes. The N–C–S angles in both cases are very close to 180° (178.4(8)° for the linear and 177.2(7)° for the angular). The presence of two kinds of NCS groups with different C–N bond lengths explains the observed doublet for $\nu_{(C-N)}$ in the infrared spectra of these complexes. Prior to this crystal, structures of six-coordinate cobalt(II) complexes containing terminal NCS ligands were not known. However, in other cobalt complexes

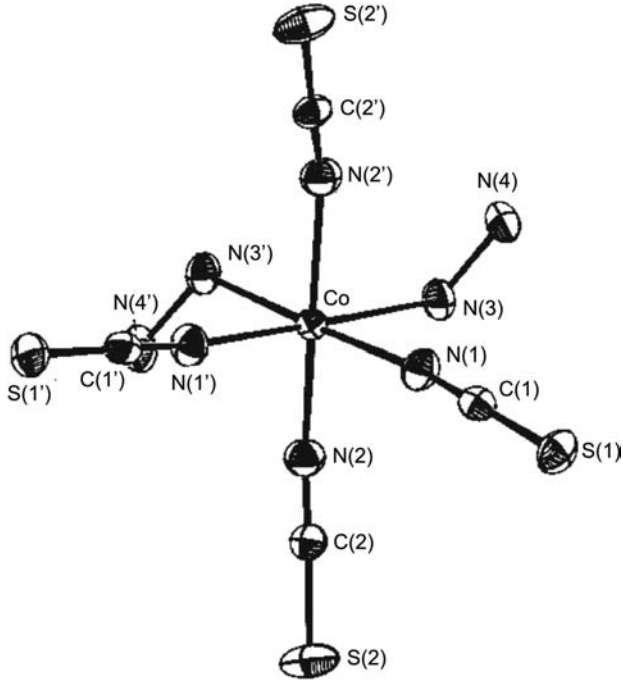

Figure 5.21 ORTEP diagram of $(N_2H_5)_2Co(NCS)_4{\cdot}2H_2O$. Reproduced from Ref. [27] with permission of The Royal Society of Chemistry © 1991.

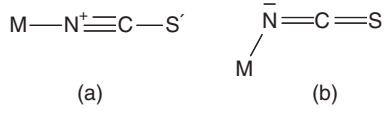

Figure 5.22 Metal thiocyanate (M–NCS) linkages: (a) linear and (b) angular. Reproduced from Ref. [27] with permission of The Royal Society of Chemistry © 1991.

containing terminal NCS ligands the Co–N–C angle ranges from 155° to 175°. The unique feature of the present structure is the existence of both bent and linear Co–NCS forms in the same molecule. Another significant aspect is that the two hydrazinium cations are in cis positions, unlike the *trans* coordination observed in chloride and sulfate complexes.

This structure is an example in which the hydrazinium cations are in cis positions. The longer bond distance of 2.243(6) Å observed for Co–N(3) compared to the value of 2.114(9) Å in $[Co(NH_3)_6]Cl_2$ indicates a weaker metal–nitrogen interaction. The N–N bond length of 1.445(8) Å observed in the present structure is comparable to the values in other hydrazinium complexes.

Table 5.19 Hydrogen bonding in $(N_2H_5)_2Co(NCS)_4{\cdot}2H_2O$.

D–H···A[a]	D–A (Å)	D–H (Å)	A···H (Å)	D–H–A (°)
N(4)–H(41)···O(1)	2.703	0.985	1.724	172.5
N(4)–H(43)···S(1^{I})	3.538	1.042	3.039	110.2
N(4)–H(32)···O(2^{II})	3.764	1.056	2.821	148.8
O(1)–H(w2)···S(2^{III})	3.517	0.895	3.063	113.5
N(3)–H(32)···S(2^{IV})	3.447	1.056	2.881	113.8
N(4)–H(43)···S(1^{V})	3.292	1.042	2.408	142.0
O(1)–H(w1)···S(1^{V})	3.437	0.821	2.869	128.1
N(3)–H(31)···S(1^{V})	3.593	0.967	2.635	171.1
N(4)–H(43)···S(1^{VI})	3.663	1.042	3.151	111.4

[a] Symmetry codes: I, x, $1+y$, z; II, x, $1-y$, $-\frac{1}{2}+z$; III, $\frac{1}{2}+x$, $\frac{1}{2}+y$, z; IV, $1-x$, $1-y$, $2-z$; V, $3/2-x$, $\frac{1}{2}+y$, $3/2-z$; VI, $=3/2-x$, $\frac{1}{2}-y$, $2-z$.

The two water molecules in the structure are located in the vicinity of NH_3 of the $N_2H_5^+$ ions, held together by N–H···O type hydrogen bonds. The sulfur atoms are also involved in N–H···S and O–H···S hydrogen bonding (Table 5.19)

Preliminary studies on single crystals of the $(N_2H_5)_2Ni(NCS)_4{\cdot}2H_2O$ complex indicate that it crystallizes in the same space group as that of cobalt complex. The unit-cell parameters obtained from these studies are $a=16.4$ Å, $b=7.7$ Å, $c=13.1$ Å, $\beta=112.0°$, $U=1534$ Å^3, $Z=4$, $D_m=1.67$ g·cm^{-3}, and $D_c=1.70$ g cm^{-3}. These data, coupled with spectral data, confirm that the nickel complex is isostructural with the cobalt complex.

5.6 RECENT STUDIES ON HYDRAZINIUM METAL COMPLEXES

In the last decade, several new hydrazinium metal complexes have been prepared and their spectra, thermal properties, and crystal structures reported [3–12]. Some of them are briefly reviewed here.

Similar to hydrazinium metal sulfates, hydrazinium metal sulfite complexes can be synthesized; the procedure is, though, slightly different. Hydrazinium transition metal sulfite dihydrate complexes of the formula $(N_2H_5)_2M(SO_3)_2(H_2O)_2$ where M = Fe, Co, Ni, Cu, and Zn are prepared from metal hydrazine carboxylates (described in Chapter 4) as the starting material. In this method, the anhydrous metal hydrazine carboxylate, $M(N_2H_3COO)_2$, is added to distilled water previously saturated with sulfur dioxide gas. The complex decomposes with the liberation of carbon

dioxide. The resulting clear solution is kept at room temperature for about 3–4 days under a sulfur dioxide atmosphere. The crystalline complex deposited is filtered off, washed several times with cold water, and dried in air [29].

The magnetic data coupled with electronic spectra of iron, cobalt, nickel, and copper complexes indicate a high-spin octahedral nature. The zinc complex is diamagnetic and shows only charge-transfer transition. Infrared studies show that both hydrazinium ions are coordinated to the metal ions and that the sulfite ions are present as bidentate ligand. When these complexes are investigated in air, their simultaneous TG-DTAs show that cobalt, nickel, and zinc complexes give the respective metal sulfate as the final residue. Iron and copper complexes, however, give a mixture of the respective metal oxide and sulfate as the decomposition product. In a nitrogen atmosphere, the respective metal sulfites are formed as the end residue.

Analogous to the synthesis method adopted for the preparation of hydrazinium metal sulfite hydrates, hydrazinium lanthanide sulfite hydrates, $N_2H_5Ln(SO_3)_2(H_2O)_2$, can be synthesized by the addition of hydrazine sulfite monohydrate to the respective anhydrous lanthanide hydrazine carboxylates $M(N_2H_3COO)_2$ [10].

As mentioned in Chapter 1, the development of inorganic derivatives by complex formation with organic anions is of interest from the viewpoint of generating new precursors [7–12]. Several hydrazinium fluorometallates have been investigated as their decomposition offers a convenient route for the synthesis of binary fluorides [6].

Nine-coordinate hydrazinium lanthanide ethylenediaminetetraacetate (EDTA) hydrates of the formula $(N_2H_5)[Ln(EDTA)(H_2O)_3](H_2O)_5$, where M = Eu, Gd, Tb and Dy, are prepared by adding an aqueous mixture of H_4EDTA and hydrazine hydrate to their respective Ln nitrate hydrate aqueous solution [10]. Crystalline solids separate after a few weeks from the clear filtered solution of the mixture. X-Ray powder diffraction patterns of each complex reveal isomorphism among them. X-Ray crystallography of single crystals of Dy shows it to be nine-coordinate with hexadentate $EDTA^{4-}$ and three more coordination sites occupied by water molecules. These EDTA complexes form the respective nano-metal oxide as end products observed in their multi-step degradation by thermal analysis.

Hydrazinium metal pyruvates $[N_2H_5]_2M[CH_3COCOO]_4$, where M = Co or Ni, are prepared from aqueous solution containing a mixture of the respective salts, pyruvic acid, and hydrazine hydrate [11]. The magnetic moments and electronic spectra of the complexes suggest a high-spin

octahedral geometry with two hydrazinium ions and four pyruvate ions showing a unidentate coordination mode, resulting in six-coordination around the metal ions. Thermal analysis in air reveals that these complexes yield Co_2O_3 and NiO as the residual product.

Dihydrazinium complexes of the type $(N_2H_5)_2M(Html)_2{\cdot}nH_2O$ with divalent transition metal trimellitate (H_3tml = trimellitic acid) hydrates of empirical formula (where $n = 1$ for M = Co or Ni, and $n = 2$ for M = Mn, Zn, or Cd) are prepared from an aqueous solution of trimellitic acid, hydrazine hydrate, and the respective metal nitrate hydrate [12]. Flake-like crystals of the complex appear after a couple of days. These are filtered off, washed with alcohol and with diethyl ether, and air-dried. While cadmium forms the mono-hydrazinium complex $[(N_2H_5)Cd(Html)_{1.5}{\cdot}2H_2O]$ with tetrahedral geometry, the rest of the dihydrazinium metal trimellitate complexes have octahedral geometry.

5.7 SUMMARY

Several hydrazinium metal sulfate, oxalate, halide (Cl^- and Br^-), and thiocyanate complexes have been synthesized and characterized by spectral, thermal, and single-crystal studies. Some of the complexes discussed are $(N_2H_5)_2M(SO_4)_2$, $N_2H_5Ln(SO_4)_2{\cdot}H_2O$ (where Ln = La, Ce, Pr, Nd, and Sm), $(N_2H_5)_2M(C_2O_4)_2{\cdot}nH_2O$, $(N_2H_5)_2(UO_2)(C_2O_4)_2{\cdot}H_2O$, $(N_2H_5)_6[UO_2(C_2O_4)_5]{\cdot}2H_2O$, $(N_2H_5)_2MCl_4{\cdot}2H_2O$, $(N_2H_5)_2MBr_4{\cdot}4H_2O$, $N_2H_5CuCl_3$, $(N_2H_5)_2ZnCl_4$, $(N_2H_5)_3MnCl_5$, $(N_2H_5)_4FeCl_6$, and $(N_2H_5)_2M(NCS)_4{\cdot}2H_2O$ (where M = Co and Ni). Single-crystal studies of the following representative compounds have also been presented: $(N_2H_5)_2M(SO_4)_2$ (M = Mn, Zn, and Cd), $N_2H_5Nd(SO_4)_2{\cdot}H_2O$, $(N_2H_5)_2Cu(C_2O_4)_2{\cdot}nH_2O$, $(N_2H_5)_2(UO_2)(C_2O_4)_2{\cdot}H_2O$, $(N_2H_5)_6[UO_2(C_2O_4)_5]{\cdot}2H_2O$, $(N_2H_5)_2FeCl_4{\cdot}2H_2O$, $(N_2H_5)_2PtCl_4{\cdot}2H_2O$, $(N_2H_5)_3MnCl_5$, and $(N_2H_5)_2Co(NCS)_4{\cdot}2H_2O$.

These studies have clearly shown the presence of a hydrazinium cation coordinated to the metal ion. Interestingly, the hydrazinium cation is both coordinated and non-coordinated to metal ions in some oxalate and chloride complexes. The valence or oxidation number of metal ion appears to dictate the bonding.

REFERENCES

1. Bottomley, F. (1970) Reactions of hydrazine with transition-metal complexes. *Quarterly Reviews, Chemical Society*, **24**, 617–638.

2. Schmidt, E.W. (2001) *Hydrazine and its Derivatives: Preparation, Properties, Applications*, 2nd edn, John Wiley & Sons, Inc.
3. David, B.M. (2005) Synthesis, structure, and thermal properties of soluble hydrazinium germanium(IV) and tin(IV)selenide salts. *Inorganic Chemistry*, **44**, 3755–3761.
4. Sonia, C., Ragul, R., and Sivasankar, B.N. (2013) Synthesis and characterization of pure nickel, copper and magnesium cobaltite using hydrazinium compounds as precursors. *Journal of Chemical and Pharmaceutical Research*, **5**, 66–72.
5. Premkumar, T. and Govindarajan, S. (2010) Thermoanalytical and spectroscopic studies on hydrazinium lighter lanthanide complexes of 2-pyrazinecarboxylic acid. *Journal of Thermal Analysis and Calorimetry*, **100**, 725–732.
6. Skapin, T., Mazej, Z., Makarowicz, A. *et al.* (2011) Aluminium(III) fluoride originating from decomposition of hydrazinium fluoroaluminate (III) under oxidative conditions: Syntheses, X-ray photoelectron spectroscopy and some catalytic reactions. *Journal of Fluorine Chemistry*, **132**, 703–712.
7. Saravanan, K. and Govindarajan, S. (2002) Dipicolinate complexes of main group metals with hydrazinium cation. *Proceedings of the Indian Academy of Sciences – Chemical Sciences*, **112**, 25–36.
8. Premkumar, T. and Govindarajan, S. (2003) Synthesis and spectroscopic, thermal, and XRD studies on trivalent lighter rare-earth complexes of 2,3-pyrazinedicorboxylate with hydrazinium cation. *Inorganic Chemistry Communications*, **6**, 1385–1389.
9. Premkumar, T., Govindarajan, S., Nigam, P., and Manivannam, V. (2009) New nine coordinated complexes of lanthanides with bidentate 2-pyrazinecarboxylate containing hydrazinium cation. *Inorganica Chimica Acta*, **326**, 619.
10. Vikram, L. and Sivasankar, B.N. (2008) New nine co-ordinated hydrated heavier lanthanide ethylenediaminetetraacetates containing hydrazinium cation: Crystal structure of $(N_2H_5)[Dy(EDTA)(H_2O)_3](H_2O)_5$. *Indian Journal of Chemistry*, **47A**, 25–31.
11. Raju, B. and Sivasankar, B.N. (2009) Spectral, thermal, and X-ray studies on some new bis and tris-hydrazine and hydrazinium metal pyruvates. *Journal of Thermal Analysis and Calorimetry*, **98**, 371–376.
12. Vairam, S., Premkumar, T., and Govindarajan, S. (2010) Trimellitate complexes of divalent transition metals with hydrazinium cation: thermal and spectroscopic studies. *Journal of Thermal Analysis and Calorimetry*, **100**, 955–960.
13. Patil, K.C., Govindarajan, S., Soundararajan, R., and Pai Verneker, V.R. (1981) Thermal analysis of hydrazinium metal sulfates and their hydrazinates. *Proceedings of the Indian Academy of Sciences – Chemical Sciences*, **90**, 421–426.
14. Govindarajan, S. and Patil, K.C. (1982) Thermal decomposition of hydrazinium aluminium sulfate hydrate and hydrazinate. *Thermochimica Acta*, **55**, 373–376.
15. Govindarajan, S., Babu, P.J., and Patil, K.C. (1986) Thermal analysis of metal sulfate hydrazinates and hydrazinium metal sulfates. *Thermochimica Acta*, **97**, 287–293.
16. Srinivasan, K., Govindarajan, S., and Harrison, W.T.A. (2007) Iron(II) hydrazinium sulfate. *Acta Crystallographica, Section E*, **63**, i41–i42.
17. Srinivasan, K., Govindarajan, S., and Harrison, W.T.A. (2006) catena-Poly[[dihydrazinecadmium(II)]-di-μ-sulfato-κ^4O:O′]. *Acta Crystallographica, Section E*, **62**, i219–i221.
18. Srinivasan, K., Govindarajan, S., and Harrison, W.T.A. (2007) *catena*-Poly[[dihydraziummanganese(II)]]-di-μ-sulfato-κ^4O:O′] from synchrotron data. *Acta Crystallographica, Section E*, **63**, i152.

19. Govindarajan, S., Patil, K.C., Manohar, H., and Werner, P.E. (1986) Hydrazinium as a ligand: structural, thermal, spectroscopic and magnetic studies of hydrazinium lanthanide di-sulfate monohydrates; crystal structure of the neodymium compound. *Journal of the Chemical Society, Dalton Transactions*, 119–123.
20. Gajapathy, D., Govindarajan, S., Patil, K.C., and Manohar, H. (1983) Synthesis, characterisation and thermal properties of hydrazinium metal oxalate hydrates. Crystal and molecular structure of hydrazinium copper oxalate monohydrate. *Polyhedron*, **2**, 865–873.
21. Poojary, M.D. and Patil, K.C. (1987) X-Ray structure of dihydrazinium uranyl dioxalate monohydrate. *Proceedings of the Indian Academy of Science*, **99**, 311–315.
22. Govindarajan, S., Patil, K.C., Poojary, M.D., and Manohar, H. (1986) Synthesis, characterization and X-ray structure of hexahydrazinium diuranyl pentaoxalate. *Inorganica Chimica Acta*, **120**, 103–107.
23. Kumar, N.R.S., Nethaji, M., and Patil, K.C. (1991) Preparation, characterization, spectral and thermal analyses of $(N_2H_5)_2MCl_4{\cdot}2H_2O$ (M=Fe, Co, Ni and Cu); crystal structure of the iron complex. *Polyhedron*, **10**, 365–371.
24. Kumar, N.R.S., Mathews, I.I., and Patil, K.C. (1991) Synthesis, spectral and structural studies on $(N_2H_5)_2MCl_4(H_2O)_2$ (M=Pt and Pd); crystal structure of the platinum complex. *Polyhedron*, **10**, 579–582.
25. Kumar, N.R.S., Nethaji, M., and Patil, K.C. (1991) Synthesis, characterization and structure of $(N_2H_5)_3MnX_5$ (X=Cl and Br). *Journal of Coordination Chemistry*, **24**, 333–337.
26. Kumar, N.R.S. (1990) Synthesis, spectra and structure of hydrazinium metal chloride and thiocyanate complexes, PhD Thesis, Indian Institute of Science, Bangalore.
27. Kumar, N.R.S., Nethaji, M., and Patil, K.C. (1991) Synthesis and characterization of bis(hydrazinium)tetra-thiocyanato-N)-cobalt(II) and -nickel(II) dihydrates; crystal structure of the cobalt complex. *Journal of the Chemical Society, Dalton Transactions*, 1251–1254.
28. Kumar, N.R.S., Nethaji, M., and Patil, K.C. (1991) Structure of bis(thiocyanato-*N*)bis-(thiosemicarbazide-N^1,*S*)nickel(II) a redetermination. *Acta Crystallographica, Section C*, **47**, 2052–2054.
29. Vikram, L., Shanthakumar, D.S., Ragul, R., and Sivasankar, B.N. (2007) Spectral and thermal studies on new hydrazinium metal sulfite dihydrates. *Journal of Thermal Analysis and Calorimetry*, **89**, 521–524.

6

Applications of Inorganic Hydrazine Derivatives

K. C. Patil[1] and Tanu Mimani Rattan[2]
[1]*Department of Inorganic and Physical Chemistry, Indian Institute of Science, Bangalore, India*
[2]*Department of Physics, Sri Sathya Sai Institute of Higher Learning, Prasanthi Nilayam, India*

6.1 INTRODUCTION

Hydrazine, monomethyl hydrazines (MMHs), and dimethyl hydrazines (UDMHs) are well-recognized fuels for rocket propulsion. Although envisaged as highly energetic compounds in the 1960s, presently new uses of hydrazine and its derivatives are emerging. Several organic derivatives of hydrazine, such as triazoles, have been patented and used as fungicides, herbicides, insecticides, and plant growth regulators. Several types of triazoles and INH (isoniazid – hydrazide of 4-pyridine-carboxylic acid) are also used as antibacterial and tuberculosis drugs. Azocarbonamide, $C_2H_4N_2O_2(NH_2CONNCONH_2)$ and other organic derivatives of hydrazine are used as blowing agents. Currently, hydrazine hydrate is used commercially in the agriculture sector (>40%), as blowing agents (33%), as boiler feed water (15%), and in pharmaceuticals

Inorganic Hydrazine Derivatives: Synthesis, Properties and Applications, First Edition.
Edited by K. C. Patil and Tanu Mimani Rattan.

(12%) [1–3]. The uses of inorganic derivatives of hydrazine as explosives and propellants (energetic materials), oxygen scavenger (boiler water treatment) and analytical reagents, and so on, although known, are not well documented. Some of these applications are discussed in this chapter.

6.2 APPLICATIONS OF HYDRAZINE SALTS

Hydrazine salts retain the reactivity and reducing property of anhydrous hydrazine or hydrazine hydrate, making them suitable as analytical agents, energetic compounds, and starting material for metal complexes. These aspects are discussed in the following sections.

6.2.1 Synthesis of Hydrazinium Metal Complexes

Most of the hydrazinium salts discussed in Chapter 2 are very reactive. This property has been used in the preparation of hydrazinium metal complexes, which offer varied applications as precursors, reagents, energetic compounds, and nanostructures among others. Chapter 3 discussed these aspects in the synthesis of hydrazinium metal chloride $[(N_2H_5)_2MCl_4{\cdot}2H_2O]$, hydrazinium metal thiocyanate $[(N_2H_5)_2M(NCS)_4{\cdot}2H_2O]$, hydrazinium metal sulfate $[(N_2H_5)_2M(SO_4)_2]$, hydrazinium metal oxalate $[(N_2H_5)_2M(C_2O_4)_2{\cdot}nH_2O]$, and so on, by reaction of the corresponding hydrazinium salts with respective metal salts.

6.2.2 Solid-State Synthesis of Ammonium Vanadyl Complex

Vanadium compounds have a complex chemistry because of the multiple oxidation states of vanadium. Among these, V_2O_5 is an important semiconducting material with potential applications as catalysts, chemical sensors, field effect transistors, and electrochemical and photochromism devices. Studies on the reactivity of hydrazinium chloride with NH_4VO_3 have led to the formation of the ammonium vanadyl complex $(NH_4)_2VO(OH)_2Cl_2$, which is a precursor to the formation of V_2O_5.

Solid-state reactions between N_2H_5Cl and NH_4VO_3 have been carried out in different mole ratios at 100 °C in air [4]. The DTA (differential thermal analysis) results of N_2H_5Cl, NH_4VO_3 and $N_2H_5Cl:NH_4VO_3$

Table 6.1 DTA results of N_2H_5Cl, NH_4VO_3, and $N_2H_5Cl : NH_4VO_3$ mixtures.

Compound/mixture	DTA peaks (°C)[a]
N_2H_5Cl	100(−), 225(+), 310(−)
NH_4VO_3	195(−), 215(−), 310(−)
N_2H_5Cl: NH_4VO_3 (20 : 1)	100(−), 225(+)
N_2H_5Cl: NH_4VO_3 (4 : 1)	100(−), 225(+), 260(+), 285(−), 300(−), 370(+)
N_2H_5Cl: NH_4VO_3 (2 : 1)	100(−), 195(+), 245(+), 260(+), 300(−), 365(+)
$(NH_4)_2VO(OH)_2Cl_2$ (green)	290(−), 365(+), 685(−)

[a] (−) = Endotherm, (+) = exotherm.

mixtures, summarized in Table 6.1, reveal details of the reaction between the two. It is noticed that NH_4VO_3 appears to sensitize the decomposition of N_2H_5Cl when present in small quantities (20 : 1). As the concentration of NH_4VO_3 is increased by changing the mole ratio of $N_2H_5Cl : NH_4VO_3$ (6 : 1, 4 : 1, and 2 : 1), additional peaks are observed at 260, 285, and ~365 °C. The additional peaks may be due to the chemical reaction between NH_4VO_3 and N_2H_5Cl. In fact, the isothermal TG (thermogravimetry) of a $NH_4VO_3 : 2N_2H_5Cl$ mixture at 100 °C is horizontal after 2 h, with 18% weight loss. To identify the reaction product at this stage, experiments have been conducted with $NH_4VO_3 : N_2H_5Cl$ in 1 : 4 and 1 : 6 proportions, heated at 100 °C. The solid dry products when analyzed gave a composition corresponding to $(NH_4)_2VO(OH)_2Cl_2$ (observed (%) $NH_3 = 18.45$, $V = 24.8$, $Cl = 33.2$; calculated (%) $NH_3 = 17.3$, $V = 24.5$, $Cl = 34.1$). This formula is also consistent with the observed weight loss in the isothermal TG (observed 18.0%; required 18.1%). Consequently, the reaction between NH_4VO_3 and N_2H_5Cl can be represented as:

$$NH_4VO_3 + 2N_2H_5Cl \rightarrow (NH_4)_2VO(OH)_2Cl_2 + NH_3 + N_2 + \tfrac{1}{2}H_2 \quad (6.1)$$

The TG of $(NH_4)_2VO(OH)_2Cl_2$ shows a weight loss of 56.8% corresponding to the formation of V_2O_5 (required 56.3%). A DTA result of this compound shows it to decompose endothermically. The exotherm at 365 °C could be attributed to the oxidation of vanadium(IV) to vanadium(V) and the sharp endotherm at 685 °C is due to melting of V_2O_5. Powder X-ray data of $(NH_4)_2VO(OH)_2Cl_2$ show that irrespective of the amount of N_2H_5Cl present the product remains the same.

The complex $(NH_4)_2VO(OH)_2Cl_2$ is thus a precursor to the formation of V_2O_5, an important semiconducting material.

6.2.3 Synthesis of 4-Amino-3,5-dimethyl-1,2,4-triazole

Hydrazinium hydrazine carboxylate is used in the preparation of 4-amino-3,5-dimethyl-1,2,4-triazole, a useful compound in agriculture and medicine. When a mixture of viscous liquid hydrazinium hydrazine carboxylate and acetonitrile is kept at room temperature, two layers appear: the top layer being acetonitrile and the lower one $N_2H_5COON_2H_3$. A pink color develops in the acetonitrile layer after about 12 h. After two to three weeks, a white crystalline compound is formed in the hydrazinium hydrazine carboxylate layer, and the pinkish acetonitrile layer disappears. The white crystals are those of 4-amino-3,5-dimethyl-1,2,4-triazole.

The synthesis of 4-amino-3,5-dimethyl-1,2,4-triazole is also carried out using hydrazinium hydrazine carboxylate as the starting material; it is boiled under reflux with acetonitrile (20 ml) for 4 h [5]. The resultant solution is evaporated over a water bath to afford colorless crystals of the triazole. The crystals are separated by filtration and washed with a small amount of acetone followed by acetonitrile, and then dried in air to give the product (1.3 g). The compound is freely soluble in DMSO and water, slightly soluble in acetone, and insoluble in benzene, carbon tetrachloride, chloroform, and acetonitrile.

The solid compound has been characterized by elemental analysis, infrared and NMR (^{1}H and ^{13}C) spectroscopy, and X-ray diffraction. The analytical and spectral data confirm that the compound is 4-amino-3,5-dimethyl-1,2,4-triazole. The mass spectral fragmentation pattern has been successfully interpreted on the basis of its structure.

Hydrazine hydrate is known to react with acetonitrile in the presence of sulfur or ethanol to form 4-amino-3,5-dimethyl-1,2,4-triazole or 3,6-disubstitued-1,2–dihydro-1,2,4,5-tetrazines. The initial product, which is disubstituted 1,2-dihydro-1,2,4,5-tetrazine, is readily oxidized to the pink colored 1,2,4,5-tetrazine; it may also rearrange at elevated temperature or on treatment with an acid to the corresponding 1,2,4-triazole. The triazole compound is obtained by the reaction of hydrazine hydrate and acetonitrile in the presence of CO_2. The presence of CO_2 in the formation of the six-membered ring intermediate is essential, and has been confirmed by repeating the experiments in the absence of CO_2. However, the exact role of CO_2 in this reaction is not clear. Figure 6.1 gives a possible mechanism for the formation of the triazole from hydrazinium hydrazine carboxylate and acetonitrile.

Hydrazine or its salts are known to form amidrazone salts (**1**) by nucleophilic attack on acetonitrile. Compound **2** (4-amino-3,5-dimethyl-1,2,4-triazole) appears to be formed through six-membered ring

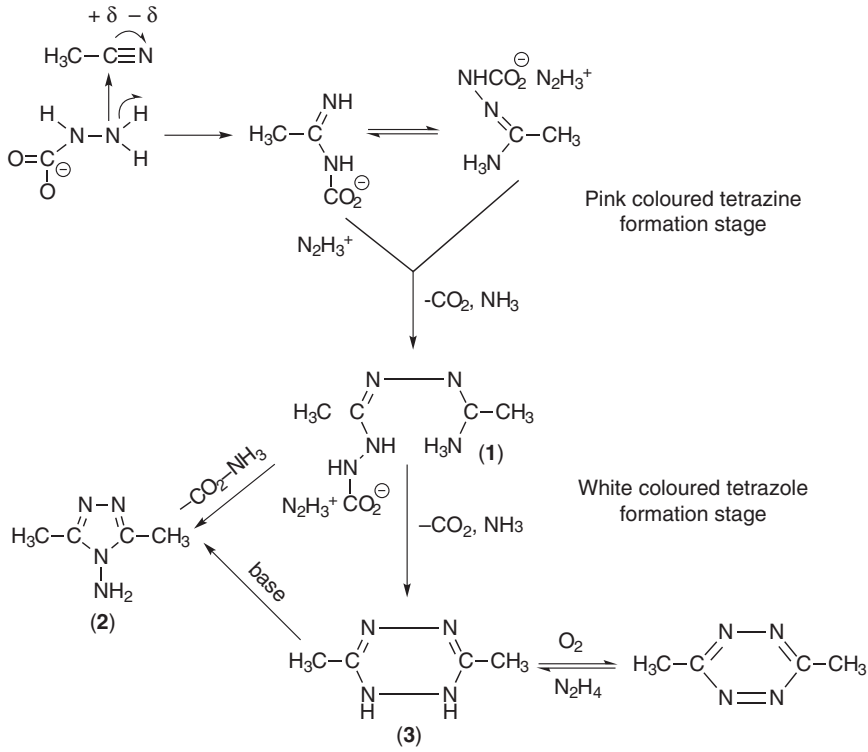

Figure 6.1 Mechanism of triazole formation. Reproduced with permission from [5] © 1989 Indian Institute of Science.

compound **3,** as established by earlier studies [5]. For the substitution, it has been observed the presence of more powerful electron-withdrawing groups tends to stabilize the six-membered ring, namely, 3,6-disubstituted-1,2-dihydro-1,2,4,5-tetrazine (pink color), while more electron-releasing groups facilitate conversion into the five-membered ring.

6.2.4 Hydrazinium Phosphates as Flame Retardants

Natural fibers such as cotton (cellulose) are intrinsically flammable and undergo combustion in air, once ignited. Phosphorous-containing compounds like ammonium phosphates have been investigated as flame retardants for cellulosic materials. This role of phosphates as useful flame retardants for cellulose is well known.

Natural cellulose is a linear polymer consisting of glucopyranose units, linked by 1,4-glycosidic bonds, with several monomeric units (up to

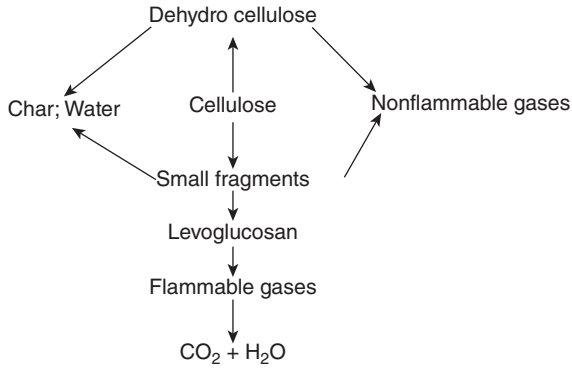

Figure 6.2 Pyrolysis of cellulose. Ph.D Thesis of Vittal, J.J. under Prof K. C. Patil at Indian Institute of Science.

5000). The combustion of cellulose is due to the production of combustible or flammable gaseous products during its pyrolysis (Figure 6.2). Additives like phosphorous-containing compounds can pyrolyze cellulose, producing char and water, instead of ill-defined tar, which decomposes to form flammable gases like 1,4-anhydro-D-glucopyranose, 1,6-anhydro-D-glucofuranose, levoglycosan, and so on. Phosphate compounds are considered to be ideal flame retardants as they act by reducing the pyrolysis temperature of cellulose, favoring the dehydration pathway of decomposition and increasing char formation rather than tar formation.

Monohydrazinium phosphate (MHP) and dihydrazinium phosphate (DHP) have also been investigated as flame retardants of cellulose and compared with the corresponding ammonium phosphates [6,7]. The flame retardant property of hydrazinium phosphates is checked using a Whatman No. 40 filter paper with an ash content of 0.018% as the cellulose source. This filter paper is treated with hydrazinium phosphates by dipping it into aqueous solutions of selected concentrations of 2.5% and 10% to ensure that the desired weight of phosphate is retained on the sample. The samples are then dried in air and used in pyrolysis experiments.

Figure 6.3 shows the DTA curves of cellulose, monohydrazinium phosphate-treated cellulose, and dihydrazinium phosphate-treated cellulose. The DTA of cellulose exhibits a large exotherm at 377 °C due to the oxidative degradation of cellulose and the oxidation of tarry products produced from the pyrolysis of cellulose. The first exothermic peak temperature is lowered from 377 °C for pure cellulose to 277 °C for

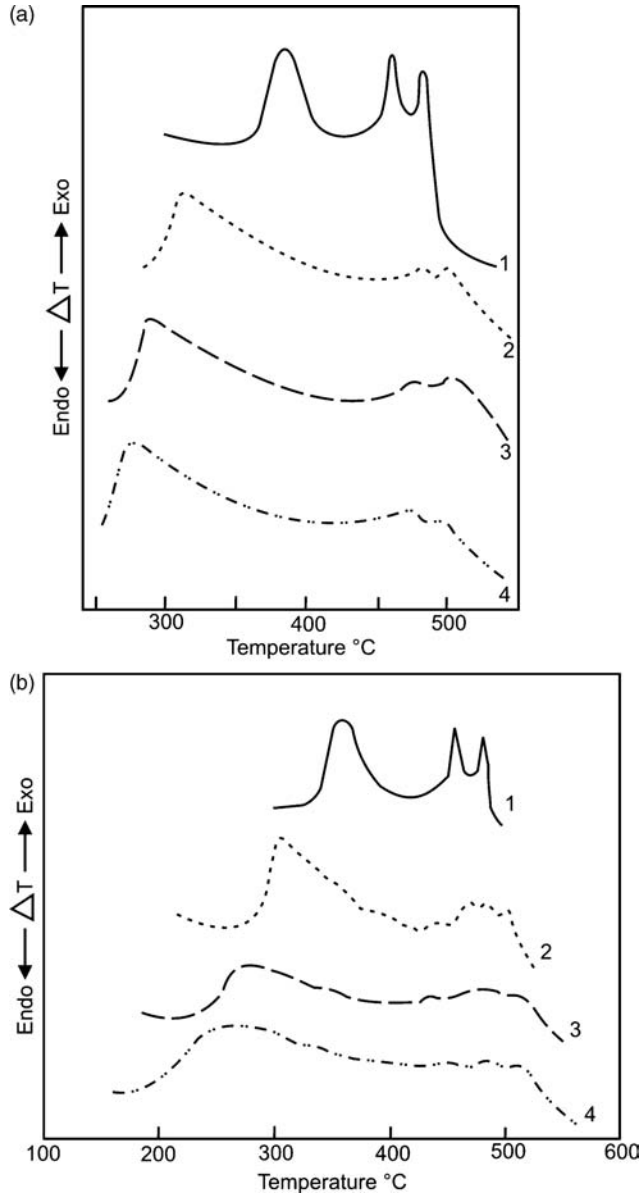

Figure 6.3 DTA curves (in air) of cellulose untreated and treated with (a) $N_2H_5H_2PO_4$: (1) untreated, (2) 2% MHP treated, (3) 5% MHP treated, and (4) 10% MHP treated; (b) $(N_2H_5)_2HPO_4$: (1) untreated, (2) 2% DHP treated, (3) 5% DHP treated, and (4) 10% DHP treated. Reproduced from Ref [6] with permission from SAGE Publications Ltd © 1980 and Ref [7] with permission from Elsevier © 1981.

Table 6.2 DTA data of untreated and monohydrazinium phosphate-treated Whatman filter paper.

Sample	DTA peak temperature (°C)[a]
$N_2H_5H_2PO_4$	82(m), 107(−), 119(−), 266(+)
Filter paper (α-cellulose)	377(+), 460(+), 488(+)
Paper dipped in 2% $N_2H_5H_2PO_4$ solution and dried	310(+), 480(+), 500(+)
Paper dipped in 5% $N_2H_5H_2PO_4$ solution and dried	288(+), 480(+), 500(+)
Paper dipped in 10% $N_2H_5H_2PO_4$ solution and dried	277(+), 480(+), 500 (+)

[a] (m) = Melting, (−) = endotherm, and (+) = exotherm.

10% monohydrazinium phosphate; the corresponding temperature is 266 °C for 10% dihydrazinium phosphate-treated cellulose. The dihydrazinium phosphate-treated cellulose samples decompose at lower temperatures. This sensitization clearly indicates the acid-catalyzed decomposition of cellulose. The last two exotherms at 460 and 488 °C could be due to the glowing of char in the condensed phase. However, the decomposition temperature of these exotherms is higher but the peak area is considerably reduced, almost disappearing for 5% and 10% dihydrazinium phosphate-treated cellulose. Since the percentage of phosphorus is higher, the oxidation and hence the glowing of char is completely prevented in these cases.

Table 6.2 summarizes the DTA data of untreated cellulose and of cellulose treated with various concentrations of monohydrazinium phosphate.

The TG curves of α-cellulose, monohydrazinium phosphate-treated cellulose, and dihydrazinium phosphate-treated cellulose show an initial weight loss (9%) at 50 °C due to dehydration (Figure 6.4). Cellulose starts decomposing slowly up to 180 °C; the weight loss is then rapid between 180 and 250 °C for mono- and dihydrazinium phosphate. This shows that phosphate acts in the condensed phase, minimizing tar formation and maximizing char formation.

Table 6.3 summarizes mass spectrometric analysis data of the decomposition gaseous products of mono- and dihydrazinium phosphate, mono- and diammonium phosphate, and phosphoric acid treated celluloses.

The ratio of the intensity of mass 18 to 44 (water and carbon dioxide, respectively) is higher for dihydrazinium phosphate-treated cellulose than for monohydrazinium phosphate-treated cellulose or even diammonium

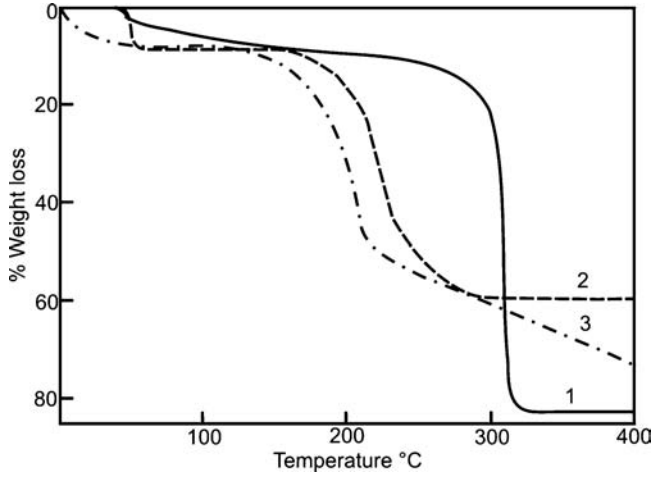

Figure 6.4 TG curves of (1) pure filter paper, (2) 5% MHP treated filter paper, and (3) 5% DHP treated filter paper. Reproduced from Ref [6] with permission from SAGE Publications Ltd © 1980 and Ref [7] with permission from Elsevier © 1981.

Table 6.3 Mass spectrometry results of untreated and treated cellulose pyrolyzed at 500 °C and 10^{-8} Torr.

Sample	Peak heights of molecular ions (*m/z*)			Peak height ratio of mass 18 to 44 (H_2O/CO_2)
	18 (H_2O)	28 (N_2)	44 (CO_2)	
Untreated cellulose filter paper	39.51	—	62.74	0.63
5% Mono-ammonium phosphate-treated cellulose	49.40	—	22.72	2.17
5% Monohydrazinium phosphate-treated cellulose	60.42	—	19.60	3.08
Dihydrazinium phosphate-treated cellulose	59.04	21.4	7.44	7.94
Diammonium phosphate-treated cellulose	51.47	13.7	6.84	7.52
Phosphoric acid treated cellulose	44.69	13.0	5.51	8.11

phosphate-treated cellulose, although the latter difference it is not significant. Considering mass 28 to be due to nitrogen alone (carbon monoxide can also be produced) it seems that more nitrogen is produced in the case of dihydrazinium phosphate-treated cellulose.

Dihydrazinium phosphate is the salt of a weak base, namely, hydrazine, having a hydrophilic hydrazinium cation and a higher percentage of nitrogen than diammonium phosphate. It is interesting to compare its flame retardant property with those of diammonium phosphate and phosphoric acid. Although thermal analysis (DTA and TG) do not show any marked difference, the mass spectrometric studies show that dihydrazinium phosphate-treated cellulose produces more water, nitrogen, and carbon dioxide compared with the other two retardants. Therefore, it appears that $N_2H_5^+$ in dihydrazinium phosphate is not reacting with phosphate to form P–N bonds, which facilitate phosphorylation. In addition, as the temperature for oxidative degradation is lowered to the same extent in all three cases, it appears that free phosphoric acid causes dehydration and degradation at a lower temperature. This pathway offers a more acidic environment in the thermal state. The decomposition temperature of dihydrazinium phosphate is comparable with that of the flammable substrate cellulose; it suffers from the disadvantage that it decomposes exothermically at 270 °C. This disadvantage appears to be more than compensated for, however, by the hydrophilic nature or hygroscopic property of the hydrazinium ion, which promotes dehydration more efficiently and limits the production of combustible hydrocarbon gases.

Furthermore, from the viewpoint of the gas theory of fire retardancy, it appears that nitrogen produced during the pyrolysis of DHP, being noncombustible, alters the flammability by dilution of the flammable gases; however, the contribution is less significant.

6.2.5 Hydrazinium Thiocyanate as Analytical Reagent for the Quantitative Estimation of Copper

The copper content in cupric compounds is usually determined by gravimetric analysis. In the conventional method, Cu^{2+} is usually reduced to Cu^+ by the addition of sulfurous acid, ammonium hydrogen sulfite, ascorbic acid, or ferrous sulfate. It is then precipitated as cuprous thiocyanate by the addition of ammonium thiocyanate and estimated gravimetrically.

The use of N_2H_5SCN as an analytical reagent for the quantitative estimation of copper has been explored since it reduces cupric to cuprous ion and precipitates as cuprous thiocyanate in a single step [8]. The procedure is as follows: A copper solution containing up to 0.3 g of copper is diluted to 150–200 ml in a 400-ml beaker. A 10% solution of

Table 6.4 Gravimetric determination of copper using N_2H_5SCN as a reagent.

Copper taken (g)	Copper found (g)	Error (%)[a]
0.0536	0.0535	−0.2
0.0717	0.0715	−0.3
0.0770	0.0769	−0.1
0.1044	0.1045	−0.1
0.1305	0.1300	−0.4
0.1750	0.1754	+0.2
0.1991	0.1984	−0.4
0.3368	0.3381	+0.4

[a] Relative standard deviation 0.13%.

hydrazinium thiocyanate is then added slowly with constant stirring. A white precipitate forms, and the supernatant liquid becomes acidic. The precipitate is digested on a water-bath for about an hour, and subsequently filtered off on a porosity-3 sintered-glass crucible. The precipitate is washed with cold distilled water and finally with alcohol. It is dried thereafter to a constant weight at 110–120 °C and weighed as $Cu_2(SCN)_2$. The reaction of hydrazinium thiocyanate, N_2H_5SCN, with Cu^{2+} can be written as follows:

$$4Cu^{2+} + 4N_2H_5SCN \rightarrow 2Cu_2(SCN)_2 + 3N_2H_5^{+} + 5H^{+} + N_2 \quad (6.2)$$

Table 6.4 gives the results of the gravimetric determination of copper.

The method of determination of copper using hydrazinium thiocyanate as a reagent is advantageous because the reduction of cupric to cuprous ions and the precipitation of cuprous thiocyanate are achieved by a single reagent. Furthermore, the time required for the determination is much less than with conventional methods. On the other hand, while ions like Fe^{3+}, Mn^{2+}, and Cr^{3+} do not interfere, ions like Ag^{+} and Hg^{+} do interfere. Interestingly, cuprous thiocyanate is not precipitated by addition of hydrazine hydrate and thiocyanate to solutions containing Cu^{2+} ions. Hydrazine hydrate is known to reduce Cu^{2+} to Cu^{+}, which either forms Cu_2O or is further reduced to metallic copper.

6.3 ENERGETIC MATERIALS

As discussed in Chapter 3 (Section 3.3), the reactivity of metal hydrazine derivatives varies from detonation to deflagration depending upon the nature of the anion (oxidizing or reducing) and cation (transition or

non-transition metal). Hydrazine salts with oxidizing anions like nitrate, perchlorate, and azide explode on ignition. This property of inorganic hydrazine derivatives has been useful in the preparation of several energetic compounds such as explosives, initiators, and energetic oxidizers for solid propellants. These are discussed in the following sections.

6.3.1 Explosives and Initiators

Transition metal perchlorate, nitrate, and azide hydrazines are explosives. They are sensitive to friction and impact. Nickel perchlorate hydrazine is reported to be explosive even under water. Metal hydrazine complexes of azide and nitrate are highly sensitive to impact and friction and so decompose violently. Table 6.5 summarizes the impact sensitivities of these complexes as determined by the drop weight method [9].

Metal hydrazine complexes of azide and nitrate have been investigated as initiators. For example, the synthesis of nickel nitrate hydrazine [$Ni(NO_3)_2(N_2H_4)_2$] described in Chapter 3 has been commercially developed for use as detonators (blasting caps) in China.

For the industrial manufacture of nickel azide hydrazine for defense applications, Zhu *et al.* have synthesized this complex with a slight modification [10,11]. They start from the corresponding nitrate and use NaAc-HAc as buffer solution to maintain a stable pH during the reaction process. The pH during the synthesis of nickel azide hydrazine is controlled by adding 20% HNO_3 to the aqueous solution of $Ni(NO_3)_2$. The hazardous gas hydrogen azide (HN_3) is released during the reaction because of the acidity of HNO_3. To overcome this problem, a weaker acetic acid (HAc) in

Table 6.5 Impact sensitivities of metal hydrazine azide and nitrate complexes.

Compound	Impact sensitivity (cm)
$M(NO_3)_2(N_2H_4)_3$	11
$Co(NO_3)_2(N_2H_4)_3$	8
$Ni(NO_3)_2(N_2H_4)_3$	9
$Zn(NO_3)_2(N_2H_4)_3$	13
$Cd(NO_3)_2(N_2H_4)_3$	8.5
$Cd(NO_3)_2(N_2H_4)_2$	12.5
$Co(N_3)_2(N_2H_4)_2$	9
$Ni(N_3)_2(N_2H_4)_2$	10
$Zn(N_3)_2(N_2H_4)_2$	12

form of its buffer solution NaAc-HAc is selected. A solution of NaN_3 and $N_2H_4{\cdot}H_2O$ is added simultaneously to the aqueous solution of $Ni(NO_3)_2$ maintained at 60 °C. To this mixture the buffer solution is added to control the pH and the resultant solution is stirred for 40 min.

A relatively recent evaluation of the performance of nickel azide hydrazine manufactured by this procedure indicates it to be a safer, lead-free, primary explosive than lead styphanate or lead azide [12]. For this reason it has also been explored as a charge for semiconductor-bridge initiators used for the initiation of high-explosive devices. Its best ignition performance parameters under optimal conditions have been evaluated by the same group [13].

Research efforts in the development of green energetic materials continues as new formulations of a series of hydrazinium salts of nitrogen-rich organic compounds have been reported, such as 5,5-bi-tetrazololates, 1*H*,1′*H*-5,5′-bitetrazole-1,1′-diol, 5-hydrazinotetrazole (HTZ), and so on [14–16]. Energetic characterizations of these salts have shown excellent thermal stabilities, despite their very high nitrogen contents. Their sensitivities towards impact, friction, and electrical discharge have been tested as possible replacements for RDX, HNS, and so on.

Transition metal hydrazine complexes like $[Cr(N_2H_4)_3](ClO_4)_3$ and $[Ni(N_2H_4)_3](NO_3)_2$ are considered to be novel explosives as their explosion parameters, such as shock wave overpressure, shock wave energy equivalent, and bubble energy equivalent are comparable to those of the classical high explosives [17].

6.3.2 Energetic Oxidizers for Solid Propellants

Ammonium perchlorate (AP) is universally used as an oxidizer in solid propellant composition. Aluminum powder is usually added to AP-based propellants to increase their energy. A high loading density (total of AP + Al 88%) is necessary to acquire the desired specific impulse (I_{sp}) for propulsion. The processing of such a propellant composition becomes difficult due to incompatibility. Therefore, to acquire a higher specific impulse, one has to take recourse to more energetic oxidizers and/or binders. Some of the alternatives considered to ammonium perchlorate are $LiClO_4$, $N_2H_5ClO_4$, $N_2H_6(ClO_4)_2$, and so on.

6.3.2.1 Metal Perchlorate Hydrazines

Most oxidizers used for propulsion suffer from disadvantages like hygroscopicity, incompatibility, and friction sensitivity. As a result, attempts

Table 6.6 Comparative data of NH_4ClO_4 and $Al(ClO_4)_3 \cdot 3N_2H_4$.

Property	NH_4ClO_4	$Al(ClO_4)_3 \cdot 3N_2H_4$
Molecular weight	117.5	421.5
Weight of % O_2	54.5	45.5
O/F	2.2	2.25
Density ($g\,cm^{-3}$)	1.9	1.6
Heat of combustion ($cal\,g^{-1}$)	470	1150
Heat of combustion of propellant ($cal\,g^{-1}$)		
Oxidizer (80): CTPB[a] (20)	800–850	1285
Burning rate ($mm\,s^{-1}$)	0.6	0.875

[a] CTPB = carboxy terminated polybutadiene.

have been made to synthesize new energetic oxidizers like metal complex perchlorates of the general formula $AM(ClO_4)_4$ (where A = Li^+, NH_4^+, $N_2H_5^+$, and so on, and M = Al and Cr) or by complexing with ammonia, for example, hydrazinium perchlorate ammoniates (Chapter 2). Among these, the oxidizer aluminum perchlorate hydrazine ($Al(ClO_4)_3 \cdot 3N_2H_4$) has better stability, endothermicity, high oxygen content, density, and storability than ammonium perchlorate (Table 6.6).

Hydrazine complexes of aluminum and magnesium, $Al(ClO_4)_3 \cdot 6N_2H_4$ and $Mg(ClO_4)_2 \cdot Al(ClO_4)_3 \cdot 8N_2H_4$, exhibit I_{sp} values in the range 270–290 s^{-1}. The heat of combustion of $Al(ClO_4)_3 \cdot 3N_2H_4$ is more than twice that of ammonium perchlorate. Although these are considered as high energetic oxidizers, some difficulties are encountered during their commercial processing as propellants. With binders like carboxy terminated polybutadiene (CTPB) there is a reaction between N_2H_4 and CTPB. However, by encapsulation of these oxidizers with polymers like cellulose acetate, phenol formaldehyde, polymethyl methacrylate, polystyrene, and so on the processing of the propellant is possible with CTPB [18]. The burning rate of compounds processed this way is further increased by mixing them with aluminum powder, which acts as a fuel.

6.3.2.2 Magnesium-Doped $N_2H_5ClO_4 \cdot 0.5H_2O$

Another method of stabilizing hygroscopic hydrazinium perchlorates is to add magnesium ions. This idea stems from the fact that the presence of magnesium ions in fertilizer grade ammonium nitrate makes it non-hygroscopic. As a case study, magnesium ion has been doped into $N_2H_5ClO_4 \cdot 0.5H_2O$ and investigated for its stability. The doped

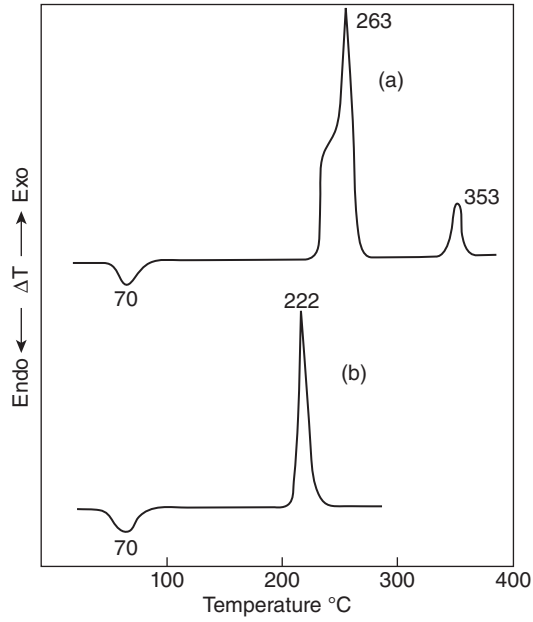

Figure 6.5 DTA curves of (a) $N_2H_5ClO_4{\cdot}0.5H_2O$ and (b) Mg^{2+}-doped $N_2H_5ClO_4{\cdot}0.5H_2O$. Ph.D Thesis of Nesamani, C. under Prof. K. C. Patil at Indian Institute of Science.

compound is prepared by dissolving trace amounts of Mg powder (less than 0.5 %) in a solution of $N_2H_5ClO_4{\cdot}0.5H_2O$ [9]. The product crystallized has been characterized by chemical analysis, infrared spectra, and TG-DTA, indicating trace quantities of magnesium present in $N_2H_5ClO_4$.

Figure 6.5 shows typical DTA curves of hydrazinium perchlorate hemihydrate versus Mg^{2+}-doped hydrazinium perchlorate hemihydrate. It can be seen that the compound prepared by using Mg^{2+}-doped hydrazinium perchlorate hemihydrate decomposes at a lower temperature of 222 °C compared to $N_2H_5ClO_4{\cdot}0.5H_2O$, which decomposes at 263 °C. This shows that Mg^{2+}-doped hydrazinium perchlorate hemihydrate displays different thermal properties than hydrazinium perchlorate. When the doped compound is heated, the crystal lattice is broken and Mg^{2+} ions are displaced from its sites. This results in an increase in the concentration of defects in the lattice. The decrease in the decomposition temperature of Mg^{2+} doped hydrazinium perchlorate compared to hydrazinium perchlorate may therefore be attributed to the production of larger

defects. Doping by magnesium not only decomposes hydrazinium perchlorate to a lower temperature, it also stabilizes it.

6.4 COMBUSTIBLE METAL HYDRAZINE COMPLEXES

Several metal hydrazine complexes are combustible solids. This property makes them as useful starting materials for various products. These complexes consist of a metal cation with hydrazine as the ligand. One or more oxidizing anions are provided to balance the charge of the complex. The metals incorporated are transition metals, alkaline earth metals, metalloids, or lanthanide metals that are capable of forming hydrazine complexes. The preferred metals include cobalt, magnesium, manganese, nickel, titanium, copper, chromium, zinc, tin, rhodium, iridium, ruthenium, palladium, and platinum. The transition metal cation or alkaline earth metal cation acts as a template at the center of the coordination complex. One or more oxidizing anions may also be coordinated with the metal cation. The complexes when heated rapidly undergo combustion, deflagration, or decomposition to produce significant quantities of gas.

The combustible nature of metal hydrazine complexes and the high exothermicity realized during heating have paved the way for using them as precursors to several useful nanocrystalline metal powders and oxide materials like Fe_3O_4, γ-Fe_3O_3, ferrites, cobaltites, manganites, and so on.

6.4.1 Synthesis of γ-Fe_2O_3 – Recording Material

Iron oxalate hydrazine, the synthesis of which is discussed in Chapter 3, is used to prepare iron oxide. The decomposition/combustion of $FeC_2O_4(N_2H_4)_2$ in air at $\approx$250 °C yields the oxide Fe_2O_3 by the following reaction:

$$2FeC_2O_4(N_2H_4)_2 + \tfrac{5}{2}O_2 \rightarrow Fe_2O_3 + 4CO_2 + 4NH_3 + 2N_2 + 2H_2O \tag{6.3}$$

However, X-ray powder diffraction of the combustion residue shows it to be a mixture of α- and γ-Fe_2O_3 [19,20]. This is further confirmed by DTA and a temperature profile study that revealed an exotherm at $\approx$630 °C corresponding to the conversion of γ- $\rightarrow$ α-Fe_2O_3.

6.4.2 Synthesis of Nano-Copper Chromite ($CuCr_2O_4$) Catalyst

Copper chromite is a well-known catalyst for the decomposition/combustion of ammonium perchlorate based solid propellants [21]. The preparation of copper chromite involves the solid-state reaction between copper oxide (CuO) and chromium oxide (Cr_2O_3) at the high temperature of 850 °C for 24 h. However, it is possible to prepare $CuCr_2O_4$ by the combustion of a mixture of $Cu(N_2H_3COO)_2{\cdot}H_2O$ and $Cr(N_2H_3COO)_3{\cdot}3H_2O$ (1 : 2 mole ratio). This mixture ignites at 250 °C and undergoes autocatalytic combustion to yield nano-oxide material. The nanopowder (~60 nm) obtained, when heated at 600 and 800 °C for an hour, shows the formation of single phase $CuCr_2O_4$ as seen in the powder XRD pattern (Figure 6.6).

The catalytic activity of the finely divided copper chromite for oxidation reactions has been investigated utilizing decomposition of N_2O as a test reaction. The kinetics of N_2O decomposition were studied in the temperature range 420–480 °C and the activation energy (E_a) for this reaction was found to be 21.8 kcal mol^{-1}.

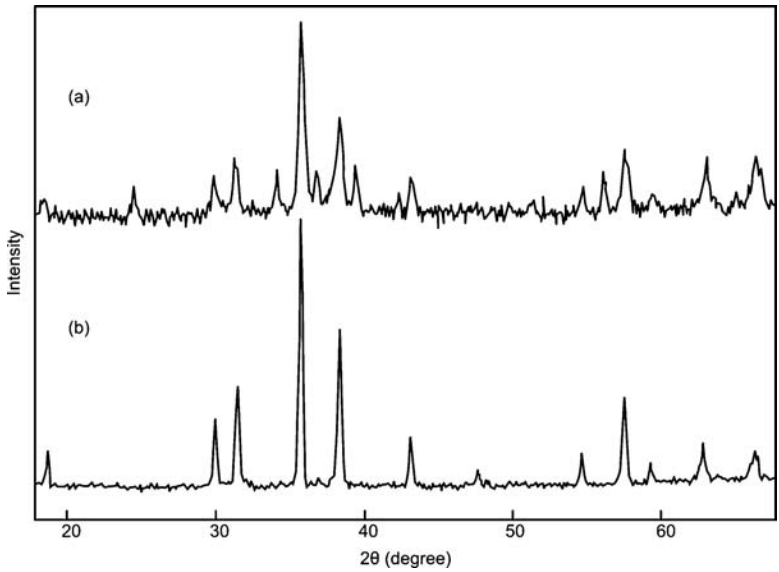

Figure 6.6 X-Ray powder diffraction of $CuCr_2O_4$ heated at (a) 600 °C and (b) 800 °C. Ph.D Thesis of Sundar Manoharan, S. under Prof. K. C. Patil at Indian Institute of Science.

6.4.3 Synthesis of Lithium Metal Oxide ($LiMO_2$) – Battery Material

Lithium-ion battery (LIB) technology is one of the most powerful rechargeable energy sources available today. In the lithium-ion cells, the cathode is a transition metal oxide, typically consisting of $LiCoO_2$, $LiMn_2O_4$, or $LiNiO_2$. As these cells show good recycling electrochemical abilities, control of the electrochemical properties of these double oxides is very important.

$[Li(H_2O)M(N_2H_3COO)_3]0.5H_2O$, M = Ni and Co, have been synthesized in moderate yield from the corresponding metal salts and hydrazine carboxylate anion, $N_2H_3COO^-$; the latter was prepared by mixing $N_2H_4{\cdot}H_2O$ and dry ice [22]. The Ni complex crystallizes as purple needles whereas Co complex crystallizes as orange-red needles. Single-crystal structures of these complexes have been determined, which show the bidentate ligand coordination of the anion to the metal.

These two compounds on pyrolysis at ~700 °C in an oxygen atmosphere give the corresponding layered materials $LiMO_2$, M = Ni and Co. They have been characterized by powder XRD, Rietveld refinement, and scanning electron microscopy. The cathodic properties of $LiMO_2$ have been evaluated by cyclic voltammetry and galvanostatic charge–discharge cycling of up to 20 cycles in the voltage ranges 2.5–4.3 and 2.5–4.5 V versus Li metal (Figure 6.7).

6.4.4 Synthesis of Nano-Titania – Photocatalyst

In recent years, the widespread presence of chemicals has posed a serious threat to the environment. When chemicals such as heavy metals, herbicides, pesticides, aliphatic and aromatic detergents, arsenic compounds, solvents, degreasing agents, volatile organics, and chlorophenols seep into water sources, contamination is really hazardous. For instance, wastewaters produced from industrial processes of textile and dyestuff contain large quantities of azo dyes. An estimated 15% of the total dye is lost during dying processes and find its way into wastewaters. Oxidation of these organic pollutants at the surface of TiO_2, acting as catalyst, is an important photocatalytic application of titania. The catalytic activity of TiO_2 is influenced by its crystal structure (anatase or rutile), surface area, size distribution, porosity, surface hydroxyl group density, and surface adsorption and desorption process.

Titanyl hydrazine carboxylate dihydrate ($TiO(N_2H_3COO)_2{\cdot}2H_2O$) is synthesized by the reaction of titanyl chloride with hydrazine carboxylate

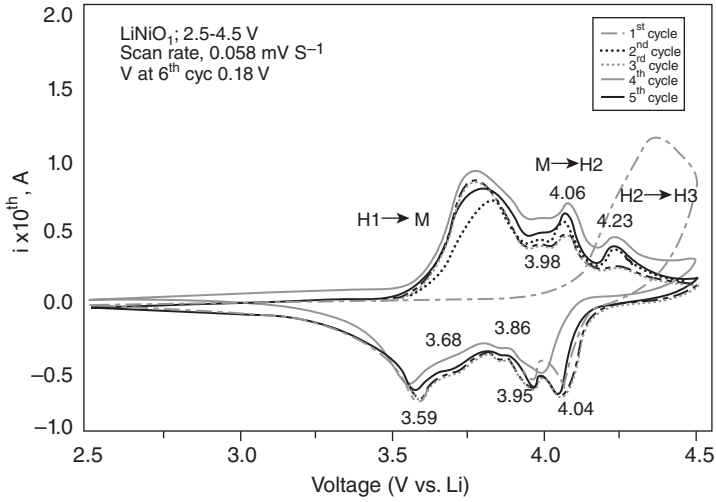

Figure 6.7 Cyclic voltammograms of $LiNiO_2$ prepared at 700 °C in an O_2 atmosphere with a scan rate of 0.058 mV s^{-1}. Lithium metal was the counter and reference electrode; voltage range 2.5–4.5 V, structural transitions (H1, M, H2, and H3) are also shown. Adapted with permission from Ref [22]. © 2006, American Chemical Society.

(Chapter 4, Section 4.3). Nano-titania is then prepared by combustion of the precursor titanyl hydrazine carboxylate at 350 °C in air. The formation of nano-titania has been confirmed by powder XRD pattern. It shows the formation of rutile titania with an average crystallite size of 8 nm. The density and surface area of the oxide are 3.04 g cm^{-3} and 110 m^2 g^{-1}, respectively. The particle size calculated from surface area is 20 nm [23].

The photocatalytic activity of nano-TiO_2 can be investigated spectroscopically by following the degradation of methylene blue with time. About 0.2 ml of methylene blue is added to 3 ml of a titania suspension (0.0015 wt% TiO_2). The sample is then irradiated by a mercury lamp. In this case, the differential absorbance at 660 nm measured with a UV/Vis spectrophotometer showed complete degradation of the dye within 10 min at room temperature (Figure 6.8), making nano-TiO_2 an important photocatalyst.

The higher photocatalytic activity of combustion-synthesized titania is due to:

1. crystalline nature of the nanoparticles;
2. hydrophilic nature of the surface, which absorbs more water molecules as seen from the TGA;

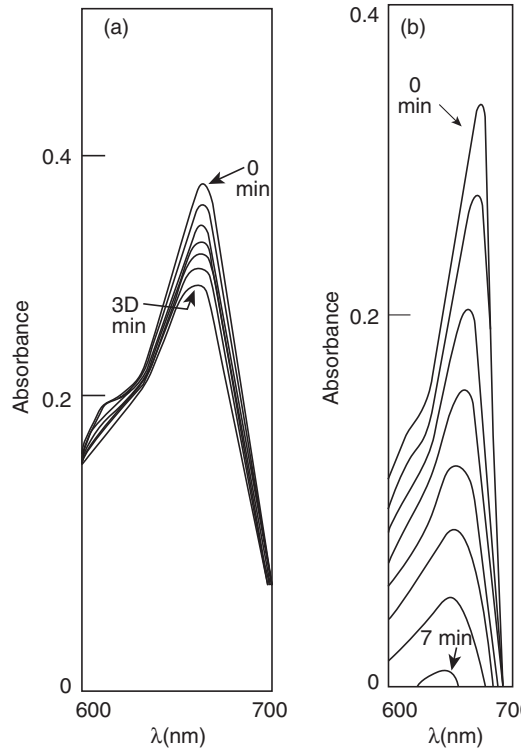

Figure 6.8 UV absorption spectra of (a) methylene blue and (b) methylene blue over nano-titania. Adapted from Ref [23]. With kind permission from Springer Science and Business Media © 1996.

3. absorption of visible radiation at about 500 nm;
4. lower band gap (2.5 eV).

Interestingly, the same TiO_2 can be reused.

6.4.5 Metal Ion Substituted Oxide Materials

It is easy to dope metal ions in metal hydrazine complexes as well as to make solid solutions of them (discussed in Chapter 4). The combustion of these metal-ion substituted metal hydrazine carboxylate complexes in air yield the corresponding nanocrystalline oxide materials with interesting catalytic, magnetic, and dielectric properties, having applications as phosphors, pigments, and so on. A few examples of the interesting

properties of nanocrystalline oxides derived from metal ion doped hydrazine complexes are:

- electronic ($Ca_{1-x}Mn_xO$),
- magnetic ($Fe_{2-x}Co_xO_{3-\delta}$),
- catalytic (Ni-Mo-S/Al_2O_3),
- spintronic ($Zn_{1-x}Mn_xO$),
- phosphor ($Y_{2-x}Eu_xO_{3-\delta}$),
- pigment ($Ce_{1-x}Pr_xO_{2-\delta}$).

Investigations on some of these nano-oxides validate their characteristic properties. For example, in cobalt-substituted γ-Fe_2O_3 a single line B-H curve (plot of applied external magnetic field H versus magnetic flux density B) indicates the presence of nanoparticles and the superparamagnetic nature of the oxide. The room temperature coercivity of this oxide varies from 130 Oe for pure γ-Fe_2O_3 to a maximum of 245.56 Oe for 5 at. % cobalt-substituted γ-Fe_2O_3; it then decreases to 105.43 Oe for 10 at.% Co/γ-Fe_2O_3. The saturation magnetization decreases with increasing percentage of cobalt. The values are 69 ($x = 0$ at.%) and 28.54 ($x = 10$ at.%). The results of temperature variations show that the coercivity increases considerably for 5 at.% from 122.78 Oe at 25 °C to 3106.10 Oe at −178 °C (liquid nitrogen temperature). This shows that coercivity is temperature dependant, and that cobalt is substituted in the γ-Fe_2O_3 matrix and not adsorbed on it [24].

The doping of Pr into ceria lattice furnishes the nano-cerium oxide pigment $Ce_{1-x}Pr_xO_{2-\delta}$, with $x = 0$–0.5. The diffuse reflectance spectra of $Ce_{1-x}Pr_xO_{2-\delta}$ pigments show an absorption edge at ≈690 nm confirming the formation of the red pigment. The surface area of this pigment is high at around 90 $m^2 g^{-1}$. A TEM of the red pigment obtained shows small spherical particles (Figure 6.9) distributed uniformly [25].

6.4.6 Synthesis of Nano-Cobaltites, -Ferrites, -Chromites, and -Manganites

The discovery, through serendipity, that the combustion of iron hydrazine carboxylate yields nano-iron oxide led to the preparation of various nano-size oxide materials by the thermal reactivity of metal hydrazine carboxylates. Hitherto, oxide materials prepared by conventional ceramic techniques used hydroxides, carbonates, nitrates, or oxalates as starting materials. The procedure involves their repeated pulverization and

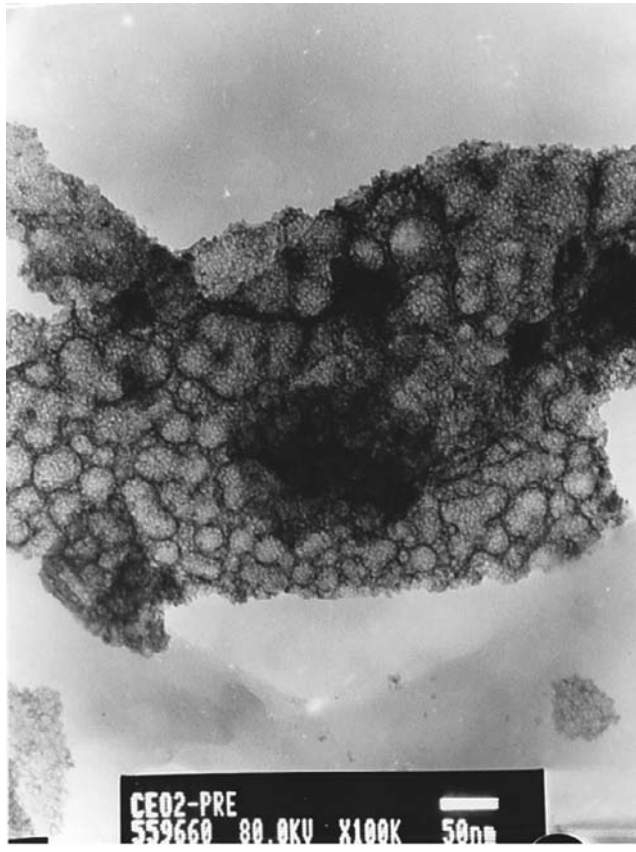

Figure 6.9 Transmission electron microscopy (TEM) micrograph of $Ce_{0.5}Pr_{0.5}O_{2-\delta}$. Reproduced from Ref [25] with permission from Elsevier © 2001.

calcinations at high temperatures (>800 °C). This causes inhomogeneity of the product and incorporation of chemical impurities during repeated grinding and heating operations. The combustion synthesis method has opened up a new vista, using hydrazine based redox complexes.

The formation of cobaltites (MCo_2O_4) from the combustion of mixed metal oxalate/acetate hydrazine complexes and solid solutions of hydrazinium metal hydrazine carboxylate hydrates have been discussed in Chapters 3 and 4, respectively (Sections 3.2.4.1, 3.2.6 and 4.6). The final product, confirmed by X-ray diffraction pattern, shows the characteristics of cobaltite spinels. Similar to cobaltites, mixed metal oxalate/acetate hydrazines complexes undergo single-step decomposition to form

corresponding ferrites (MFe_2O_4) at temperatures as low as 150–160 °C (Sections 3.2.6, 3.2.7.2, and 4.6). Interestingly, the mixed metal oxalate hydrazine precursors ignite while undergoing suction filtration, if allowed to dry.

Mixed metal oxalate hydrates do not yield ferrites at such low temperatures. However, complex formation with hydrazine makes it possible to obtain ferrites from the oxalates precursors at low temperatures of ~150 °C. This shows that the exothermic decomposition of hydrazine plays a vital role in the formation of these spinels at such temperatures. Properties of the ferrites formed are summarized in Table 6.7.

Notably, traditional ceramic approaches to synthesizing cobaltites or ferrites result in crystalline material, but with a low surface area, limiting their applications as catalysts or high frequency core. The severity of the reaction conditions necessary in ceramic approaches to overcome the slow reaction kinetics that occur when two solids are brought together causes this limitation. Repeated high-temperature firing of the component oxides with frequent re-grindings result in low surface area crystalline ferrites. To overcome all such difficulties, requires spinel formation in a short time and a considerable reduction in temperature. This allows for mixing of the component cations on an atomic scale. Mixed metal hydrazine precursors offer a new method for obtaining a wide variety of nano-spinels like $Co_{0.5}Zn_{0.5}Fe_2O_4$, $Co_{0.5}Ni_{0.5}Fe_2O_4$, and $Mn_{0.6}Zn_{0.4}Fe_2O_4$ from mixed metal, cinnamate fumerate, and succinate hydrazine complexes (Figure 6.10) [26–29].

Cobaltites and ferrites also find application as catalysts in dehydrogenation reactions. As a consequence, ferrites with large surface area are needed to function effectively as catalysts. For example, hydrogen peroxide, a well-known disinfectant that liberates nascent oxygen is widely used in operation theatres of hospitals. It is essential that to

Table 6.7 X-ray, Mössbauer, and surface area data of the ferrites.

Ferrite	X-ray data, a_0 (Å)	Mössbauer data		Surface area ($m^2\,g^{-1}$)
		Isomer shift ($mm\,s^{-1}$)	Internal field (kOe)	
$MgFe_2O_4$	8.42	0.3002	497.7	76
$MnFe_2O_4$	8.51	0.3850	524.2	31
$CoFe_2O_4$	8.37	0.4790	505.6	47
$NiFe_2O_4$	8.35	0.4690	511.0	–
$ZnFe_2O_4$	8.44	0.4100	508.4	22

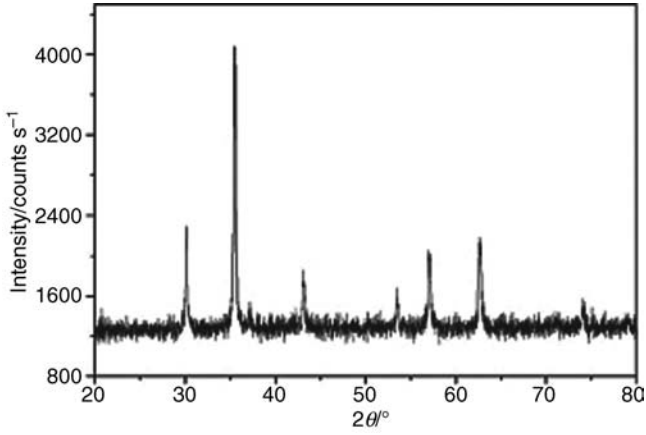

Figure 6.10 XRD pattern of $Mn_{0.6}Zn_{0.4}Fe_2O_4$. Reproduced from Ref [29]. With kind permission from Springer Science and Business Media © 2010.

liberate this oxygen, the decomposition of H_2O_2 takes place at room temperature and the use of catalysts plays a significant role in achieving this. The kinetics of the heterogeneous decomposition of hydrogen peroxide on nano-size ferrites MFe_2O_4 and cobaltites MCo_2O_4 (where M = Mn, Fe, Co, Ni, Zn, and Mg) have been investigated. A gasometric method is utilized to study the kinetics of H_2O_2 decomposition. The $KMnO_4$ titrimetric method cannot be used as such oxides are nano-size and ultra fine, causing difficulty in the separation of the dispersed fine particles from H_2O_2 [30].

The decomposition of H_2O_2 is found to be first order at low concentration (0.3%) and zero order at high concentration (30%). The catalytic activity of cobaltites on the decomposition of H_2O_2 is found to be better than that of ferrites (Figure 6.11). The observed catalytic behavior of ferrites and cobaltites has been attributed to their fine particle nature, large surface area, and electronic structure.

Hydrazinium metal chromium oxalate hydrazine complexes, $(N_2H_5)_2MCr_2(C_2O_4)_5{\cdot}xN_2H_4$ (M = Mg, Co, Ni, Cu, and Cd and $x = 1$–3), have been synthesized and investigated as precursors to metal chromites, MCr_2O_4 [31]. Like cobaltites and ferrites, chromites also find application as catalysts. The preparation of these complexes involves the reaction of respective metal carbonates with chromic acid and reduction of Cr(VI) to Cr(III) with oxalic acid and hydrazine hydrate or dihydrazinium oxalate, $(N_2H_5)_2C_2O_4$. Precipitation of the pinkish violet colored crystals of mixed metal chromium oxalate complex takes place.

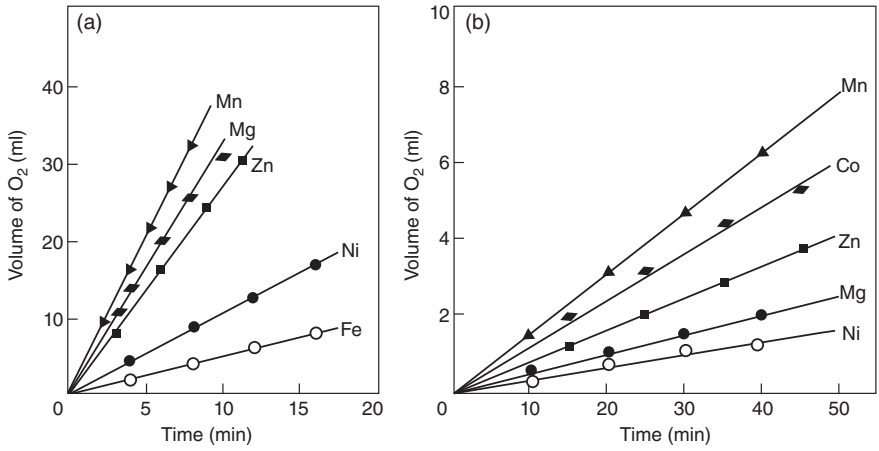

Figure 6.11 Decomposition of H_2O_2 (30%) on (a) cobaltites and (b) ferrites at 30 °C. Reproduced with permission from [30] © 1987 Indian Academy of Sciences.

All the complexes decompose exothermically at ~300 °C to their respective green metal chromites (Table 6.8). The formation of chromites has been confirmed by TG weight loss (Figure 6.12). The decomposed products have also been characterized by their XRD patterns.

Recently, this method of synthesis has been extended to prepare nano-size nickel manganite ($NiMn_2O_4$). Hydrazine complexes of the formula $NiMn_2(C_4H_2O_4)_3{\cdot}6N_2H_4$ and $NiMn_2(C_4H_4O_4)_3{\cdot}6N_2H_4$ containing organic anions like fumerate and succinate, respectively, are precursors to these oxides [32,33].

Table 6.8 Thermal analysis data of $(N_2H_5)_2MCr_2(C_2O_4)_5{\cdot}nN_2H_4$.

Compound	Thermogravimetry			DTA peak temperature (°C)[a]	Product
	Temperature range (°C)	% Weight loss			
		Obsd.	Calcd.		
$(N_2H_5)_2MgCr_2(C_2O_4)_5{\cdot}2N_2H_4$	32–280	30.0	31.2	—	$MgCr_2(C_2O_4)_4$
	280–450	73.0	72.5	330 (+)	$MgCr_2O_4$
$(N_2H_5)_2CoCr_2(C_2O_4)_5{\cdot}2N_2H_4$	32–270	30.0	29.7	—	$CoCr_2(C_2O_4)_5$
	270–370	68.0	69.0	310 (+)	$CoCr_2O_4$.
$(N_2H_5)_2CdCr_2(C_2O_4)_5{\cdot}2N_2H_4$	32–580	64.0	64.3	310 (+)	$CdCr_2O_4$
$(N_2H_5)_2CuCr_2(C_2O_4)_5{\cdot}N_2H_4$	32–450	67.0	67.2	310 (+)	$CuCr_2O_4$
$(N_2H_5)_2NiCr_2(C_2O_4)_5{\cdot}3N_2H_4$	32–280	31.0	32.7		$NiCr_2(C_2O_4)_4$
	280–620	70.5	70.4	290 (+)	$NiCr_2O_4$

[a] (+) = Exotherm.

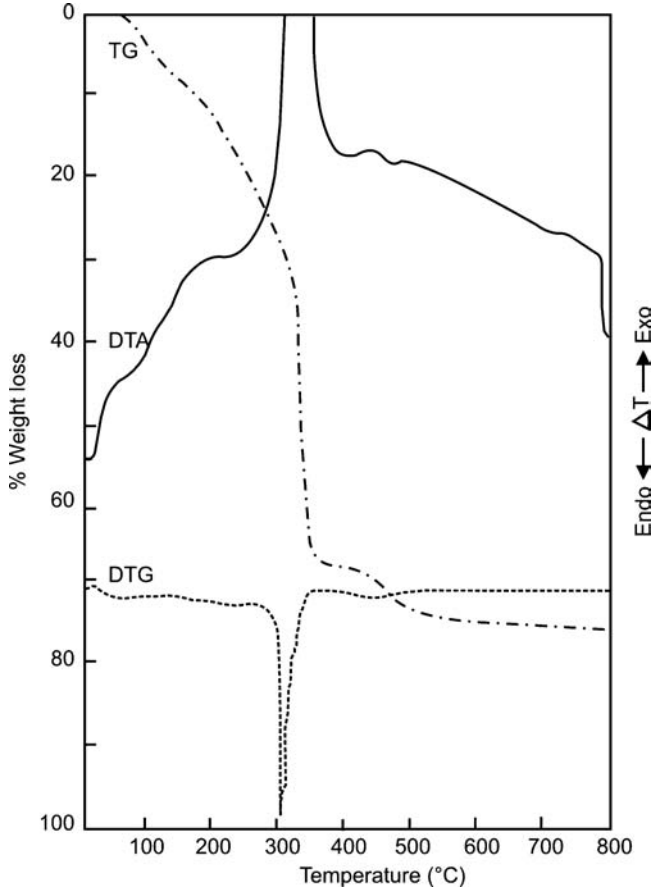

Figure 6.12 Simultaneous TG-DTA-DTG curves of $(N_2H_5)_2MgCr_2(C_2O_4)_5{\cdot}2N_2H_4$. M.Phil Dissertation evaluated by Prof. K. C. Patil, and Dr. Gajapathy, Indian Institute of Science.

6.4.7 Synthesis of Nano-Metal Powders as Catalysts

Catalytic studies of the hydrodesulfurization of thiophene performed at atmospheric pressure in a single-pass microreactor has been studied with Ni-Mo-S/Al_2O_3 catalysts derived from the decomposition of $(N_2H_5)Ni(N_2H_3COO)_3{\cdot}H_2O$ (Figure 6.13). This hydrazinium precursor based catalyst performs better than industrial catalysts [34]. Scanning transmission electron microscopy (STEM) spot analysis shows that Mo is not phase segregated from the promoter metals (Co, Ni, and Co-Ni) on the

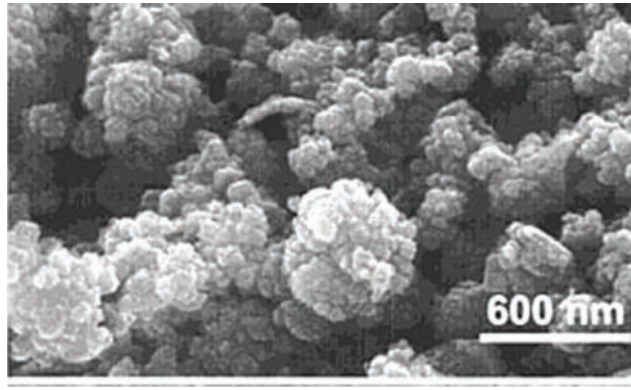

Figure 6.13 Scanning electron microscopy (SEM) micrograph of sonochemically prepared Ni-Mo-S/Al_2O_3. Reprinted with permission from Ref [34]. © 2001, American Chemical Society.

scale of ~3 nm, indicating the formation of binary metal sulfide M-Mo-S structures.

Metallic clusters of pure nanocrystalline Ni of ~3 nm size have been prepared by decomposing nickel hydrazine carboxylate complex under a 1 : 10 H_2/He flow. Low temperature autocatalytic decomposition of the complex furnishes the nanopowders [35]. In another study, nano-size Ni powders with narrow size distribution have been prepared via the reduction of nickel hydrazine complexes of the type $Ni(N_2H_4)_nCl_2$ ($n = 2$–3) as precursors in aqueous solution [36].

6.5 MISCELLANEOUS APPLICATIONS

In recent times, the new use of hydrazine has been towards the development of nanomaterials because of its strongly reducing, solvating, and ligating properties. This has enabled its application as precursors to a diverse group of metal oxide and metal chalcogenide-based nanostructures of considerable importance [37–39]. The following sections describe some of the recent applications of these inorganic hydrazine derivatives.

6.5.1 Reducing Agents

Similar to hydrazine hydrate, a good reducing agent, other inorganic salts like hydrazinium sulfate and hydrazinium halides are also used as reducing

agents. A recent study has shown that hydrazonium sulfate ($N_2H_6SO_4$) acts a reducing agent in the synthesis of inorganic phosphate hydrates like ammonium manganese phosphate monohydrate ($NH_4MnPO_4{\cdot}H_2O$). Control of the oxidation state of the metal ion like manganese, which exhibits multiple oxidation states, is challenging. This problem is overcome by the addition of $N_2H_6SO_4$ into the reaction mixture under basic condition to prevent an aerobic oxidation of Mn^{2+} [40].

6.5.2 Antibacterial Agents

Some hydrazinium salts of organic acids like pyrazine, pyrazole, and imidazole carboxylates discussed in Chapter 2 have proved useful as antibacterial agents. The *in vitro* antibacterial screening of the free acids and their hydrazinium salts has been carried out against *Escherichia coli*, *Salmonella typhi*, and *Vibrio cholerae*, the results of which are presented here [41].

6.5.2.1 Antibacterial Activity Testing

The antibacterial activity of the compounds is determined by the disc diffusion method [42]. The bacteria are cultured in nutrient agar medium and used as inoculum for the study. Bacterial cells are swabbed onto nutrient agar medium (prepared from NaCl (5.0 g), peptone (5 g), beef extract powder (3 g), yeast extract powder (3 g), and agar (20 g) in 1000 ml distilled H_2O); pH 7.5 ± 0.2 in Petri dishes. The test solutions are prepared in distilled water to a final concentration of 1%, 2%, and 4% and then applied to filter paper discs (Whatman No. 4, 5 mm diameter). These discs are placed on the already seeded plates and incubated at 35 ± 2 °C for 24 h. The zones of inhibition around the discs are measured after 24 h. Co-trimoxazole is used as a standard positive control (Table 6.9).

The antibacterial activities of the prepared hydrazinium salts show more promising activity than the corresponding free acids against the standard positive control antibiotic, Co-trimoxazole.

6.5.3 Synthesis of 1D and 2D Nanostructures

Hydrazine hydrate offers a facile method for the preparation of 1D structures of ZnO. These nanorods are produced by microwave

Table 6.9 Antibacterial activity of hydrazinium salts and their free acids.

Compound	Diameter of inhibition zone (mm)[a]								
	Escherichia coli			*Salmonella typhi*			*Vibrio cholerae*		
	1%	2%	4%	1%	2%	4%	1%	2%	4%
Hpyz(COO)	—	9	11	—	—	9	6	8	10
$N_2H_5pyz(COO)$	9	10	12	7	8	11	9	11	24
$N_2H_5pyz(COO)\cdot H_2O$	8	9	12	7	7	10	8	10	19
$H_2pyz(COO)_2$	—	9	11	9	9	12	9	11	14
$N_2H_5Hpyz(COO)_2$	9	11	15	—	10	21	9	13	32
$(N_2H_5)_2pyz(COO)_2$	10	13	28	9	16	37	10	14	35
$(N_2H_5)_2pyz(COO)_2\cdot H_2O$	10	13	29	9	17	36	11	13	34
$N_2H_5Hpyz(COO)_2$. $H_2pyz(COO)_2$	10	11	13	9	10	14	11	11	15
$H_2pz(COO)_2\cdot H_2O$	—	6	8	—	7	9	—	6	7
$N_2H_5Hpz(COO)_2$	—	8	11	6	9	12	6	8	10
$(N_2H_5)_2pz(COO)_2$	9	16	25	10	16	34	10	17	32
$N_2H_5Hpz(COO)_2\cdot H_2pz(COO)_2$	—	8	10	6	8	12	7	7	11
$N_2H_5Hpz(COO)_2\cdot (H_2pz(COO)_2)_3$	6	8	10	—	8	8	7	9	10
H_2imdc[b]	—	—	—	—	—	—	—	—	—
N_2H_5Himdc	6	8	11	6	9	12	—	11	12
$N_2H_5Himdc.\ H_2O$	6	8	11	6	8	11	—	11	12
Co-trimoxazole	6	7	10	6	9	11	7	8	10

[a] Diameter of inhibition zone is a mean of triplicates.
[b] Insoluble.

irradiation of zinc acetate and hydrazine hydrate, which appear to form a zinc acetate hydrazine hydrate complex that undergoes *in situ* decomposition to form the nano-oxide rods [43]:

$$m\mathrm{Zn(CH_3COO)_2} + n\mathrm{N_2H_4} \rightarrow [\mathrm{Zn(CH_3COO)_2}]_m[\mathrm{N_2H_4}]_n \qquad (6.4)$$

Interestingly, under similar microwave irradiation, when zinc acetate is made to react with ammonium hydroxide, nanostructures of the material are not formed. Hence it may be concluded that it is the hydrazine hydrate that acts as ligand and capping agent facilitating the formation of 1D nanomaterial of ZnO (Figure 6.14).

The unique solvent properties of hydrazine have further been used to produce a range of 2D nanostructures of first and second row transition metal chalcogenides by the solvothermal method. Hydrazine, being a small volatile molecule, capable of forming coordinate complexes or

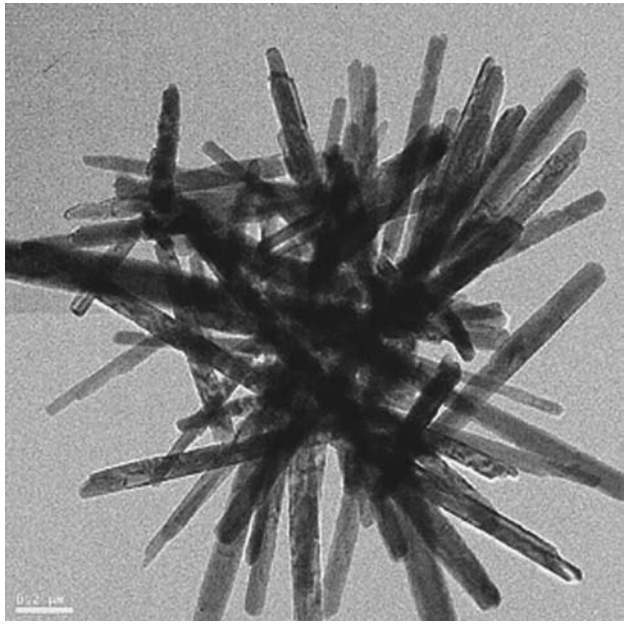

Figure 6.14 TEM micrograph of ZnO nanorods. Reproduced from Krishna Bhat, D. (2008) Facile synthesis of ZnO nanorods by microwave irradiation of zinc–hydrazine hydrate complex. *Nanoscale Res. Lett.*, **3**, 31–35 © 2008.

precursors with metals, has rendered this process as a new soft synthetic route to prepare novel metal chalcogenide based materials at low temperatures. A major advantage of this method is that it has thin-film forming capabilities and produces no carbon or other contaminants in the product. It is proposed that the parent framework metal chalcogenide is broken up during its interactions with the hydrazinium moieties (Figure 6.15). The resulting metal chalcogenide hydrazine building units are later reorganized into network structures during their decomposition at low temperatures [44].

A similar solvothermal process has been used to synthesize the new thioantimonate compound $[Mn_2Sb_4S_8(N_2H_4)_2]$ by reacting Mn and $Sb_2S_3$with S in hydrazine hydrate solution. This compound is a semiconductor with a band gap of 1.59 eV and displays paramagnetic behavior at high temperature and switches to antiferromagnetic ordering at 40 K [45].

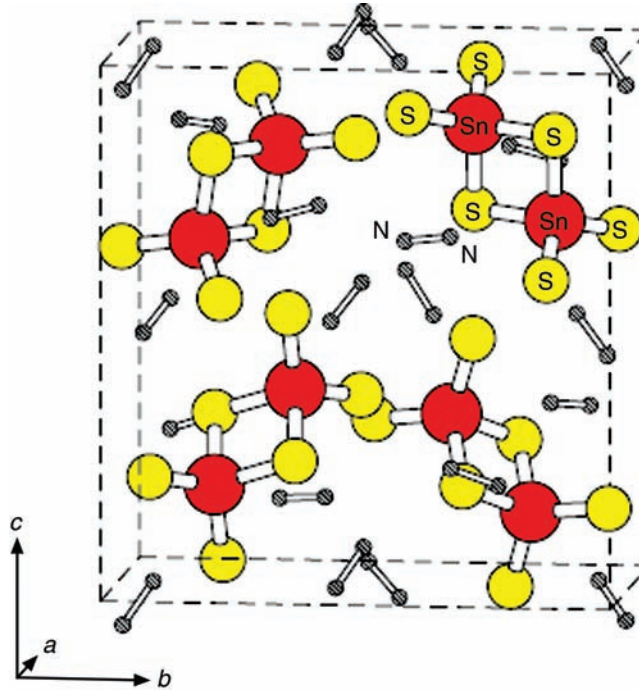

Figure 6.15 Crystal structure of $(N_2H_5)_4Sn_2S_6$. Reprinted from Ref [39] by permission from Macmillan Publishers Ltd © 2009.

REFERENCES

1. Rothgery, E.F. (2004) Hydrazine and its derivatives, in *Kirk-Othmer Encyclopedia of Chemical Technology*, vol. 13, John Wiley & Sons, Inc., pp. 562–607.
2. Schmidt, E.W. (2001) *Hydrazine and its Derivatives: Preparation, Properties, Applications*, 2nd edn, John Wiley & Sons, Inc.
3. Makled, A.E. and Belal, H. (2009) Modeling of hydrazine decomposition for monopropellant thrusters. 13th International Conference on Aerospace Sciences & Aviation Technology pp. 22.
4. Kumar, N.R.S. and Patil, K.C. (1987) Thermal reactivity of hydrazinium halides. Solid state reaction of N_2H_5Cl with $NHVO_3$. Symposium on Solid Propellants for Rocketry and Explosives 241–243.
5. Vittal, J.J., Angadi, V.B., and Patil, K.C. (1989) Reactivity of hydrazinium hydrazinecarboxylate-synthesis of 4-amino-3,5-dimethyl-1,2,4-triazole. *Journal of the Indian Institute of Science*, **69**, 119–124.
6. Patil, K.C., Vittal, J.J., and Patel, C.C. (1980) Monohydrazinium phosphate as flame retardant. *Journal Fire Retardant Chemistry*, **7**, 3–8.
7. Patil, K.C., Vittal, J.J., and Patel, C.C. (1981) Pyrolysis and combustion of α-cellulose: effect of dihydrazinium phosphate $(N_2H_5)_2HPO_4$. *Thermochimica Acta*, **43**, 213–219.

8. Vittal, J.J., Anantasubramaniam, C.R., Soundararajan, R., and Patil, K.C. (1979) Hydrazinium thiocyanate as a reagent for determination of copper. *Talanta*, **26**, 1041–1042.
9. Nesamani, C. (1983) *Studies on high energy hydrazine compound*, Ph.D Thesis, Indian Institute of Science, Bangalore.
10. Zhu, S.G., Xu, D., Cao, S. *et al.* (2005) The powerful coordination compound-nickel hydrazine azide. *Explosive Materials*, **34**, 17–18.
11. Zhu, S.G., Li, Y., Zhang, L., and Mou, J. (2010) *The preparation of NHA [P]*. China: ZL200810122840. X, 2010-01-06.
12. Talwar, M.B., Agrawal, A.P., Chabbra, J.S. *et al.* (2004) Studies on nickel hydrazinium nitrate (NHN) and *bis*-(5-nitro-2H-tetrazolato-N^2) tetraamino cobalto(III) perchlorato (BNCP): potential lead-free advanced primary explosives. *Journal of Scientific and Industrial Research*, **63**, 677–681.
13. Peng, M.A., Zhu, S.G., Zhang, L. *et al.* (2010) Ignition of semiconductor bridge with nickel hydrazine azide. *Chinese Journal of Energetic Materials*, **18**, 213–216.
14. Fischer, N., Klapötke, T.M., Reymann, M., and Stierstorfer, J. (2013) Nitrogen-rich salts of 1*H*,1′*H*-5,5′-bitetrazole-1,1′-diol: energetic materials with high thermal stability. *European Journal of Inorganic Chemistry*, 2167–2180.
15. Fischer, N., Iszak, D., Klapötke, T.M. *et al.* (2012) Nitrogen-rich 5,5′-bistetrazolates and their potential use in propellant systems: a comprehensive study. *Chemistry - A European Journal*, **18**, 4051–4062.
16. Lin, Q.H., Li, U.C., Qi, C. *et al.* (2013) Nitrogen-rich salts based on 5-hydrazino-1H-tetrazole: a new family of high-density energetic materials. *Journal of Materials Chemistry A*, **1**, 6776–6785.
17. Ramnath, M. (1979) Studies on solid composite propellant combustion: Effect of additives and encapsulation, PhD Thesis, Indian Institute of Science, Bangalore.
18. Wojewodka, A., Beøzowski, J., Wilk, Z., and Stas, J. (2009) Energetic characteristics of transition metal complexes. *Journal of Hazardous Materials*, **171**, 1175–1177.
19. Gajapathy, D. (1983) *Studies on metal–hydrazine system*, Ph.D Thesis, Indian Institute of Science, Bangalore.
20. Patil, K.C. and Pai Verneker, V.R. (1980) A novel method of preparing γ-Fe_2O_3. *Magnetics Society of India Transactions*, **4**, 8–10.
21. Sundar, Manoharan, S. (1991) Combustion synthesis and properties of fine particle spinel, perovskite and K_2NiF_4 type oxides, PhD Thesis, Indian Institute of Science, Bangalore.
22. Tey, S.L., Reddy, M.V., Subba Rao, G.V. *et al.* (2006) Synthesis, structure, and magnetic properties of $[Li(H_2O)M(N_2H_3CO_2)_3]\cdot 0.5H_2O$ (M=Co, Ni) as single precursors to $LiMO_2$ battery materials. *Chemistry of Materials*, **18**, 1587–1594.
23. Aruna, S.T. and Patil, K.C. (1996) Synthesis and properties of nanosize titania. *Journal of Materials Synthesis and Processing*, **4**, 175–179.
24. Suresh, K., Mahesh, G.V., and Patil, K.C. (1989) Preparation of cobalt doped γ-Fe_2O_3 and Mn-Zn ferrites by the thermal decomposition of the hydrazine precursors. *Journal of Thermal Analysis*, **35**, 1137–1143.
25. Aruna, S.T., Ghosh, S., and Patil, K.C. (2001) Combustion synthesis and properties of $Ce_{1-x}Pr_xO_{2-\delta}$ red ceramic pigments. *International Journal of Inorganic Materials*, **3**, 387–392.
26. Rakkiyasamy, M., Kalimuthu, K., and Rangasamy, S. (2012) Synthesis and characterization of nickel cobalt cinnamate hydrazinate: a precursor for cobaltite nanoparticles. *Scientific Reviews & Chemical Communications*, **2**, 597–601.

27. Rakkiyasamy, M., Kalimuthu, K., and Rangasamy, S. (2013) Preparation and characterization of nickel cobalt phenylacetate hydrazinate – a precursor for cobaltite nanoparticles. *Research Journal of Chemical Science*, **3**, 76–78.
28. Gonsalves, L.R., Mojumdar, S.C., and Verenkar, V.M.S. (2010) Synthesis of cobalt nickel ferrite nanoparticles via autocatalytic decomposition of the precursor. *Journal of Thermal Analysis and Calorimetry*, **100**, 789–792.
29. Gawas, U.B., Mojumdar, S.C., and Verenkar, V.M.S. (2010) Synthesis, characterization, infrared studies and thermal analysis of $Mn_{0.6}Zn_{0.4}Fe_2(C_4H_2O_4)_3{\cdot}6N_2H_4$ and its decomposition product $Mn_{0.6}Zn_{0.4}Fe_2O_4$. *Journal of Thermal Analysis and Calorimetry*, **100**, 867–871.
30. Mimani, T., Ravindranthan, P., and Patil, K.C. (1987) Catalytic decomposition of hydrogen peroxide on fine particle ferrites and cobaltites. *Proceedings of the Indian Academy of Sciences – Chemical Sciences*, **99**, 209–215.
31. Margasahayam, S. (1986) *Hydrazine complexes of chromium as precursors to chromites*, MPhil Dissertation, University of Madras.
32. Sawant, S.Y., Verenkar, V.M.S., and Mojumdar, S.C. (2007) Preparation, thermal, XRD, chemical and FTIR spectral analysis of $NiMn_2O_4$ nanoparticles and respective precursor. *Journal of Thermal Analysis and Calorimetry*, **90**, 669–672.
33. Porob, R.A., Khan, S.Z., Mojumdar, S.C., and Verenkar, V.M.S. (2006) Synthesis, TG, DSC and infrared spectral study of $NiMn_2(C_4H_4O_4)_3{\cdot}6N_2H_4$: a precursor for $NiMn_2O_4$ nanoparticles. *Journal of Thermal Analysis and Calorimetry*, **86**, 605–608.
34. Arul Dhas, N., Arash, E., and Kenneth, S.S. (2001) Sonochemical preparation of supported hydrodesulfurization catalysts. *Journal of the American Chemical Society*, **123**, 8310–8316.
35. Mastai, Y. and Gedankan, A. (2004) Sonochemistry and other novel methods developed for the synthesis of nanoparticles, in *The Chemistry of Nanomaterials*, vol. 1 (eds C.N.R. Rao, A. Müller, and A.K. Cheetham), Wiley-VCH Verlag GmbH, Weinheim, ch. 6, pp. 116.
36. Huang, G.Y., Xu, S.M., Xu, G. *et al.* (2009) Preparation of fine nickel powders via reduction of nickel hydrazine complex precursors. *Transactions of Nonferrous Metals Society of China*, **19**, 389–393.
37. Patil, K.C., Hegde, M.S., Tanu, Rattan, and Aruna, S.T. (2008) *Chemistry of Nanocrystalline Oxide Materials: Combustion Synthesis, Properties, and Applications*, World Scientific Publishing Co. Pte. Ltd., Singapore.
38. Mitzi, D.B. (2009) Solution processing of chalcogenide semiconductors via dimensional reduction, in *Solution Processing of Inorganic Materials*, John Wiley & Sons, Inc., Hoboken, ch. 3, pp. 77–104.
39. Mitzi, D.B., Kosbar, L.L., Murray, C.E. *et al.* (2004) High-mobility ultrathin semiconducting films prepared by spin coating. *Nature*, **428**, 299–303.
40. Danvirutai, C., Noisong, P., and Youngme, S. (2010) Some thermodynamic functions and kinetics of thermal decomposition of $NH_4MnPO_4{\cdot}H_2O$ in nitrogen atmosphere. *Journal of Thermal Analysis and Calorimetry*, **100**, 117–124.
41. Premkumar, T. (2002) Synthesis and structural, spectroscopic, and thermal characterization of pyrazine, pyrazole and imidazole carboxylates of metal with hydrazine, Ph.D Thesis, Bharathiar University, Coimbatore, India.
42. Cruickshank, R. (1968) *Medical Microbiology: A Guide to Diagnosis and Control of Infection*, 11th edn, E & S Livingstone Ltd. Cruickshank, Edinburgh and London.

43. Krishna Bhat, D. (2008) Facile synthesis of ZnO nanorods by microwave irradiation of zinc–hydrazine hydrate complex. *Nanoscale Research Letters*, **3**, 31–35.
44. Yuan, M. and Mitzi, D.B. (2009) Solvent properties of hydrazine in the preparation of metal chalcogenide bulk materials and films. *Dalton Transactions*, 6078–6088.
45. Liu, Y., Tian, Y., and Wei, F.X. *et al.* (2011) A new hydrazine-bridged thioantimonate $Mn_2Sb_4S_8(N_2H_4)_2$: synthesis, structure, optical and magnetic properties. *Inorganic Chemistry Communications*, **14**, 884–888.

Index

Inorganic Hydrazine Derivatives: Synthesis, Properties and Applications, First Edition.
Edited by K. C. Patil and Tanu Mimani Rattan.